SÓNIA FERNANDA ALMEIDA SANTOS

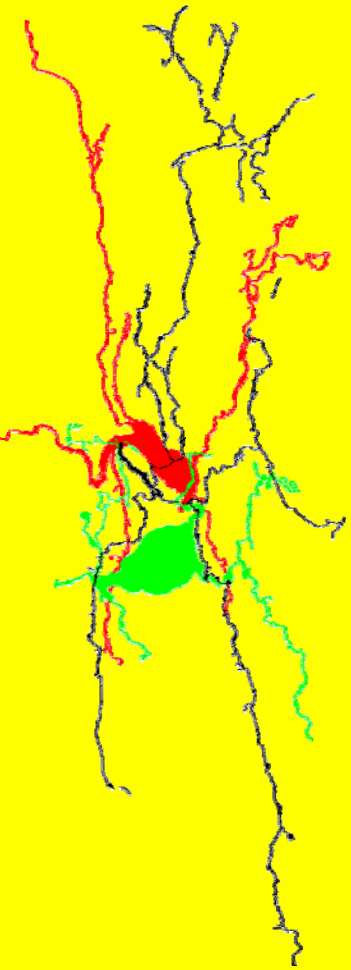

MECANISMOS DE PROCESSAMENTO DA DOR:

Diversidade dos Padrões de Disparo em Neurónios Sensoriais Espinhais e a sua Modificação por Agonistas de Receptores de Opioides

Dissertação de candidatura ao grau de Doutor apresentada à Faculdade de Medicina da Universidade do Porto

PORTO

2010

SÓNIA FERNANDA ALMEIDA SANTOS

MECANISMOS DE PROCESSAMENTO DA DOR:

Diversidade dos Padrões de Disparo em Neurónios Sensoriais Espinhais e a sua Modificação por Agonistas de Receptores de Opioides

PORTO

2010

Dissertação de candidatura ao grau de Doutor apresentada à Faculdade de Medicina da Universidade do Porto

Artigo 48º, § 3º

“ A Faculdade não responde pelas doutrinas expendidas na dissertação”

(Regulamento da Faculdade de Medicina do Porto, Decreto-Lei nº 19337 de 29 de Janeiro de 1931)

CORPO CATEDRÁTICO DA FACULDADE DE MEDICINA DO PORTO

Professores Efectivos

MANUEL MARIA PAULA BARBOSA
MANUEL ALBERTO COIMBRA SOBRINHO SIMOES
JORGE MANUEL MERGULHAO CASTRO TAVARES
MARIA AMELIA DUARTE FERREIRA
JOSÉ AGOSTINHO MARQUES LOPES
PATRÍCIO MANUEL VIEIRA ARAÚJO SOARES SILVA
DANIEL FILIPE LIMA MOURA
BELMIRO DOS SANTOS PATRICIO
ALBERTO MANUEL BARROS DA SILVA
JOSE MANUEL LOPES TEIXEIRA AMARANTE
JOSE HENRIQUE DIAS PINTO DE BARROS
MARIA FÁTIMA MACHADO HENRIQUES CARNEIRO
ISABEL MARIA AMORIM PEREIRA RAMOS
DEOLINDA MARIA VALENTE ALVES LIMA TEIXEIRA
MARIA DULCE CORDEIRO MADEIRA
ALTAMIRO MANUEL RODRIGUES COSTA PEREIRA
RUI MANUEL ALMEIDA MOTA CARDOSO
ANTONIO CARLOS FREITAS RIBEIRO SARAIVA
ÁLVARO JERONIMO LEAL MACHADO DE AGUIAR
ANTÓNIO JOSÉ PACHECO PALHA
JOSE LUÍS MEDINA VIEIRA
JOSE CARLOS NEVES DA CUNHA AREIAS
MANUEL JESUS FALCAO PESTANA VASCONCELOS
JOÃO FRANCISCO MONTENEGRO ANDRADE LIMA BERNARDES
MARIA LEONOR MARTINS SOARES DAVID
RUI MANUEL LOPES NUNES
AMADEU PINTO DE ARAUJO PIMENTA
ANTÓNIO ALBINO COELHO MARQUES ABRANTES TEIXEIRA
JOSÉ EDUARDO TORRES ECKENROTH GUIMARÃES
FRANCISCO FERNANDO ROCHA GONÇALVES
JOSE MANUEL PEREIRA DIAS DE CASTRO LOPES
MANUEL ANTONIO CALDEIRA PAIS CLEMENTE
ABEL VITORINO TRIGO CABRAL

Professores Jubilados ou Aposentados

ABEL JOSÉ SAMPAIO DA COSTA TAVARES
ALEXANDRE ALBERTO GUERRA SOUSA PINTO
AMÂNDIO GOMES SAMPAIO TAVARES
ANTÓNIO AUGUSTO LOPES VAZ
ANTÓNIO CARVALHO ALMEIDA COIMBRA
ANTÓNIO FERNANDES DA FONSECA
ANTÓNIO FERNANDES OLIVEIRA BARBOSA RIBEIRO BRAGA
ANTÓNIO GERMANO PINA SILVA LEAL
ANTÓNIO LUÍS TOMÉ DA ROCHA RIBEIRO
ANTÓNIO MANUEL SAMPAIO DE ARAÚJO TEIXEIRA
ARTUR MANUEL GIESTEIRA DE ALMEIDA
CÂNDIDO ALVES HIPÓLITO REIS
CARLOS RODRIGO MAGALHÃES RAMALHÃO
DANIEL SANTOS PINTO SERRÃO
EDUARDO JORGE CUNHA RODRIGUES PEREIRA
FERNANDO DE CARVALHO CERQUEIRA MAGRO FERREIRA
FERNANDO TAVARELA VELOSO
FRANCISCO JOSÉ ZARCO CARNEIRO CHAVES
FRANCISCO DE SOUSA LÉ
HENRIQUE JOSÉ FERREIRA GONÇALVES LECOUR DE MENEZES
JOÃO SILVA CARVALHO
JOAQUIM GERMANO PINTO MACHADO CORREIA DA SILVA
JOAQUIM OLIVEIRA COSTA MAIA
JOSÉ AUGUSTO FLEMING TORRINHA
JOSÉ CARVALHO DE OLIVEIRA
JOSÉ FERNANDO BARROS CASTRO CORREIA
JOSÉ MANUEL COSTA MESQUITA GUIMARÃES
LEVI EUGÉNIO RIBEIRO GUERRA
LUÍS ALBERTO MARTINS GOMES DE ALMEIDA
MANUEL MACHADO RODRIGUES GOMES
MANUEL TEIXEIRA AMARANTE JÚNIOR
MARIA DA CONCEIÇÃO FERNANDES MARQUES MAGALHÃES
MÁRIO JOSÉ CERQUEIRA GOMES BRAGA
SERAFIM CORREIA PINTO MAGALHÃES
VALDEMAR MIGUEL BOTELHO DOS SANTOS CARDOSO
WALTER FRIEDRICH ALFRED OSSWALD

Ao Professor Doutor Boris Safronov

À Professora Doutora Deolinda Maria Alves de Lima Teixeira

Aos meus pais

Ao Cid

PREFÁCIO

O meu percurso no campo das Neurociências iniciou-se com uma bolsa de investigação orientada pelo Doutor Boris Safronov. O objectivo do projecto em que fui incluída inicialmente, consistia em estudar os diferentes tipos de disparo de potenciais de acção exibidos pelos neurónios de uma das lâminas da medula espinhal, envolvida no processamento da dor, recorrendo à técnica patch-clamp. Nessa altura, o conhecimento científico adquirido na universidade apenas me havia fornecido algumas ferramentas, contudo, a perspectiva de poder estudar pequenas correntes eléctricas neuroniais através do recurso a uma técnica da qual nunca ouvira falar, surpreendentemente, não me intimidou.

Assim começou este percurso e com grande entusiasmo dediquei-me a esta dissertação.

Entretanto, no início de 2007, fui convidada a integrar o corpo docente da Faculdade de Medicina do Porto, na função de assistente convidado, e esta tem sido uma experiência gratificante de aprendizagem e partilha mútuas.

Foram muitas as pessoas que, durante estes anos, contribuíram directa ou indirectamente para a realização desta tese. Ao mentor do trabalho científico, Professor Doutor Boris Safronov, o meu sincero agradecimento por me ter dado a oportunidade de participar no trabalho experimental que alargou os meus horizontes. Reconheço e admiro a sua rara capacidade e rigor científico, o seu dinamismo e entusiasmo permanentes, fundamentais ao progresso desta dissertação. Ao Doutor Igor Melnick, um agradecimento especial por me ter iniciado na electrofisiologia, pelo convívio e companheirismo. À Professora Doutora Deolinda Lima, agradeço todo o entusiasmo científico contagiante, a sua determinação e as palavras preciosas com que sempre contei durante todo o percurso desta dissertação. Admiro-a profundamente como pessoa, brilhante cientista, comunicadora e líder.

Agradeço ao Doutor Victor Derkach pelo enorme contributo que deixou na presente dissertação e pelos ensinamentos que em muito aumentaram as minhas competências científicas.

Várias pessoas do IBMC, do Instituto de Histologia e Laboratório de Biologia Celular contribuíram para a concretização deste projecto. Agradeço ao Dr. Vítor Pinto pela força nos momentos difíceis e solitários no laboratório, ao Professor Doutor Vasco Galhardo pela amabilidade permanente, à Drª. Clara Monteiro pelo valioso apoio amigo, ao Doutor Paulo

Aguiar pela atenção e disponibilidade, ao Dr. Hélder Cruz pelos valiosos conhecimentos informáticos, ao Doutor Miguel Pais Vieira pela boa disposição e companheirismo e ao Sr. Carlos pela paciência e prontidão com que sempre me respondeu.

Agradeço também à Drª. Isabel Martins pela paciência, amizade, suporte, partilha de secretária e experiências.

Ao Professor Doutor António Avelino, um muito obrigada pela experiência inesquecível da degustação de capsaicina e pelos gestos fundamentais nos momentos certos.

O meu especial agradecimento à Professora Doutora Delminda Magalhães pela disponibilidade e convívio enriquecedor.

Aos restantes elementos docentes e/ou investigadores, agradeço os momentos passados.

A todo o corpo técnico do Instituto de Histologia e Embriologia, o meu agradecimento pela ajuda prestada, em especial à Elisa e Anabela pelo apoio laboratorial, à D. Ana Tavares e Raquel pelo apoio de secretariado, à D. Glória Alves e Sr. Fernando Pinto, um muito obrigada pela generosidade permanente em tempo de aulas, e não só.

O meu agradecimento à Fundação para a Ciência e a Tecnologia (FCT) pela oportunidade que me deu ao conceder-me uma bolsa de doutoramento (SFRH / BD /12318/2003).

Quero também expressar um muito especial agradecimento ao colega de curso Luís Cruz pelo companheirismo, amizade, dedicação e paciência durante todos estes anos.

Aos meus Pais agradeço tudo aquilo que sou hoje. O apoio, a crença e os valores, mas também o amor e apoio fundamentais com que me brindaram em todos os momentos. Dedico-lhes esta dissertação.

A dedicatória extende-se ao meu querido Cid, pela sua companhia nesta jornada e nos obstáculos vencidos, mas também pelo apoio e afecto incondicional que sempre me dedicou.

Por fim, dedico esta tese ao nosso encantador e muito querido filho, Valentim.

Sónia Santos

Em obediência ao disposto no Decreto-Lei nº388/70, artigo 8º, parágrafo 2, declaro que efectuei o planeamento e execução das experiências, observação do material e análise dos resultados discutidos durante esta dissertação. Declaro ainda que participei activamente na redacção de todas as publicações que fazem parte integrante desta dissertação:

I Santos SFA, Melnick IV & Safronov BV. (2004) Selective postsynaptic inhibition of tonic-firing neurons in substantia gelatinosa by μ-opioid agonist. *Anesthesiology* **101**: 1177-1183.

II Santos SFA**,** Rebelo S**,** Safronov BV & Derkach VA. (2007) Excitatory interneurons dominate sensory processing in the spinal substantia gelatinosa of rat. *J Physiol* **581**: 241-254.

III Santos SFA**,** Luz LL, Szucs P, Lima D, Derkach VA & Safronov BV. (2009) Transmission efficacy and plasticity in glutamatergic synapses formed by excitatory interneurons of the substantia gelatinosa in the rat spinal cord. *PlosOne* **4**: e8047, p1-18.

IV Melnick IV, Santos SFA, Szokol K, Szucs P & Safronov BV. (2004) Ionic basics of tonic firing in spinal substantia gelatinosa neurons of rat. *J Neurophysiol* **91**: 646-655.

V Melnick IV**,** Santos SFA & Safronov BV. (2004) Mechanism of spike frequency adaptation in substantia gelatinosa neurons of rat. *J Physiol* **559**: 383-395.

A reprodução destas publicações foi feita com autorização das respectivas editoras.

Com excepção do resumo e conclusões, a restante parte desta Dissertação será escrita em Inglês.

ABBREVIATIONS

AFN	adapting firing neuron
AIS	axon initial segment
AMPA	α-amino-3-hydroxy-5-methyl-4-isoxazolepropionic acid
BAPTA	1,2-Bis (2-Aminophenoxy) ethane-*N,N,N′,N′*-tetraacetic acid
CNQX	6-cyano-7-nitroquinoxaline-2,3-dione
DAMGO	**[**D-Ala^2, N- Me- Phe^4, Gly^5–ol**]**– enkephalin
DFN	delayed firing neuron
DOR	δ-opioid receptor
EPSC	excitatory postsynaptic current
EPSP	excitatory postsynaptic potential
GABA	γ-aminobutiric acid
GIRK	G-protein dependent inward rectifying potassium (channel)
IPSC	inhibitory postsynaptic current
IPSP	inhibitory postsynaptic potential
KOR	κ-opioid receptor
K_A	A-type potassium (channels)
K_{CA}	Ca^{2+} -dependent potassium (channels)
K_{DR}	delayed-rectifier potassium (channels)
LTD	long term depression
LTP	long term potentiation
MOR	μ-opioid receptor
NMDA	N-methyl-D-aspartate
R_{IN}	input resistance
r.m.s.	root mean square
SDH	superficial dorsal horn
SG	substantia gelatinosa
TFN	tonic firing neuron
TEA	tetraethilammonium
TTX	tetrodotoxin
V_R	membrane potential

CONTENTS

I. INTRODUCTION

1. Modulation of Nociceptive Transmission - General Aspects

The pain processing starts at nociceptors, receptors for noxious stimuli located in the peripheral terminals of afferents in skin, muscles, tendons, joints and viscera. These receptors allow detection of both somatic and visceral pain. Unlike the innocuous receptors, nociceptors often respond to multiple stimulus modalities and are therefore considered as polymodal. They can be activated by painful stimulus including noxious heat or cold, intense pressure or irritants (reviewed by Hill, 2001 and Julius & Basbaum, 2001).

Primary afferents which conduct nociceptive information from the periphery to the dorsal horn of the spinal cord are thinly myelinated Aδ- and unmyelinated C-fibres (reviewed by Warren *et al*., 2000 and Schaible, 2006; Gardner *et al*., 2000; Bielefeldt & Gebhart, 2006). Their different axon conduction velocities (reviewed by Todd & Koerber, 2006) is on the basis of the division of pain into two sensations: the first sharp pain is mediated by the activation of the faster conducting Aδ-fibres, whereas the second dull pain is transmitted by the slowly conducting C-fibres. The latter are thought to mediate the burning pain sensation, whereas the former evoke pricking pain, sharpness and also aching pain (reviewed by Julius & Basbaum, 2001).

Noxious stimuli open membrane cation channels, permeable to sodium and/or calcium, and lead to a depolarization of the primary afferent terminal. If the stimulus is strong enough, the depolarizing currents are transduced into electrical activity. The resulting action potentials are propagated via the axon to the central nervous system and, after activation of voltage-gated calcium channels, fast excitatory, glutamatergic synaptic transmission is initiated (reviewed by Woolf & Salter, 2000; Yoshimura & Jessel, 1990).

The onset, duration, and intensity of a painful stimulus are coded by the generated action potentials. Tetrodotoxin (TTX)-sensitive and -resistant types of voltage-gated Na^+-channel are involved in spike initiation and propagation in the peripheral axon (Khasar *et al*., 1998; Pinto *et al*., 2008). TTX-sensitive type of sodium channel dominates conduction in both types of thin primary afferent fibres. The TTX-sensitive channel determines the physiological conduction velocity and synaptic transmission in C-fibres, being the only type of sodium channel underlying conduction in Aδ-fibres (Pinto *et al*., 2008). TTX-resistant sodium channels are molecules for nociception in the cold and for cold pain, designated for the peripheral sensory nerve endings (Zimmermann *et al*., 2007; Pinto *et al*., 2008).

The sensory barrage produced by the activation of primary afferents is transmitted to neurons in the superficial dorsal horn (SDH) of the spinal cord or the corresponding region of the trigeminal brain stem complex (reviewed by Woolf & Salter, 2000), which project through a thalamic relay to the cortex as the nociceptive transmission system, eliciting pain (reviewed by Hunt & Mantyh, 2001).

A mechanism of spinal pain processing was proposed by Melzack and Wall (1965) as the 'gate control theory'. They suggested that there is a gating mechanism in the spinal dorsal horn through which pain information has to pass on its way to the brain. Whether the gate is opened or closed depends on which fibres are activated, e.g. large diameter fibres activate inhibitory interneurons that prevent noxious information from being further transduced to the thalamus (closing the gate).

Besides being involved in pain conduction (Rethelyi, 1977; Light & Perl, 1979; Sugiura *et al*., 1986; Cervero, 1987), SDH also plays a key role in the system of pain control. In fact, a population of spinal dorsal horn neurons includes both enkephalin-ergic cells and those specifically expressing opioid receptors, indicating its involvement in endogenous mechanisms of anti-nociception (Merchenthaler *et al*., 1986; Ribeiro-da-Silva *et al*., 1991; Arvidson *et al*., 1995a,b,c). These cells also play an important role in analgesic effects induced by opioids during systemic administration or local injection (Light & WillcocKson, 1999). However, little is known about the types of spinal neurons serving as specific postsynaptic targets for opioid action.

Spinal cord neurons can be distinguished on the basis of their membrane properties and intrinsic firing (Thomson *et al*., 1989; Yoshimura & Jessel, 1989; Lopez-Garcia & King, 1994; Grudt & Perl, 2002). In turn, the firing pattern of a neuron can determine the efficiency of its output. Therefore, it is necessary to study the neuron firing patterns in relation to its synaptic connectivity. Although a number of studies were done on synapses formed by the primary afferents, little is known about synapses between two intrinsic dorsal horn neurons. Until recently, this knowledge was mostly based on recordings of spontaneous activity of unidentified origin. Such an approach did not allow to describe basic properties or activity dependent modulation of synapses connecting two local neurons. A direct way to study such synapses, simultaneous patch-clamp recording from a couple of monosynaptically connected neurons, could be hardly applied due to a very low probability of finding connected cells in the spinal cord (Lu & Perl, 2003; 2005).

Still many questions remain unanswered in what concerns to the evaluation of sensory processing in the spinal cord. For this reason, this work has the purpose to clarify different aspects of the spinal nociceptive processing and mechanisms of opioidergic analgesia. Therefore, we analysed the firing properties, synaptic connections and activity-dependent modulation of synaptic strength (plasticity) of spinal neurons involved in sensory processing.

1.1. Sensory Processing in the SDH

SDH is the first relay station in processing the sensory information on its way from periphery to the brain. It is formed by laminae I-II which differ from each other on the basis of neuronal morphology as well as types of terminating primary afferents (Brown, 1981). Lamina II, or substantia gelatinosa (SG), is mostly formed by local excitatory and inhibitory interneurons, some of which relay the primary afferent inputs to projection neurons in lamina I (reviewed by Basbaum & Jessel, 2000; Lu & Perl, 2003, 2005; Kato *et al*., 2007). It is believed that diverse sensory modalities are also encoded by the intrinsic firing properties and synaptic connectivity of SDH neurons (reviewed by Willis & Coggeshall, 1991; Brown, 1981; Cervero, 1987).

1.1.1. Types of intrinsic firing properties

Besides morphology (Beal & Cooper, 1978; Gobel *et al*., 1980; Grudt & Perl, 2002), the neurons from SG are also distinguished on the basis of intrinsic firing properties (Thomson *et al.*, 1989; Lopez-Garcia & King, 1994; Grudt & Perl, 2002) which can be studied by both sharp electrode (Yoshimura & Jessell, 1989; Thomson *et al*., 1989; Lopez-Garcia & King, 1994) and tight-seal recordings (Grudt & Perl, 2002; Ruscheweyh & Sandkuhler, 2002; Graham *et al*., 2004). Intracellular stimulation of lamina I-II neurons revealed three distinct groups with different intrinsic firing properties (Figure 1).

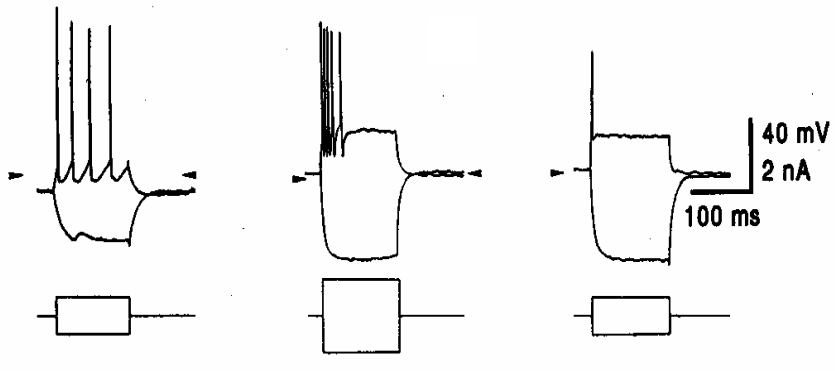

Figure 1. *Characterization of three types of dorsal horn neurons according to their intrinsic firing properties*. Sustained hyper- or depolarizing current pulses were applied to test membrane responses and firing patterns. The small arrow heads indicate -75 mV membrane potential on all records (From Safronov, 1999).

The neurons from the first group responded with a tonic firing to injection of sustained depolarizing currents (tonic-firing neurons, TFNs). Neurons from the second group fired trains of action potentials only at the beginning of a depolarization (adapting-firing neurons, AFNs), whereas the third group of neurons generated only one or two spikes during sustained depolarization (single-spike neurons). The functional relevance of this classification was further supported by observation that the intrinsic firing patterns correlated with those appearing after stimulation of afferent inputs (Thomson *et al*., 1989; Lopez-Garcia & King, 1994). The neurons responding to a low threshold (non-noxious) and a high threshold (noxious) cutaneous stimulation by generation of action potentials, a number of which increased with the strength of the stimulation, wide-dynamic-range neurons, belonged predominantly to TFN group. The neurons firing equal number of spikes in response to both non-noxious and noxious stimuli, low-threshold neurons, were either TFNs or AFNs. The neurons excited by noxious stimulation only, nociceptive-specific neurons, were mostly AFNs. By contrast, in most of the single-spike neurons the cutaneous stimulation evoked inhibitory postsynaptic potentials and a reduction of spontaneous firing. Therefore, the type-specific intrinsic firing of SG neurons forms the basis of the diverse modalities of sensory, including noxious, input.

The intrinsic firing properties of the neuron, in turn, are determined by the specific properties and distributions of voltage-gated ion channels as well as by the electrotonic architecture of the cell. The development of several techniques (Hamill *et al.*, 1981; Edwards *et al*., 1989; Safronov *et al*., 1997) has made it possible to study the ion channels and their distribution in intact dorsal horn neurons. The distributions of voltage-gated Na^+ and K^+ channels between the soma, axon and dendrites in SDH neurons were studied in spinal cord slices by the 'entire soma isolation' method (Safronov *et al*., 1997), showing that 96 % of Na^+ channels are located in the axon initial segment (AIS) (Safronov *et al.*, 1999), while the soma and dendrites are mostly equipped with K^+ channels (Wolff *et al*., 1998). This uneven distribution of both Na^+ and K^+ channels plays a major role in determination of excitability in dorsal horn neurons (reviewed by Safronov, 1999).

1.1.2. Neuronal connectivity and synaptic plasticity

Sensory processing is also determined by the pattern of synaptic connectivity between SDH neurons. Activity of a neuron and the strength of its synapses are related. Activity-dependent modification of synaptic strength, or synaptic plasticity, (Malenka & Nicoll, 1999; Malenka & Bear, 2004; Turrigiano & Nelson, 2004; Lisman & Spruston, 2005) plays a key role in nociceptive processing and chronic pain development (Woolf & Salter, 2000; Ji *et al*., 2003; Salter, 2005).

Long term potentiation, LTP, causes excitatory synapses to be strengthened for prolonged periods and regulates their postsynaptic glutamate receptors. LTP can elicit postsynaptic responses mediated through AMPA/Kainate (Yoshimura & Jessel, 1990; Kocsis *et al*., 2003) or NMDA receptors (Kauer *et al*., 1988; Liao *et al*., 1995). Ca^{2+} entry through the NMDA receptors and Ca^{2+}-permeable type of AMPA receptors (Wollmuth & Sakmann, 1998) leads to an increase in intracellular Ca^{2+} and subsequent activation of intracellular kinases, which feed back on cellular excitability. For instance, activation of protein kinase C leads to a phosphorylation of the NMDA receptor and its enhanced activation (MacDonald *et al*., 2001). The Ca^{2+}-calmodulin dependent protein kinase II is expressed in the SDH (Fang *et al*., 2002; Larsson & Broman, 2005) and is also involved in plasticity induction upon Ca^{2+} entry in glutamatergic synapses (Pedersen *et al*., 2005; Derkach *et al*., 2007). These kinases may act postsynaptically to insert new AMPA receptors.

Long term depression, LTD, can counterbalance LTP (Stanton, 1996). LTD appears to result from activation of Ca^{2+}-dependent phosphatases which cause internalization of postsynaptic AMPA receptors in hippocampus (Mulkey *et al*., 1993). However, in the cerebellum, LTD requires the activity of a protein kinase, rather than a phosphatase, and involves internalization of postsynaptic AMPA receptors but also involves metabotropic glutamate receptors (reviewed by Ito, 2002; Sakurai, 1987).

2. Mechanisms of opioidergic analgesia

2.1. Opioid receptors

Opioids inhibit the spinal pain processing by two mechanisms, a direct pre- and postsynaptic inhibition in the SDH and a centrally-mediated activation of the descending pain inhibitory system (reviewed by Millan, 2002).

Spinal SG is characterized by high densities of enkephalin-containing neurons, axon terminals and opiate binding sites (Merchenthaler *et al*., 1986; Ribeiro-da-Silva *et al*., 1991; Arvidson *et al*., 1995a,b,c), and therefore, contributes to the analgesic actions of the opioidergic system (Proudfit, 1980; Jensen & Yaksh, 1986). Usually, three types of opioid receptors are considered: μ-opiod receptor (MOR), κ-opiod receptor (KOR), and δ-opiod receptor (DOR) (reviewed by Martin, 1983 and Massote & Kieffer, 1998). In addition, a fourth opioid receptor type, named ORL-1 ('opioid receptor-like 1') is also considered by some authors (reviewed by Calo *et al*., 2000 and Stucky *et al*., 2001; Meunier *et al*., 1995). Although opioid receptors are located both pre- and postsynaptically (reviewed by Simon, 1991), DORs are predominantly presynaptic (Arvidson *et al*., 1995a), while KORs

(Arvidson *et al*., 1995b) and mostly MORs (Arvidson *et al*., 1995c) are predominantly postsynaptic. The postsynaptic MORs are specifically targeted to excitatory SG interneurons (Kemp *et al*., 1996), but no any correlation between neuronal sensitivity to MOR agonists and cellular morphology or neuronal intrinsic firing properties has ever been established. Indeed, all SG morphologic groups (Todd, 1988; Eckert *et al*., 2003) are sensitive to MOR agonists (Light & Willcockson, 1999; Eckert *et al*., 2003) and little is known about the types of neurons serving as specific postsynaptic targets for opioid action within the SG.

2.2. Cellular efects of opioid receptor activation

Most opioid receptors belong to the group of G protein coupled receptors (reviewed by Childers, 1991 and Satoh & Minami, 1995; Mann, 2003). The opioids act through the following three mechanisms:

1) activation of K^+ channels (G-protein dependent inward rectifying K^+ channel, GIRK) (reviewed by Ikeda *et al*., 2002; Yoshimura & North, 1983);

2) inactivation of voltage dependent Ca^{2+} channels (Ikeda, 1996) and

3) inhibition of adenylate cyclase (reviewed by Childers, 1991, Hawes *et al*., 2000 and Moran *et al*., 2000; Chieng & Williams, 1998).

As a result, opioids inhibit neurotransmission both pre- and postsynaptically (Schneider *et al*., 1998; Eckert *et al*., 2003). Presynaptic inhibition depends mostly on the direct inhibitory effect on transmitter exocytosis from membrane associated storage vesicles, but also on the inactivation of voltage dependent Ca^{2+} channels (Ikeda, 1996). Postsynaptic inhibition depends on GIRK channels activation which induces membrane hyperpolarization associated with an increase in K^+ conductance (reviewed by North, 1989 and Ikeda *et al*., 2002).

Additional opioids actions are activation of protein kinase C (Chen & Huang, 1991; Shukla *et al*., 2006), release of Ca^{2+} from intracellular stores (Quillan *et al*., 2002), activation of MAP-kinases (Li & Chang, 1996; Schulz *et al*., 2004) and receptor traficking (Tölle *et al*., 1996).

3. Work objectives and technical considerations

The experimental research work making up this doctoral thesis was designed in order to provide new knowledge for understanding cellular and molecular events underlying SG sensory integration. We characterized SG neurons with different firing patterns as excitatory or inhibitory and subsequently performed a study on functional, pharmacological and structural organization of synapses formed by the excitatory interneurons. We were also interested in studying the neuron types serving as specific postsynaptic targets to the action of a MOR agonist, as well as the contribution of ionic conductances to the cell-specific of SG neurons firing patterns.

The experiments were performed in the rat, an animal extensively used in electrophysiological studies.

The present dissertation includes five publications arranged according to the results sequence logic and the questions raised by them.

In the *first publication* we were interested in:

1) the classification of the different intrinsic firing patterns of SG neurons. Since the first classification of the neurons was done with the classical sharp electrode introducing a low input resistance of 50-70 MΩ (Thomson *et al*., 1989; Yoshimura & Jessell, 1989; Lopez-Garcia & King, 1994), it was necessary to first check whether the same firing patterns would be present in recordings with a patch-clamp electrode, where the input resistance of the neuron is about ten times higher (0.5-2.0 GΩ). On the other hand, the lack of uniform criteria used in the classification of the different types of neuronal firing patterns reported in several patch-clamp studies (Grudt & Perl, 2002; Ruscheweyh & Sandkühler, 2002; Graham *et al*., 2004) led us to create specific classification criteria, in order to reduce the number of putative factors responsible for the determination of the firing patterns and allow a standard functionally relevant classification;

2) the spinal mechanisms of opioidergic analgesia, by comparing the action of a MOR agonist on SG neurons with different intrinsic firing properties. Until now, the responsiveness of the neuron to opioids had never been correlated with its firing type, and the opioid-induced modifications of neuronal firing patterns were not reported.

In the *second publication* we intended to characterize SG neurons with different firing patterns as excitatory or inhibitory interneurons, by performing paired whole-cell patch-clamp recordings. However, since simultaneous patch-clamp recording from a couple of monosynaptically connected neurons could be hardly applied to the SG, due to a very low probability of finding connected cells (Lu & Perl, 2003; 2005), we first had to develop a new technique allowing efficient identification of monosynaptically coupled neurons. In this newly created technique, a tight-seal whole-cell contact was established with a postsynaptic neuron located in laminae I-III (regions where axons of SG interneurons terminate), and a second pipette was used for highly specific cell-attached (loose-seal) stimulation of SG neurons, until a connected presynaptic neuron was found.

Although this new technique of identification of monosynaptically coupled neurons allowed us to do the first step in characterization of interneuron synapses, a number of principal questions about the synaptic function still remained to be answered, namely:

1) how effective is synaptic transmission between two spinal neurons?

2) which temporal pattern of firing in a presynaptic neuron is needed to evoke an action potential generation in a postsynaptic neuron?

3) how intrinsic firing pattern of a presynaptic neuron is converted by synapse into postsynaptic potentials?

4) do the synapses between two intrinsic spinal neurons exhibit any form of synaptic plasticity?

5) which subunit composition of postsynaptic receptors is critical for synaptic function and plasticity?

6) how do the kinetics of excitatory postsynaptic currents (EPSCs) change with the synapse location, along the dendritic tree of the postsynaptic neuron?

5) does an SG excitatory interneuron form multiple synapses on a postsynaptic neuron?

6) what is the release probability in an individual synapse?

7) how do the experimental conditions, lowering input resistance (R_{IN}) in the postsynaptic neuron, affect both the resolution and the efficacy of distal synaptic inputs?

To answer those questions, in the *third publication*, we combined paired recording, computer simulation and biocytin-labelling to study functional organization and activity-dependent modification of glutamatergic synapses of SG interneurons.

For the recordings involving induction of plasticity, special precautions were taken in order to preserve cytoplasmic composition in connected cells. The efficacy of synaptic transmission depends

on passive membrane properties of a postsynaptic neuron (R_{IN} and membrane time constant) which vary with the composition of intracellular recording solution: R_{IN} values in SG neurons are lower when measured in whole-cell with Ca^{2+} chelator-free solutions (Hantman *et al*., 2004) than the R_{IN} values measured in the whole-cell mode with pipette solutions containing strong Ca^{2+} chelators or in the perforated-patch mode, preventing the dialysis of cytoplasmic factors and Ca^{2+} (Horn & Marty, 1988; Rae *et al*., 1991). However, since the presence of a strong Ca^{2+} chelator in the presynaptic neuron may affect synaptic release (Ohana & Sakmann, 1998), we did recording from the postsynaptic neuron in the perforated-patch mode, while the intact presynaptic SG excitatory interneuron was stimulated through a cell-attached pipette, also used for the labelling with biocytin (Szucs *et al*., 2009).

In the *fourth* and *fifth publications* we combined electrophysiological, anatomical and computational methods, in order to determine the basic conductances (Na^+, K_{DR} and K_A) and structural elements responsible for appearance of, respectively, cell-specific tonic- and adapting-firing patterns in SG neurons.

All conclusions about the roles of ion channels in determining the firing patterns of the neurons were tested. Computer simulations were done using NEURON software and a SG neuron model specially created. The passive membrane properties and the ion channel expression were modelled on the basis of our recordings, in order to reconstruct the basic firing patterns observed in the experiments. The analysis of the current magnitudes provided an evidence for the involvement of a certain current type in determination of firing pattern.

References

Arvidson U, Dado RJ, Riedl M, Lee J-H, Law PY, Loh HH, Elde R & Wessendorf MW (1995a). Delta-opioid receptor immunoreactivity: distribution in brainstem and spinal cord, and relationship to biogenic amines and enkephalin. *J Neurosci* **15**: 1215-1235.

Arvidson U, Riedl M, Chakrabarti S, Vulchanova L, Lee J-H, Nakano AH, Lin X, Loh HH, Law P-Y, Wessendorf MW & Elde R (1995b). The κ–opioid receptor is primarily postsynaptic: combined immunohistochemical localization of the receptor and endogenous opioids. *Proc Natl Acad Sci* **92**: 5062-5066.

Arvidson U, Riedl M, Chakrabarti S, Lee J-H, Nakano AH, Dado RJ, Loh HH, Law P-Y, Wessendorf MW & Elde R (1995c). Distribution and targeting of a μ-opioid receptor (MOR1) in brain and spinal cord. *J Neurosci* **15**: 3328-3341.

Basbaum A & Jessel TM (2000). The perception of pain. In *Principles of neural science* (Kandel ER, Schwartz JH & Jessell TM), 4th edn, pp 472-491. McGraw Hill.

Beal JA & Cooper MH (1978). The neurons in the gelatinosal complex (laminae II and III) of the monkey (Macaca mulatta): A Golgi Study. *J Comp Neurol* **179**: 89-122.

Bielefeldt K & Gebhart GF (2006). Visceral pain: basic mechanisms. In: *Wall and Melzack's Textbook of Pain* (McMahon SB & Koltzenburg M, ed), 5th edn, pp 721-736. Elsevier Churchill Livingstone.

Brown AG (1981). Organization in the Spinal Cord. Berlin, Heidelberg, New York: Springer-Verlag.

Calo G, Bigoni R, Rizzi A, Guerrini R, Salvadori S & Regoli D (2000). Nociceptin/orpanin FQ receptor ligands. *Peptides* **21**: 935-947.

Cervero F (1987). Dorsal horn neurones and their sensory inputs. In *Spinal Afferent Processing* (Yaksh TL, ed) pp 197-216. Plenum press, New York.

Chen L & Huang LY (1991). Sustained potentiation of NMDA receptor-mediated glutamate responses through activation of protein kinase C by a mu-opioid. *Neuron* **7**: 319-326.

Chieng B & Williams JT (1998). Increased opioid inhibition of GABA release in nucleus accumbens during morphine withdrawal. *J Neurosci* **18**: 7033-7039.

Childers SR (1991). Opioid receptor-coupled second messenger systems. *Life Sci* **48**: 1991-2003.

Derkach VA, Oh MC, Guire ES & Soderling TR (2007). Regulatory mechanisms of AMPA receptors in synaptic plasticity. *Nat Rev Neurosci* **8**: 101-113.

Eckert III WA, McNaughton KK & Light AR (2003). Morphology and axonal arborization of rat spinal inner lamina II neurons hyperpolarized by μ-opioid-selective agonists. *J Comp Neurol* **458**: 240–256.

Edwards FA, Konnerth A, Sakmann B, & Takahashi T (1989). A thin slice preparation for patch clamp recordings from neurones of the mammalian central nervous system. *Pfluegers Arch* **414**: 600-612.

Fang L, Wu J, Lin Q & Willis WD (2002). Calcium-calmodulin-dependent protein kinase II contributes to spinal cord central sensitization. *J Neurosci* **22**: 4196-4204.

Gardner EP, Martin JM & Jessell TM (2000). The Bodily Senses. In: *Principles of Neural Science* (Kandel ER, Schwartz JH & Jessell TM, ed), 4th edn, pp 430-449. McGraw-Hill.

Gobel S, Falls WM, Bennett GJ, Abdelmoumene M, Hayashi H & Humphrey E (1980). An EM analysis of the synaptic connections of horseradish peroxidase-filled stalked cells and islet cells in the Substantia Gelatinosa of adult cat spinal cord. *J Comp Neurol* **194**: 781-807.

Graham BA, Brichta AM & Callister RJ (2004). In vivo responses of mouse superficial dorsal horn neurones to both current injection and peripheral cutaneous stimulation. *J Physiol* **561**: 749-763.

Grudt TJ & Perl ER (2002). Correlations between neuronal morphology and electro-physiological features in the rodent superficial dorsal horn. *J Physiol* **540**: 189-207.

Hamill OP, Marty A, Neher E, Sakmann B & Sigworth FJ (1981). Improved patch-clamp techniques for high-resolution current recording from cells and cell-free membrane patches. *Pfluegers Arch* **391**: 85-100.

Hantman AW, van den Pol AN & Perl ER (2004). Morphological and physiological features of a set of spinal substantia gelatinosa neurons defined by green fluorescent protein expression. *J Neurosci* **24**: 836-842.

Hawes BE, Graziano MP & Lambert DG (2000). Cellular actions of nociceptin: transduction mechanisms. *Peptides* **21**: 961–967.

Hill RG (2001). Molecular basis for the perception of pain. *Neuroscientist* **7**: 282-292.

Horn R & Marty A (1988). Muscarinic activation of ionic currents measured by a new whole-cell recording method. *J Gen Physiol* **2**: 145-159.

Hunt SP & Mantyh PW (2001). The molecular dynamics of pain control. *Nat Rev Neurosci* **2**: 83-91.

Ikeda SR (1996). Voltage-dependent modulation of N-type calcium channels by G-protein beta gamma subunits. *Nature* **380**: 255-258.

Ikeda K, Kobayashi T, Kumanishi T, Yano R, Sora I & Niki H (2002). Molecular mechanisms of analgesia induced by opioids and ethanol: is the GIRK channel one of the keys? *Neurosci Res* **44**: 121-131.

Ito M (2002). The molecular organization of cerebellar long-term depression. *Nat Rev Neurosci* **3**: 896-902.

Jensen TS & Yaksh TL (1986). Comparison of the antinociceptive action of mu and delta opioid receptor ligands in the periaqueductal gray matter, medial and paramedial ventral medulla in the rat as studied by the microinjection technique. *Brain Res* **372**: 301-312.

Ji RR, Kohno T, Moore KA & Woolf CJ (2003). Central sensitization and LTP: do pain and memory share similar mechanisms? *Trends Neurosci* **26**: 696–705.

Julius D & Basbaum AI (2001). Molecular mechanisms of nociception. *Nature* **413**: 203-210.

Kato G, Kawasaki Y, Ji R-R & Strassman AM (2007). Differential wiring of local excitatory and inhibitory synaptic inputs to islet cells in rat spinal lamina II demonstrated by laser scanning photostimulation. *J Physiol* **580**: 815-833.

Kauer JA, Malenka RC & Nicoll RA (1988). NMDA application potentiates synaptic transmission in the hippocampus. *Nature* **334**: 250-252.

Kemp T, Spike RC, Watt C & Todd AJ (1996). The mu-opioid receptor (MOR1) is mainly restricted to neurons that do not contain GABA or glycine in the superficial dorsal of the rat spinal cord. *Neurosci* **75**: 1231-1238.

Kocsis P, Tarnawa I, Szombathelyi Z & Farkas S (2003). Participation of AMPA- and NMDA-type excitatory amino acid receptors in the spinal reflex transmission, in rat. *Brain Res Bull* **60**: 81-91.

Larsson M & Broman J (2005). Different basal levels of CaMKII phosphorylated at Thr286/287 at nociceptive and low-threshold primary afferent synapses. *Eur J Neurosci* **21**: 2445-2458.

Li LY & Chang KJ (1996). The stimulatory effect of opioids on MAP-Kinase in Chinese hamster ovary cells transfected to express mu-opioid receptors. *Mol Pharmacol* **50**: 599-602.

Liao D, Hessler NA & Malinow R (1995). Activation of postsynaptically silent synapses during pairing-induced LTP in CA1 region of hippocampal slice. *Nature* **375**: 400-404.

Light AR & Perl ER (1979). Spinal termination of functionally identified primary afferent neurons with slowly conducting myelinated fibers. *J Comp Neurol* **186**: 133–150.

Light AR & Willcockson HH (1999). Spinal laminae I-II neurons in rat recorded *in vivo* in whole cell, tight seal configuration: properties and opioid responses. *J Neurophysiol* **82**: 3316-3326.

Lisman J & Spruston N (2005). Postsynaptic depolarization requirements for LTP and LTD: a critique of spike timing-dependent plasticity. *Nat Neurosci* **8**: 839-841.

Lopez-Garcia JA & King AE (1994). Membrane properties of physiologically classified rat dorsal horn neurons in vitro: correlation with cutaneous sensory afferent input. *Eur J Neurosci* **6**: 998-1007.

Lu Y & Perl ER (2003). A specific inhibitory pathway between substantia gelatinosa neurons receiving direct C-fiber input. *J Neurosci* **23**: 8752-8758.

Lu Y & Perl ER (2005). Modular organization of excitatory circuits between neurons of the spinal superficial dorsal horn (laminae I and II). *J Neurosci* **25**: 3900-3907.

MacDonald JF, Kotecha SA, Lu WY & Jackson MF (2001). Convergence of PKC-dependent kinase signal cascades on NMDA receptors. *Curr Drug Targets* **2**: 299-312.

Malenka RC & Bear MF (2004). LTP and LTD: an embarrassment of riches. *Neuron* **44**: 5–21.

Malenka RC & Nicoll RA (1999). Long-term potentiation—a decade of progress? *Science* **285**: 1870-1874.

Mann E (2003). Chronic pain and opioids: dispelling myths and exploring facts. *Prof Nurse* **187**: 408-411.

Martin WR (1983). Pharmacology of opioids. *Pharmacol Rev* **35**: 283-323.

Massote D & Kieffer BL. (1998). A molecular basis for opiate action. *Essays Biochem* **33**: 65-77.

Melzack R & Wall PD (1965). Pain mechanisms: a new theory. *Science* **150**: 971-979.

Merchenthaler I, Maderdrut JL, Altschuler RA & Petrusz P (1986). Immunocytochemical localization of proenkephalin-derived peptides in the central nervous system of the rat. *Neurosci* **17**:325–48.

Meunier JC, Mollereau C, Toll L, Suaudeau C, Moisand C, Alvinerie P, Butour JL, Guillemot JC, Ferrara P & Monsarrat B (1995). Isolation and structure of the endogenous agonist of opioid receptor-like ORL1 receptor. *Nature* **377**: 532-535.

Millan MJ (2002). Descending control of pain. *Progress in Neurobiology* **66**: 355-474.

Moran TD, Abdulla FA & Smith PA (2000). Cellular neurophysiological actions of nociceptin/orphanin FQ. *Peptides* **21**: 969–976.

Mulkey RM, Herron CE & Malenka RC (1993). An essential role for protein phosphatases in hippocampal long-term depression. *Science* **261**: 1051-1055.

North RA (1989). Drug receptors and the inhibition of nerve cells. *Br J Pharmacol* **98**: 13-28.

Ohana O & Sakmann B (1998). Transmitter release modulation in nerve terminals of rat neocortical pyramidal cells by intracellular calcium buffers. *J Physiol* **513**: 135-148.

Pinto V, Derkach VA & Safronov BV (2008). Role of TTX-sensitive and TTX-resistant sodium channels in Adelta- and C-fiber conduction and synaptic transmission. *J Neurophysiol* **99**: 617-628.

Proudfit HK (1980). Effects of raphe magnus and raphe pallidus lesions on morphine-induced analgesia and spinal cord monoamines. *Pharmacol Biochem Behav* **13**: 705-714.

Quillan JM, Carlson KW, Song C, Wang D & Sadee W (2002). Differential effects of mu-opioid receptor ligands on Ca^{2+} signaling. *J Pharmacol Exp Ther* **302**: 1002-1012.

Rae J, Cooper K & Gates P (1991). Low access resistance perforated patch recordings using amphotericin B. *J Neurosci Methods* **37**: 15-26.

Rethelyi M (1977). Preterminal and terminal axon arborizations in the substantia gelatinosa of cat's spinal cord. *J Comp Neurol* **172**: 511–521.

Ribeiro-da-Silva A, Pioro EP & Cuello AC (1991). Substance P- and enkephalin-like immunoreactivities are colocalized in certain neurons of the substantia gelatinosa of the rat spinal cord: An ultrastructural double-labeling study. *J Neurosci* **11**: 1068-1080.

Ruscheweyh R & Sandkühler J (2002). Lamina-specific membrane and discharge properties of rat spinal dorsal horn neurones in vitro. *J Physiol* **541**: 231-244.

Safronov BV (1999). Spatial distribution of Na^+ and K^+ channels in spinal dorsal horn neurones: role of the soma, axon and dendrites in spike generation. *Progress in Neurobiology* **59**: 217-241.

Safronov BV, Wolff M & Vogel W (1999). Axonal expression of sodium channels in rat spinal neurones during postnatal development. *J Physiol* **514**: 729-734.

Safronov BV, Wolff M & Vogel W (1997). Functional distribution of three types of Na^+ channel on soma and processes of dorsal horn neurones of rat spinal cord. *J Physiol* **503**: 371-385.

Sakurai M (1987). Synaptic modification of parallel fibre-Purkinje cell transmission in in vitro guinea-pig cerebellar slices. *J Physiol* **394**: 463-480.

Salter MW (2005). Cellular signalling pathways of spinal pain neuroplasticity as targets for analgesic development. *Curr Top Med Chem* **5**: 557–567.

Satoh M & Minami M (1995). Molecular pharmacology of the opioid receptors. *Pharmacol Ther* **68**: 343-364.

Schaible H (2006). Basic mechanisms of deep somatic pain. In: *Wall and Melzack's Textbook of Pain* (McMahon SB, Koltzenburg M, edn), 5th edn, pp 621-633. Elsevier Churchill Livingstone.

Schneider SP, Eckert III WA & Light AR (1998). Opioid- activated postsynaptic, inward rectifying potassium currents in whole cell recordings in substantia gelatinosa neurons. *J Neurophysiol* **80**: 2954 - 2962.

Shukla PK, Tang L & Wang ZJ (2006). Phosphorylation of neurogranin, protein kinase C, and Ca^{2+}/calmodulin dependent protein kinase II in opioid tolerance and dependence. *Neurosci Lett* **404**: 266-269.

Schulz R, Eisinger DA & Wehmeyer A (2004). Opioid control of MAP Kinase cascade. *Eur J Pharmacol* **500**: 487-497.

Simon EJ (1991). Opioid receptors and endogenous opioid peptides. *Medicinal Res Rev* **11**: 357-374.

Stanton PK (1996). LTD, LTP, and the sliding threshold for long-term synaptic plasticity. *Hippocampus* **6**: 35-42.

Stucky CL, Gold MS & Zhang X (2001). Mechanisms of pain. *Proc Natl Acad Sci USA* **9821**: 11845-11846.

Szucs P, Pinto V & Safronov BV (2009). Advanced technique of infrared LED imaging of unstained cells and intracellular structures in isolated spinal cord, brainstem, ganglia and cerebellum. *J Neurosci Methods* **177**: 369-380.

Thomson AM, West DC & Headley PM (1989). Membrane characteristics and synaptic responsiveness of superficial dorsal horn neurons in a slice preparation of adult rat spinal cord. *Eur J Neurosci* **1**: 479-488.

Todd AJ (1988). Electron microscope study of Golgi-stained cell in lamina II of the rat spinal dorsal horn. *J Comp Neurol* **275**:145–157.

Todd AJ & Koerber HR (2006). Neuroanatomical substrates of spinal nociception. In: *Wall and Melzack's Textbook of Pain* (McMahon SB, Koltzenburg M, ed), 5th edn, pp 73-90. Elsevier Churchill Livingstone.

Tölle TR, Berthele A, Shadrack J & Zieglgäsberger W (1996). Involvement of glutamatergic neurotransmission and protein kinase C in spinal plasticity and the development of chronic pain. *Progress in Brain Research* **110**: 193-206.

Turrigiano GG & Nelson SB (2004). Homeostatic plasticity in the developing nervous system. *Nat Rev Neurosci* **5**: 97–107.

Warren S, Yezierski RP & Capra NF (2000). The Somatosensory System II: Touch, Thermal Sense, and Pain. In: Fundamental Neuroscience for Basic and Clinical Applications (Haines DE, ed), 3th edn, pp 280–301. Churchill Livingstone.

Willis WD & Coggeshall RE (1991). Sensory Mechanisms of the Spinal Cord. Plenum Press, New York.

Wollmuth LP & Sakmann B (1998). Different mechanisms of Ca^{2+} transport in NMDA and Ca^{2+}-permeable AMPA glutamate receptor channels. *J Gen Physiol* **112**: 623-636.

Wolff M, Vogel W & Safronov BV (1998). Uneven distribution of K+ channels in soma, axon and dendrites of rat spinal neurones: functional role of the soma in generation of action potentials. *J Physiol* **509**: 767-776.

Woolf CJ & Salter MW (2000). Neuronal plasticity: increasing the gain in pain. *Science* **288**: 1765-1769.

Yoshimura M & Jessell TM (1989). Membrane properties of rat substantia gelatinosa neurons in vitro. *J Neurophysiol* **62**: 109-118.

Yoshimura M & Jessell TM (1990). Amino acid-mediated EPSPs at primary afferent synapses with substantia gelatinosa neurons in the rat spinal cord. *J Physiol* **430**: 315-335.

Yoshimura M & North RA (1983). Substantia gelatinosa neurones hyperpolarized in vitro by enkephalin. *Nature* **305**: 529-530.

Zimmermann K, Leffler A, Babes A, Cendan CM, Carr RW, Kobayashi J, Nau C, Wood JN & Reeh PW (2007). Sensory neuron sodium channel $Na_V1.8$ is essential for pain at low temperatures. *Nature* **447**: 855-858.

II. PUBLICATIONS

First publication

PAIN AND REGIONAL ANESTHESIA

Anesthesiology 2004; 101:1177–83

Selective Postsynaptic Inhibition of Tonic-firing Neurons in Substantia Gelatinosa by μ-Opioid Agonist

Sónia F. A. Santos, Igor V. Melnick, Ph.D.,† Boris V. Safronov, P.D., Ph.D.‡*

Background: **Spinal substantia gelatinosa (SG) is a site of action of administered and endogenous opioid agonists and is an important element in the system of antinociception. However, little is known about the types of neurons serving as specific postsynaptic targets for opioid action within the SG. To study the spinal mechanisms of opioidergic analgesia, the authors compared the action of μ-opioid agonist [D-Ala^2, N-Me-Phe^4, Gly^5-ol]-enkephalin (DAMGO) on SG neurons with different intrinsic firing properties.**

Methods: **Whole cell patch clamp recordings from spinal cord slices of Wistar rats were used to study the sensitivity of SG neurons to DAMGO.**

Results: **Three groups of neurons with distinct distributions in SG were classified: tonic-, adapting-, and delayed-firing neurons. DAMGO at 1 μM concentration selectively hyperpolarized all tonic-firing neurons tested, whereas none of the adapting- or delayed-firing neurons were affected. The effect of DAMGO on tonic-firing neurons was due to activation of G protein–coupled inward-rectifier K^+ conductance, which could be blocked by 500 μM Ba^{2+} and 500 μM Cs^+ but increased by 50 μM baclofen. As a functional consequence of DAMGO action, a majority of tonic-firing neurons changed their pattern of intrinsic firing from tonic to adapting.**

Conclusions: **It is suggested that tonic-firing neurons, presumably functioning as excitatory interneurons, are primary postsynaptic targets for administered and endogenous opioid agonists in spinal SG. Functional transition of cells in this group from tonic to adapting firing mode may represent an important mechanism facilitating opioidergic analgesia.**

SUBSTANTIA gelatinosa (SG) of the spinal cord is a site of termination of most fine-caliber primary afferent fibers and is therefore involved in pain conduction.[1–4] However, SG also represents one of the key elements in the system of pain control. High densities of enkephalin-containing neurons and axon terminals as well as opiate binding sites found in SG indicate its role in endogenous enkephalinergic antinociception.[5–8] Besides, SG is a site for the analgesic action of administered exogenous opioids.[9–11] It was shown that enkephalins inhibit SG neurons *via* a combination of presynaptic and postsynaptic mechanisms. The presynaptic effects are mediated *via* both μ- and δ-opioid receptors located in axons, whereas the postsynaptic inhibition is mostly attributed to activation of μ-opioid receptors in somatodendritic domains.[6,7,12,13] The postsynaptic μ-opioid receptors are specifically targeted to excitatory SG interneurons,[14] the inhibition of which may be important for the spinal mechanisms of antinociception.

The postsynaptic action of opioid agonists on SG neurons results in a robust membrane hyperpolarization associated with an increase in K^+ conductance.[13,15–17] This conductance mediated through G protein–coupled inward-rectifier K^+ (GIRK) channels could be blocked by low concentrations of external Ba^{2+} and Cs^+ but enhanced by the γ-aminobutyric acid type B ($GABA_B$) receptor agonist baclofen.[18,19]

There are several morphologic groups of SG neurons.[20–23] It was shown that the neurons of all these groups can be sensitive to the μ-opioid agonist [D-Ala^2, N-Me-Phe^4, Gly^5-ol]-enkephalin (DAMGO),[17,22] implying the lack of strict correlation between cell morphology and sensitivity to the drug. In addition to morphology, SG neurons are also distinguished on the basis of their membrane properties and intrinsic firing.[24–27] The actions of opioids on neurons with different patterns of intrinsic firing, however, have not been compared so far. Here, we report a striking correlation between the firing pattern of rat SG neurons and their sensitivity to DAMGO. The DAMGO-induced hyperpolarization was only observed in neurons with tonic-firing pattern, which possessed a functional combination of both μ-opioid receptors and GIRK channels. In addition, it has been found that the inhibition was facilitated by a transition of most neurons from tonic to adapting firing mode. It is suggested that the tonic-firing SG neurons can function as excitatory interneurons and that their selective inhibition by opioid agonists is involved in analgesic postsynaptic effects of endogenous enkephalins and administered opioids.

Materials and Methods

Tight-seal recordings were done using 200- or 300-μm coronal slices prepared from the lumbar enlargement of the spinal cord of 2- to 7-week-old Wistar rats.[28] The animals were killed in accordance with the national guidelines (Direcção Geral de Veterinária, Ministério da Agricultura, Lisboa, Portugal). After anesthesia by intraperitoneal injection of Na^+ pentobarbital (30 mg/kg), the vertebral column was quickly cut out and immersed

* Ph.D. Student, ‡ Associate Research Professor, Departamento de Neurobiologia Básica e Clínica, Instituto de Biologia Molecular e Celular, and Instituto de Histologia e Embriologia, Faculdade de Medicina, Universidade do Porto, Porto, Portugal. † Postdoctoral Fellow, Departamento de Neurobiologia Básica e Clínica, Instituto de Biologia Molecular e Celular.

Received from the Departamento de Neurobiologia Básica e Clínica, Instituto de Biologia Molecular e Celular, Porto, Portugal. Submitted for publication March 23, 2004. Accepted for publication June 21, 2004. Supported by a grant from the Fundação para a Ciência e a Tecnologia (Portuguese Foundation for Science and Technology), Lisboa, Portugal.

Address reprint requests to Dr. Safronov: Instituto de Biologia Molecular e Celular, Rua do Campo Alegre 823, 4150-180 Porto, Portugal. Address electronic mail to: safronov@ibmc.up.pt.

Table 1. Parameters of Neurons and Their Responses to 1 μM DAMGO and 50 μM Baclofen

	V_R, mV	R_{IN}, GΩ	Responses to DAMGO	ΔV_{DAMGO}, mV	$R_{IN\text{-}DAMGO}/R_{IN}$	Responses to Baclofen
TFN	−71.3 ± 5.5 n = 53	1.67 ± 0.2 n = 53	53 of 53	−10.1 ± 3.0 n = 53	0.23 ± 0.07 n = 53	21 of 21
AFN	−71.5 ± 6.6 n = 46	1.48 ± 0.4 n = 46	0 of 30	−0.1 ± 0.6 n = 30	1.01 ± 0.12 n = 30	12 of 12
DFN	−76.8 ± 3.4 n = 47	0.77 ± 0.3 n = 47	0 of 31	0.0 ± 0.2 n = 31	1.02 ± 0.08 n = 31	12 of 12

Values are presented as mean ± SD. Responsiveness to baclofen was tested in voltage clamp mode, whereas all other measurements were performed in current clamp mode.

AFN = adapting-firing neuron; ΔV_{DAMGO} = membrane polarization in 1 μM [D-Ala^2, N-Me-Phe^4, Gly^5-ol]-enkephalin measured from −70 mV, at which each neuron was held in current clamp mode before the drug was applied; DFN = delayed-firing neuron; R_{IN} = input resistance; $R_{IN\ DAMGO}$ = input resistance in 1 μM [D-Ala^2, N-Me-Phe^4, Gly^5-ol]-enkephalin; TFN = tonic-firing neuron; V_R = membrane resting potential.

in ice-cold oxygenated artificial cerebrospinal fluid. The segment of the lumbar enlargement was dissected and glued to the stage of the tissue slicer. Slices were prepared and incubated for 40–60 min in oxygenated artificial cerebrospinal fluid at 33°C. For recording, the slices were transferred into a 0.7-ml chamber and continuously perfused at a rate of 8 ml/min. All recordings were done at 22°–24°C. SG (lamina II) was identified as a translucent band in the dorsal horn. Each neuron was localized during recording according to the position of the pipette tip on the video image of SG.

Artificial cerebrospinal fluid contained 115 mM NaCl, 5.6 mM KCl, 2 mM $CaCl_2$, 1 mM $MgCl_2$, 11 mM glucose, 1 mM NaH_2PO_4, and 25 mM $NaHCO_3$ (pH 7.4 when bubbled with a 95%–5% mixture of oxygen–carbon dioxide). Standard pipette solution contained 6 mM NaCl, 128 mM KCl, 2 mM $MgCl_2$, 10 mM EGTA, and 10 mM HEPES. The pH value was adjusted to 7.3 with KOH (final $[K^+]$ was 160.5 mM). In 36 experiments, guanosine 5'-triphosphate (100 μM) and adenosine 5'-triphosphate (2 mM) were added to the pipette solution. All chemicals were purchased from Sigma-Aldrich (Sintra, Portugal). DAMGO, baclofen, and naloxone (antagonist of μ-opioid receptors) were dissolved in distilled water and stored in aliquots of 4, 1.5, and 0.125 mM, respectively, at −20°C. Fresh dilutions were made with artificial cerebrospinal fluid just before the experiment. Adenosine 5'-triphosphate and guanosine 5'-triphosphate were dissolved in internal solution at final concentrations and kept in aliquots at −20°C until the experiment.

The patch pipettes had a resistance of 3–5 MΩ after fire polishing. An EPC-9 amplifier (HEKA, Lambrecht, Germany) was used in all experiments. The effective corner frequency of the low-pass filter was 3 kHz, and traces were digitized at 10 kHz. For measurements of transient K^+ (K_A) currents, a standard P/n protocol was used for transients and leakage subtraction. Offset and liquid junction potentials were corrected for in all experiments. In neurons subjected to detailed analysis, the series resistance was 6–20 MΩ and was compensated by 60%. Fast current clamp mode of the EPC-9 amplifier was used for voltage recording. Input resistance (R_{IN}) of SG neurons was measured in current clamp mode using negative 500-ms current pulses of 5–10 pA.

Special precautions were taken to correctly measure the resting potential in SG neurons. In current clamp mode, most commercially available patch clamp amplifiers inject into the cell a small uncompensated current of 5–20 pA, which can vary from day to day and cannot be compensated by users in a simple way (our personal observations with several EPC7, EPC9, and Axopatch 200B [Axon Instruments, Union City, CA] amplifiers). Such a current can depolarize by tens of millivolts the cells with R_{IN} in GΩ range. Therefore, before each experiment, we measured in current clamp mode a voltage decrease on a 0.5-GΩ resistor and determined the current needed to bring it to an expected 0 mV. In all following current clamp recordings, this sustained current was applied to the neuron and was considered zero current level. Under these conditions, the resting potential measured in current clamp mode was equal to the potential at which zero absolute current was recorded in voltage clamp mode. This correction may explain, at least in part, more negative resting potential values obtained here than in other patch clamp studies of dorsal horn neurons.[27,29]

All numbers in the text and figures are given as mean ± SEM; numbers in table 1 are given as mean ± SD. The parameters were compared using a paired or independent Student *t* test. The current study is based on recordings from 149 SG neurons.

Results

Classification of SG Neurons

Based on several criteria, SG neurons (n = 146) were separated into three groups (fig. 1): tonic-firing neurons (TFNs), adapting-firing neurons (AFNs), and delayed-firing neurons (DFNs). Three additional neurons could not be clearly classified and therefore were not subjected to study.

Tonic-firing neurons (n = 53) were able to support firing during 500-ms depolarization induced by a sustained current injection (fig. 1, *A1*). They had a low firing

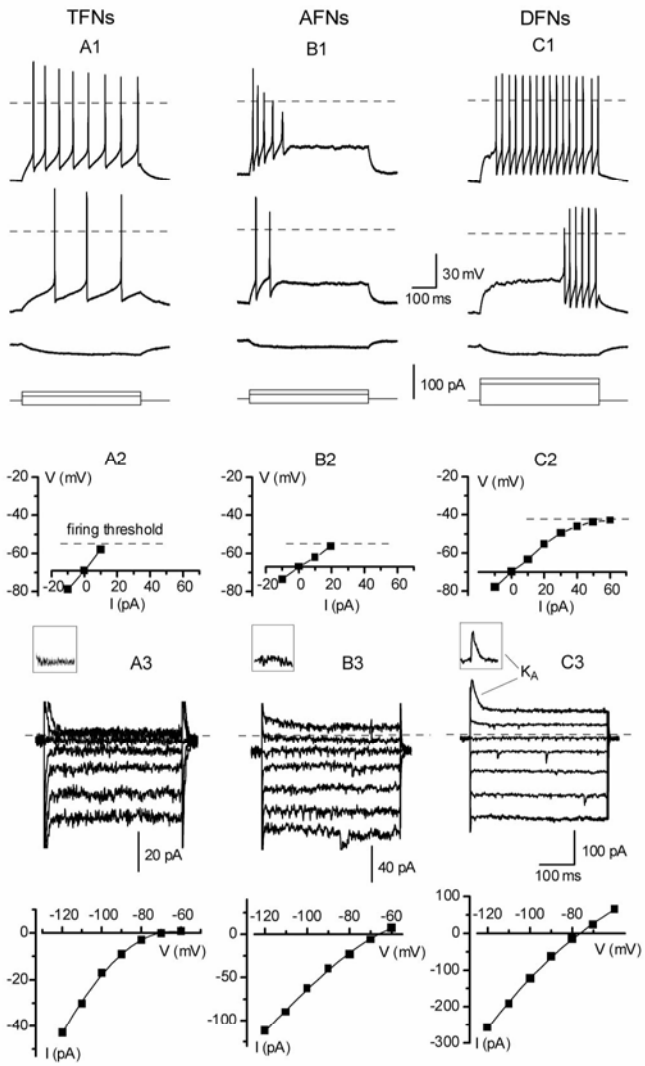

Fig. 1. Classification of three groups of substantia gelatinosa neurons: tonic-firing neurons (TFNs, *A*), adapting-firing neurons (AFN, *B*), and delayed-firing neurons (DFNs, *C*). (*A1*, *B1*, and *C1*) Each neuron was kept at −70 mV, and 500-ms hyperpolarizing or depolarizing current pulses were applied to test membrane responses and firing patterns. *Dashed lines* indicate 0 mV. (*A2*, *B2*, and *C2*) Subthreshold membrane polarization as a function of injected current. Neurons were kept at their resting potentials. (*A3*, *B3*, and *C3*) Voltage clamp recordings of membrane currents. All neurons were held at −80 mV, and 300-ms voltage pulses to potentials from −120 to −60 mV in 10-mV steps were applied. Transient K^+ (K_A) currents at −60 mV given in *insets* were obtained by subtracting the transients and leakage currents using a standard P/n protocol. Current and voltage clamp recordings are from different neurons.

threshold (−51.2 ± 1.7 mV, n = 11), and 10- to 20-pA current pulses were sufficient to evoke firing (fig. 1, *A2*). Under the voltage clamp condition, the current–voltage relations in all TFNs showed pronounced inward rectification (fig. 1, *A3*). A characteristic feature of AFNs (n = 46) was a burst-like firing of only two to six spikes at the beginning of depolarization (fig. 1, *B1*). At any stimulus intensity, AFN discharges could not continue during the whole pulse. The firing threshold of −50.7 ± 1.4 mV (n = 10) was not significantly different from that in TFNs ($P > 0.75$, independent Student *t* test). The membrane properties of AFNs (fig. 1, *B2* and *B3*) were fairly similar to those of TFNs. In both TFNs and AFNs, a K_A current was not seen at voltage steps from −80 to −60 mV (fig. 1, *A3* and *B3*, *insets*).

A principal difference of DFNs (n = 47) was a presence of large K_A current (137.9 ± 10.5 pA at voltage step from −80 to −60 mV, n = 10; $P < 0.001$, independent Student *t* test, for comparison with either TFN or AFN group; fig. 1, *C3*, *inset*), which substantially influenced the firing pattern (fig. 1, *C1* and *C2*). The spike threshold in DFNs (−36.4 ± 1.6 mV, n = 10) was considerably higher than in TFNs ($P < 0.001$, independent Student *t* test) or AFNs ($P < 0.001$, independent Student *t* test) and was reached at stimulation as strong as 50–70 pA because a large portion of injected current was compensated by activating K_A current. In DFNs, the first spikes typically occurred with a considerable time delay at the end of the pulse and moved to its beginning as the stimulation increased. R_{IN} in DFNs was approximately half of that in the other cell types ($P < 0.001$ for TFNs and $P < 0.001$ for AFNs, independent Student *t* tests), but a more negative resting potential (table 1; $P < 0.05$ for either TFN or AFN group, independent Student *t* tests) was closer to K^+ equilibrium potential of −84 mV, indicating a presence of larger resting K^+ conductance. An inward rectification was less pronounced in DFNs (fig. 1, *C3*). However, there were some minor variations in discharge patterns of DFNs at strong stimulation. Some cells discharged regularly during the whole pulse (fig. 1, *C1*), whereas others belonging to this group showed interrupted bursts of even single spikes (not shown).

In all three types of neurons, membrane response to hyperpolarizing voltages consisted of dominating fast inward-rectifier current. A slow hyperpolarization-activated I_H-like current carried by both K^+ and Na^+ ions[24,30,31] was negligible in majority of SG neurons studied here using both normal and adenosine 5'-triphosphate/guanosine 5'-triphosphate–containing (n = 36) pipette solutions.

Distribution of Neuron Types in SG

Each group of neurons had its specific distribution pattern within SG (figs. 2A and B). TFNs were relatively homogeneously distributed over the whole length of SG. Few AFNs were found in medial and intermediate region, but most of them were localized in a lateral SG, especially its ventral part. Although DFNs could be found in all SG regions, their density in the medial and lateral parts was higher. The sensitivity to DAMGO was tested for the neurons of each type located in different SG regions (indicated by crosses).

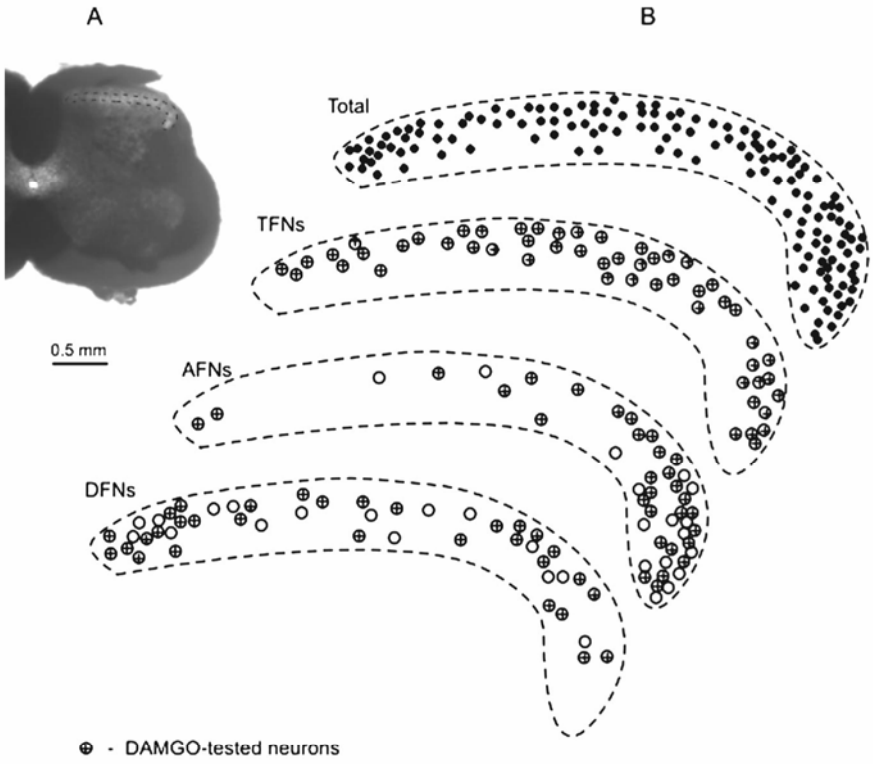

Fig. 2. Distribution of tonic-firing neurons (TFNs), adapting-firing neurons (AFNs), and delayed-firing neurons (DFNs). (*A*) Spinal cord slice from a 19-day-old rat with substantia gelatinosa appearing as a translucent band in the dorsal horn. (*B*) All neurons studied were plotted together as *circles* on a top schematic drawing of substantia gelatinosa. Each of three drawings below shows a distribution of one particular cell group. Neurons that were tested for their sensitivity to DAMGO are marked by *crosses*.

Sensitivity to DAMGO

Only one neuron per slice was tested for its sensitivity to DAMGO, and the slice was not exposed to the drug before beginning of the recording to avoid a desensitization of opioid responses.[16,32]

In each of 53 TFNs tested, a 30-s application of 1 μM DAMGO evoked a robust hyperpolarization ranging from 5 to 13 mV, which was accompanied by a considerable decrease in R_{IN} (fig. 3, *A1*, and table 1; $P < 0.001$, paired Student *t* test). Membrane currents were reversibly increased in such a way that the current–voltage curves in control and 1 μM DAMGO crossed each other at a po-

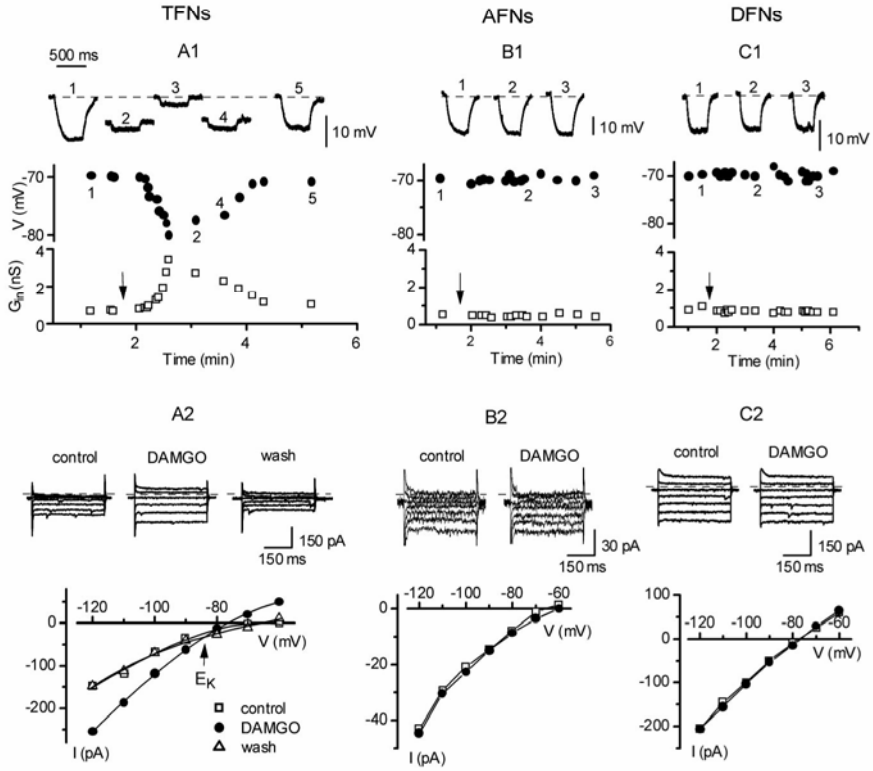

Fig. 3. Effect of DAMGO on tonic-firing neurons (TFNs, *A*), adapting-firing neurons (AFNs, *B*), and delayed-firing neurons (DFNs, *C*). (*A1*, *B1*, and *C1*) In current clamp mode, membrane potentials were uniformly adjusted to −70 mV (by a sustained current injection) before 1 μM DAMGO was applied for 30 s. The beginning of the application is indicated by an *arrow*. The effect of DAMGO was monitored by repetitive membrane hyperpolarization for 500 ms by 10-pA current. *Trace 3* in *A1* was recorded when additional current was injected into a DAMGO-hyperpolarized neuron to return membrane potential to −70 mV. Membrane conductance (G_{IN}) was calculated from changes in membrane potential during 10-pA hyperpolarizing current pulses. (*A2*, *B2*, and *C2*) Voltage clamp recordings of membrane currents (the same pulse protocol as in fig. 1, *A3*, *B3*, and *C3*) in the absence and presence of 1 μM DAMGO.

tential close to the K^+ equilibrium potential (fig. 3, *A2*), indicating an activation of K^+ selective current. Although the DAMGO-activated hyperpolarization lasted several minutes (up to 18 min) without remarkable inactivation, most TFNs responded to the drug only once, and only some cells responded to several applications. Presence of 2 mM adenosine 5'-triphosphate and 100 μM guanosine 5'-triphosphate in the pipette solution[16] in 9 of 53 tested TFNs did not improve their responsiveness to repetitive DAMGO applications. The hyperpolarization in TFNs was prevented if DAMGO was applied together with 100 nM naloxone (n = 7).

Neither AFNs (n = 30) nor DFNs (n = 31) responded to 1 μM DAMGO, and their R_{IN} did not change (figs. 3B and C and table 1; $P > 0.85$ for AFNs and $P > 0.8$ for DFNs, paired Student *t* tests). Increasing the duration of DAMGO application to 1–3 min in all AFNs and DFNs or inclusion of 2 mM adenosine 5'-triphosphate and 100 μM guanosine 5'-triphosphate to the pipette solution in 15 of 30 AFNs and 12 of 31 DFNs did not affect their sensitivity to DAMGO.

Therefore, only TFNs and not AFNs or DFNs were hyperpolarized by DAMGO, which activated K^+-selective conductance. The sensitivity of a neuron to DAMGO depended on its type rather than its location within the SG (fig. 2B).

Effects of Ba^{2+}, Cs^+, and Baclofen on Membrane Conductance

In experiments shown in figure 4, the effects of Ba^{2+}, Cs^+, and baclofen were studied. In seven TFNs, membrane currents were first activated by 1 μM DAMGO, and then 500 μM Ba^{2+} was added. In all these neurons, Ba^{2+} blocked the DAMGO-activated current (fig. 4, *A1*). Direct application of 500 μM Ba^{2+} (without DAMGO) blocked the resting membrane conductance in all cell types in a voltage-independent manner. At −120 mV, the inward current was blocked to 38.8 ± 4.3% in TFNs (n = 4, not shown; $P < 0.01$, paired Student *t* test), 32.4 ± 3.8% in AFNs (n = 8; fig. 4B1; $P < 0.001$, paired Student *t* test), and 30.9 ± 3.1% in DFNs (n = 11; fig. 4, *C1*; $P < 0.001$, paired Student *t* test). Application of 500 μM Cs^+ also blocked the resting K^+ conductance in all groups of neurons with stronger effects seen at more negative potentials (fig. 4, *A2*, *B2*, and *C2*). At −120 mV, an inward current was suppressed to 42.0 ± 3.9% in TFNs (n = 6; $P < 0.001$, paired Student *t* test), 43.9 ± 5.4% in AFNs (n = 8; $P < 0.001$, paired Student *t* test), and 30.4 ± 3.4% in DFNs (n = 5; $P < 0.001$, paired Student *t* test). All tested TFNs (n = 21), AFNs (n = 12), and DFNs (n = 12) responded to the $GABA_B$ receptor agonist baclofen (table 1), which, similar to DAMGO, was applied to one neuron per slice. In all three groups, 50 μM baclofen reversibly induced K^+ current (fig. 4, *A3*, *B3*, and *C3*). At −120 mV, the baclofen-induced current was −90.7 ± 7.1 pA in TFNs (n = 21), −73.4 ± 10.1 pA in AFNs (n = 12), and −72.9 ± 7.1 pA in DFNs (n = 12). In contrast to DAMGO, all neurons responded to several applications of baclofen. Therefore, all groups of SG neurons possessed GIRK conductance, which could be blocked by Ba^{2+} and Cs^+ but activated by baclofen *via* the $GABA_B$ receptor pathway.

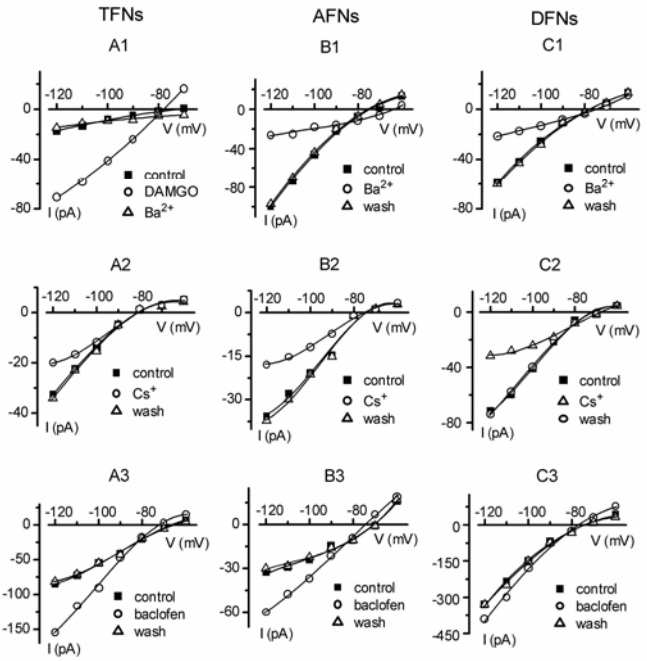

Fig. 4. Effects of external 500 μM Ba^{2+}, 500 μM Cs^+, and 50 μM baclofen on membrane currents in tonic-firing neurons (TFNs, *A*), adapting-firing neurons (AFNs, *B*), and delayed-firing neurons (DFNs, *C*). (*A1*) Current–voltage (I-V) curves obtained from one TFN in control solution and after addition of 1 μM DAMGO and Ba^{2+}. (*B1* and *C1*) I-V curves for AFNs and DFNs, respectively, in control, Ba^{2+}, and after wash. (*A2*, *B2*, and *C2*) Cs^+ exerted a voltage-dependent block in all three groups of substantia gelatinosa neurons. (*A3*, *B3*, and *C3*) Reversible increase in membrane currents by baclofen.

Modification of Discharge Pattern in TFNs by DAMGO

To study the functional consequences of postsynaptic effect of opioids, the firing patterns before and after 30-s application of 1 μM DAMGO were compared in all 53 TFNs. In 44 of them (83%), the DAMGO application reversibly induced a spike frequency adaptation in such a way that the neurons were not able to support tonic firing at any stimulation strength (fig. 5A). In addition, much stronger current injection was needed to reach the firing threshold of the first spike (fig. 5A). The discharge pattern modified by DAMGO was not improved when the membrane potential was returned to −70 mV by injecting persistent current through the recording pipette (fig. 5A, 5 min after DAMGO application). In the other 9 TFNs (17%), the tonic discharge pattern remained after DAMGO application. However, the firing characteristic constructed for those 9 TFNs was considerably shifted to the right (fig. 5B).

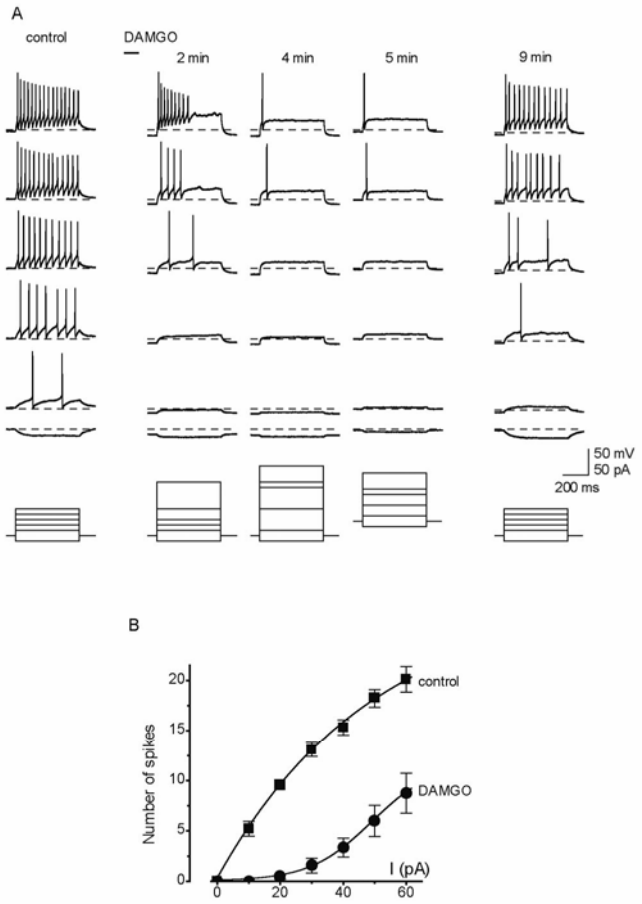

Fig. 5. DAMGO-induced modification of firing pattern in tonic-firing neurons. (*A*) Induction of spike-frequency adaptation observed in majority of tonic-firing neurons (44 of 53). The firing patterns were recorded 2, 4, 5, and 9 min (recovery) after DAMGO application. The recording at 5 min was done when the membrane potential was returned to −70 mV by current injection. *Dashed line* indicates −70 mV. (*B*) DAMGO-induced shift in firing characteristics for the rest (9 of 53) of the tonic-firing neurons. The characteristics were constructed as the number of spikes fired during 500-ms depolarization as a function of injected current. Each *point* is a mean of nine measurements. The data points are fitted by eye.

Discussion

The current results have shown that the μ-opioid agonist DAMGO selectively inhibits TFNs in SG, whereas it had no effect on AFNs and DFNs. Our finding implies that TFNs, which receive direct inputs from Aδ- and C-type afferents,[27] represent a primary postsynaptic target for both administered opioids and endogenous enkephalins in the spinal cord. Cell classification on the basis of firing patterns was important for this study. Our data support several patch clamp investigations showing that SG is formed by neurons with diverse intrinsic firing properties[23,27,33,34] but conflict with Ruscheweyh and Sandkuhler,[29] who have found only adapting discharge patterns in neurons from rat lamina II (SG). Our classification is also similar to those suggested on the basis of recordings with a sharp electrode.[25,26] However, it cannot be excluded that some TFNs from the current study would appear as AFNs if recorded with a sharp electrode introducing larger somatic shunt.

Each group of neurons had its specific distribution pattern within SG. The intermediate SG was dominated by TFNs, the medial region contained both TFNs and DFNs, and the lateral zone contained all three types of cells with a high percentage of AFNs. This is in good agreement with Melnick *et al.*,[23] who showed that in parasagittal spinal cord slices, including mostly the intermediate region of SG, TFNs represent 70% of the total neuronal population. The sensitivity of a given neuron to DAMGO depended on its firing properties rather than its location within the SG. Therefore, our results suggest that the percentage of neurons responding to opioids might vary along the medial–lateral axis of SG, being highest in the intermediate zone.

Agonists binding to μ-opioid receptors hyperpolarize membrane through the activation of GIRK (also known as Kir3) channels functioning as effectors.[19,35,36] It seems that all three types of SG neurons possess GIRK conductance, which could be blocked by Ba^{2+} and Cs^{+} as well as activated by baclofen *via* the $GABA_B$ receptor pathway.[18] Selective inhibition of TFNs by DAMGO could therefore be explained by a specific targeting of postsynaptic μ-opioid receptors to TFNs rather than AFNs and DFNs. Alternatively, it is possible that AFNs and DFNs also express μ-opioid receptors but that the G protein coupling them to GIRK channels is not present. Because the majority of SG neurons expressing μ-opioid receptors do not contain GABA or glycine and therefore are excitatory interneurons,[14] we suggest that TFNs can function as excitatory interneurons. The intrinsic firing properties would allow them to convert stronger synaptic inputs into higher discharge frequencies in a broad range of synaptic stimulation.

The current results show that the mechanism of postsynaptic action of opioids on SG neurons is more complex and effective than it was assumed so far. Membrane hyperpolarization due to activation of GIRK conductance resulted in increased stimulation intensity needed to reach the firing threshold. In addition, most TFNs showed a transition from tonic to adapting firing mode. Therefore, the input–output characteristics of the neurons were modified in such a way that stronger synaptic input could no longer be converted into increasing numbers of generated spikes. It should be also noted that the opioid-induced plasticity of firing behavior reported here can be a complex phenomenon, which, in addition to modulation of GIRK channels,[37] may also involve G protein–dependent regulation of some other ion channel systems.[38–40]

DAMGO-sensitive interneurons from SG send some of their axons to lamina I and V,[22] where most projection neurons that target supraspinal regions are located.[41,42] Therefore, μ-opioid agonists can inhibit SG neurons that

relay primary nociceptive afferent inputs to ascending projection neurons. Suppression of excitatory interneurons with a tonic-firing pattern by enkephalins may be an important mechanism of endogenous pain control because μ-opioid receptor–expressing dorsal horn neurons were shown to be located in close proximity to enkephalinergic terminals.[7,43] Under physiologic conditions, they may be involved in an endogenous, *i.e.*, stress-induced, analgesia.

Furthermore, TFNs possessing μ-opioid receptors are likely to participate in analgesic effects of administered opioids. High sensitivity of TFNs to μ-opioid agonist implies their involvement in analgesic effects of spinal, epidural, and systemic opioids, like morphine.[9–11,44] At low doses, opioids do not block voltage-gated Na^+ and K^+ channels,[45–47] and therefore, their specific action *via* opioid receptors in tonic-firing spinal sensory neurons may contribute to profound and prolonged relief of pain with virtually no motor blockade.

The authors thank Helena Pereira (Technician, Departamento de Neurobiologia Básica e Clínica, Instituto de Biologia Molecular e Celular, Porto, Portugal) for technical assistance.

References

1. Rethelyi M: Preterminal and terminal axon arborizations in the substantia gelatinosa of cat's spinal cord. J Comp Neurol 1977; 172:511–21
2. Light AR, Perl ER: Spinal termination of functionally identified primary afferent neurons with slowly conducting myelinated fibers. J Comp Neurol 1979; 186:133–50
3. Sugiura Y, Lee CL, Perl ER: Central projections of identified, unmyelinated (C) afferent fibers innervating mammalian skin. Science 1986; 234:358–61
4. Cervero F: Dorsal horn neurons and their sensory inputs, Spinal Afferent Processing. Edited by Yaksh TL. New York, Plenum Press, 1987, pp 197–216
5. Ribeiro-da-Silva A, Pioro EP, Cuello AC: Substance P- and enkephalin-like immunoreactivities are colocalized in certain neurons of the substantia gelatinosa of the rat spinal cord: An ultrastructural double-labeling study. J Neurosci 1991; 11:1068–80
6. Arvidson U, Dado RJ, Riedl M, Lee J-H, Law P-Y, Loh HH, Elde R, Wessendorf MW: δ-Opioid receptor immunoreactivity: Distribution in brainstem and spinal cord, and relationship to biogenic amines and enkephalin. J Neurosci 1995; 15:1215–35
7. Arvidson U, Riedl M, Chakrabarti S, Lee J-H, Nakano AH, Dado RJ, Loh HH, Law P-Y, Wessendorf MW, Elde R: Distribution and targeting of a μ-opioid receptor (MOR1) in brain and spinal cord. J Neurosci 1995; 15:3328–41
8. Merchenthaler I, Maderdrut JL, Altschuler RA, Petrusz P: Immunocytochemical localization of proenkephalin-derived peptides in the central nervous system of the rat. Neurosci 1986; 17:325–48
9. Duggan AW, Hall JG, Headley PM: Suppression of transmission of nociceptive impulses by morphine: Selective effects of morphine administered in the region of the substantia gelatinosa. Br J Pharmacol 1977; 61:65–76
10. Johnston SM, Duggan AW: Evidence that opiate receptors of the substantia gelatinosa contribute to the depression, by intravenous morphine, of the spinal transmission of impulses in unmyelinated afferents. Brain Res 1981; 207:223–8
11. Eltzschig HK, Lieberman ES, Camann WR: Regional anesthesia and analgesia for labor and delivery. N Engl J Med 2003; 348:319–32
12. Dado RJ, Law PY, Loh HH, Elde R: Immunofluorescent identification of a delta (δ)-opioid receptor on primary afferent nerve terminals. Neuroreport 1993; 5:341–4
13. Grudt TJ, Williams JT: μ-Opioid agonists inhibit spinal trigeminal substantia gelatinosa neurons in guinea pig and rat. J Neurosci 1994; 14:1646–54
14. Kemp T, Spike RC, Watt C, Todd AJ: The μ-opioid receptor (MOR1) is mainly restricted to neurons that do not contain GABA or glycine in the superficial dorsal horn of the rat spinal cord. Neurosci 1996; 75:1231–8
15. Yoshimura M, North RA: Substantia gelatinosa neurones hyperpolarized in vitro by enkephalin. Nature 1983; 305:529–30
16. Schneider SP, Eckert WA, Light AR: Opioid-activated postsynaptic, inward rectifying potassium currents in whole cell recordings in substantia gelatinosa neurons. J Neurophysiol 1998; 80:2954–62
17. Light AR, Willcockson HH: Spinal laminae I-II neurons in rat recorded in vivo in whole cell, tight seal configuration: Properties and opioid responses. J Neurophysiol 1999; 82:3316–26
18. Sodickson DL, Bean B: $GABA_B$ receptor-activated inwardly rectifying potassium current in dissociated hippocampal CA3 neurons. J Neurosci 1996; 16:6374–85
19. Svoboda KR, Lupica CR: Opioid inhibition of hippocampal interneurons via modulation of potassium and hyperpolarization-activated cation (I_h) currents. J Neurosci 1998; 18:7084–98
20. Gobel S: Golgi studies of the neurons in layer II of the dorsal horn of the medulla (trigeminal nucleus caudalis). J Comp Neurol 1978; 180:395–414
21. Todd AJ: Electron microscope study of Golgi-stained cell in lamina II of the rat spinal dorsal horn. J Comp Neurol 1988; 275:145–57
22. Eckert WA, McNaughton KK, Light AR: Morphology and axonal arborization of rat spinal inner lamina II neurons hyperpolarized by μ-opioid-selective agonists. J Comp Neurol 2003; 458:240–56
23. Melnick IV, Santos SFA, Szokol K, Szucs P, Safronov BV: Ionic basis of tonic firing in spinal substantia gelatinosa neurons of rat. J Neurophysiol 2004; 91: 646–55
24. Yoshimura M, Jessel TM: Membrane properties of rat substantia gelatinosa neurons in vitro. J Neurophysiol 1989; 62:109–18
25. Thomson AM, West DC, Headley PM: Membrane characteristics and synaptic responsiveness of superficial dorsal horn neurons in a slice preparation of adult rat spinal cord. Eur J Neurosci 1989; 1:479–88
26. Lopez-Garcia JA, King AE: Membrane properties of physiologically classified rat dorsal horn neurons in vitro: Correlation with cutaneous sensory afferent input. Eur J Neurosci 1994; 6:998–1007
27. Grudt TJ, Perl ER: Correlations between neuronal morphology and electrophysiological features in the rodent superficial dorsal horn. J Physiol 2002; 540:189–207
28. Edwards FA, Konnerth A, Sakmann B, Takahashi T: A thin slice preparation for patch clamp recordings from neurones of the mammalian central nervous system. Pflugers Arch 1989; 414:600–12
29. Ruscheweyh R, Sandkuhler J: Lamina-specific membrane and discharge properties of rat spinal dorsal horn neurones in vitro. J Physiol 2002; 541:231–44
30. Mayer ML, Westbrook GL: A voltage-clamp analysis of inward (anomalous) rectification in mouse spinal sensory ganglion neurones. J Physiol 1983; 340: 19–45
31. Pape H-C: Queer current and pacemaker: The hyperpolarization-activated cation current in neurons. Annu Rev Physiol 1996; 58:299–327
32. Blanchet C, Luscher C: Desensitization of mu-opioid receptor-evoked potassium currents: Initiation at the receptor, expression at the effector. Proc Natl Acad Sci U S A 2002; 99:4674–9
33. Lu Y, Perl ER: A specific inhibitory pathway between substantia gelatinosa neurons receiving direct C-fiber input. J Neurosci 2003; 23:8752–8
34. Hu H-J, Gereau RW: ERK integrates PKA and PKC signaling in superficial dorsal horn neurons: II. Modulation of neuronal excitability. J Neurophysiol 2003; 90:1680–8
35. Wimpey TL, Chavkin C: Opioids activate both an inward rectifier and a novel voltage-gated potassium conductance in the hippocampal formation. Neuron 1991; 6:281–9
36. Ikeda K, Kobayashi T, Yano R, Sora I, Niki H: Molecular mechanisms of analgesia induced by opioids and ethanol: Is the GIRK channel one of the keys? Neurosci Res 2002; 44:121–31
37. Derjean D, Bertrand S, Masson GL, Landry M, Morisset V, Nagy F: Dynamic balance of metabotropic inputs causes dorsal horn neurons to switch functional states. Nature Neurosci 2003; 6:274–81
38. Ma JY, Li M, Catterall WA, Scheuer T: Modulation of brain Na^+ channels by a G-protein-coupled pathway. Proc Natl Acad Sci U S A 1994; 91:12351–5
39. Müller W, Hallermann S, Swandulla D: Opioidergic modulation of voltage-activated K^+ currents in magnocellular neurons of the supraoptic nucleus in rat. J Neurophysiol 1999; 81:1617–25
40. Law PY, Wong YH, Loh HH: Molecular mechanisms and regulation of opioid receptor signaling. Annu Rev Pharmacol Toxicol 2000; 40:389–430
41. Trevino DL, Coulter JD, Willis WD: Location of cells of origin of spinothalamic tract in lumbar enlargement of the monkey. J Neurophysiol 1973; 36: 750–61
42. Lima D: Anatomical basis for the dynamic processing of nociceptive input. Eur J Pain 1998; 2:195–202
43. Song B, Marvizon JC: Peptidases prevent mu-opioid receptor internalization in dorsal horn neurons by endogenously released opioids. J Neurosci 2003; 23:1847–58
44. Wang JK, Nauss LA, Thomas JE: Pain relief by intrathecally applied morphine in man. ANESTHESIOLOGY 1979; 50:149–51
45. Hu S, Rubly N: Effects of morphine on ionic currents in frog node of Ranvier. Eur J Pharmacol 1983; 95:185–92
46. Bräu ME, Koch ED, Vogel W, Hempelmann G: Tonic blocking action of meperidine on Na^+ and K^+ channels in amphibian peripheral nerves. ANESTHESIOLOGY 2000; 92:147–55
47. Wolff M, Olschewski A, Vogel W, Hempelmann G: Meperidine suppresses the excitability of spinal dorsal horn neurons. ANESTHESIOLOGY 2004; 100:947–55

Second publication

J Physiol 581.1 (2007) pp 241–254

Excitatory interneurons dominate sensory processing in the spinal substantia gelatinosa of rat

Sónia F. A. Santos[1,2], Sandra Rebelo[2], Victor A. Derkach[3] and Boris V. Safronov[1,2]

[1]Instituto de Biologia Molecular e Celular – IBMC, Universidade do Porto, Rua do Campo Alegre 823, 4150-180 Porto, Portugal
[2]Laboratório de Biologia Celular e Molecular, Faculdade de Medicina, Universidade do Porto, Alameda Professor Hernâni Monteiro, 4200-319 Porto, Portugal
[3]Vollum Institute, Oregon Health & Science University, 3181 SW Sam Jackson Park Road, Portland, OR 97239, USA

Substantia gelatinosa (SG, lamina II) is a spinal cord region where most unmyelinated primary afferents terminate and the central nociceptive processing begins. It is formed by several distinct groups of interneurons whose functional properties and synaptic connections are poorly understood, in part, because recordings from synaptically coupled pairs of SG neurons are quite challenging due to a very low probability of finding connected cells. Here, we describe an efficient method for identifying synaptically coupled interneurons in rat spinal cord slices and characterizing their excitatory or inhibitory function. Using tight-seal whole-cell recordings and a cell-attached stimulation technique, we routinely tested about 1500 SG interneurons, classifying 102 of them as monosynaptically connected to neurons in lamina I–III. Surprisingly, the vast majority of SG interneurons ($n = 87$) were excitatory and glutamatergic, while only 15 neurons were inhibitory. According to their intrinsic firing properties, these 102 SG neurons were also classified as tonic ($n = 49$), adapting ($n = 17$) or delayed-firing neurons ($n = 36$). All but two tonic neurons and all adapting neurons were excitatory interneurons. Of 36 delayed-firing neurons, 23 were excitatory and 13 were inhibitory. We conclude that sensory integration in the intrinsic SG neuronal network is dominated by excitatory interneurons. Such organization of neuronal circuitries in the spinal SG can be important for nociceptive encoding.

(Received 21 December 2006; accepted after revision 28 February 2007; first published online 1 March 2007)
Corresponding authors B. V. Safronov: Instituto de Biologia Molecular e Celular-IBMC, Universidade do Porto, Rua do Campo Alegre 823, 4150-180 Porto, Portugal. Email: safronov@ibmc.up.pt
V. A. Derkach: Vollum Institute, Oregon Health & Science University, 3181 SW Sam Jackson Park Rd, Portland, OR 97239, USA. Email: derkachv@ohsu.edu

The spinal substantia gelatinosa (SG), a dorsal horn region where most fine-calibre C- and Aδ-fibres terminate (Rethelyi, 1977; LaMotte, 1977; Light & Perl, 1977; Sugiura et al. 1986), is a key element in the nociceptive processing system. Diverse sensory modalities are encoded in the SG by the types of terminating afferents, the firing properties of intrinsic SG neurons and their synaptic connectivity (Brown, 1981; Cervero, 1987; Willis & Coggeshall, 1991).

Several groups of SG neurons with distinct intrinsic firing properties were characterized by both sharp electrode (Yoshimura & Jessell, 1989; Thomson *et al.* 1989; Lopez-Garcia & King, 1994) and tight-seal recordings (Grudt & Perl, 2002; Ruscheweyh & Sandkuhler, 2002; Santos *et al.* 2004; Graham *et al.* 2004). SG neurons with distinct firing properties show type-specific morphological features and intralaminar distributions (Grudt & Perl, 2002; Melnick *et al.* 2004*a*,*b*; Santos *et al.* 2004), but little is known about their synaptic connections. This knowledge is, however, important because neuronal firing activity and the strength of its synapses are related. Indeed, activity-dependent modification of synaptic strength, or synaptic plasticity, is an essential property of neuronal networks (Malenka & Nicoll, 1999; Turrigiano & Nelson, 2004; Malenka & Bear, 2004; Lisman & Spruston, 2005) and plays a key role in nociceptive processing and chronic pain development (Woolf & Salter, 2000; Ji *et al.* 2003; Salter, 2005). Thus, the firing pattern of a neuron can critically determine the efficiency of its functional connections and ultimately its contribution to the network activity. Therefore, to better understand how nociceptive information is processed within the superficial dorsal horn, it is essential to study firing patterns of SG interneurons and their synaptic connections.

Such investigation relies on identifying pairs of monosynaptically coupled neurons. This is a difficult task, however, if a conventional double patch-clamp recording technique is used, since the probability of finding monosynaptically connected neurons in slices of the

 DOI: 10.1113/jphysiol.2006.126912

superficial dorsal horn is very low (Lu & Perl, 2003). Indeed, recent studies have provided the first insight into the neuronal architecture of SG network showing that SG neurons form specific excitatory and inhibitory circuitries in the SG as well as lamina I (Lu & Perl, 2003, 2005). However, the total number of recordings from pairs of SG neurons is quite limited as well as the knowledge on the network organization. Therefore, we implemented a novel approach for efficiently identifying monosynaptic connections and studied discharge properties of excitatory and inhibitory SG interneurons. This approach combines a tight-seal whole-cell recording from postsynaptic neuron with a specific cell-attached stimulation of presynaptic neuron. We focused on two critical and unknown aspects of SG network organization: (1) the functional balance between the excitatory and inhibitory modes of sensory processing, and (2) whether and how neuronal firing properties correlate with their synaptic connections. We have characterized synaptic connections for SG neurons with different firing patterns and found that signalling within the SG network is dominated by excitatory glutamatergic interneurons.

Methods

Tight-seal recordings were made using both 200 μm transverse and 300 μm parasagittal slices prepared from the lumbar enlargement of the spinal cord of 2- to 7-week-old rats (Bentley & Gent, 1994; Melnick *et al.* 2004*a*). The animals were killed in accordance with the national guidelines (Direcção Geral de Veterinária, Ministério da Agricultura). After the anaesthesia by intraperitoneal injection of sodium pentobarbital (30 mg kg^{-1}), the vertebral column was quickly cut out and immersed in ice-cold oxygenated artificial cerebrospinal fluid (ACSF). The 5–7 mm segment of the lumbar enlargement was dissected and the slices were prepared using the tissue slicer (Leica VT 1000S). The slices were then incubated for 40–60 min in ACSF at 33°C. The SG (lamina II) was identified in the dorsal horn as a translucent band of about 60 μm thickness in its intermediate region (see Fig. 6). The marginal 20 μm layer of the dorsal horn separating the SG from the white matter was considered as lamina I. Neurons were localized during recording according to a position of the pipette tip on the video image of a superficial dorsal horn.

ACSF contained (mM): NaCl 115, KCl 3, $CaCl_2$ 2, $MgCl_2$ 1, glucose 11, NaH_2PO_4 1, $NaHCO_3$ 25, and glucose 11 (pH 7.4 when bubbled with 95%/5% mixture of O_2/CO_2). $MgCl_2$ was excluded from the ACSF used for recordings to avoid a possible block of the NMDA receptor-gated postsynaptic currents at potentials close to the resting membrane potential. Standard pipette solution contained (mM): KCl 3, potassium gluconate 150.5, $MgCl_2$ 1, BAPTA 1 and Hepes 10 (pH 7.3 adjusted with KOH, final $[K^+]$ was 160.5 mM). The theoretical reversal potential for Cl^- (E_{Cl}) was −81 mV in all experiments. The pipettes used for perforated-patch recordings were filled with solution containing (mM): NaCl 5, potassium gluconate 145, Hepes 10, amphotericin B (final concentration 100 μg ml^{-1}, freshly prepared from a 60 mg ml^{-1} stock solution). All chemicals were purchased from Sigma.

Recording pipettes were pulled from thick-walled borosilicate glass tubes (Modulohm, Denmark), fire-polished, and had a resistance of 3–5 MΩ. The pipettes used for cell-attached stimulation were narrower than those for the tight-seal recordings and had a resistance of 13–27 MΩ when fire-polished and filled with ACSF. An EPC-10-Double amplifier (HEKA, Lambrecht, Germany) was used in all experiments. The voltage-follower circuitry of the amplifier was employed for the current-clamp measurements. The effective corner frequency of the low-pass filter in voltage-clamp mode was 3 kHz. The frequency of digitization was always 10 kHz. Offset potentials were compensated directly before formation of a seal. Liquid junction potentials were calculated and corrected for in all experiments. The series resistance, determined in the current-clamp mode from the instantaneous voltage change produced by a current step injection, did not exceed 14 MΩ (with an exception of one cell). The voltage error due to resistance in series did not exceed 2 mV in all current-clamp recordings and was below 3 mV in all but three voltage-clamp experiments. Input resistances (R_{IN}) of neurons were measured in both current-clamp (using a −10 pA hyperpolarizing current of 500 ms duration) and voltage-clamp modes (from a change in a leakage current at a 100 ms voltage step from −80 to −120 mV).

Recordings in perforated patch mode were made 20–30 min after establishing the gigaseal contact with the cell. This time period allowed amphotericin B to perforate the membrane under the pipette and reduce the access resistance. Stable recording with perforated patches lasted for up to 2 h. Stability of perforated patches was controlled by adding to the pipette solution fluorescent dye Alexa 694. Only when patch membrane had been ruptured did the cell body also become fluorescent.

Resting membrane potential (V_R) is critical for pattern identification in some types of SG neurons and therefore special precaution was taken to correctly estimate it. Since the R_{IN} in SG neurons is in the gigaohm range, an unbalanced steady-state current of just a few picoamps at the amplifier input could substantially influence the measured V_R value (Santos *et al.* 2004). Thus, we balanced the input of the amplifier in a current-clamp mode before each experiment using a 0.5 GΩ resistor model circuitry in accordance with a procedure described by Santos *et al.* (2004). The remaining uncompensated input current was less than 1 pA.

SG neurons were separated into three groups on the basis of their firing properties, tonic neurons (TNs), adapting neurons (ANs) and delayed-firing neurons (DNs) as described in detail by Santos *et al.* (2004). In brief, TNs were able to support tonic firing during 500 ms depolarization induced by a sustained current injection. They had a low mean firing threshold of about −50 mV and 10–20 pA current pulses were sufficient to evoke firing (Santos *et al.* 2004; Melnick *et al.* 2004*a*). Under voltage-clamp condition, TNs showed inward rectification. A characteristic feature of ANs was a burst-like firing of spikes only at the beginning of depolarization. The mean firing threshold of about −50 mV was not significantly different from that in TNs (Santos *et al.* 2004; Melnick *et al.* 2004*b*). In both TNs and ANs, a transient K^+ current was not seen at voltage steps from −80 to −60 mV (Melnick *et al.* 2004*a*,*b*). A principal difference of DNs was the presence of a large transient K^+ current that substantially influenced the firing pattern. The spike threshold in DNs (about −40 mV, Santos *et al.* 2004) was considerably higher than in TNs or ANs and was reached at stimulation as strong as 50–70 pA, since a large portion of injected current was compensated by activating the transient K^+ current. In DNs the first spikes typically appeared with a considerable time delay at the end of the pulse and moved to its beginning as the stimulation increased. An inward rectification was less pronounced in DNs. There were, however, some minor variations in discharge patterns of DNs at strong stimulation. Some cells discharged regularly during the whole pulse, while others belonging to this group showed either interrupted bursts or single spikes (Santos *et al.* 2004). In Table 3 these subtypes of DNs are called DN_1, DN_2 and DN_3, respectively.

All numbers are given as mean ± standard error of the mean (S.E.M.). The parameters were compared by independent Student's *t* test. The present study is based on recordings from 249 superficial dorsal horn neurons, 217 of which were located in the SG. These statistics do not include the cells from the control experiments, in which inhibitory interneurons were selectively searched, to avoid bias toward the contribution of inhibitory neurons. All experiments, except those in Fig. 2*B*, were carried out at room temperature of 22–24°C.

Results

Our experiments were designed to (1) find monosynaptically connected pairs of superficial dorsal horn neurons with a presynaptic neuron located in the SG, (2) identify excitatory or inhibitory nature of the synapse, (3) correctly record the intrinsic firing patterns of presynaptic neurons, and (4) map the network connections of SG neurons within the superficial dorsal horn.

Identification of monosynaptic connections

Throughout this study the action potentials in presynaptic neurons were evoked using a cell-attached stimulation, specific for stimulated cell. The efficiency of this technique was first tested by the simultaneous whole-cell current-clamp recording from extracellularly stimulated neuron (Fig. 1*A*, $n = 12$). A 1 ms current pulse of 100 nA was applied to a stimulation pipette at a frequency of 1 Hz as it was approaching the cell. The stimulation artifacts were clearly recorded by the whole-cell electrode but a membrane depolarization was very small. After the stimulation pipette has been brought in a contact with the membrane of the cell soma, the amplitude of the stimulation artifact recorded by the whole-cell electrode increased but the membrane depolarization was still insufficient to excite the cell. An application of a slight negative pressure to the stimulation electrode, which increased the seal resistance several times, resulted in a membrane depolarization sufficient for activation of a spike at each stimulation pulse. The overshoot of the extracellularly activated spike was similar to that of the first spike in a train evoked by direct injection of depolarizing current through the whole-cell electrode (Fig. 1*A*). If a stronger negative pressure was applied to the stimulation electrode, the overshoot potential in all cells increased to non-physiological values of more than +100 mV (not shown). When the contact between the membrane and the stimulation pipette had been broken, the neuron no longer responded to the extracellular stimulation, indicating that the stimulation was efficient only for the attached neuron. The stimulation technique was effective for all three types of neurons studied. One pipette could be repeatedly used to stimulate different cells, thus providing an efficient method for searching presynaptic neurons.

To identify SG neurons as excitatory or inhibitory interneurons, we used the experimental protocol shown in Fig. 1*B*. First, a postsynaptic neuron located in laminae I–III was voltage clamped at −80 mV. The extracellular pipette was then brought in contact with a SG neuron which was presumably presynaptic, and a slight negative pressure was applied. After this, a voltage command changed the membrane potential in the postsynaptic neuron for 100 ms to −100 and −60 mV before returning back to −80 mV. Thirty milliseconds after beginning of each voltage step, a 1 ms current pulse of 100 nA was applied through the cell-attached pipette to the presynaptic neuron. If the neurons were connected, synaptic responses were evoked in a postsynaptic neuron at three different potentials at a 10 Hz frequency (100 ms stimulation interval). The same voltage command was repeated three more times (without stimulating a presynaptic neuron) in order to obtain an averaged trace used for subtraction of transients, leakage currents

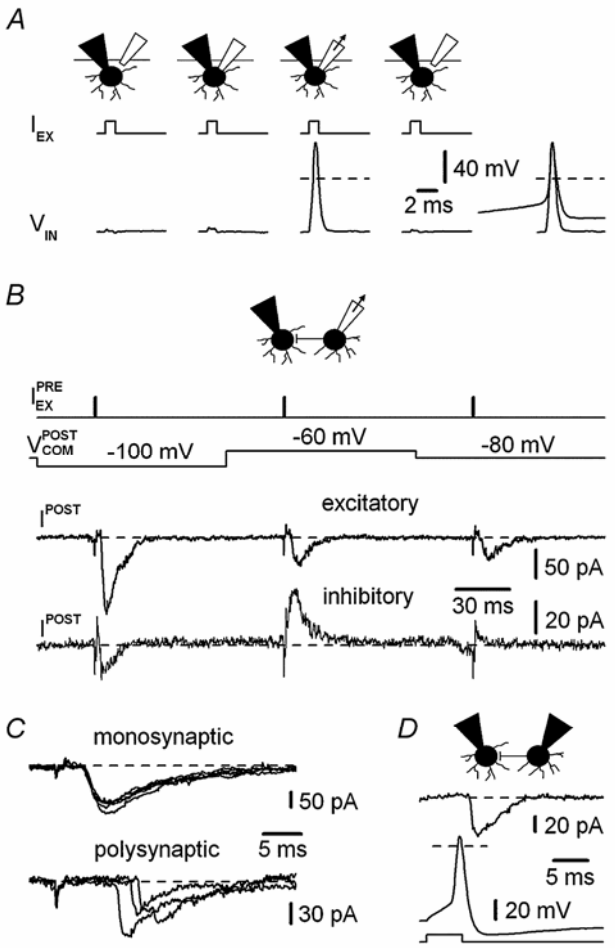

Figure 1. Focal cell-attached stimulation
A, in control experiments a direct whole-cell current-clamp recording from the extracellularly stimulated neuron was done. A 1 ms current pulse of 100 nA was injected through an artificial cerebrospinal fluid (ACSF)-filled stimulation pipette at a frequency of 1 Hz. Note the stimulation artifacts recorded intracellularly. Simple touching of the cell by the stimulation pipette (without pressure application) did not result in spike activation. However, spikes appeared at each current pulse after a slight negative pressure had been applied to the stimulation electrode and disappeared after an electrode had been withdrawn (with a positive pressure). The rightmost traces show superimposed the extra- and intracellularly (the first spike in a train) activated spikes. *B*, experimental procedure used for identifying the excitatory and inhibitory neurons. The postsynaptic currents (I_{POST}) were recorded in a voltage-clamped neuron at −100, −60 and −80 mV (each potential applied for 100 ms, $V_{COM,POST}$) while the presynaptic neuron was focally stimulated at 100 ms intervals (frequency of 10 Hz, $I_{EX,PRE}$). Recordings from two different neurons allowing characterization of their presynaptic connections as excitatory (upper) and inhibitory (lower). *C*, comparison of mono- and polysynaptic responses. Monosynaptic connection: first pulses (to −100 mV) from five consecutive voltage commands similar to those in part *B* are shown superimposed. The interval between voltage commands was 1.5 s. Polysynaptic connection: three non-consecutive pulses to −100 mV (empty episodes recorded in between are not shown). *D*, simultaneous whole-cell recordings from two synaptically connected neurons. An action potential activated by a direct injection of current pulse (100 pA, 5 ms) in a presynaptic neuron evoked a short latency inward current in a postsynaptic neuron voltage clamped at −80 mV.

and voltage-gated K^+ currents (activated at −60 mV). Thus, corrected traces shown in all figures contain only stimulation artifacts and postsynaptic currents. If the neurons appeared to be not connected, we progressively increased a negative pressure in the stimulation pipette to evoke large overshoot spikes in the presumably presynaptic neuron to ensure that lack of a postsynaptic response was not caused by insufficient stimulation of the presynaptic neuron.

A presynaptic neuron was considered as excitatory if its stimulation evoked inward postsynaptic currents at −100, −60 and −80 mV. A neuron was considered as inhibitory if the currents were inward at −100 mV and outward at −60 mV, becoming negligible at −80 mV, a potential close to an E_{Cl} of −81 mV. If the postsynaptic neuron was switched to current clamp, the corresponding excitatory or inhibitory postsynaptic potentials, EPSPs or IPSPs, were observed. This classification was also confirmed by specific receptor pharmacology: excitatory postsynaptic currents (EPSCs) were blocked by the AMPA/kainate receptor antagonist 6-cyano-7-nitroquinoxaline-2,3-dione (CNQX) (10 μM, $n = 16$), while inhibitory postsynaptic currents (IPSCs) were blocked by the glycine receptor antagonist strychnine (1 μM, $n = 6$). In eight early experiments, excitatory connections were identified on the basis of EPSPs recorded in a current-clamped postsynaptic neuron.

The responses were considered monosynaptic if they showed a constant latency and low percentage of failures at 10 Hz stimulation (Fig. 1*B*, three postsynaptic currents were recorded at different potentials with intervals of 100 ms). Figure 1*C* shows monosynaptic EPSCs recorded at first voltage steps to −100 mV from five consecutive voltage commands similar to those shown in Fig. 1*B*. In contrast, polysynaptic EPSCs could be clearly distinguished on the basis of variable latencies and frequent failures (Fig. 1*C*, failures are not shown). Polysynaptic connections were not included into this study.

The percentage of monosynaptically connected neurons in both parasagittal and transversal slices was low. A total of 173 connections (156 excitatory and 17 inhibitory) were found by testing about 1500 presumably presynaptic neurons. A tight-seal recording could be, however, established with 102 presynaptic neurons (87 excitatory and 15 inhibitory) that are described in this study. Recordings of postsynaptic currents and potentials, as well as blocker testing, were done using the cell-attached stimulation of a presynaptic neuron. At the end of the experiment we retained the stimulation pipette as a marker of the presynaptic neuron position, while the other pipette had been changed to establish a whole-cell mode and to record discharge pattern in the presynaptic neuron. In five control experiments, simultaneous whole-cell recordings from connected neurons were done (Fig. 1*D*). In this case, the recording from the postsynaptic neuron continued,

while a position and a shape of the presynaptic neuron was carefully marked on the video monitor and the stimulation pipette had been substituted with the second whole-cell electrode. In all five connections, an action potential elicited by a direct current injection to a presynaptic neuron was followed by the EPSCs in a postsynaptic one. The time delays and the kinetics of EPSCs were indistinguishable from those seen with the extracellular cell-attached stimulation.

Determination of firing patterns. We have previously characterized three types of SG neurons – TNs, ANs and DNs – on the basis of their firing patterns (Santos *et al.* 2004; Melnick *et al.* 2004*a*,*b*; see Methods). However, the reports on the discharge properties of SG neurons studied by the patch-clamp technique are controversial (Grudt & Perl, 2002; Lu & Perl, 2003; Hantman *et al.* 2004; but see Ruscheweyh & Sandkuhler, 2002). Differences in firing patterns reported in our studies and others may be a consequence of a number of experimental factors, such as measured mean values of V_R (varying from −48 to −77 mV) and R_{IN} (ranging from about 160 MΩ to 1.7 GΩ) or usage of different intracellular solutions. In addition, intrinsic discharge patterns might depend on whether the measurements are carried out at room temperature or at 37°C. Therefore, we first tested the firing patterns and measured V_R and R_{IN} in SG neurons using the least invasive form of the patch-clamp technique, perforated-patch recording (Horn & Marty, 1988; Rae *et al.* 1991), which prevents dialysis of cytoplasmic factors and alteration in divalent cation concentrations that normally occur in the whole-cell mode.

In experiments with perforated patches shown in Fig. 2*A* we recorded the same three basic types of SG neurons, TNs ($n = 10$), ANs ($n = 10$) and DNs ($n = 10$), as described by Santos *et al.* (2004). We found that the firing patterns were stable and could be recorded without modification for up to 2 h. The V_R values measured with a balanced amplifier input were close to −70 mV, and the mean R_{IN} obtained in current clamp was above 1 GΩ for all three types of neurons (Table 1). For five neurons of each type, the temperature of the solution was increased to 35–37°C (Fig. 2*B*). This did not modify the characteristic discharge pattern, implying that a correct identification of SG neuron could be done at room temperature.

In whole-cell recordings with our pipette solution (1 mM BAPTA) the same three types of SG neurons were seen. In test experiments with 15 neurons (five of each type) stable unmodified firing patterns were recorded during periods of 42 min to 2 h 1 min. Altogether, the whole-cell recordings were made from 186 SG neurons of which 89 were classified as TNs, 37 as ANs and 60 as DNs. The mean V_R and R_{IN} measured in whole-cell mode (see Table 1) were close to those of perforated-patch recordings. We thus concluded that the whole-cell recording with our internal solution was adequate for correctly characterizing pattern, V_R and R_{IN} in SG neurons.

Presynaptic TNs

Of the total 102 presynaptic SG neurons that were studied, 49 were identified as TNs (Fig. 3*A*). A majority of their synaptic connections (36 of 49; 73%) were intralaminar with another SG neurons, whereas only eight were found with lamina I, and five with lamina III neurons (Fig. 6*A* and Table 2). According to firing patterns, 31 of 49 connections were formed with TNs, 8 with ANs and 10 with DNs (Fig. 6*A* and Table 2). It should be noted that all postsynaptic neurons located in lamina I were TNs.

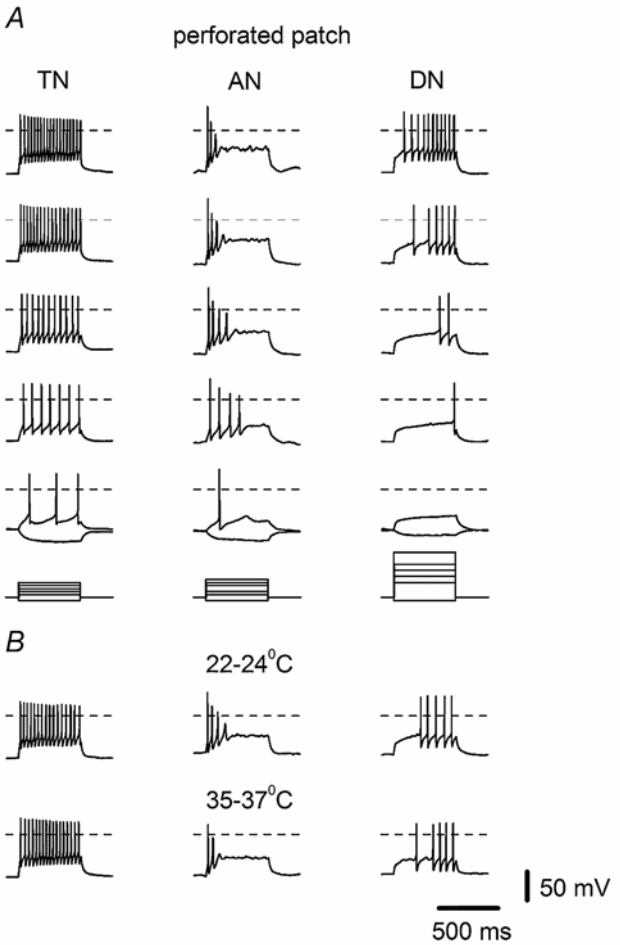

Figure 2. Perforated-patch recording of firing patterns of substantia gelatinosa (SG) neurons
A, membrane responses in a tonic neuron (TN), an adapting neuron (AN) and a delayed-firing neuron (DN) to 500 ms current injections. Stimulation protocols are shown below the traces. Passive membrane responses were elicited by an injection of a hyperpolarizing current of 10 pA (all depolarizing currents are appropriately scaled). *B*, discharge patterns of a TN, an AN and a DN at 22–24°C and 35–37°C. In all traces in this and the following figures dashed lines indicate 0 mV or 0 pA.

Table 1. The mean V_R and R_{IN} values measured in perforated-patch and whole-cell recordings

	R_{IN} (GΩ)		V_R (mV)	
	Whole cell	Perforated patch	Whole cell	Perforated patch
TN	2.26 ± 0.12 (89)	2.22 ± 0.48 (10)	−72.8 ± 0.4 (89)	−71.4 ± 0.5 (10)
AN	1.90 ± 0.18 (37)	2.02 ± 0.31 (10)	−71.8 ± 0.5 (37)	−70.3 ± 0.8 (10)
DN	1.69 ± 0.11 (60)	1.59 ± 0.37 (10)	−74.1 ± 0.4 (60)	−74.7 ± 0.7 (10)

R_{IN}, input resistance. The membrane potential (V_R) was measured with a balanced amplifier input (see Methods) in a total of 186 whole-cell modes and 30 perforated patches. Numbers of recordings are given in parentheses.

The distances between synaptically coupled neurons varied from 6 to 75 μm, with a mean distance of 19.2 ± 2.1 μm ($n = 49$).

All but two connections of TNs were excitatory. The mean maximum EPSC amplitude measured at −100 mV was 90.3 ± 10.6 pA ($n = 20$). The time course of decay was monoexponential with a mean time constant of 5.0 ± 0.5 ms ($n = 20$). The mean latency of responses, calculated as a time interval between the end of the stimulation artifact and the beginning of the EPSC, was 2.6 ± 0.4 ms ($n = 20$). The EPSCs evoked by TN stimulations were completely blocked by the glutamate AMPA receptor antagonist CNQX (10 μM; $n = 5$) but were insensitive to the NMDA receptor blocker D-aminophosphonovalerate (D-AP5; 50 μM, $n = 5$, Fig. 3*B*).

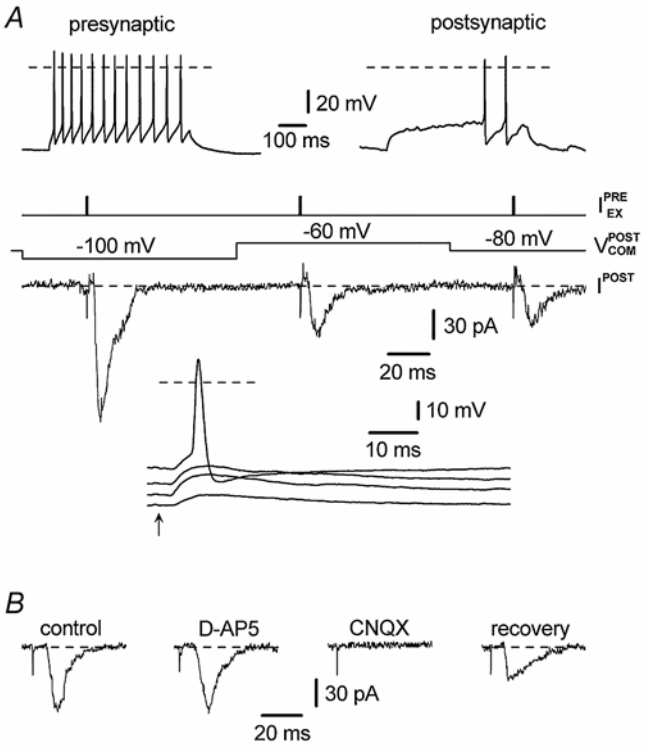

Figure 3. Connections of presynaptic TNs from the SG
A, examples of recordings obtained from one monosynaptic excitatory connection between a TN from the SG and a postsynaptic DN from the SG (25-day-old rat). Recorded EPSCs are given with the corresponding stimulation protocols (above). The current-clamp traces show EPSPs at different membrane potentials in a postsynaptic neuron. The time moment of a cell-attached stimulation of a presynaptic neuron is indicated by an arrow. Note that substantial membrane depolarization of postsynaptic DN was needed for EPSPs to reach the threshold of action potential firing. *B*, EPSCs in the control solution and in the presence of 10 μM CNQX and 50 μM D-aminophosphonovalerate (D-AP5).

The two inhibitory connections of TNs from the SG were interlaminar with a TN from lamina I and with a DN from lamina III (Fig. 6*A*, marked by asterisk).

Presynaptic ANs

All 17 presynaptic ANs were excitatory interneurons (Fig. 4*A*). In accordance with our previous results (Santos *et al.* 2004; Melnick *et al.* 2004*b*), they were mostly found in the lateral SG. In parasagittal sections, ANs were seen only if the surface of the slice included a part of the lateral SG (Fig. 6*B*). Of 17 presynaptic ANs, 12 formed intralaminar contacts with SG neurons (71%), three with lamina I neurons, and two had terminals in lamina III (Table 2). On the basis of firing patterns, presynaptic ANs formed contacts with 6 TNs, 1 AN and 10 DNs. All three excitatory connections to lamina I neurons recorded here were with TNs. The distances between coupled neurons varied from 9 to 54 μm, the mean distance being 21.1 ± 2.9 μm ($n = 17$).

The mean maximum EPSC amplitude was 103.3 ± 33.8 pA ($n = 15$) and the time constant of a decay was 5.0 ± 0.4 ms ($n = 15$). The mean latency was 2.6 ± 0.3 ms ($n = 15$). As with the presynaptic TNs, we also found that EPSCs associated with AN firing were completely blocked by 10 μM CNQX ($n = 4$) but not 50 μM D-AP5 ($n = 4$; Fig. 4*B*).

Excitatory DNs

Of 36 presynaptic DNs 23 were excitatory interneurons (Fig. 5*A*), and 74% of their connections ($n = 17$) were intralaminar with another SG neuron (Fig. 6*C*): 10 with TNs, 6 with ANs, and only 1 with a DN. Beyond the

Table 2. Connections of presynaptic SG neurons

	Postsynaptic neuron									
	Lamina I			Lamina II (SG)			Lamina III			
Presynaptic neuron (SG)	TN	AN	DN	TN	AN	DN	TN	AN	DN	Total
All connections ($n = 102$)										
TN	7 + 1*	—	—	21	8	7	2	—	2 + 1*	49
AN	3	—	—	3	1	8	—	—	2	17
DN (inhibitory)	7	—	—	2	—	3	—	—	1	13
DN (excitatory)	3	—	—	10	6	1	—	—	3	23
2 weeks ($n = 11$)										
TN	1	—	—	1	—	—	1	—	—	3
AN	1	—	—	2	—	—	—	—	—	3
DN (inhibitory)	2	—	—	1	—	—	—	—	—	3
DN (excitatory)	—	—	—	2	—	—	—	—	—	2
3 weeks ($n = 36$)										
TN	3 + 1*	—	—	15	4	2	1	—	1*	27
AN	1	—	—	—	1	2	—	—	—	4
DN (inhibitory)	—	—	—	—	—	2	—	—	—	2
DN (excitatory)	1	—	—	2	—	—	—	—	—	3
4–7 weeks ($n = 55$)										
TN	3	—	—	5	4	5	—	—	2	19
AN	1	—	—	1	—	6	—	—	2	10
DN (inhibitory)	5	—	—	1	—	1	—	—	1	8
DN (excitatory)	2	—	—	6	6	1	—	—	3	18

TN, tonic neuron; AN, adapting neuron; DN, delayed-firing neuron. The upper part of the table summarizes all connections obtained in this study. In lower parts of the table, the data are separated in three groups being presented for 2-week-old rats (postnatal days 15–20), 3-week-old rats (postnatal days 21–27) and 4- to 7-week-old rats (postnatal days 28–49). *Inhibitory connections of presynaptic TNs.

SG, DNs showed excitatory connections with three TNs in lamina I and 3 DNs in lamina III.

The mean value of maximum EPSC was 75.1 ± 16.8 pA ($n = 10$) at -100 mV, with a latency of 2.5 ± 0.4 ms ($n = 10$). The time constant of EPSC decay was 4.5 ± 0.5 ms ($n = 10$). We found that CNQX at 10 μM ($n = 7$), but not 50 μM D-AP5 ($n = 7$), completely blocked the EPSCs (Fig. 5*B*). The mean distance between coupled neurons was 23.8 ± 3.3 μm ($n = 23$; range from 6 to 59 μm).

Inhibitory DNs

The remaining 13 presynaptic DNs were identified as inhibitory interneurons (Fig. 7*A*). A majority of their postsynaptic connections were formed with lamina I neurons ($n = 7$), while only 38% ($n = 5$) with SG neurons (Fig. 7*C* and Table 2). A remaining connection was with another DN from lamina III. Thus, most connections of inhibitory DNs were interlaminar. All seven connections formed in lamina I were with TNs. In total, 13 DNs inhibited 9 TNs and 4 DNs. The distances between coupled neurons varied from 9 to 36 μm, and the mean distance was 21.6 ± 2.5 μm ($n = 13$).

The mean maximum IPSC amplitude was 75.8 ± 28.9 pA ($n = 10$) for inward currents at -100 mV, and 26.5 ± 3.3 pA ($n = 10$) for outward currents at -60 mV. The latency of the inhibitory synaptic response was 2.4 ± 0.4 ms ($n = 10$). The decay kinetics of the IPSCs were fast, the mean time constant was 5.3 ± 0.8 ms ($n = 11$) measured at -100 mV. These IPSCs were completely blocked by the glycine receptor antagonist strychnine (1 μM, $n = 6$, Fig. 7*B*), but not by picrotoxin (100 μM, $n = 5$, Fig. 7*B*).

Finally, we compared major parameters of inhibitory and excitatory DNs: R_{IN}, V_R, the current-clamp membrane time constant, the threshold of the action potential and the spike overshoot (Table 3). None of these parameters was found to be significantly different between two populations of DNs.

Control experiments

To test whether the low frequency of recording from inhibitory SG interneurons might be due to some limitations in the experimental protocol, we changed several parameters and specifically searched for inhibitory interneurons (for this reason the data were not included in the main statistics). First, although the slice thickness in

the above experiments was sufficient to preserve dendritic trees in most types of SG neurons (Grudt & Perl, 2002; Melnick *et al.* 2004*a*,*b*), we further increased the thickness to 500–600 μm in both parasagittal and transverse slices to ensure a complete preservation of distal dendrites. In these parasagittal sections, the slice thickness exceeded the mediolateral extensions of dendrites in all types of SG and lamina I neurons (Grudt & Perl, 2002). In transverse slices, the thickness exceeded the rostrocaudal dimensions of all SG neurons and nonprojection lamina I neurons (Grudt & Perl, 2002). Lamina I projection neurons, with the largest rostrocaudal dendritic extension (mean >700 μm), probably also preserved distal parts of dendrites remaining in the slice, if it was taken into consideration that any sectioning close to the soma of a superficial neuron unavoidably cut about a half of its dendritic tree and the other half is smaller than the thickness of our transverse slice. Second, we changed the amplitude of the first step in the testing voltage command to −120 mV to increase the driving force for IPSCs and therefore their resolution. Third, we made recordings from presumably not connected neuron pairs in 10 μM CNQX, to ensure that IPSCs in these pairs were not masked by glutamate-mediated EPSCs of the same magnitude, and finally we made recordings from pairs of neurons located in the centre of the SG near the interface of laminae II_i and II_o, where Lu & Perl (2003) found inhibitory GABAergic connections.

Under these conditions, we tested an additional 409 pairs of neurons: 107 in parasagittal and 302 in transverse slices. Only 24 neuron pairs (5.9%) were monosynaptically connected. Nineteen connections were excitatory and therefore were not subjected to further study. The remaining five connections were inhibitory. In three of them, the IPSCs were blocked by 1 μM strychnine but not by 100 μM picrotoxin, indicating a glycinergic nature of presynaptic neurons. One of these presynaptic neurons was a DN and two were TNs. In the two remaining connections, the IPSCs were completely blocked by addition of 100 μM picrotoxin but not by 1 μM strychnine. One of these GABAergic presynaptic neurons was a DN shown in Fig. 8, while the other was a TN (not shown). In both GABAergic neurons, the IPSCs were clearly seen at −120 and −60 mV (Fig. 8*A* and *B*) as well as at −100 mV (not shown). Both GABAergic neurons were found near the interface of lamina II_o and II_i, where a total of 54 neuron pairs were

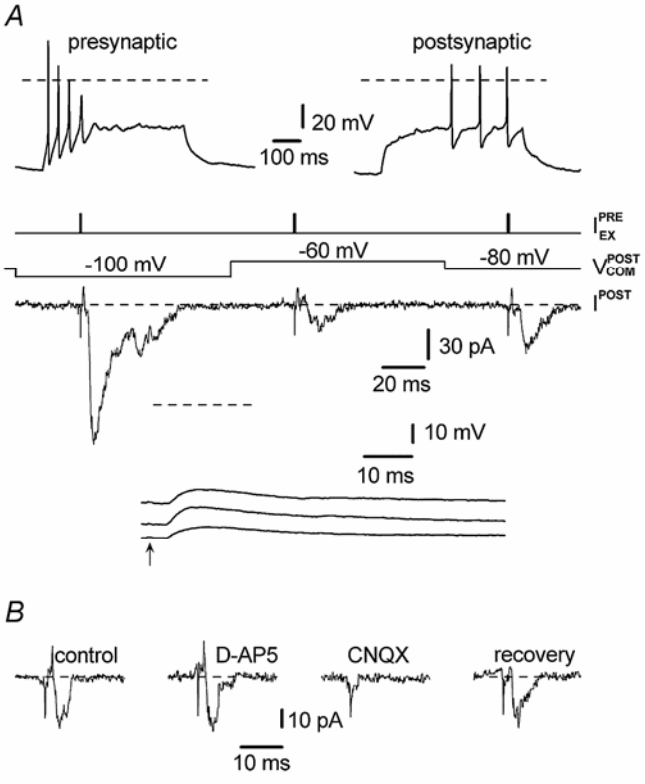

Figure 4. Excitatory connections of ANs
A, examples of recordings obtained from one connection between a presynaptic AN from the SG and a postsynaptic DN from lamina III (26-day-old rat). EPSCs and EPSPs at different voltages in the postsynaptic neuron. The time moment of a cell-attached stimulation of a presynaptic neuron in current-clamp traces is indicated by an arrow. *B*, EPSCs in control solution and in the presence of 10 μM CNQX and 50 μM D-AP5.

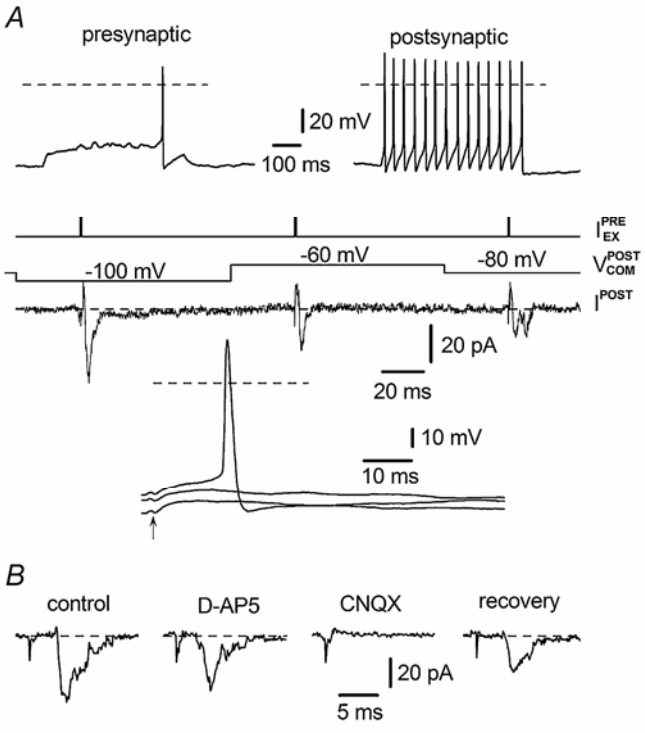

Figure 5. Monosynaptic excitatory connections of DNs
A, examples of recordings from a connection between a presynaptic DN from the SG and a postsynaptic TN from lamina I (26-day-old rat). EPSCs and EPSPs at different voltages were recorded in the postsynaptic neuron. The time moment of a cell-attached stimulation of a presynaptic neuron in current-clamp traces is indicated by an arrow. *B*, EPSCs in control solution and in the presence of 10 μM CNQX and 50 μM D-AP5.

tested. In eight pairs of apparently not connected neurons, recordings were also done in the presence of 10 μM CNQX. In none of them IPSCs became visible after addition of the blocker, indicating that in these pairs IPSCs were not masked by EPSCs.

Thus, these control experiments confirmed the adequate resolution of IPSCs in all our experiments and the overall low percentage of inhibitory connections of SG neurons with their possible region-specific localization.

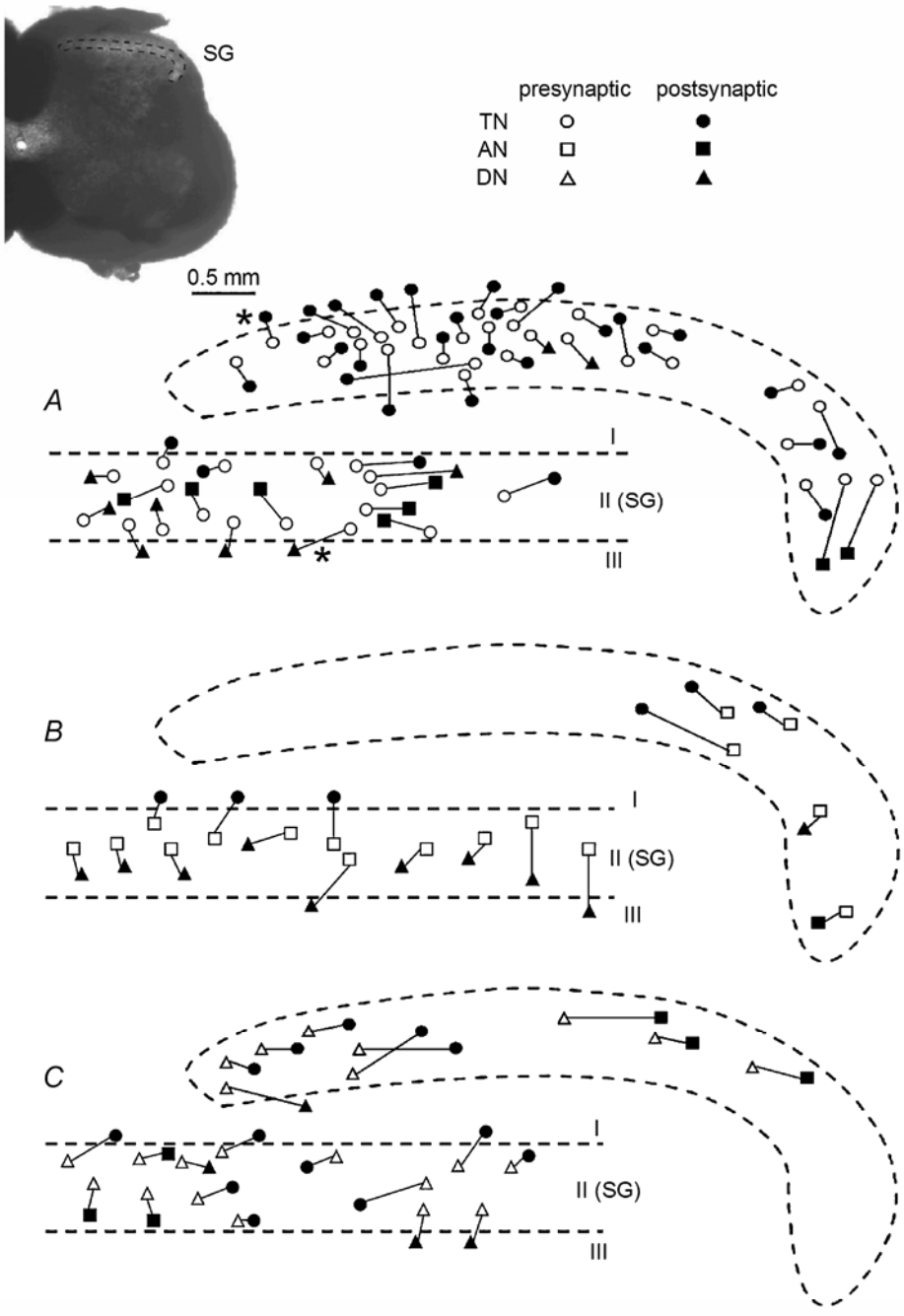

Figure 6. Distribution of excitatory connections of presynaptic SG interneurons
The diagrams of distributions of excitatory connections between presynaptic TNs (*A*), ANs (*B*) and DNs (*C*) from the SG and different types of postsynaptic neurons located in laminae I, II (SG) and III. Data from both transverse (upper) and parasagittal (lower) sections. Dashed lines indicate the border of the SG. In this and the following figure, all pre- and postsynaptic neurons are indicated by open and filled symbols, respectively. The two inhibitory connections of TNs are marked by asterisks in *A*.

Table 3. Comparison of inhibitory and excitatory DNs

	R_{IN}	V_R	Membrane time constant	Spike threshold	Spike overshoot	DN subtype			
	(GΩ)	(mV)	(ms)	(mV)	(mV)	DN_1	DN_2	DN_3	Total
Inhibitory	1.74 ± 0.43 (10)	−74.1 ± 0.7 (10)	64.3 ± 15.5 (10)	−45.7 ± 1.2 (10)	+17.4 ± 3.1 (10)	8	3	2	13
Excitatory	1.72 ± 0.18 (10)	−73.4 ± 0.9 (10)	63.5 ± 7.19 (10)	−46.3 ± 1.6 (10)	+11.6 ± 1.6 (10)	9	7	7	23
t Test	$P = 0.98$, n.s.	$P = 0.55$, n.s.	$P = 0.97$, n.s.	$P = 0.77$, n.s.	$P = 0.11$, n.s.	—	—	—	—

The parameters were compared by independent Student's *t* test, n.s., not significant. Description of minor differences between subtypes DN_1, DN_2 and DN_3 of DNs is given in Methods. Numbers of recordings are given in parentheses.

Discussion

The principal finding of this study is that the intrinsic integration in the SG is dominated by excitatory processing. We implemented a novel experimental strategy for efficiently identifying neuronal connections and found that 85% of axosomatic or axodendritic connections formed by SG interneurons were excitatory. Such a high proportion of excitatory interneurons is in a good agreement with previous morphological studies. *In situ* hybridization for three types of vesicular glutamate transporters VGLUT1, 2 and 3 revealed their expression in 38, 33 and 6% of laminae I–II neurons, respectively (Landry *et al.* 2004). Since 14% of neurons positive for either VGLUT1 or VGLUT2 were also positive for both these transporters, one can estimate that glutamatergic neurons represent 68% of the neuronal population. Another study found that 31 and 14% of SG neurons were GABA and glycine

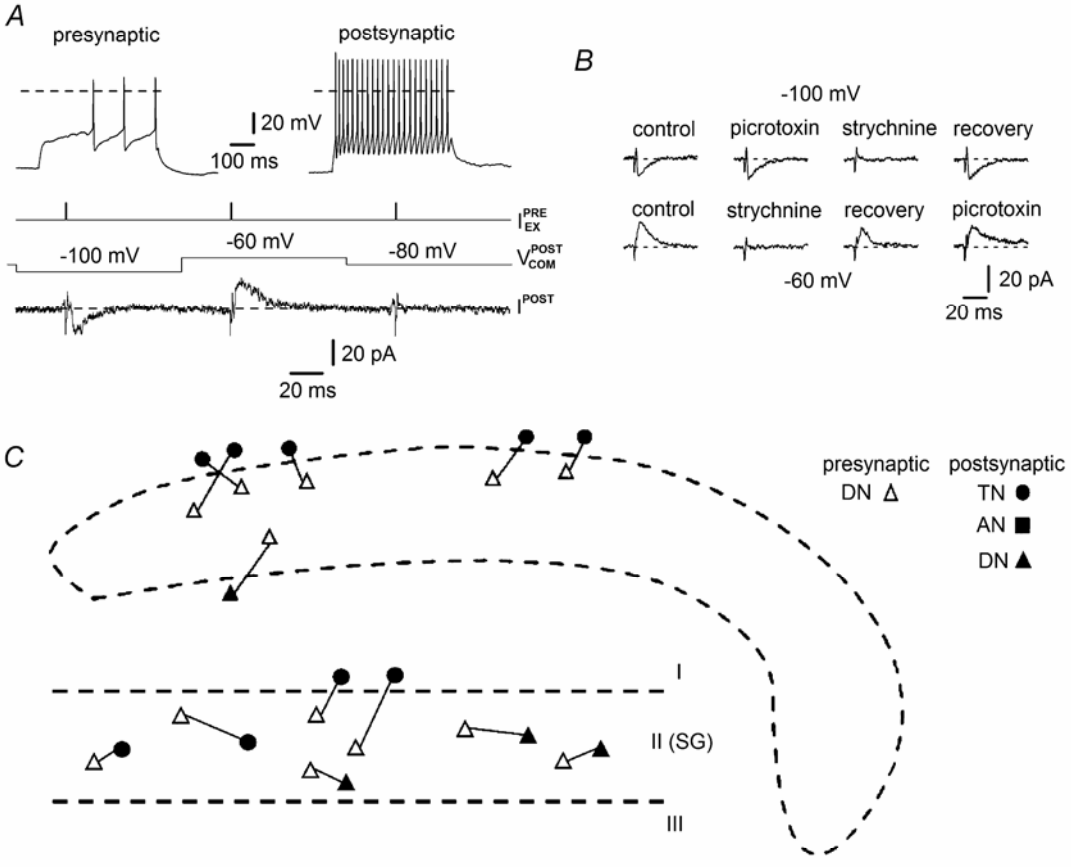

Figure 7. Monosynaptic connections of inhibitory DNs
A, recordings from an inhibitory connection between a presynaptic DN from the SG and a postsynaptic TN from the SG (19-day-old rat). IPSCs at different voltages in the postsynaptic neuron. *B*, IPSCs in control solution and in the presence of 1 μM strychnine or 100 μM picrotoxin. Recordings were made at −100 and −60 mV from the same neuron. *C*, the distributions of monosynaptic connections between inhibitory DNs from the SG and different postsynaptic neurons located in laminae I–III.

immunoreactive, respectively, and all glycine-immunoreactive cells were also GABA immunoreactive (Todd & Sullivan, 1990), suggesting that inhibitory interneurons represented 31% of SG neurons. These estimates for excitatory and inhibitory neurons are highly consistent with our data if one assumes that some inhibitory neurons may form presynaptic axoaxonic synapses and therefore cannot be detected by our technique. It is also possible that somata of excitatory interneurons originate a larger number of axonal collaterals and functional synapses than the somata of inhibitory interneurons.

In terms of integral organization of the SG neuronal network, our data suggest that, regardless of firing pattern, a majority of SG excitatory interneurons form intralaminar connections, while those of inhibitory SG neurons are mostly interlaminar. The relative number of inhibitory connections was higher for projections from the SG to lamina I (8 of 21, Table 2) and to lamina III (2 of 11, Table 2) being lower for internal projections within the SG (5 of 70, Table 2). The latter may indicate that spontaneous miniature IPSCs recorded in a vast majority of SG neurons (Chéry & De Koninck, 1999) are mostly induced by neurons located outside the SG.

We have also demonstrated that intrinsic firing of a SG neuron correlates with its function in such a way that a vast majority of TNs and ANs are excitatory interneurons, whereas DNs could be both excitatory and inhibitory interneurons. An adequate classification of neuronal firing patterns was critical for this study. Because of conflicting reports on discharge properties and membrane parameters of SG neurons, we took several precautions to ensure correct identification. In particular, we used the voltage-follower with a balanced input (Santos *et al.* 2004) to measure V_R and R_{IN}, studied passive membrane properties and discharge patterns at physiological temperatures and recorded through perforated patches to maximally preserve the intracellular environment critical for measured parameters. These experiments confirmed the three basic types of SG neurons, i.e. TNs, ANs and DNs, proposed previously (Grudt & Perl, 2002; Santos *et al.* 2004). Our whole-cell recordings have also shown that a BAPTA-based internal solution preserved the physiological firing patterns. This suggests that (1) these neurons have highly buffered Ca^{2+} under normal physiological conditions, and (2) firing patterns are highly Ca^{2+} dependent.

Our observations may also help to explain discrepancies in firing patterns between different reports. We found that the mean R_{IN} was above 1 GΩ and V_R was close to −70 mV for all cell types. High R_{IN} appears to be important for correct identification of TNs. Indeed, in the majority of them, the tonic firing could be selectively transformed into adapting upon R_{IN} reduction, for example, due to GIRK current activation by μ-opioids (Santos *et al.* 2004). Likewise, lowering R_{IN} in ANs frequently transformed their typical pattern into a single spike (unpublished observations). However, the basic firing pattern of both TNs and ANs was weakly sensitive to V_R, due to low expression of transient K^+ channels (Melnick *et al.* 2004*a*,*b*). In contrast, V_R was critical for correctly identifying DNs. Membrane depolarization can inactivate a pronounced transient K^+ current conductance and shorten the characteristic delay of the firing onset (Yoshimura & Jessell, 1989), thus inducing a tonic-like discharge. Furthermore, transient K^+ current in dorsal horn neurons was inhibited by Ca^{2+}-dependent protein kinase C and A (Hu & Gereau, 2003; Hu *et al.* 2003), suggesting that insufficient buffering for Ca^{2+} may transform the delayed-onset firing into tonic firing.

TNs in the SG can function as signal integrators (Prescott & De Koninck, 2002) because their discharge frequency increases with the stimulation intensity being regulated by the apamin-sensitive Ca^{2+}-activated K^+ conductance (Melnick *et al.* 2004*a*). Their axons project to the SG itself as well as to neighbouring laminae I and III (Melnick *et al.* 2004*a*). The present study shows that the vast majority of TNs are excitatory neurons interconnecting laminae I, II and III. The most abundant type of their connection was intralaminar with other

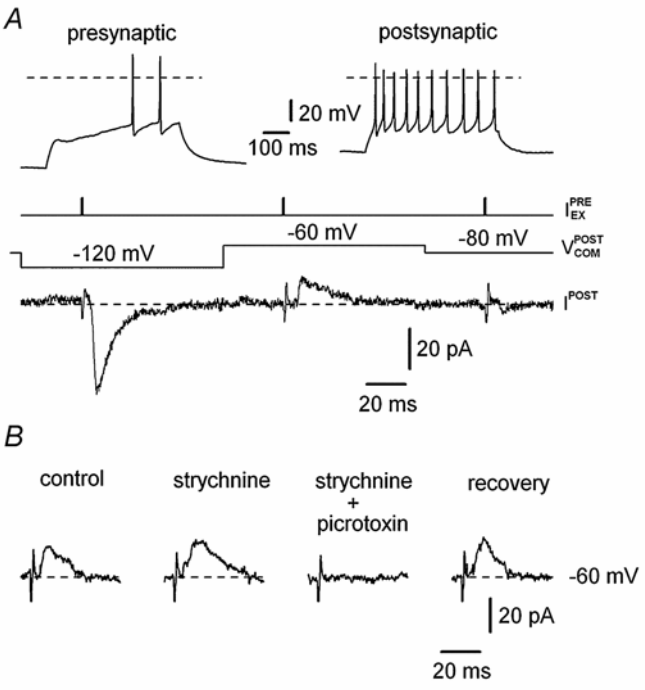

Figure 8. Monosynaptic connection of a GABAergic inhibitory DN

A, an inhibitory connection between a presynaptic DN and a postsynaptic TN in the SG (17-day-old rat). IPSCs recorded at −120, −60 and −80 mV in the postsynaptic neuron. *B*, IPSCs in control solution, in the presence of 1 μM strychnine and in the presence of 1 μM strychnine and 100 μM picrotoxin. At −60 mV, all recordings are from the same neuron.

TNs. This implies that excitatory circuitry involving two intrinsic TNs form an important block in SG processing. Importantly, excitatory TNs synapse on TNs from lamina I, a region where most nociceptive projection neurons are located (Burstein *et al.* 1987; Lima & Coimbra, 1988; Lima, 1998).

We have recently shown that TN is the only SG cell type directly inhibited by the μ-opioid agonist (Santos *et al.* 2004). The present classification of TNs as predominantly excitatory interneurons strongly supports the idea of specific targeting of postsynaptic μ-opioid receptors to excitatory SG interneurons (Kemp *et al.* 1996). Because of their numerous excitatory connections throughout the superficial dorsal horn, a selective inhibition of TNs may underlie the analgesic postsynaptic effects of endogenous enkephalins and administered opioids (Duggan *et al.* 1977; Johnston & Duggan, 1981).

ANs are preferentially located in the lateral SG and their dendritic tree and axonal arborization have pronounced rostrocaudal orientation, with a limited spread in the mediolateral and dorsoventral dimentions (Santos *et al.* 2004; Melnick *et al.* 2004*b*). Their characteristic firing adaptation results from a relatively low expression of voltage-gated Na^+ channels and is not regulated by Ca^{2+}-dependent K^+ mechanisms (Melnick *et al.* 2004*b*). The 'input–output' properties allow ANs to function as coincidence detectors (Prescott & De Koninck, 2002). Here we further show that ANs are excitatory interneurons forming most of their functional connections with local SG neurons. In the context of neuronal network therefore ANs appear to be mostly involved in the intralaminar excitatory processing within the lateral SG.

DNs can be both excitatory and inhibitory interneurons. Our statistical analysis did not reveal differences in membrane parameters between these two subpopulations. The majority of excitatory DNs made connections within the SG with local TNs. In contrast, inhibitory DNs formed most connections with lamina I TNs. Some of them released glycine acting on the strychnine-sensitive receptors. This is in accordance with observations that spontaneous miniature IPSCs in lamina I neurons were almost exclusively mediated through strychnine-sensitive glycine receptors (Chéry & De Koninck, 1999). The mean time constant of the IPSC decay (5.3 ms) obtained here is close to that of glycine-receptor-mediated IPSCs in lamina I–II neurons (Chéry & De Koninck, 1999). In general, membrane properties of DNs allow them to act as input integrators with a high firing threshold regulated by transient K^+ current. Modulation of transient K^+ current by protein kinase A and C, as well as by membrane potential, provides the mechanisms for the regulation of sensory processing in both excitatory and inhibitory circuitries.

The present data are in agreement with excitatory connections reported for ANs and DNs (Lu & Perl, 2005). According to our control experiments, a few per cent of TNs and DNs in the SG can also be GABAergic interneurons. Indeed, the GABAergic neurons with tonic firing were identified by simultaneous recordings (Lu & Perl, 2003) or green fluorescent protein expression (Hantman *et al.* 2004). It seems that neuron pairs with GABAergic connections are mostly localized in a narrow transitional zone between laminae II_i and II_o (Lu & Perl, 2003; our observations) and therefore the probability of finding them in the rest of the SG is very low. It is also possible that (1) in the majority of inhibitory synapses formed by SG neurons, $GABA_A$ receptors are extrasynaptic and therefore coreleased GABA and glycine predominantly evoke glycine-mediated IPSCs (Chery & De Koninck, 1999); and/or (2) some GABAergic neurons in the SG are involved in presynaptic inhibition of primary afferent terminals (reviewed in Lima, 1996), and thus cannot be identified by simultaneous recording from neuronal pairs.

One essential finding of this study is that excitatory synapses dominating the neuronal network in the SG are glutamatergic. Our results also indicate that fast synaptic transmission in these synapses is mediated through AMPA and/or kainate receptors, since EPSCs were completely blocked by CNQX. Although kainate receptors had been implicated in the synaptic transmission of Aδ- and C-fibre inputs to the SG (Youn & Randic, 2004) and in the modulation of transmitter release (Engelman & MacDermott, 2004), their activation under our experimental conditions was unlikely because it required much higher intensity of stimulation (Frerking *et al.* 1998; Lee *et al.* 2004), and EPSCs mediated by kainate receptors had much slower kinetics (Frerking *et al.* 1998; Cossart *et al.* 2002). In contrast, our data imply involvement of AMPA receptors, thus being consistent with observations of others that AMPA receptors are highly expressed in the superficial dorsal horn synapses (Tachibana *et al.* 1994; Tolle *et al.* 1995; Petralia *et al.* 1997) and modulate spinal synaptic plasticity and inflammatory pain (Hartmann *et al.* 2004).

In conclusion, the present study has revealed that the sensory integration in the SG is dominated by excitatory processing and that the intrinsic firing properties of SG interneurons correlate with their functions. Excitatory processing is mostly intralaminar, in contrast to the inhibition, which is preferentially interlaminar. This organization of neuronal circuitries in the spinal SG can be important for nociceptive encoding.

References

Bentley GN & Gent JP (1994). Electrophysiological properties of substantia gelatinosa neurones in a novel adult spinal slice preparation. *J Neurosci Methods* **53**, 157–162.

Brown AG (1981). *Organization in the Spinal Cord*. Springer-Verlag, Berlin, Heidelberg.

Burstein R, Cliffer KD & Giesler GJ Jr (1987). Direct somatosensory projections from the spinal cord to the hypothalamus and telencephalon. *J Neurosci* **7**, 4159–4164.

Cervero F (1987). Dorsal horn neurones and their sensory inputs. In *Spinal Afferent Processing*, ed.Yaksh TL, pp. 197–216. Plenum Press, New York.

Chéry N & De Koninck Y (1999). Junctional versus extrajunctional glycine and $GABA_A$ receptor-mediated IPSCs in identified lamina I neurons of the adult rat spinal cord. *J Neurosci* **19**, 7342–7355.

Cossart R, Epsztein J, Tyzio R, Becq H, Hirsch J, Ben-Ari Y & Crepel V (2002). Quantal release of glutamate generates pure kainate and mixed AMPA/kainate EPSCs in hippocampal neurons. *Neuron* **35**, 147–159.

Duggan AW, Hall JG & Headley PM (1977). Suppression of transmission of nociceptive impulses by morphine: selective effects of morphine administered in the region of the substantia gelatinosa. *Br J Pharmacol* **61**, 65–76.

Engelman HS & MacDermott AB (2004). Presynaptic ionotropic receptors and control of transmitter release. *Nat Rev Neurosci* **5**, 135–145.

Frerking M, Malenka RC & Nicoll RA (1998). Synaptic activation of kainate receptors on hippocampal interneurons. *Nat Neurosci* **1**, 479–486.

Graham BA, Brichta AM & Callister RJ (2004). *In vivo* responses of mouse superficial dorsal horn neurones to both current injection and peripheral cutaneous stimulation. *J Physiol* **561**, 749–763.

Grudt TJ & Perl ER (2002). Correlations between neuronal morphology and electrophysiological features in the rodent superficial dorsal horn. *J Physiol* **540**, 189–207.

Hantman AW, van den Pol AN & Perl ER (2004). Morphological and physiological features of a set of spinal substantia gelatinosa neurons defined by green fluorescent protein expression. *J Neurosci* **24**, 836–842.

Hartmann B, Ahmadi S, Heppenstall PA, Lewin GR, Schott C, Borchardt T, Seeburg PH, Zeilhofer HU, Sprengel R & Kuner R (2004). The AMPA receptor subunits GluR-A and GluR-B reciprocally modulate spinal synaptic plasticity and inflammatory pain. *Neuron* **44**, 637–650.

Horn R & Marty A (1988). Muscarinic activation of ionic currents measured by a new whole-cell recording method. *J Gen Physiol* **92**, 145–159.

Hu H-J & Gereau RW (2003). ERK integrates PKA and PKC signaling in superficial dorsal horn neurons. II. Modulation of neuronal excitability. *J Neurophysiol* **90**, 1680–1688.

Hu H-J, Glauner KS & Gereau RW (2003). ERK integrates PKA and PKC signalling in superficial dorsal horn neurons. I. Modulation of A-type K^+ currents. *J Neurophysiol* **90**, 1671–1679.

Ji RR, Kohno T, Moore KA & Woolf CJ (2003). Central sensitization and LTP: do pain and memory share similar mechanisms? *Trends Neurosci* **26**, 696–705.

Johnston SM & Duggan AW (1981). Evidence that opiate receptors of the substantia gelatinosa contribute to the depression, by intravenous morphine, of the spinal transmission of impulses in unmyelinated afferents. *Brain Res* **207**, 223–228.

Kemp T, Spike RC, Watt C & Todd AJ (1996). The μ-opioid receptor (MOR1) is mainly restricted to neurons that do not contain GABA or glycine in the superficial dorsal horn of the rat spinal cord. *Neurosci* **75**, 1231–1238.

LaMotte C (1977). Distribution of the tract of lissauer and the dorsal root fibers in the primate spinal cord. *J Comp Neurol* **172**, 529–561.

Landry M, Bouali-Benazzouz R, El Mestikawy S, Ravassard P & Nagy F (2004). Expression of vesicular glutamate transporters in rat lumbar spinal cord, with a note on dorsal root ganglia. *J Comp Neurol* **468**, 380–394.

Lee CJ, Labrakakis C, Joseph DJ & Macdermott AB (2004). Functional similarities and differences of AMPA and kainate receptors expressed by cultured rat sensory neurons. *Neuroscience* **129**, 35–48.

Light AR & Perl ER (1977). Differential termination of large-diameter and small-diameter primary afferent fibers in the spinal dorsal gray matter as indicated by labelling with horseradish peroxidase. *Neurosci Lett* **6**, 59–63.

Lima D (1996). Endogenous pain modulatory system in the light of the gate control theory. *Pain Forum* **5**, 31–39.

Lima D (1998). Anatomical basis for the dynamic processing of nociceptive input. *Eur J Pain* **2**, 195–202.

Lima D & Coimbra A (1988). The spinothalamic system of the rat: structural types of retrogradely labelled neurons in the marginal zone (lamina I). *Neurosci* **27**, 215–230.

Lisman J & Spruston N (2005). Postsynaptic depolarization requirements for LTP and LTD: a critique of spike timing-dependent plasticity. *Nat Neurosci* **8**, 839–841.

Lopez-Garcia JA & King AE (1994). Membrane properties of physiologically classified rat dorsal horn neurons *in vitro*: correlation with cutaneous sensory afferent input. *Eur J Neurosci* **6**, 998–1007.

Lu Y & Perl ER (2003). A specific inhibitory pathway between substantia gelatinosa neurons receiving direct C-fiber input. *J Neurosci* **23**, 8752–8758.

Lu Y & Perl ER (2005). Modular organization of excitatory circuits between neurons of the spinal superficial dorsal horn (laminae I and II). *J Neurosci* **25**, 3900–3907.

Malenka RC & Bear MF (2004). LTP and LTD: an embarrassment of riches. *Neuron* **44**, 5–21.

Malenka RC & Nicoll RA (1999). Long-term potentiation – a decade of progress? *Science* **285**, 1870–1874.

Melnick IV, Santos SFA & Safronov BV (2004*b*). Mechanism of spike frequency adaptation in substantia gelatinosa neurones of rat. *J Physiol* **559**, 383–395.

Melnick IV, Santos SFA, Szokol K, Szucs P & Safronov BV (2004*a*). Ionic basics of tonic firing in spinal substantia gelatinosa neurons of rat. *J Neurophysiol* **91**, 646–655.

Petralia RS, Wang YX, Mayat E & Wenthold RJ (1997). Glutamate receptor subunit 2-selective antibody shows a differential distribution of calcium-impermeable AMPA receptors among populations of neurons. *J Comp Neurol* **385**, 456–476.

Prescott SA & De Koninck Y (2002). Four cell types with distinctive membrane properties and morphologies in lamina I of the spinal dorsal horn of the adult rat. *J Physiol* **539**, 817–836.

Rae J, Cooper K, Gates P & Watsky M (1991). Low access resistance perforated patch recordings using amphotericin B. *J Neurosci Methods* **37**, 15–26.

Rethelyi M (1977). Preterminal and terminal axon arborizations in the substantia gelatinosa of cat's spinal cord. *J Comp Neurol* **172**, 511–521.

Ruscheweyh R & Sandkuhler J (2002). Lamina-specific membrane and discharge properties of rat spinal dorsal horn neurones *in vitro*. *J Physiol* **541**, 231–244.

Salter MW (2005). Cellular signalling pathways of spinal pain neuroplasticity as targets for analgesic development. *Curr Top Med Chem* **5**, 557–567.

Santos SFA, Melnick IV & Safronov BV (2004). Selective inhibition of tonic-firing neurons in substantia gelatinosa by μ-opioid agonist. *Anesthesiology* **101**, 1177–1183.

Sugiura Y, Lee CL & Perl ER (1986). Central projections of identified, unmyelinated (C) afferent fibers innervating mammalian skin. *Science* **234**, 358–361.

Tachibana M, Wenthold RJ, Morioka H & Petralia RS (1994). Light and electron microscopic immunocytochemical localization of AMPA-selective glutamate receptors in the rat spinal cord. *J Comp Neurol* **344**, 431–454.

Thomson AM, West DC & Headley PM (1989). Membrane characteristics and synaptic responsiveness of superficial dorsal horn neurons in a slice preparation of adult rat spinal cord. *Eur J Neurosci* **1**, 479–488.

Todd AJ & Sullivan AC (1990). Light microscope study of the coexistence of GABA-like and glycine-like immunoreactivities in the spinal cord of the rat. *J Comp Neurol* **296**, 496–505.

Tolle TR, Berthele A, Zieglgansberger W, Seeburg PH & Wisden W (1995). Flip and Flop variants of AMPA receptors in the rat lumbar spinal cord. *Eur J Neurosci* **7**, 1414–1419.

Turrigiano GG & Nelson SB (2004). Homeostatic plasticity in the developing nervous system. *Nat Rev Neurosci* **5**, 97–107.

Willis WD & Coggeshall RE (1991). *Sensory Mechanisms of the Spinal Cord*. Plenum Press, New York.

Woolf CJ & Salter MW (2000). Neuronal plasticity: increasing the gain in pain. *Science* **288**, 1765–1769.

Yoshimura M & Jessell TM (1989). Membrane properties of rat substantia gelatinosa neurons *in vitro*. *J Neurophysiol* **62**, 109–118.

Youn DH & Randic M (2004). Modulation of excitatory synaptic transmission in the spinal substantia gelatinosa of mice deficient in the kainate receptor GluR5 and/or GluR6 subunit. *J Physiol* **555**, 683–698.

Acknowledgements

We thank Drs Larry Trussell, John Williams and Ed McCleskey for insightful comments and discussions. The work was supported by the grant from the Portuguese Foundation for Science and Technology funded by POCTI2010 and FEDER (to B.V.S.), Medical Research Foundation grant (to V.A.D.) and NIH grant (to V.A.D. and Dr Thomas Soderling).

Third publication

OPEN ACCESS Freely available online

PLoS one

Transmission Efficacy and Plasticity in Glutamatergic Synapses Formed by Excitatory Interneurons of the Substantia Gelatinosa in the Rat Spinal Cord

Sónia F. A. Santos[1,2]*, Liliana L. Luz[1,2], Peter Szucs[1], Deolinda Lima[2], Victor A. Derkach[3], Boris V. Safronov[1,2]

1 Instituto de Biologia Molecular e Celular (IBMC), Universidade do Porto, Porto, Portugal, **2** Laboratório de Biologia Celular e Molecular, Faculdade de Medicina, Universidade do Porto, Porto, Portugal, **3** Vollum Institute, Oregon Health and Science University, Portland, Oregon, United States of America

Abstract

Background: Substantia gelatinosa (SG, lamina II) is a spinal cord region where most unmyelinated primary afferents terminate and the central nociceptive processing begins. The glutamatergic excitatory interneurons (EINs) form the majority of the SG neuron population, but little is known about the mechanisms of signal processing in their synapses.

Methodology: To describe the functional organization and properties of excitatory synapses formed by SG EINs, we did non-invasive recordings from 183 pairs of monosynaptically connected neurons. An intact presynaptic SG EIN was specifically stimulated through the cell-attached pipette while the evoked EPSCs/EPSPs were recorded through perforated-patch from a postsynaptic neuron (laminae I-III).

Principal Findings: We found that the axon of an SG EIN forms multiple functional synapses on the dendrites of a postsynaptic neuron. In many cases, EPSPs evoked by stimulating an SG EIN were sufficient to elicit spikes in a postsynaptic neuron. EPSCs were carried through both Ca^{2+}-permeable (CP) and Ca^{2+}-impermeable (CI) AMPA receptors (AMPARs) and showed diverse forms of functional plasticity. The synaptic efficacy could be enhanced through both activation of silent synapses and strengthening of already active synapses. We have also found that a high input resistance (R_{IN}, >0.5 GΩ) of the postsynaptic neuron is necessary for resolving distal dendritic EPSCs/EPSPs and correct estimation of their efficacy.

Conclusions/Significance: We conclude that the multiple synapses formed by an SG EIN on a postsynaptic neuron increase synaptic excitation and provide basis for diverse forms of plasticity. This functional organization can be important for sensory, i.e. nociceptive, processing in the spinal cord.

Citation: Santos SFA, Luz LL, Szucs P, Lima D, Derkach VA, et al. (2009) Transmission Efficacy and Plasticity in Glutamatergic Synapses Formed by Excitatory Interneurons of the Substantia Gelatinosa in the Rat Spinal Cord. PLoS ONE 4(11): e8047. doi:10.1371/journal.pone.0008047

Editor: Hitoshi Okazawa, Tokyo Medical and Dental University, Japan

Received June 5, 2009; **Accepted** November 4, 2009; **Published** November 30, 2009

Funding: The work was supported by the grant from the Portuguese Foundation for Science and Technology (to B.V.S.), Medical Research Foundation grant (to V.A.D.) and NIH grant NS027037 (to Thomas Soderling and V.A.D.). The funders had no role in study design, data collection and analysis, decision to publish, or preparation of the manuscript.

Competing Interests: The authors have declared that no competing interests exist.

* E-mail: safronov@ibmc.up.pt

Introduction

The spinal SG is an important part of the nociceptive processing system. It is mostly formed by local excitatory and inhibitory interneurons, some of which relay the primary afferent inputs to projection neurons in lamina I [1 6]. The SG is frequently considered in terms of the gate control theory [7] emphasising the role of inhibitory circuits, and perhaps for this reason, organization of excitatory circuits was less studied [6]. There are however a number of reports indicating importance of SG EINs. Independent studies using *in situ* hybridization, immunocytochemistry and paired electrophysiological recordings showed that the majority of SG neurons are excitatory, while inhibitory neurons represent a minority [4,8,9]. Immunocytochemistry and EM studies have also revealed that excitatory synapses in the superficial dorsal horn express both GluR2-containing CI-AMPARs and GluR2-lacking CP-AMPARs [10 13]. The contribution of CP-AMPARs to transmission may increase under chronic pain conditions [14 17]. The superficial dorsal horn also expresses Ca^{2+}-calmodulin dependent protein kinase II [18,19] involved in plasticity induction upon Ca^{2+} entry in glutamatergic synapses [11,20,21]. Therefore, non-NMDAR synapses of SG EINs [4] might undergo plasticity based on CP-AMPARs. The physiological evidences for plasticity in the SG EIN synapses and for involvement of CP-AMPARs in transmission from SG EINs have not been reported so far.

Here we combined paired recording, computer simulation and biocytin-labelling to study functional organization and activity-dependent modification of glutamatergic synapses of SG EINs. Special care was taken to choose experimental conditions for recording from pairs of monosynaptically connected cells. It is known that the efficacy of synaptic transmission depends on passive membrane properties of a postsynaptic neuron, i.e. R_{IN} and membrane time constant, which vary with the composition of intracellular recording solution. R_{IN} in SG neurons is above 1 GΩ

when measured in the whole-cell mode with pipette solutions containing strong Ca^{2+} chelators [4,22,23] or in the perforated-patch mode [4] which prevents dialysis of cytoplasmic factors and Ca^{2+} [24,25]. R_{IN} is lower when measured in whole-cell with Ca^{2+}-chelator-free solutions (158 MΩ, [26]). On the other hand, the presence of a strong Ca^{2+} chelator in the presynaptic neuron may affect synaptic release [27]. For these reasons, we did paired recordings under conditions preserving the cytoplasmic composition in both neurons. Recording from the postsynaptic neuron was done in the perforated-patch mode while the intact presynaptic SG EIN was specifically stimulated through a cell-attached pipette. The cell-attached pipette was also used for the SG EIN labelling with biocytin [28] for the analysis of its axon terminals.

We show that axon of an SG EIN forms multiple functional synapses on dendrites of a postsynaptic neuron. In many cases, EPSPs evoked by stimulating an SG EIN initiated postsynaptic spikes. The EPSCs were carried through both CP- and CI-AMPARs, and showed different forms of plasticity. The synaptic efficacy could be increased through the activation of silent synapses and through the increase in the strength of active synapses. We also show that a high R_{IN} (>0.5 GΩ) in a postsynaptic neuron is necessary for resolving the distal dendritic inputs. It is concluded that the multiple synapses of an SG EIN on a postsynaptic neuron increase efficacy of transmission and provide basis for diverse forms of plasticity.

Methods

Preparation

Rats (2-6-weeks) were sacrificed in accordance with the national guidelines (Direcção Geral de Veterinária, Ministério da Agricultura) after the anaesthesia by intraperitoneal injection of Na^+-pentobarbital (30 mg/kg) and subsequent check for lack of pedal withdrawal reflexes. The procedure has been approved by the institutional ethics committee (Comissão de Ética do Instituto de Biologia Molecular e Celular). Transverse slices (200 300 μm) were prepared from the lumbar spinal cord as described [22,23]. Neurons were visualized in slices using the oblique LED illumination technique [28,29]. The SG was identified in the dorsal horn as a light band of about 60 μm thickness in its intermediate region as previously described [4]. The marginal 20 μm layer separating the SG from the white matter was considered as lamina I.

Solutions and Junction Potentials

ACSF contained (in mM): NaCl 115, KCl 3, $CaCl_2$ 2, $MgCl_2$ 1, NaH_2PO_4 1, $NaHCO_3$ 25 and glucose 11 (pH 7.4; bubbled with 95% O_2/5% CO_2). The perforated-patch pipettes were filled with solution containing (in mM): NaCl 5, K-gluconate 145, HEPES 10 (pH 7.3 adjusted with KOH, final $[K^+]$ was 148 mM) and amphotericin B (100 μg/ml). Amphotericin B forms pores permeable to small monovalent ions Na^+, K^+ and Cl^-, but not to Ca^{2+} and large cytoplasmic anions [25,30]. In pipette solution, we used impermeable gluconate as the major anion and set $[Cl^-]$ to its cytoplasmic level (5 mM) to have negligible Donnan equilibrium junction potential [24,30]. The liquid junction potential [31,32] between the pipette and bath solutions was 15.5 mV; it was corrected for in all recordings. The stimulating pipettes were filled with ACSF. D-AP5, GYKI-52466, SYM 2081 and IEM 1460 were from Tocris. All the remaining chemicals were from Sigma.

Biocytin Labelling

In the labelling experiments, a postsynaptic neuron was filled by biocytin in the whole-cell mode using pipette containing (in mM): KCl 3, K-gluconate 150.5, $MgCl_2$ 1, BAPTA 1 and HEPES 10 (pH 7.3 adjusted with KOH, final $[K^+]$ was 160.5 mM) and 1% biocytin. An intact presynaptic SG EIN was filled (without rupturing the patch membrane) through the cell-attached stimulating pipette [28] which contained 500 mM NaCl and 1.5% biocytin. Increased osmomolarity improved biocytin efflux from the cell-attached pipette and filling the neuron. Labelled neurons were processed and reconstructed as described [28]. Due to different experimental conditions, these recordings were not included in the statistics based on perforated-patch recordings.

Computer Simulation

Simulations were done using NEURON software [33,34] and the SG neuron model from [23] (http://senselab.med.yale.edu/ModelDb, 62285). This basic model had R_{IN} of 1.6 GΩ, the membrane time constant of 91 ms and the dendrite electrotonic length of 0.68 λ [23]. Voltage-dependent Na^+ and K^+ conductances were set to zero, while the electrotonic EPSC/EPSP propagation was analysed. A two-state kinetic scheme was used to model the synaptic response. The current flowing through the channels in the synapse activated by transmitter release (I_S) was described by the following equation:

$$I_S = \tau_D/(\tau_D - \tau_R) * [\exp(-t/\tau_D) - \exp(-t/\tau_R)] * g_M * (V - E_{Rev}),$$

where τ_R is the conductance rise time constant, τ_D is the conductance decay time constant, g_M is the maximum conductance, V is the membrane potential and E_{Rev} is the reversal potential (set to 0 mV). According to our Results, the constants τ_R and τ_D were set to 0.5 ms and 5 ms, respectively. R_{IN} was reduced from 1.6 GΩ to 1 GΩ, 500 MΩ, 300 MΩ, 200 MΩ and 100 MΩ by increasing the specific passive membrane conductance from $1.1*10^{-5}$ S/cm^2 to $1.9*10^{-5}$ S/cm^2, $4.8*10^{-5}$ S/cm^2, $1.05*10^{-4}$ S/cm^2, $2.1*10^{-4}$ S/cm^2 and $6.6*10^{-4}$ S/cm^2, respectively. Simulations were done for the resting/holding potential of −70 mV. The synapse location and g_M are specified in figures.

Electrophysiology

Recording pipettes were pulled from thick-walled glass (BioMedical Instruments, Germany) and fire-polished (resistance, 3 5 MΩ). The stimulating pipettes were also fire-polished (resistance, 12 24 MΩ). The amplifier was EPC-10-Double (HEKA, Lambrecht, Germany); its voltage-follower circuitry was used in current-clamp (CC). The low-pass filter frequency in voltage-clamp (VC) was 3 kHz. The frequency of digitization was 10 kHz. Offset potentials were compensated before seal formation. The series resistance was 6 19 MΩ. R_{IN} was measured in CC using hyperpolarizing currents (10 pA, 500 ms). Resting potential was measured with the balanced amplifier input [35]. The perforated-patch recordings were done 20 30 min after establishing the gigaseal to allow membrane perforation and reduction of the access resistance. Recordings were done at 22 24°C.

Membrane noise was measured in the perforated-patch mode using 100 ms traces (digitalized at 0.1 ms; repeated 10 times for each potential) resembling those used for the recording of synaptic responses. Noise was analyzed in the frequency range between 10 Hz (determined by the trace length) and 3 kHz (low-pass filter frequency in VC). The noise was presented as the root mean square (r.m.s.) noise, or σ, which is also identical to the square root of the variance [36]. The intrinsic noise of the amplifier measured before the experiment was <90 fA.

Monosynaptic connections of SG EINs were identified by paired recording as described in [4]. The present study, however, demanded long-lasting recordings with continuous cell-attached

stimulation of the presynaptic neuron. As we have found, the pulse (100 nA; 1 ms) used in [4] was too strong for continuous stimulations and provoked damage of the presynaptic neuron before the end of the protocol. Therefore, we first tested how the pulse amplitude could be reduced to provide reliable and non-damaging stimulation for longer periods of time.

An SG neuron was kept in CC at −70 mV through the perforated-patch recording pipette (Fig. 1A). The tip of the stimulating pipette was attached to the same neuron with application of a slight suction. The neuron was stimulated through the cell-attached pipette by currents of increasing amplitude (10 nA, increment). The first stimulation eliciting spike was considered as threshold. The threshold stimulation increased by 20 nA (threshold +20 nA) reliably evoked spikes in all SG neurons tested (n = 10). In paired recording (Fig. 1B), a connection was first identified using a 100 nA stimulation [4], but then the pulse amplitude was appropriately adjusted. The postsynaptic neuron was in VC at −80 mV while the presynaptic SG EIN was stimulated at 10 nA increment. The first pulse eliciting EPSC was considered as threshold. The 'threshold +20 nA' pulse was used in the following experiment (n = 183). For different connections, it ranged between 30 nA and 100 nA (in most cases, 40 50 nA) and provided reliable stimulation of the presynaptic neuron for periods up to 1 hour.

It was also tested whether the cell-attached stimulation can evoke a high-frequency firing needed for plasticity-induction protocols. Three types of SG neurons with distinct firing patterns and thresholds were described in our experiments [4,35]. In 15 neurons (n = 5, for each type), we recorded spikes induced by a train of 10 pulses (1 ms) applied at 100 Hz (Fig. 2). In all neurons tested, the cell-attached stimulation evoked firing at 100 Hz. Thus, the 'threshold+20 nA' pulses could be used for repetitive stimulation of all types of SG neurons.

All numbers are given as mean ± SEM unless otherwise mentioned. The parameters were compared by paired Student's *t* test.

Results

We identified 221 monosynaptic connections with presynaptic SG neurons by testing ~900 presumably presynaptic neurons. The probability of finding connections in this study (~25%) was higher than in [4] (~10%) because of the implementation of the oblique LED illumination technique [28,29] allowing selection of neurons from a larger pool of visible cells. Inhibitory connections (n = 38) were not subjected to analysis. The excitatory connections (n = 183) form the basis of the present study. Of 183 postsynaptic neurons, 16 were in lamina I, 144 in the SG and 23 in lamina III. The resting potential, R_{IN} and the slowest membrane time constant in postsynaptic neurons were −74.3±0.5 mV (n = 183), 1.77±0.08 GΩ (n = 183) and 79.6±3.5 ms (n = 162), respectively.

The experiments were done to study 1) the threshold of spike initiation in an SG neuron, 2) the pharmacological properties of synapses formed by SG EINs, 3) the kinetics of EPSCs and their change with the synapse location along the dendritic tree of the postsynaptic neuron, 4) how the experimental conditions lowering R_{IN} in the postsynaptic neuron affect both the resolution and the efficacy of distal synaptic inputs, 5) the efficacy of EPSPs to evoke spikes in a postsynaptic neuron, 6) whether synapses of SG EINs can show short- and long-term plasticity, 7) whether an SG EIN forms single or multiple synapses on a postsynaptic neuron, and 8) the release probability in the individual synapse.

Spike Initiation in an SG Neuron

The estimation of firing threshold in a neuron is needed for evaluation of efficacy of synaptic transmission. In addition, correct

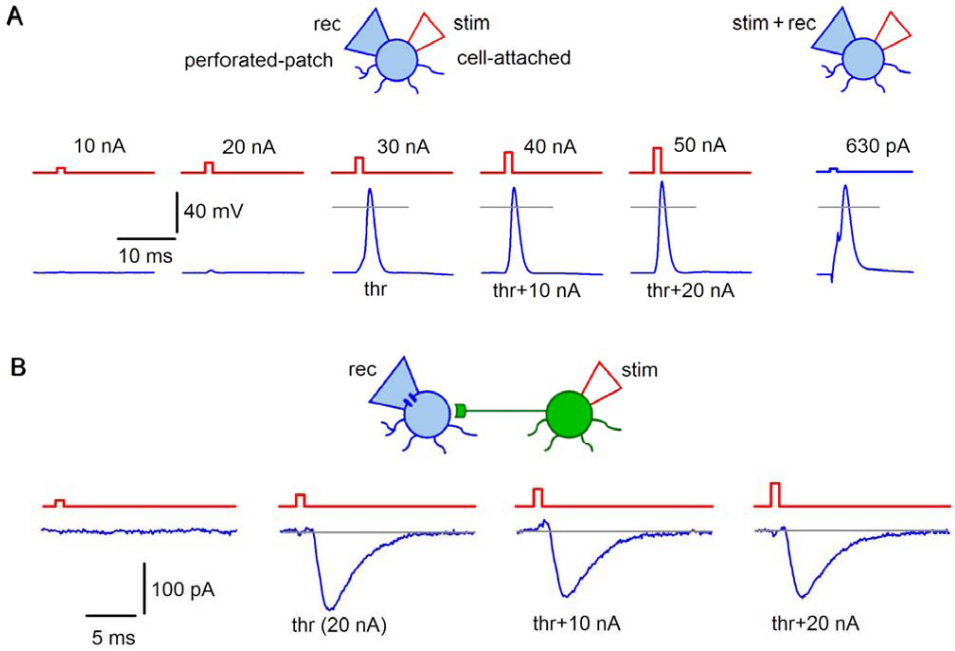

Figure 1. Adjustment of the stimulation strength. A, an SG neuron current-clamped via the perforated-patch recording pipette was stimulated by the current injection (1 ms; 10 nA increment) through the cell-attached pipette. The first spike was evoked at 30 nA (threshold). Right, spike evoked in the same neuron by a 1 ms current injection through the recording pipette. It is seen that the initiation phase of the spike evoked by the cell-attached stimulation does not show voltage distortions which typically appear when one electrode is used for both stimulation and recording. Grey line, 0 mV. B, the strength of the cell-attached stimulation for the SG EIN in a connection was adjusted by recording the evoked EPSCs (−80 mV). For this connection, the threshold was at 20 nA, and therefore, the stimulation at 40 nA (threshold+20 nA) was used throughout the experiment. doi:10.1371/journal.pone.0008047.g001

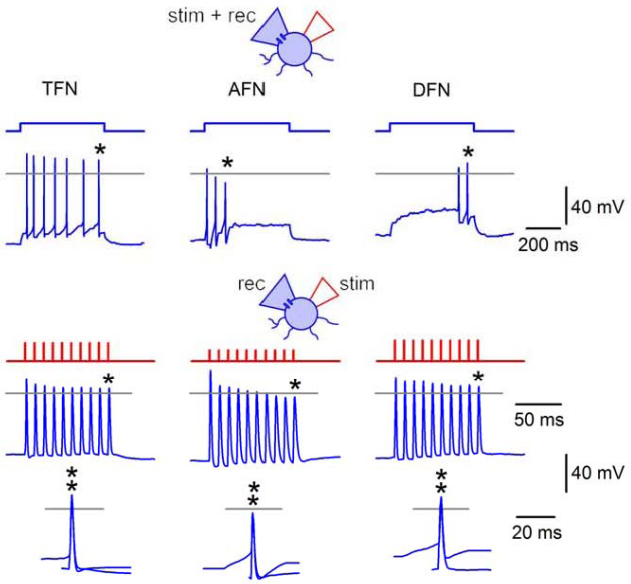

Figure 2. Stimulation of SG neurons at 100 Hz. The perforated-patch pipette and the cell-attached pipette were placed on the soma of an SG neuron. Depolarizing currents (500 ms; 40 pA) were first injected through the perforated-patch and the neuron was classified according to its firing pattern as tonic-firing neuron (TFN), adapting-firing neuron (AFN) or delayed-firing neuron (DFN) [4,35]. Following classification, the same neuron was stimulated through the cell-attached pipette at 100 Hz (10 pulses). Each pulse (1 ms) had the 'threshold+20 nA' amplitude. The last spikes in trains (asterisks) elicited by these stimulation techniques are shown superimposed on the bottom.
doi:10.1371/journal.pone.0008047.g002

estimation of the spike initiation time in the axon initial segment (AIS) of the presynaptic neuron is critical for determining the latency of the postsynaptic response. These estimations can hardly be done in experiments where one electrode is used for both stimulation and recording (Fig. 1A, right), since injections of large currents needed to evoke spike by short pulses (1 ms) cause capacitance transients and voltage drop on the access resistance which, even after compensation, distort recording at the moment of spike initiation. Undistorted spike could however be recorded when stimulation was delivered via the cell-attached pipette (Fig. 1A). Therefore, we studied the spike initiation in an SG neuron stimulated via the cell-attached pipette (Fig. 3). At subthreshold level, a small passive intracellular response was observed which increased linearly with stimulation intensity. This response was appropriately scaled and superimposed on the suprathreshold traces, to estimate the contribution of the passive component. At the firing threshold, the amplitude of the passive component was 10.7±1.7 mV (n = 10) when measured from the resting potential. This passive depolarization was sufficient to trigger a spike consisting of two components separated by an inflexion point (arrowhead, Fig. 3). These components were similar to those described in the classical studies of motoneurons [37 39], which attributed the fast and slow components to the spike invasion to the AIS and the soma, respectively. Since the soma of dorsal horn neurons has low density of Na^+ channels and is not able itself to generate spikes [40,41], the two components of the spike in SG neurons could be explained by the spike generation in the AIS and its antidromic invasion to the tightly coupled electrotonic domain consisting of the axon hillock and the soma (AH+S) [42,43]. At a threshold (Fig. 3), the AIS component of the spike was initiated during the 1 ms stimulation, and the interval between the initial phases of the AIS and AH+S components was 0.99±0.18 ms (n = 9; range 0.4 1.9 ms; in 1 of 10 cells the components could not be distinguished). The amplitude of the AIS component was 15.1±2.1 mV (n = 9; measured from the passive component) and varied from cell to cell as shown in Fig. 3 (threshold). At 'threshold +10 nA' stimulations, the AIS component was completely activated during the stimulation pulse.

Thus, short depolarizations (~10 mV) induced by the cell-attached stimulation were sufficient to elicit spike in the AIS. From the AIS, the spike propagated in two directions: orthodromically, towards the axon terminals, and antidromically, to the soma. For this reason, we considered the end of the stimulation pulse, where the AIS spike has already been generated, as a moment from which the EPSC latency has to be measured. These experiments have also indicated that the traditional measurement of the latency from the peak of the somatic spike can overestimate the true latency by adding the time needed for the antidromic spike propagation from the AIS to the soma (up to ~2 ms). This overestimation can vary from spike to spike, since the time interval between the AIS and AH+S components varies with stimulation intensity and alterations in the membrane potential [42,44].

Pharmacological Properties of Synapses Formed by SG EINs

Pharmacological properties of EPSCs were studied in 68 connected cell pairs. The postsynaptic receptor antagonists were applied for 30 60 s (perfusion rate, 1 volume of the experimental chamber per 5 s), but if a complete block was not achieved by the end of the application, its duration was increased, in some cases to 20 21 min (to allow drug diffusion to deeper synapses in the spinal cord slices).

The AMPA/kainate receptor blocker CNQX (10 20 μM) was tested in 10 pairs. A complete EPSC block was obtained in 5 cases (full recovery, n = 4). In the remaining pairs, both blocks (by 43.4±11.4%, n = 5) and recoveries were incomplete, probably, due to diffusion problems for some deep synapses in the spinal cord slice. The AMPAR blocker GYKI-52466 (100 μM) was tested in 21 pairs. The EPSC block was complete in 14 cases (recovery, n = 12). In 7 pairs, the block was partial (by 72.3±6.8%) and recovery was obtained in only 2 cases. The specific blocker of CP-AMPARs IEM 1460 (20 μM) was tested in 43 pairs (Fig. 4). In 22 cases, a complete block with recovery was observed. In 15 pairs, the block was partial (by 44.0±7.2%) and the recovery to >80% was obtained in 9 cases. In the remaining 6 connections, the EPSCs were insensitive to IEM 1460. The kainate receptor blocker SYM 2081 (1 μM) was tested in 25 pairs. In no case was a full block observed. A partial block (by 43.2±10.1%) was seen in 6 pairs but recovery was obtained in only 2 cases. In 19 pairs, SYM 2081 had no effect. The NMDAR blocker D-AP5 (50 μM) had no effect on EPSCs recorded in 1 mM Mg^{2+}-containing ACSF (n = 5), and we also did not see effect of the blocker when tested in Mg^{2+}-free ACSF [4]. The EPSCs were not reduced by a mixture of the $GABA_A$ receptor blocker picrotoxin (100 μM) and the glycine receptor blocker strychnine (1 μM) (n = 5).

These tests have shown that transmission from an SG EIN involves both the CP- and CI-AMPARs.

Time Course of EPSCs

We measured the rise time and the decay time constant of EPSCs evoked by stimulating SG EINs. The rise time ranged from 0.46 ms to 5.4 ms giving the histogram peak at 0.5 1.0 ms (Fig. 5A). The EPSC decay was analysed by fitting traces with one (n = 172) or two (n = 11) exponential functions (Fig. 5B). Eighty-

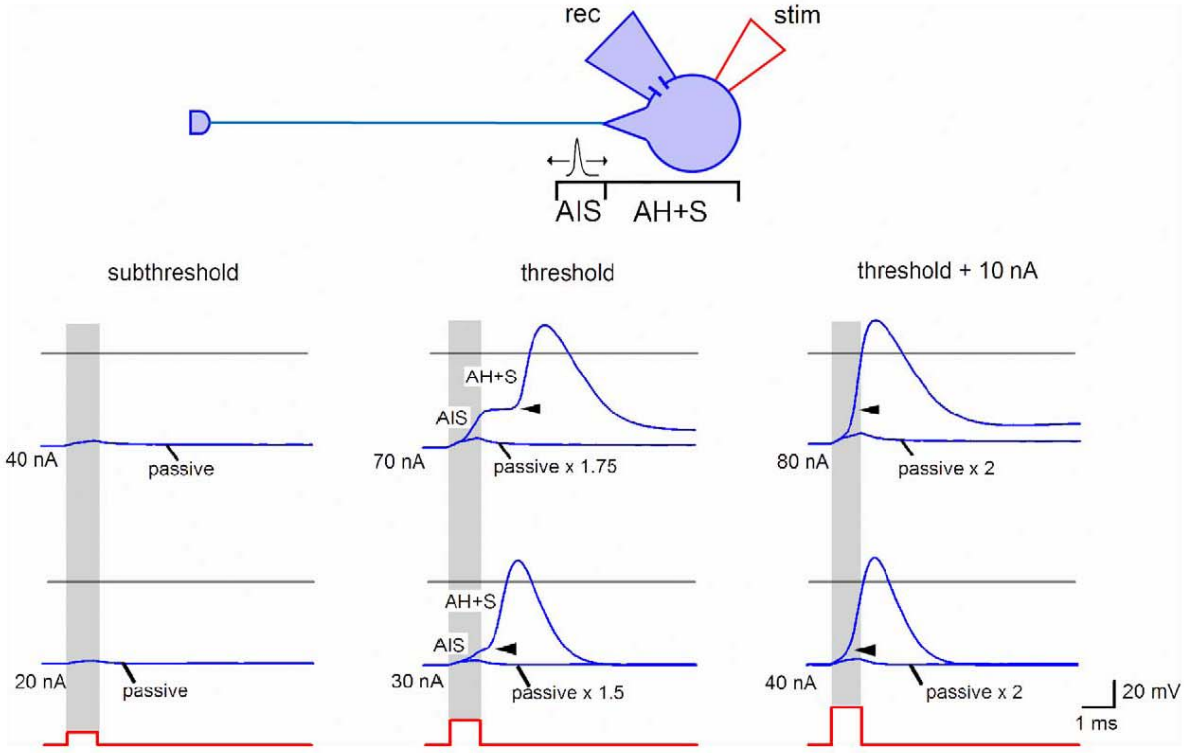

Figure 3. Spike initiation in an SG neuron. Stimulating (cell-attached) and recording (perforated-patch) pipettes were placed on the soma of an SG neuron. Stimulation (1 ms) increased with a 10 nA increment. Subthreshold, the membrane responses were considered as passive. Threshold, the AIS and AH+S components could be best distinguished (transitions are indicated by arrowheads). The AIS component was initiated within the 1 ms of the stimulation. The passive response was multiplied by the corresponding scaling factor. Threshold+10 nA, the interval between the AIS and AH+S components became shorter. The AIS component was completely generated within the 1 ms of the stimulation. Two SG neurons shown have different proportions between the amplitudes of the AIS and AH+S components and different kinetics of transitions. Horizontal grey lines, 0 mV. Resting potentials were about −70 mV.
doi:10.1371/journal.pone.0008047.g003

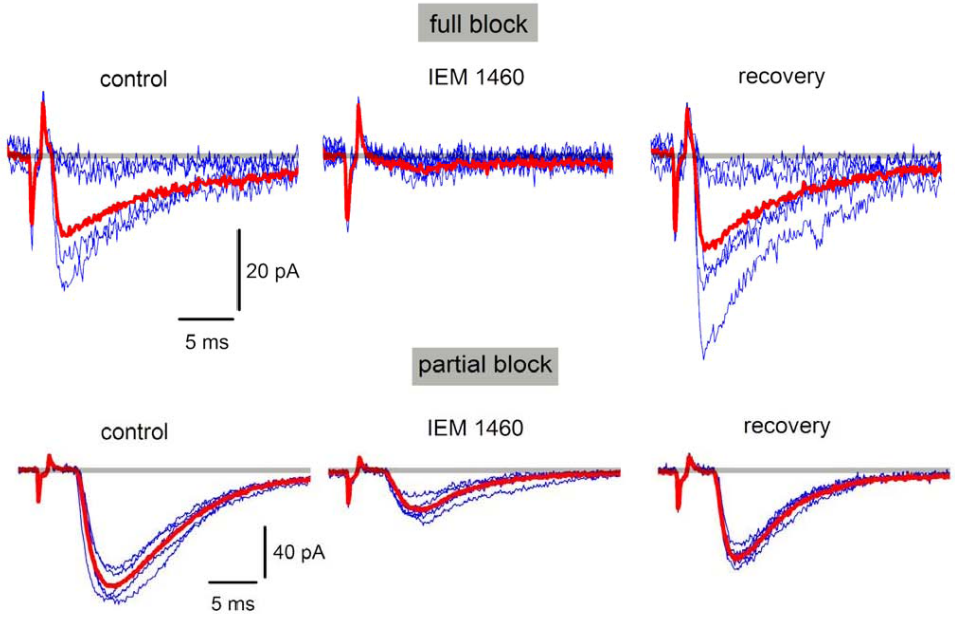

Figure 4. Effect of a CP-AMPAR blocker on evoked EPSCs. EPSCs evoked in two different cells by stimulation of SG EINs. EPSCs were recorded in the absence and presence of the specific CP-AMPAR blocker IEM 1460 (20 μM). The EPSCs were completely blocked in some neuron pairs (top), whereas the blockade was only partial in other cases (bottom). The drug was washed-out (recovery) after the steady-state level of block has been reached. Red traces are averages of five consecutive EPSCs (blue).
doi:10.1371/journal.pone.0008047.g004

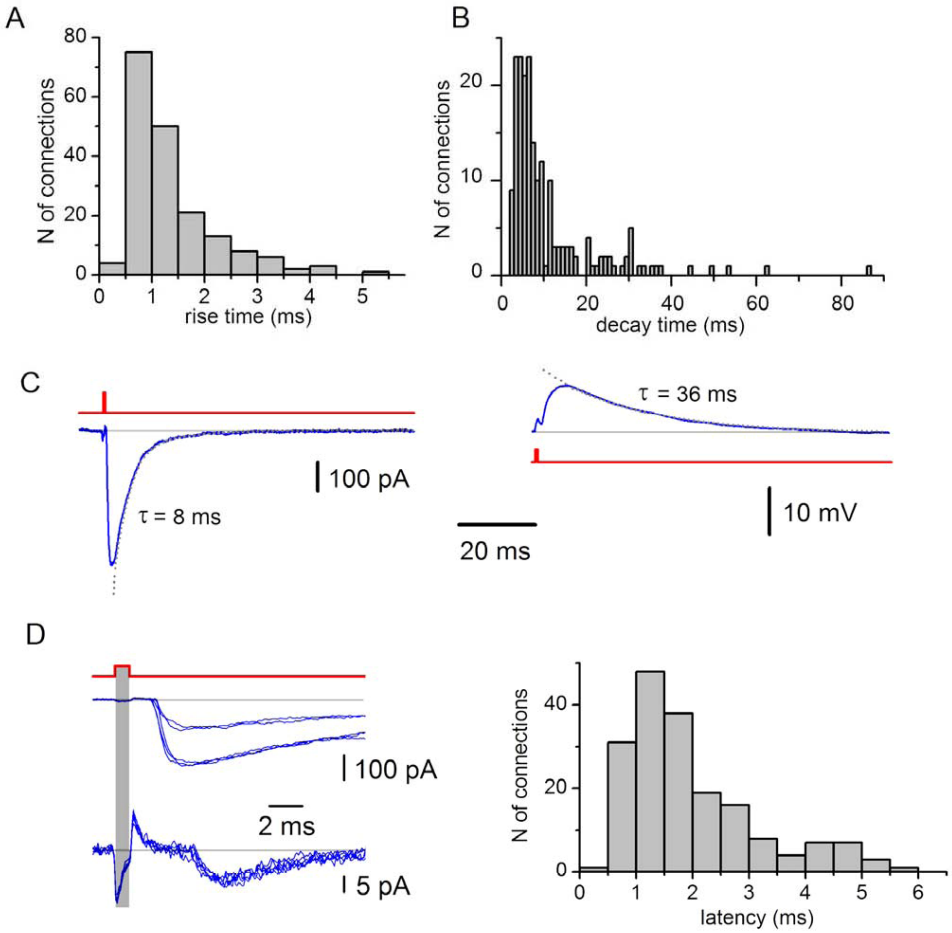

Figure 5. Time course and latency of monosynaptic EPSCs. A, the distribution of the rise times from 10% to 80% of the EPSC amplitude (n = 183). The rise time was measured in averaged (15–30) traces. B, the distribution of the EPSC decay time constants (n = 194; 183 connections). In 11 connections, the decay was fitted with two exponentials. C, monosynaptic EPSC (−80 mV) and EPSP (−70 mV) elicited in the same neuron by stimulating an SG EIN. The decays are fitted with exponentials. D, the distribution of the latency times (n = 183). Latencies were measured as an interval between the end of the stimulation (grey bar) and the beginning of the EPSC measured at 10% of the amplitude. Recordings (each family of traces contains 5 EPSCs evoked by consecutive stimulations) are shown for two connections with different latencies.
doi:10.1371/journal.pone.0008047.g005

four percent of the decay time constants were in the interval between 2 ms and 17 ms. The time courses of EPSCs and EPSPs are illustrated in Fig. 5C. In all connections, EPSCs decayed faster than EPSPs. In 8 pairs analysed, the EPSC and EPSP decay time constants were 8.9±0.7 ms and 35.8±2.1 ms, respectively.

Variable EPSP Latencies Explained by Different Location of the Synapses along the Dendritic Tree

The latency times ranged for different connections from 0.48 ms to 5.5 ms (Fig. 5D; mean 1.9±0.1 ms, n = 183).

For the reason given in Discussion, the longest latencies observed could not be explained by spike propagation in the presynaptic neuron and transmitter release. Therefore, computer simulations were done to test whether additional delay could be caused by the electrotonic EPSC propagation in the postsynaptic neuron, when release occurred at distal synapses. We also studied whether different dendritic locations of the synapse can explain observed variations of the rise and decay kinetics.

Recording was simulated for the electrode placed at the soma, while a synapse was moved along the somatodendritic domain (Fig. 6A). In VC, the proximal EPSC showed fast decay with the time constant (~5 ms) resembling τ_D of the kinetic scheme describing synapse (see Methods). When this synapse was moved distally (dendrite 0.95), the EPSC became slower (decay time constant, 16.4 ms) and smaller. The electrotonic delay of the EPSC increased from 0.05 ms for the somatic synapse to 3.51 ms for the distal (dendrite 0.95) synapse (Fig. 6B). The EPSC rise time also changed with the synapse location from 0.5 ms (soma) to 5.35 ms (dendrite 0.95) (Fig. 6C). In CC (Fig. 6D), the proximal EPSP had two components in the decay kinetics, of which the slow one corresponded to the membrane time constant of the model neuron. The distal EPSP had slower rising phase and monoexponential decay. The electrotonic delays were 2.2 ms and 8.1 ms for the proximal and distal EPSPs, respectively.

Thus, our experiments have shown that SG EINs elicit fast EPSCs. The variation range of their kinetics, in the majority of cases, can be explained by different dendritic locations of the synapse. Electrotonic propagation in the postsynaptic neuron can substantially increase the latency of distal EPSCs.

Detection of Distal Dendritic Inputs at the Soma

VC is widely used as a principal mode for recording spontaneous and evoked synaptic activity in the superficial dorsal

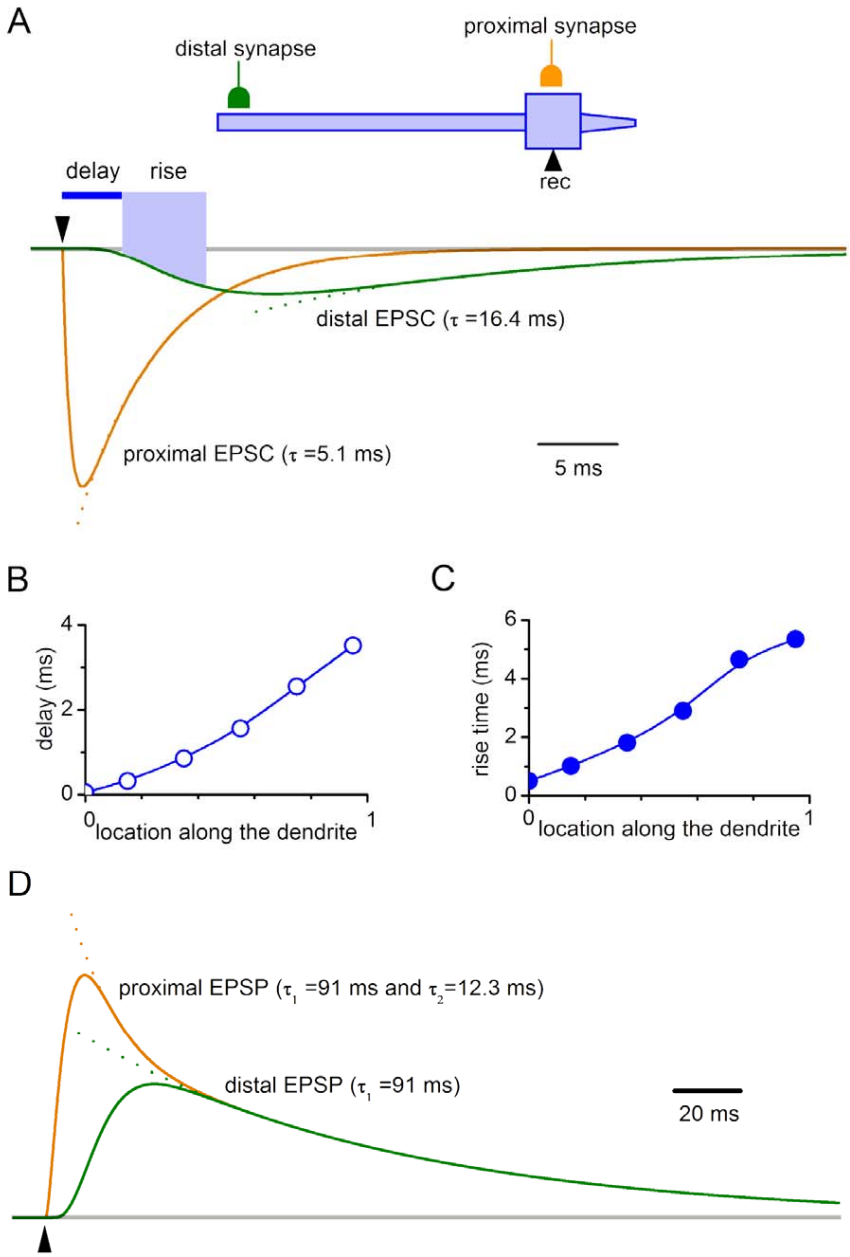

Figure 6. Simulation of proximal and distal inputs. A, simulation of proximal (soma) and distal EPSCs seen with electrode placed at the soma. Distal synapse is at dendrite 0.95; assuming 0 as the proximal end and 1 as the distal end. Both synapses have the same kinetics and g_M ($9.2*10^{-5}$ μS). The EPSC decay was fitted with an exponential. B, the electrotonic delay of the EPSC propagation to the soma as a function of the synapse location at the dendrite. The delay was measured to the moment when the EPSC seen at the soma reached 10% of its amplitude. C, the EPSC rise time (from 10% to 80%) as a function of the synapse location. D, simulation of proximal (soma) and distal (dendrite 0.95) EPSPs seen at the soma. The decay of the distal EPSP is fitted with one exponential, whereas that for the proximal EPSP with two exponential functions.
doi:10.1371/journal.pone.0008047.g006

horn [4,14,45 48]. However, its applicability for detection of weak distal, i.e. inhibitory, inputs has recently been questioned [49,50]. Lower signal-to-noise ratio in VC has been assumed as major reason for the different proportions of excitatory and inhibitory connections seen in CC [2,3,50] and VC [4] experiments. Therefore, we compared the resolution power of both techniques in detecting distal synapses. Recording of weak distal inputs was assumed to be affected by the membrane noise, R_{IN} and the driving force for the carrier ion. Effects of the first two factors were studied experimentally and the last one is analyzed in Discussion.

Membrane noise was measured at potentials used for recording of synaptic inputs. VC identification in this study and [4] was done at −80 mV and −100 mV (a pulse to −60 mV was only applied to see the IPSC reversion). CC identification in [2,3,50] was done at −50 mV and −60 mV. Therefore, the current noise at −80 mV and −100 mV was compared with the voltage noise at −60 mV and −55 mV in the same 10 SG neurons. In VC, the current noise at −80 mV ($\sigma_I = 1.47 \pm 0.14$ pA) and −100 mV was low (Fig. 7A) but increased with depolarization (Fig. 7C) due to subthreshold activity of voltage-gated Na^+ and K^+ channels [36,51]. In CC, the

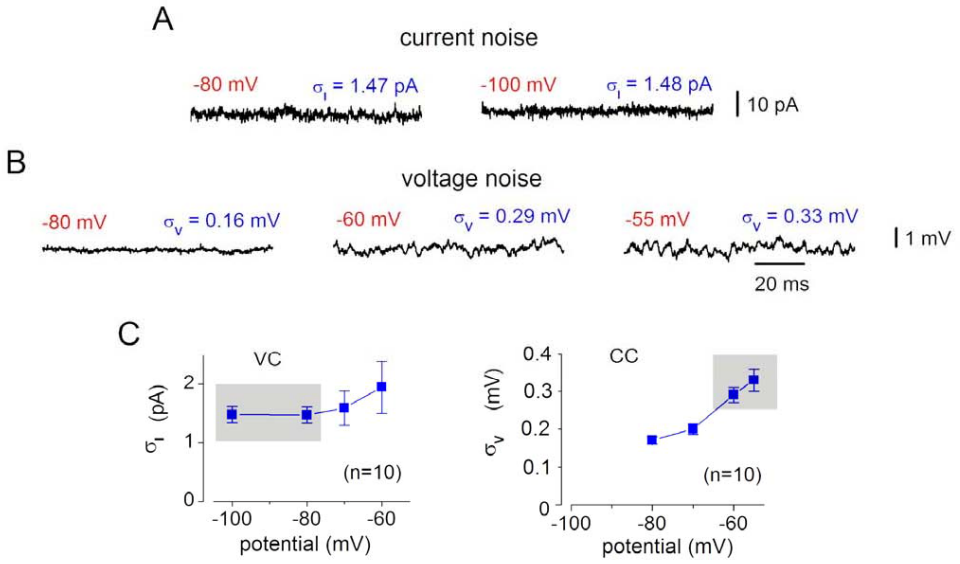

Figure 7. Membrane noise in SG neurons. A, the current noise in VC (filter, 3 kHz). The σ_I values represent the means of measurements in 10 SG neurons. B, the voltage noise in CC. The σ_V values are the means (n = 10). Note increase in the voltage-noise at -60 mV and −55 mV due to subthreshold activity of Na^+ channels [36]. C, σ_I and σ_V as functions of membrane potential. VC and CC data are from the same neurons. Grey boxes indicate the current and voltage noise at potentials used for comparison with other studies.
doi:10.1371/journal.pone.0008047.g007

voltage noise also increased with depolarization to −60 mV ($\sigma_V = 0.29 \pm 0.02$ mV) and −55 mV (Fig. 7B and C), where it showed a typical component with a frequency of >100 Hz caused by the subthreshold activity of Na^+ channels [36,51]. At all potentials analyzed (Fig. 7C), our σ_I and σ_V values were in good agreement with those from specialized studies [36,51].

To determine the resolution limits, which also depend on spectral compositions of responses and noise, simulated EPSC and EPSP were added to original recordings of current and voltage noise, respectively (Fig. 8). In VC, the EPSC could be already detected at $2\sigma_I$ amplitude, and was clearly resolved at $3\sigma_I$ amplitude. Detection was more difficult in CC, where the Na^+-channel-dependent component of the membrane noise [36] masked the EPSP. Reliable detection of EPSP could not be done for amplitudes below $3\sigma_V$. Therefore, the resolution limit of 3σ was assumed for both VC and CC. Our data (Fig. 7C) suggest that the smallest EPSC adequately resolved at −80 mV has amplitude of ~5 pA. This limit could be also validated by inspecting the traces in Fig. 5D (lower traces) and Fig. 15A. Similar signal-to-noise ratio for the EPSP recorded at −60 mV is achieved at 0.9 mV.

R_{IN} affects detection of distal inputs because an increase in the membrane conductance associated with its drop shunts EPSC/EPSP propagation to the soma. The mean R_{IN} is >1.6 GΩ in the present study and [4] but drops to 158±68 MΩ [26] when Ca^{2+}-chelator-free pipette solution is used [2,3,26]. Therefore, we studied effect of R_{IN} variation from 1.6 GΩ to 100 MΩ in the SG neuron model with the distal and proximal synapses (Fig. 9). Synapses were adjusted in the basic model to give EPSCs of 5 pA (VC, 1.6 GΩ). This model of the smallest distal and proximal inputs resolved in our experiments (>$3\sigma_I$) was used to study effects of the R_{IN} drop in both VC and CC. In VC, R_{IN} had virtually no

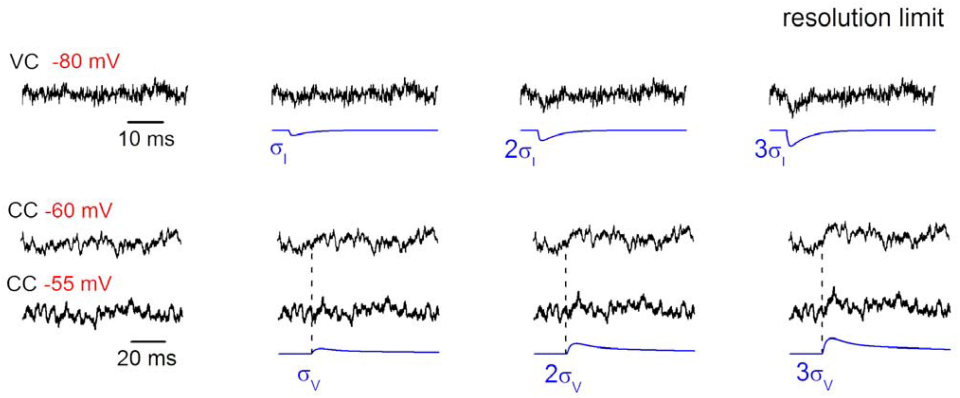

Figure 8. Resolution limits. Determination of the resolution limits for VC and CC recordings. Simulated (noise-free) EPSCs and EPSPs were added to the original recordings of current noise at −80 mV and voltage noise at −60 mV and −55 mV, respectively. The amplitude of the EPSC and EPSP was expressed in the corresponding σ (σ, 2σ and 3σ) calculated for each individual recording. Synaptic responses were considered as resolved at the 3σ level.
doi:10.1371/journal.pone.0008047.g008

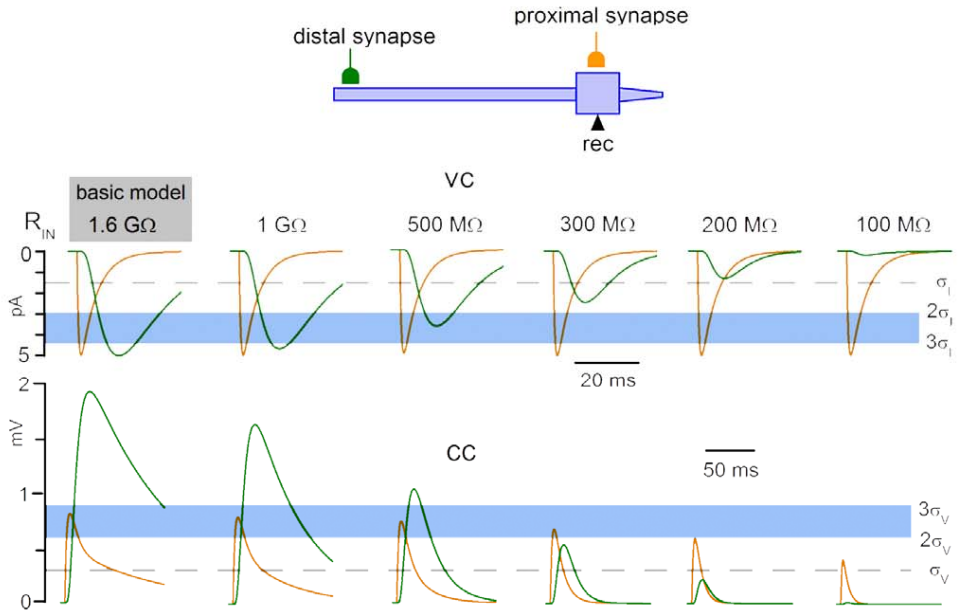

Figure 9. Effect of R_{IN} on the resolution of distal inputs. Computer model of SG neuron was used to simulate somatic recordings of the distal (dendrite 0.95) and proximal (soma) inputs at varying R_{IN}. The g_M values, $9.2*10^{-5}$ μS for the proximal synapse and $5*10^{-4}$ μS for the distal synapse, were adjusted in the basic model to give EPSCs of 5 pA. Horizontal lines indicate the σ, 2σ and 3σ levels of resolution. The σ values were from our experiments: $\sigma_I = 1.47$ pA (−80 mV) and $\sigma_V = 0.29$ mV (−60 mV).
doi:10.1371/journal.pone.0008047.g009

effect on the proximal EPSC which always remained $>3\sigma_I$ (Fig. 9, VC). However, the distal EPSC became $<2\sigma_I$ at 300 MΩ and $<\sigma_I$ at 200 MΩ. In CC, the proximal EPSP was $<3\sigma_V$ at 1.6 GΩ and became $<2\sigma_V$ at 100 MΩ. The distal EPSP was $>3\sigma_V$ and could be well resolved at $R_{IN}>500$ MΩ. For R_{IN} <500 MΩ, the distal EPSP became $<2\sigma_V$ at 300 MΩ and $<\sigma_V$ at 200 MΩ, and could no longer be considered as resolved. Thus, the smallest distal EPSC recorded under our conditions could not be adequately resolved in VC or CC experiments with $R_{IN}<500$ MΩ. The amplitudes of simulated EPSCs and EPSPs expressed in the corresponding σ (Fig. 9) allowed a comparison of the signal-to-noise ratios for recording distal inputs in high-R_{IN} VC and low-R_{IN} CC experiments. The signal-to-noise ratio in VC at 1.6 GΩ (3.4 σ_I) was 1.8, 4.5 and 34 times higher than in CC at 300 MΩ (1.9 σ_V), 200 MΩ (0.76 σ_V) and 100 MΩ (0.1 σ_V), respectively.

This analysis has shown that, for both proximal and distal synaptic inputs, high-R_{IN} VC has higher signal-to-noise ratio than low-R_{IN} CC. Furthermore, the efficacy of distal EPSPs is reduced with the drop in R_{IN}.

Efficacy of Synaptic Transmission

Transmission efficacy was studied in 22 connections. The postsynaptic neuron was kept in CC at a potential close to its resting potential of −70 mV, while the presynaptic SG EIN was stimulated each 20 s.

In 3 connections (Fig. 10A), the input from the SG EIN was classified as subthreshold and neither single nor summed EPSPs elicited spikes. The largest single or summed EPSPs were 5 8 mV. The mean EPSP failure rate was 0.46±0.06 (n = 3; range, 0.37 0.58; 56 episodes analysed). The mean EPSCs ranged from 15 pA to 90 pA.

In 3 connections (Fig. 10B), the input was at the level of firing threshold with the probability of eliciting spike by single EPSPs below 20% (9.7±3.1%, n = 3). Spikes could be also evoked by the EPSP summation. The largest EPSPs which did not evoke spikes were 11 16 mV. The EPSP failure rate was 0.38±0.24 (n = 3; range, 0.13 0.84; 258 episodes analysed). The mean EPSC amplitudes were 37 52 pA.

In 8 connections (Fig. 10C), the input was classified as suprathreshold and single EPSPs initiated spikes with a probability of 67.4±7.5% (n = 8). The EPSP summation could evoke multiple spikes. The largest EPSPs which did not evoke spikes were 8 25 mV. The EPSP failure rate was 0.35±0.10 (n = 8; range, 0 0.91; 649 episodes analysed). The mean EPSC amplitudes were 37 399 pA.

In the remaining 8 connections, spontaneous synaptic plasticity was observed. In the experiment shown in Fig. 10D, the EPSC was small during the first 10 min of recording (mean, 20 pA; first 15 EPSCs) but then dramatically increased (mean, 610 pA; last 15 EPSCs). Following this, single EPSPs became suprathreshold. In these connections, the EPSC amplitude increased by a factor of 8.5±3.3 (n = 8).

Thus, an SG EIN evokes substantial depolarization of the postsynaptic neuron and individual or summed EPSPs can frequently elicit spikes. Moreover, synapses of SG EINs showed plasticity, which was studied in the following experiments.

Short-Term Plasticity

Short-term plasticity (sub-second range) was induced in 7 connections using a standard paired-pulse protocol (Fig. 11A). No interaction between the paired responses was seen for intervals up to 160 ms (Fig. 11C). At longer intervals (320 ms and 640 ms), a depression of the second response was observed (0.64±0.08, n = 7; at 640 ms, $P<0.001$). The failure rate for the first EPSC was 0.37±0.14 (n = 7) and for the second EPSC at 320 and 640 ms intervals (pooled) was 0.44±0.13 (n = 14). Thus, the change in the failure rate could not explain the depression observed for these intervals.

Long-Term Plasticity

Different forms of long-term plasticity (tens of minutes) was induced by stimulating SG EINs at 1 Hz, 10 Hz and 100 Hz. Before and after the induction protocol application, the EPSCs

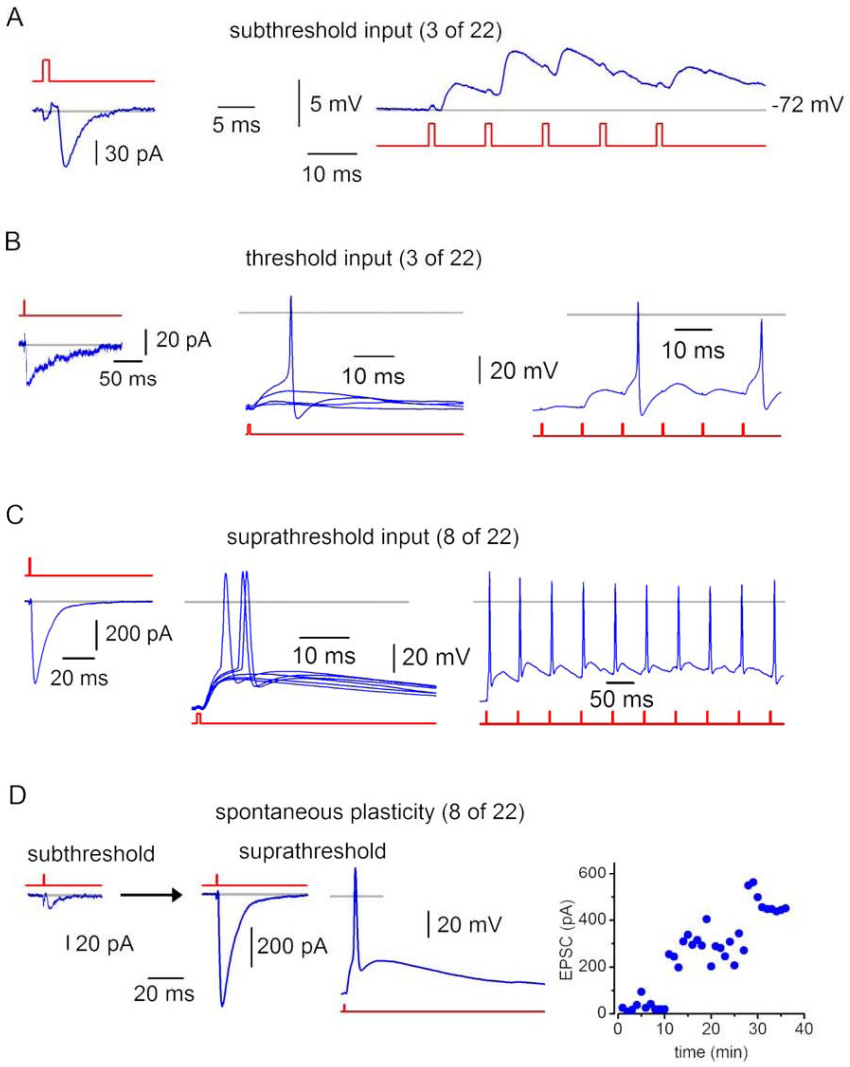

Figure 10. Efficacy of synaptic transmission. A, EPSCs (−80 mV) and EPSPs recorded in a neuron with the subthreshold input from an SG EIN. The EPSP summation was evoked by 5 stimulations of the presynaptic SG EIN at 100 Hz. B, connection with the threshold input. Some single EPSPs elicited spikes. The EPSP summation evoked by 6 stimulations of the presynaptic SG EIN at 100 Hz elicited two spikes. C, connection with the suprathreshold input. Single EPSPs frequently initiated spikes. Repetitive firing could be induced in the postsynaptic neuron by the EPSP summation (the SG EIN was stimulated at 20 Hz). D, recordings from the connection which showed spontaneous plasticity. Each point in the graph represents the EPSC amplitude obtained by averaging 3 consecutive episodes recorded within 1 min. Grey lines, 0 mV or 0 pA.
doi:10.1371/journal.pone.0008047.g010

were evoked each 20 s. At this interval, EPSCs remained stable in 6 of 8 control experiments (Fig. 12), while in 2 cases spontaneous potentiation occurred as reported above (not shown). Induction protocols were applied in 73 connections and the plasticity was considered as induced (n = 66) if its appearance correlated with the induction protocol application and the EPSC amplitude changed by more than 25%.

Stimulation at 1 Hz applied for 2 min was tested in 42 pairs. In 22 cases, it caused a significant and irreversible increase in synaptic strength observed for 12 52 min until the end of the recording (Fig. 12, LTP, 1 Hz). The EPSC increased by a factor of 2.9±0.4 (n = 22, P<0.001, range from 1.27 to 6.6) at 12 min and 3.2±0.4 (n = 14, P<0.001) at 30 min. In 15 pairs, the protocol induced depression (Fig. 12, LTD, 1 Hz) recorded for 14 50 min. The EPSC amplitude reduced to 0.41±0.05 (n = 15, P<0.001, range from 0.11 to 0.64) at 14 min and 0.36±0.05 (n = 8, P<0.001) at 30 min. In the remaining 5 pairs neither LTP nor LTD were induced.

Stimulation at 10 Hz applied for 1 min was tested in 22 pairs, in 9 of which potentiation was induced (Fig. 12; LTP; 10 Hz) and lasted for 12 50 min. The EPSC was increased by a factor of 4.7±1.1 (n = 9, P<0.001, range from 1.41 to 10.1) at 12 min and 4.0±1.9 (n = 5, P<0.2) at 30 min. In the remaining 11 pairs, depression was induced and lasted for 10 40 min (Fig. 12; LTD; 10 Hz). The EPSCs decreased to 0.51±0.04 (n = 11, P<0.001, range from 0.33 to 0.7) at 10 min and 0.43±0.08 (n = 7, P<0.001) at 30 min.

High-frequency stimulation (100 Hz applied for 1 s, repeated 3 times with 1 s intervals) was tested in 9 pairs. In 3 cases, LTP was induced and observed for 11 46 min. The EPSC increased by a factor of 2.2±0.3 (n = 3, P<0.05, range 1.82 to 2.68) at 11 min and 2.3±0.5 (n = 2, P<0.2) at 30 min. In 6 pairs, we observed LTD (15 35 min). The EPSCs decreased to 0.36±0.05 (n = 6, P<0.001, range from 0.2 to 0.48) at 15 min and 0.21±0.02 (n = 3; P<0.001) at 30 min.

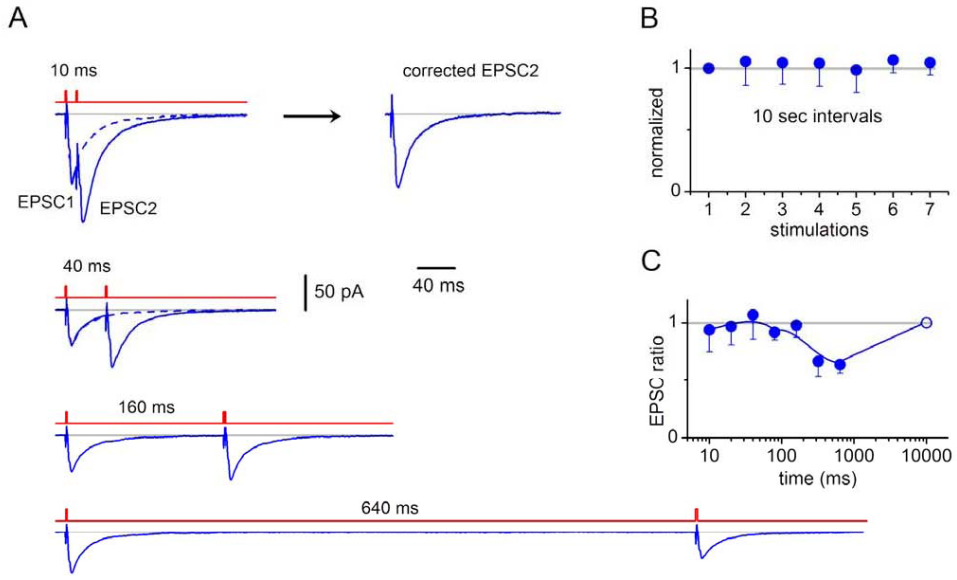

Figure 11. Short-term plasticity. A, EPSCs (−80 mV, averages of 24 traces) elicited by paired-pulse stimulations of a presynaptic SG EIN. Intervals between the paired stimulations were 10 s. The intervals between the pulses in the pair varied from 10 ms to 640 ms. At short intervals, the second EPSC in the pair was corrected for the overlap with the first EPSC as shown for 10 ms. For this, the first EPSC from the trace without overlap (at 640 ms) was scaled to fit the peak of the first EPSC with overlap and then was subtracted from it. B, test for stability of EPSCs at stimulations with 10 s intervals. For each connection, the amplitudes of the first EPSCs (non-averaged) in the first 7 paired stimulations were plotted (the first EPSC was normalized to 1). Each point shows the mean value for 7 connections. C, the ratio between the peak amplitudes of the second and first EPSCs as a function of the interval. For each connection (n = 7), the ratio was calculated from the average of 10–36 traces. The point at 10 s was set to 1 according to data from B.
doi:10.1371/journal.pone.0008047.g011

Thus, synapses of SG EINs show diverse forms of functional plasticity.

Monosynaptic EPSCs Are Evoked by Transmitter Release in Multiple Synapses of the Same Axon

In the majority of pairs (152 of 183), the EPSCs were composite and at least two components could be distinguished on their rising phase. In some cases, transitions between the components were seen as inflexion points (Fig. 13A), however, in other cases, the components were clearly separated in time (Fig. 13B1). In all these pairs, we also recorded individual components (Fig. 13A and B1) which had the same latencies as in the composite EPSC. The time interval between the first two components of the composite EPSC (Δ) remained constant during recording and ranged from 0.3 ms (3 kHz filter) to 3.1 ms.

Since a composite EPSC was elicited by one spike, one could rule out the possibility that the components appeared due to variation in the presynaptic spike initiation time. Two hypotheses could explain the appearance of composite EPSCs. 1) The axon of an SG EIN forms multiple synapses on a postsynaptic neuron; in this case, simultaneous activation of synapses with different electrotonic locations elicits EPSCs reaching the soma with different delays. 2) In addition to a monosynaptic connection, the neurons are also connected via an intercalated neuron; different conduction times in these pathways might also explain appearance of composite EPSCs. Although an involvement of an intercalated neuron was unlikely in connections with Δ<1 ms (Fig. 13A), it could not be excluded for those with larger Δ (Fig. 13B1). Therefore, we analysed 5 connections with large Δ to distinguish between the hypotheses.

For the composite EPSC from Fig. 13B1, the latency distributions for both components was constructed and showed two distinct peaks (Fig. 13B2). The width of each peak, corresponding to the latency variation for each component, was within 1 ms (grey boxes). Thus, each EPSC component could be independently identified as monosynaptic based on the standard criterion of latency stability. We also analyzed the Δ variation in the composite EPSCs (Fig. 13B3). With the exception of 6 measurements, all values were within the 1 ms range (grey box). Similar variations (<1 ms) of Δ was seen in all 5 analysed connections with large Δ (2.5±0.3 ms, n = 5). The following analysis was done to test whether such small Δ variations can be consistent with the idea of involvement of the intercalated neuron.

The delay on the intercalated neuron consists of the time taken for the presynaptic spike to begin the EPSP (synaptic delay), the time necessary for the EPSP to grow and initiate the spike (initiation time), and the time needed for the spike propagation along the axon of the intercalated neuron (propagation time) [52]. Since the synaptic delay and the propagation time are short (<1 ms), the initiation time was assumed to be the major contributor to the conduction delay. In addition, the initiation time should vary with the spontaneous changes in the quantal transmitter release from the presynaptic neuron. Therefore we analysed the spike initiation time and its variation to rule out the possibility of involvement of the intercalated neuron.

For these experiments, 9 connections were chosen with suprathreshold EPSPs and rapid spike initiation. The postsynaptic neurons had high R_{IN} (2.2±0.4 GΩ, n = 9). In the connection shown in Fig. 13C, the EPSP failure rate was low (0.10) and the probability of spike initiation by a single EPSP was high (62%). In VC, the EPSC amplitude varied from episode to episode indicating variation in the transmitter release (Fig. 13C). In CC, the fluctuations in the quantal transmitter release caused variation of the spike initiation time. The histogram showed a broad distribution of the initiation times from 1.9 ms to 18.2 ms (mean

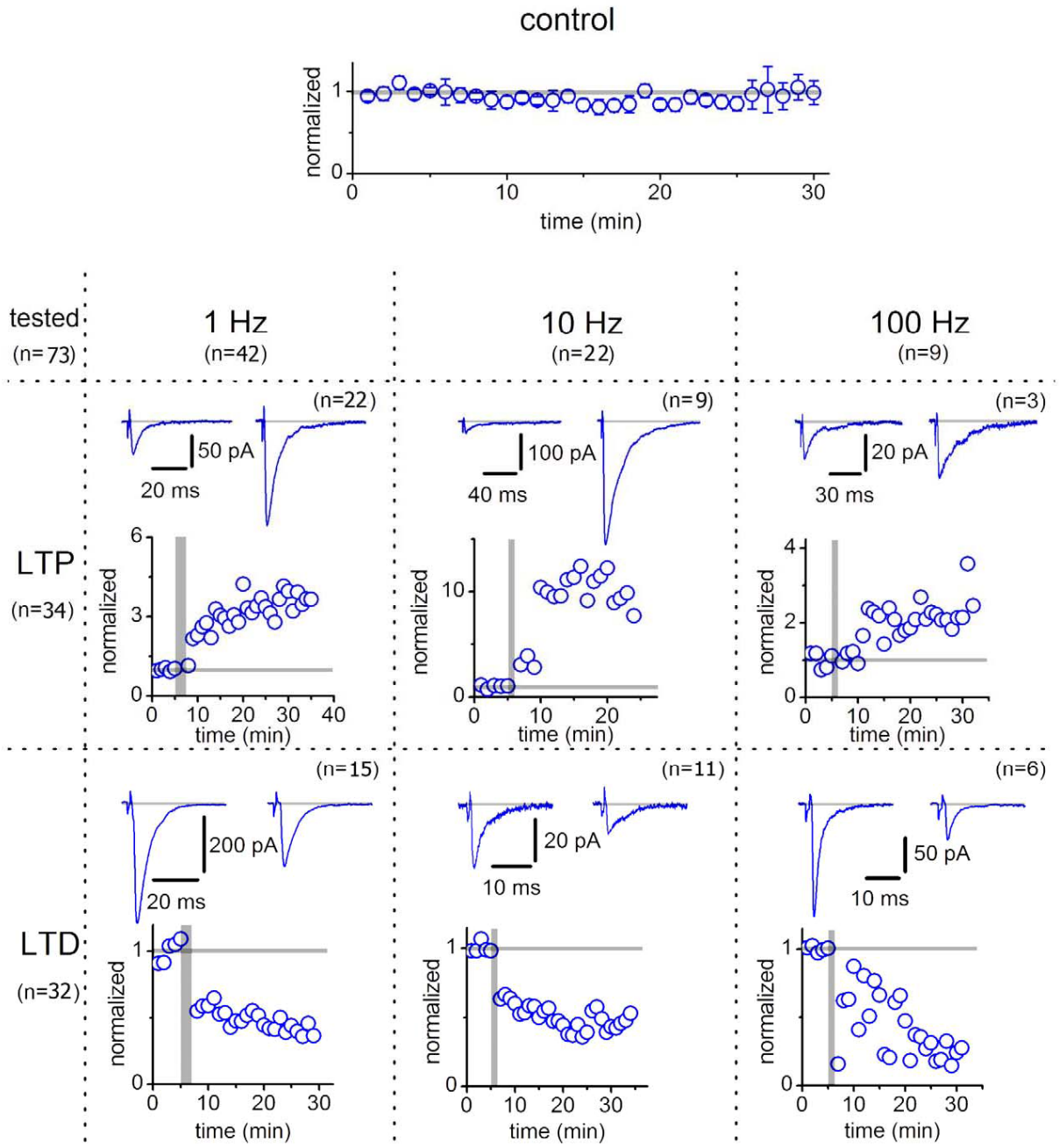

Figure 12. Long-term plasticity in synapses of SG EINs. Control, the postsynaptic neuron was in VC at −80 mV and the presynaptic SG EIN was stimulated each 20 s. EPSCs obtained by 3 consecutive stimulations were averaged and presented as one point. The control graph shows the average of normalized values (n = 6). LTP and LTD were induced by three different protocols of stimulations at 1 Hz, 10 Hz and 100 Hz. During application of the induction protocol, the postsynaptic neuron was switched to CC. Illustrations of induced plasticity are based on recordings from individual neurons. Before induction of plasticity (indicated by the vertical grey bar), each connection was stimulated during 5 min. The mean EPSC amplitude measured before induction was normalized to 1. The times, at which the changes in the EPSC amplitudes are reported in the text, were calculated from the end of the application of the induction protocol.
doi:10.1371/journal.pone.0008047.g012

6.2±0.3 ms, n = 142). This histogram was binned at 1 ms which is usually considered as the largest latency variation allowed for the monosynaptic connection. The maximum bin (grey) contained only 26% of events, indicating that it was not possible to select a 1 ms range of delay variation containing more than about one-fourth of initiated spikes. The mean initiation time in all 9 connections was 8.9±2.1 ms. The largest bin contained 28±3% (n = 9) of events, indicating that the vast majority of synaptically evoked spikes showed the initiation time variation >1 ms.

These experiments have shown that the spike initiation time and its variation in the intercalated neuron should be substantially larger than Δ and its variation in the composite EPSC. Therefore, an existence of multiple synapses between the neurons is likely explanation for the composite EPSC.

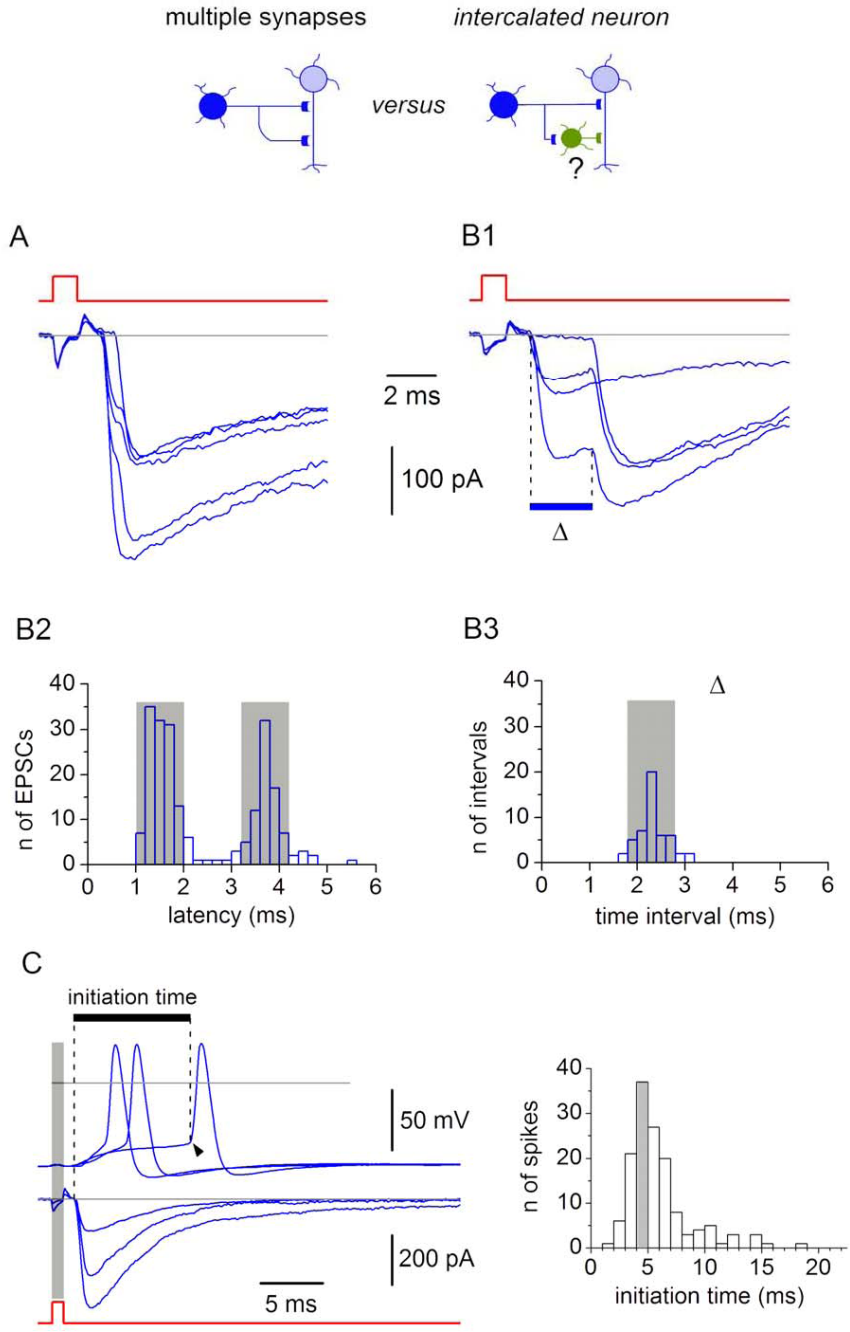

Figure 13. Composite EPSCs evoked by transmitter release in multiple synapses. A, EPSCs with a fast transition on the rising phase. The interval between the components (Δ) was 0.4 ms. B1, EPSCs with Δ of 2.3 ms. B2, latency distributions for individual components of the EPSC from B1. Width of grey boxes is 1 ms. The histogram includes the episodes with both components and one of the components (n = 212). B3, distribution of Δ for the composite EPSC from B1. The histogram is based on 50 episodes with both components. The grey box has a width of 1 ms. C, spike initiation by EPSPs. The moment of the transmitter release (left vertical dashed line) was determined in VC, where the measurement was more precise. In CC, the postsynaptic neuron was at −70 mV and spikes were evoked by stimulating the presynaptic SG EIN. Beginning of the spike depolarization (arrowhead) was considered as the moment of the spike initiation in the AIS (see Fig. 3). Right, distribution of the spike initiation times (n = 142), calculated as an interval between the transmitter release and the spike initiation moments. Bin width, 1 ms. The largest bin (grey) contains 37 of 142 events.

doi:10.1371/journal.pone.0008047.g013

We also tested whether composite EPSCs could be modelled by simultaneously activating synapses with different somatodendritic locations. In the simulation shown in Fig. 14A, one synapse was positioned at the soma, while the other one was moved along the dendrite (points 1 6). Simultaneous activation of both synapses gave composite EPSCs, in which Δ increased with the distance between the synapses. A composite EPSC could also be simulated for two dendritic synapses (Fig. 14B). These simulations confirmed that the composite EPSCs could be evoked by the activation of multiple synapses of one presynaptic neuron distributed along the

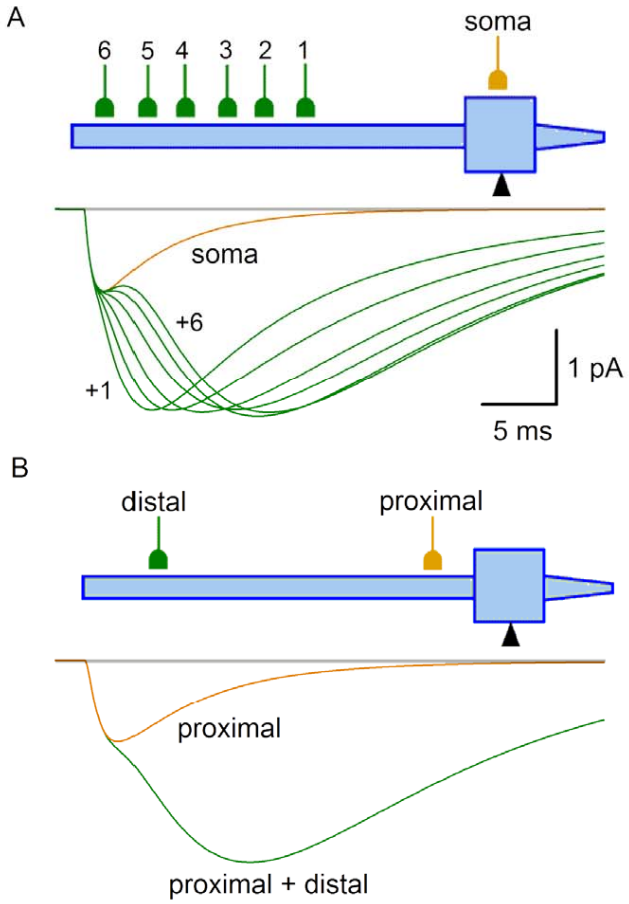

Figure 14. Modelling of composite EPSC. A, the proximal synapse was at the soma ($g_M = 2*10^{-5}$ μS), while the distal synapse was moved along the dendrite and its g_M was changed to keep the amplitude of composite EPSC. Points 1–6 and the g_M values were: dendrite 0.41 and $1.3*10^{-4}$ μS, dendrite 0.51 and $1.7*10^{-4}$ μS, dendrite 0.61 and $2.1*10^{-4}$ μS, dendrite 0.71 and $2.3*10^{-4}$ μS, dendrite 0.81 and $2.5*10^{-4}$ μS, and dendrite 0.91 and $2.5*10^{-4}$ μS, respectively. A simple EPSC was simulated by activating the somatic synapse only (trace, soma). Simultaneous activation of somatic and dendritic synapses gave composite EPSCs (traces, soma+1 to +6). B, simulation with two dendritic synapses, proximal (dendrite 0.11, $g_M = 3*10^{-5}$ μS) and distal (dendrite 0.81, $g_M = 2.3*10^{-4}$ μS). Simultaneous activation of these synapses gave a composite EPSC seen at the soma.
doi:10.1371/journal.pone.0008047.g014

somatodendritic domain of the postsynaptic neuron. In this case, Δ reflects the electrotonic distance between the synapses.

Finally, in two connections with composite EPSCs we have succeeded to obtain a detailed filling with biocytin of both the axon terminals of the presynaptic SG EIN and the dendritic arbores of the postsynaptic neuron. In the connection shown in Fig. 15, the composite EPSC had three components (Fig. 15A). The presynaptic cell axon formed a dense network in the vicinity of the postsynaptic cell body (Fig. 15B). At higher magnification (Fig. 15C), a number of close appositions (indicating putative synaptic contacts) between the varicosities of the presynaptic axon and the dendrites and soma of the postsynaptic neuron were detected in regions 1 3. In the other labelled connection, three putative synaptic contacts have also been revealed. Although it was not possible to estimate the electrotonic distance between the synapses and their total number, or to attribute the groups of synapses to the components of a composite EPSC, the labelling experiments suggested that multiple synaptic contacts between an SG EIN and a postsynaptic neuron can form the anatomical basis for the composite EPSCs.

Thus, paired recordings, computer simulation and biocytin labelling indicated that the majority of the monosynaptic EPSCs are likely to be generated by transmitter release in multiple synapses formed by the axon of an SG EIN on a postsynaptic neuron.

Probability of Release in an Individual Synapse

In the experiments described above, we calculated the failure rates for composite EPSC/EPSP to characterize transmitter release in multiple synapses. In some connections, however, it was possible to analyse individual components of the composite EPSC and estimate the release probability of the corresponding synapses. We analysed 10 such synapses in 5 connections. The release probability in these synapses was 0.51 ±0.07 (n = 10). If two such synapses were single and independent, the expected failure rate for their composite response (no synapse activated) would be $(1\ 0.51)^2 = 0.24$. Indeed, the mean failure rate for the bi-component response in these connections was 0.21 ±0.07 (n = 5). These values suggested that the two synapses were individual and operated independently.

Role of Individual Synapses in Plasticity

In 10 of 36 connections with induced LTP (Fig. 12) and in 3 of 8 connections with spontaneous LTP (Fig. 10D), some components of composite EPSCs could be well identified and it was possible to follow the changes in properties of individual synapses. In 6 cases, LTP (induced, n = 3; spontaneous, n = 3) was probably associated with an activation of previously silent synapses. One of these connections first showed EPSCs with only one component corresponding to activation of more distal synapse 2 (Fig. 16A1). After the application of induction protocol, a new component corresponding to activation of more proximal synapse 1 appeared (Fig. 16A2). These components could be seen both individually and overlapping (as a composite EPSC). We plotted the amplitudes of the components corresponding to synapse 1 and synapse 2 (Fig. 16A, right). In the episodes with overlapping responses, the EPSC amplitude for synapse 1 was measured from the baseline to the inflection point, and for synapse 2 from the inflexion point to the peak. As one can judge from the plot, the LTP was caused by the activation of previously silent proximal synapse 1, while the distal synapse 2 did not show substantial alteration of activity.

In the remaining 7 connections, the induced LTP was associated with an increase in the amplitude of components forming the composite EPSC. In the connection shown in Fig. 16B1 and B2, the EPSC components corresponding to activation of both the proximal synapse 1 and the distal synapse 2 were potentiated (Fig. 16B, right).

Thus, transmission efficacy can be increased through activation of silent synapses and potentiation of already active synapses.

Discussion

In this study we have described several novel properties of the neuronal network in the spinal SG. In particular, we have characterized excitatory synapses formed by glutamatergic SG interneurons on postsynaptic neurons located in laminae I-III. The major findings of this study are: 1) short (1 ms) depolarization of ~10 mV can initiate spike in the AIS of an SG neuron; 2) both CP- and CI-AMPARs are involved in transmission from an SG EIN; 3) the axon of an SG EIN forms multiple synapses on a

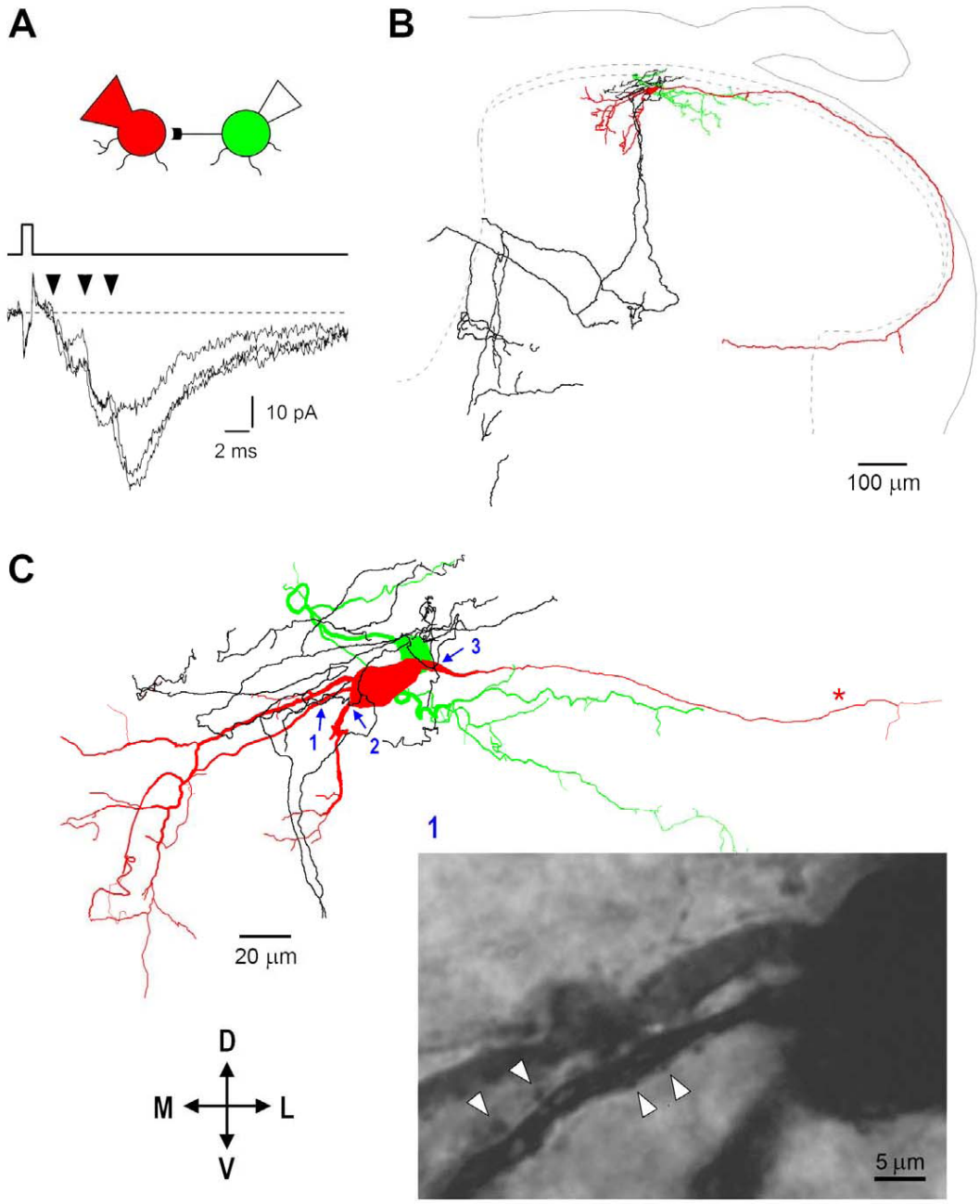

Figure 15. Reconstruction of synaptically connected neurons. A, composite EPSCs (−80 mV) with at least three components (arrowheads). The postsynaptic neuron was filled with biocytin in whole-cell mode, while the presynaptic one through the cell-attached pipette [28]. B, both cell bodies were in the SG. The axon of the postsynaptic neuron (red) ran along the dorsal surface of the grey matter, gave a collateral in the lateral column, and turned medially to re-enter the grey matter. The presynaptic cell axon (black) formed a dense network in the vicinity of the cell bodies and divided into two major branches which travelled to deeper laminae and turned towards the dorsal grey commissure. Soma and dendrites of the presynaptic neuron are shown in green. C, a number of close appositions between the varicosities of the presynaptic axon and the dendrites and soma of the postsynaptic neuron were detected in regions 1–3 (blue arrows). Some of them are shown (arrowheads) on the photomicrograph of the region 1. Objective; 100x (oil-immersion), numerical aperture 1.25.
doi:10.1371/journal.pone.0008047.g015

postsynaptic neuron; 4) synapses of SG EINs show broad somatodendritic distribution in the postsynaptic neuron; 5) high-R_{IN} recording from the postsynaptic neuron is necessary for correct estimation of transmission efficacy; 6) in many cases, release from one SG EIN is sufficient to elicit spike in a postsynaptic neuron; 7) synapses of the SG EINs undergo diverse forms of plasticity.

Rapid Spike Initiation in SG Neurons

Implementation of independent electrodes for stimulation of and recording from one neuron allowed study of the spike initiation process. Spikes in SG neurons consisted of two components similar to those described in motoneurons [37 39]. The fast one was an electrotonic projection of the spike generated in the AIS while the slow one corresponded to the antidromic spike invasion to the axon

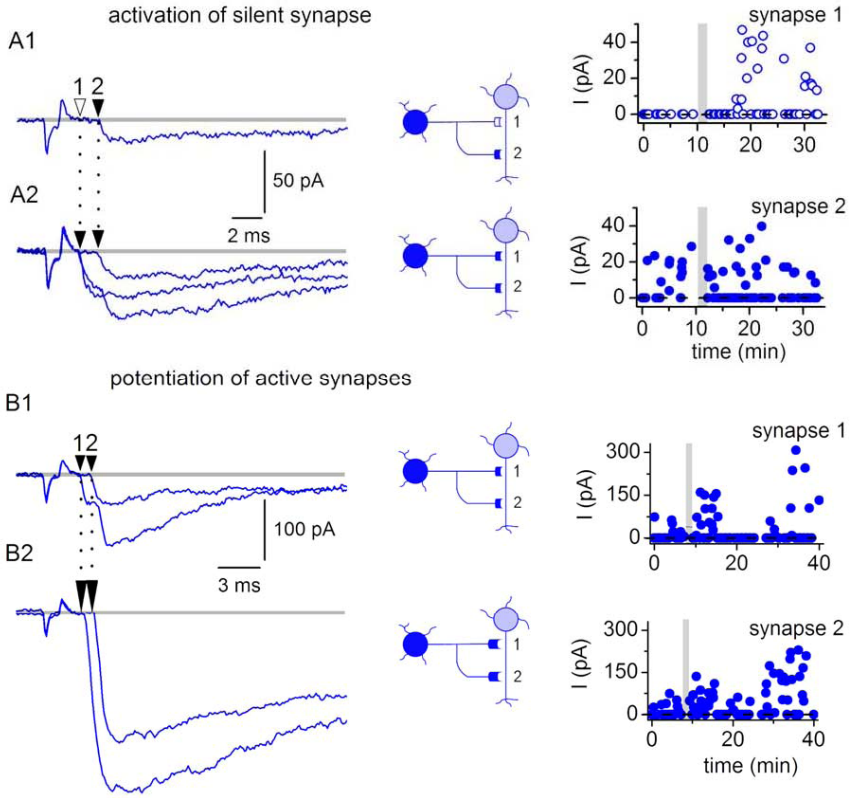

Figure 16. Role of individual synapses in plasticity. A1-2, LTP associated with an activation of a previously silent synapse. A1, EPSC elicited before the application of the induction protocol corresponded to activation of more distal synapse 2. A2, EPSC recorded after induction of LTP (1 Hz protocol). A new component corresponded to activation of more proximal synapse 1. Two plots show the amplitudes of the EPSC components corresponding to synapse 1 and synapse 2 during the experiment. The amplitudes were measured from non-averaged traces. B1-2, LTP associated with an increase in the amplitude of components forming the composite EPSC. Recordings before (B1) and after (B2) the LTP induction (1 Hz protocol). Two plots show the EPSC components corresponding to synapse 1 and synapse 2.
doi:10.1371/journal.pone.0008047.g016

hillock and soma [42,43]. Short (1 ms) depolarization of ~10 mV induced by the cell-attached stimulation was sufficient to trigger spike in the AIS, where the ratio of the Na^+ conductance to the passive capacitive load is high [43]. Similar thresholds were also obtained for synaptically evoked spikes in paired recordings. Substantially higher firing thresholds, however, were seen in our experiments with intracellular injections of 500 ms pulses (19 34 mV, measured from −70 mV [35]). It is likely that the slow depolarization evoked by a long pulse leads to a partial inactivation of Na^+ channels and activation of K_A channels prior to spike initiation, and therefore, increases the firing threshold and delay.

Multiple Synapses Formed by the Axon of an SG EIN

Analysis of composite EPSCs, computer simulations and labelling experiments indicated that the axon of an SG EIN forms multiple synapses on a postsynaptic neuron. In 83% of connections, the composite EPSCs showed visible transitions between the components. The true number of EINs forming multiple synapses may be even higher. The filter frequency (3 kHz) used in our experiments did not allow to see transitions faster than 0.3 ms, and responses from synapses separated by a short electrotonic distance could not be distinguished. Furthermore, there are silent synapses between the neurons which may become active under certain conditions. Therefore, formation of multiple synapses on a postsynaptic neuron appears to be a general property of an SG EIN.

The time intervals between the components of composite EPSCs could be explained by the electrotonic distances between the synapses in a postsynaptic neuron. In some cases, however, components with longer latency did not have apparently slower rise predicted from our simulations (see Figs. 13B1 and 15A). Therefore, it is possible that some presynaptic factors, like different axonal conduction time for each synaptic terminal, could also contribute to different latencies of the EPSC components. For example, different spike propagation delays at the branching points of the presynaptic axon could contribute to the intervals between the EPSC components.

Both CP- and CI-AMPARs are involved in transmission from SG EINs. AMPARs are known as main transducers of fast central glutamatergic synapses [53]. In agreement with this, EPSCs evoked by the SG EIN stimulations were fast. The distributions of the rise times and the decay time constants were in the range predicted by the model for the fast synapses located at different electrotonic distances from the soma. The longest EPSC latencies obtained (~5 ms) could not be explained by the time needed for the presynaptic spike propagation and transmitter release. Assuming the conduction velocity in an unmyelinated axon of 1 m/s and the length of the axon branch connecting neurons of <500 μm (our data), the propagation time could be estimated as <0.5 ms. Allowing 0.5 ms for transmitter release, the conduction delay in the presynaptic axon could be estimated as 1 ms. This time might further increase due to the spike propagation delays at

the axon branching points. However, the long latencies observed in our study were likely to be caused by the EPSC propagation in the dendrites of postsynaptic neuron. As modelling predicts, the electrotonic delay varies with the synapse location and it takes >3 ms for the distal EPSC to reach the soma. Thus, the variations in the EPSC kinetics and latencies reflected a broad somatodendritic distribution of synapses in the postsynaptic neuron.

Transmission Efficacy and Synaptic Plasticity

It is believed that excitatory connections between dorsal horn neurons are weak, and EPSPs of 0.9 2.6 mV [2] and 0.5 8.5 mV [50] are not sufficient to elicit postsynaptic spikes [50]. However, these conclusions were based on low-R_{IN} recording from a postsynaptic neuron, which reduced the amplitude of depolarization induced by activation of a given synaptic conductance (see Fig. 9, CC). Furthermore, dialysis of the presynaptic neuron could affect its capacity of transmitter release in multiple synapses. Small EPSCs (mean, 19 pA) in [50] corresponded to release in a single synapse. Thus, the true efficacy of excitatory transmission in those studies appeared to be underestimated.

Our data show that transmission between dorsal horn neurons can be effective. First, a non-dialysed SG EIN releases transmitter in multiple synapses, thus, increasing effective conductance depolarizing the postsynaptic membrane. Second, a high R_{IN} preserved in postsynaptic neuron allows better conversion of the synaptic conductance into membrane depolarization. Therefore, single EPSPs of >10 mV were regularly recorded. In many cases, input from an SG EIN was sufficiently strong to elicit spike in a postsynaptic neuron kept in CC at −70 mV. In some pairs, an SG EIN could even evoke repetitive firing in the postsynaptic neuron.

R_{IN} in dorsal horn neurons was shown to change with temperature [54]. Assuming that both the leak K^+ conductance (determining R_{IN}) and the glutamate-activated conductance (generating EPSP) have similar Q10 (aqueous diffusion of ions [55]) one can conclude that the ratio between them, and therefore, synaptic efficacy should not change with temperature.

We have found that synapses of SG EINs undergo diverse forms of functional plasticity. LTP could be induced through activation of silent synapses and through potentiation of already active synapses. One cannot exclude, however, that potentiation of the components of a composite EPSC was also caused by recruitment of silent synapses with similar electrotonic location, so that their activation did not result in generation of an apparently new component. It is possible that the activation of silent synapses and the strengthening of already active synapses can cooperate in induction of LTP. This plasticity might be induced by Ca^{2+} influx through CP-AMPARs [56] which are expressed in the superficial dorsal horn [10 13] and, as we show, are activated by release from SG EINs. It is also possible that heterogeneity of synaptic properties observed in the present study, like CP- and/or CI-AMPAR expression and plasticity, might correlate with the postsynaptic cell type [56].

Functional Balance between the Excitatory and Inhibitory Inputs

Reports about the balance between the excitatory and inhibitory connections in the spinal dorsal horn are contradictory. Studies using *in situ* hybridization [8], immunocytochemistry [9] and the high-R_{IN} paired recordings in VC ([4] and this study) showed that the majority of SG neurons are excitatory, whereas inhibitory neurons form a minority. In contrast, the low-R_{IN} CC recordings revealed more numerous inhibitory connections, and the authors suggested that the difference in the results was caused by a better detection of weak distal inhibitory inputs in CC [49,50]. However, our measurements of the membrane noise have shown that the high-R_{IN} VC has higher signal-to-noise ratio. The last factor which has not been considered so far is the driving force for the inhibitory inputs.

IPSPs in [3] were recorded at a 20 mV driving force (recording, −50 mV; E_{Rev} = −70 mV). IPSCs in [4] and here were recorded at similar driving force for both inward (−100 mV) and outward (−60 mV) currents (E_{Rev} = −82 mV). Thus, analyses of all factors showed that our VC recording has higher detection power. The true reason for lower frequency of excitatory connections in [2,3,49] can be a shunt of distal inputs by low-R_{IN} recording. Indeed, the longest latencies of IPSPs (3.3 ms) in [3] and EPSPs (2.1 ms) in [2] were short for CC recording, and indicated that none of inputs reported was distal. A recent study using the laser scanning photostimulation technique revealed that the inhibitory receptors are confined to the narrow peri-somatic region of an SG neuron while the glutamate receptors are more widespread [5]. Therefore, shunt of weak distal inputs [2,3,49], which are mostly excitatory [5], led to an underestimation of the number of excitatory connections.

The driving force for inhibitory inputs in [50] is unclear. IPSPs were recorded at −60 mV as hyperpolarizations, although at the Cl^- gradient used (20 mM/135.5 mM, E_{Cl} = −49 mV) they had to be depolarizing. This implied a voltage error of >15 mV. Furthermore, identification of monosynaptic IPSPs demands analysis of latency variations for individual traces. The voltage noise at −60 mV [36,51] does not allow reliable detection of non-averaged IPSPs of <0.5 mV. Therefore, many IPSPs in [50] (smallest 0.1 mV) were below the detection limit. Although in some traces apparent noise was lower than expected at −60 mV, this could mean that the true potential was more negative, for example, due to uncompensated liquid junction potential of 13 mV (calculated according to [32]). This, however, would increase the voltage error to ~30 mV. Thus, uncontrolled voltages and consideration of IPSPs with amplitudes below the resolution limit allowing tests for monosynaptic connectivity question conclusions about the high percentage of inhibitory connections [50].

In conclusion, we have shown that the EIN is an important processing element in the spinal SG. Its axon forms multiple synapses on the soma and dendrites of a postsynaptic neuron. Many of those synapses have functional CP-AMPARs. The excitatory transmission is frequently effective and an SG EIN can elicit spike in a postsynaptic neuron. The excitatory synapses are dynamic and can change their functional state through diverse forms of plasticity. These properties of the SG EINs are important for understanding the mechanisms of the spinal nociceptive processing.

Author Contributions

Conceived and designed the experiments: PS VD BVS. Performed the experiments: SFS LLL. Analyzed the data: SFS LLL DL BVS. Wrote the paper: PS VD BVS.

References

1. Basbaum A, Jessel T (2000) The perception of pain. In: Kandel E, Schwartz J, Jessel T, eds. Principles of neural science. 4th ed. New York: Mc Graw Hill. pp 472 491.

2. Lu Y, Perl ER (2005) Modular organization of excitatory circuits between neurons of the spinal superficial dorsal horn (laminae I and II). J Neurosci 25: 3900 3907.

3. Lu Y, Perl ER (2003) A specific inhibitory pathway between substantia gelatinosa neurons receiving direct C-fiber input. J Neurosci 23: 8752 8758.
4. Santos SF, Rebelo S, Derkach VA, Safronov BV (2007) Excitatory interneurons dominate sensory processing in the spinal substantia gelatinosa of rat. J Physiol 581: 241 254.
5. Kato G, Kawasaki Y, Ji RR, Strassman AM (2007) Differential wiring of local excitatory and inhibitory synaptic inputs to islet cells in rat spinal lamina II demonstrated by laser scanning photostimulation. J Physiol 580: 815 833.
6. Graham BA, Brichta AM, Callister RJ (2007) Moving from an averaged to specific view of spinal cord pain processing circuits. J Neurophysiol 98: 1057 1063.
7. Melzack R, Wall PD (1965) Pain mechanisms: a new theory. Science 150: 971 979.
8. Landry M, Bouali-Benazzouz R, El Mestikawy S, Ravassard P, Nagy F (2004) Expression of vesicular glutamate transporters in rat lumbar spinal cord, with a note on dorsal root ganglia. J Comp Neurol 468: 380 394.
9. Todd AJ, Sullivan AC (1990) Light microscope study of the coexistence of GABA-like and glycine-like immunoreactivities in the spinal cord of the rat. J Comp Neurol 296: 496 505.
10. Nagy GG, Al-Ayyan M, Andrew D, Fukaya M, Watanabe M, et al. (2004) Widespread expression of the AMPA receptor GluR2 subunit at glutamatergic synapses in the rat spinal cord and phosphorylation of GluR1 in response to noxious stimulation revealed with an antigen-unmasking method. J Neurosci 24: 5766 5777.
11. Larsson M, Broman J (2006) Pathway-specific bidirectional regulation of Ca2+/calmodulin-dependent protein kinase II at spinal nociceptive synapses after acute noxious stimulation. J Neurosci 26: 4198 4205.
12. Antal M, Fukazawa Y, Eordogh M, Muszil D, Molnar E, et al. (2008) Numbers, densities, and colocalization of AMPA- and NMDA-type glutamate receptors at individual synapses in the superficial spinal dorsal horn of rats. J Neurosci 28: 9692 9701.
13. Polgar E, Al-Khater KM, Shehab S, Watanabe M, Todd AJ (2008) Large projection neurons in lamina I of the rat spinal cord that lack the neurokinin 1 receptor are densely innervated by VGLUT2-containing axons and possess GluR4-containing AMPA receptors. J Neurosci 28: 13150 13160.
14. Vikman KS, Rycroft BK, Christie MJ (2008) Switch to Ca2+-permeable AMPA and reduced NR2B NMDA receptor-mediated neurotransmission at dorsal horn nociceptive synapses during inflammatory pain in the rat. J Physiol 586: 515 527.
15. Larsson M, Broman J (2008) Translocation of GluR1-containing AMPA receptors to a spinal nociceptive synapse during acute noxious stimulation. J Neurosci 28: 7084 7090.
16. Katano T, Furue H, Okuda-Ashitaka E, Tagaya M, Watanabe M, et al. (2008) N-ethylmaleimide-sensitive fusion protein (NSF) is involved in central sensitization in the spinal cord through GluR2 subunit composition switch after inflammation. Eur J Neurosci 27: 3161 3170.
17. Park JS, Voitenko N, Petralia RS, Guan X, Xu JT, et al. (2009) Persistent inflammation induces GluR2 internalization via NMDA receptor-triggered PKC activation in dorsal horn neurons. J Neurosci 29: 3206 3219.
18. Fang L, Wu J, Lin Q, Willis WD (2002) Calcium-calmodulin-dependent protein kinase II contributes to spinal cord central sensitization. J Neurosci 22: 4196 4204.
19. Larsson M, Broman J (2005) Different basal levels of CaMKII phosphorylated at Thr286/287 at nociceptive and low-threshold primary afferent synapses. Eur J Neurosci 21: 2445 2458.
20. Pedersen LM, Lien GF, Bollerud I, Gjerstad J (2005) Induction of long-term potentiation in single nociceptive dorsal horn neurons is blocked by the CaMKII inhibitor AIP. Brain Res 1041: 66 71.
21. Derkach VA, Oh MC, Guire ES, Soderling TR (2007) Regulatory mechanisms of AMPA receptors in synaptic plasticity. Nat Rev Neurosci 8: 101 113.
22. Melnick IV, Santos SF, Safronov BV (2004) Mechanism of spike frequency adaptation in substantia gelatinosa neurones of rat. J Physiol 559: 383 395.
23. Melnick IV, Santos SF, Szokol K, Szucs P, Safronov BV (2004) Ionic basis of tonic firing in spinal substantia gelatinosa neurons of rat. J Neurophysiol 91: 646 655.
24. Horn R, Marty A (1988) Muscarinic activation of ionic currents measured by a new whole-cell recording method. J Gen Physiol 92: 145 159.
25. Rae J, Cooper K, Gates P, Watsky M (1991) Low access resistance perforated patch recordings using amphotericin B. J Neurosci Methods 37: 15 26.
26. Hantman AW, van den Pol AN, Perl ER (2004) Morphological and physiological features of a set of spinal substantia gelatinosa neurons defined by green fluorescent protein expression. J Neurosci 24: 836 842.
27. Ohana O, Sakmann B (1998) Transmitter release modulation in nerve terminals of rat neocortical pyramidal cells by intracellular calcium buffers. J Physiol 513(Pt 1): 135 148.
28. Szucs P, Pinto V, Safronov BV (2009) Advanced technique of infrared LED imaging of unstained cells and intracellular structures in isolated spinal cord, brainstem, ganglia and cerebellum. J Neurosci Methods 177: 369 380.
29. Safronov BV, Pinto V, Derkach VA (2007) High-resolution single-cell imaging for functional studies in the whole brain and spinal cord and thick tissue blocks using light-emitting diode illumination. J Neurosci Methods 164: 292 298.
30. Marty A, Neher E (1995) Tight-seal whole-cell recording. In: Sakmann B, Neher E, eds. Single-channel recording 2nd ed. New York: Kluwer Academic/Plenum Publishers. pp 31 52.
31. Barry PH, Lynch JW (1991) Liquid junction potentials and small cell effects in patch-clamp analysis. J Membr Biol 121: 101 117.
32. Barry PH (1994) JPCalc, a software package for calculating liquid junction potential corrections in patch-clamp, intracellular, epithelial and bilayer measurements and for correcting junction potential measurements. J Neurosci Methods 51: 107 116.
33. Hines ML, Carnevale NT (1997) The NEURON simulation environment. Neural Comput 9: 1179 1209.
34. Hines M (1993) Neuron- a program for stimulation of nerve equation. In: Eeckman F, eds. Neural Systems: Analysis and Modeling. Boston: Kluwer Academic Publishers. pp 127 136.
35. Santos SF, Melnick IV, Safronov BV (2004) Selective postsynaptic inhibition of tonic-firing neurons in substantia gelatinosa by mu-opioid agonist. Anesthesiology 101: 1177 1183.
36. Diba K, Lester HA, Koch C (2004) Intrinsic noise in cultured hippocampal neurons: experiment and modeling. J Neurosci 24: 9723 9733.
37. Coombs JS, Curtis DR, Eccles JC (1957) The interpretation of spike potentials of motoneurones. J Physiol 139: 198 231.
38. Coombs JS, Curtis DR, Eccles JC (1957) The generation of impulses in motoneurones. J Physiol 139: 232 249.
39. Araki T, Terzuolo CA (1962) Membrane currents in spinal motoneurons associated with the action potential and synaptic activity. J Neurophysiol 25: 772 789.
40. Safronov BV, Wolff M, Vogel W (1997) Functional distribution of three types of Na+ channel on soma and processes of dorsal horn neurones of rat spinal cord. J Physiol 503(Pt 2): 371 385.
41. Safronov BV, Wolff M, Vogel W (1999) Axonal expression of sodium channels in rat spinal neurones during postnatal development. J Physiol 514(Pt 3): 729 734.
42. Safronov BV, Wolff M, Vogel W (2000) Excitability of the soma in central nervous system neurons. Biophys J 78: 2998 3010.
43. Safronov BV (1999) Spatial distribution of NA+ and K+ channels in spinal dorsal horn neurones: role of the soma, axon and dendrites in spike generation. Prog Neurobiol 59: 217 241.
44. Coombs JS, Eccles JC, Fatt P (1955) The electrical properties of the motoneurone membrane. J Physiol 130: 291 325.
45. Yoshimura M, Nishi S (1993) Blind patch-clamp recordings from substantia gelatinosa neurons in adult rat spinal cord slices: pharmacological properties of synaptic currents. Neuroscience 53: 519 526.
46. Chery N, de Koninck Y (1999) Junctional versus extrajunctional glycine and GABA(A) receptor-mediated IPSCs in identified lamina I neurons of the adult rat spinal cord. J Neurosci 19: 7342 7355.
47. Morisset V, Urban L (2001) Cannabinoid-induced presynaptic inhibition of glutamatergic EPSCs in substantia gelatinosa neurons of the rat spinal cord. J Neurophysiol 86: 40 48.
48. Lu VB, Biggs JE, Stebbing MJ, Balasubramanyan S, Todd KG, et al. (2009) Brain-derived neurotrophic factor drives the changes in excitatory synaptic transmission in the rat superficial dorsal horn that follow sciatic nerve injury. J Physiol 587: 1013 1032.
49. Lu Y (2008) Synaptic wiring in the deep dorsal horn. Focus on "Local circuit connections between hamster laminae III and IV dorsal horn neurons". J Neurophysiol 99: 1051 1052.
50. Schneider SP (2008) Local circuit connections between hamster laminae III and IV dorsal horn neurons. J Neurophysiol 99: 1306 1318.
51. Jacobson GA, Diba K, Yaron-Jakoubovitch A, Oz Y, Koch C, et al. (2005) Subthreshold voltage noise of rat neocortical pyramidal neurones. J Physiol 564: 145 160.
52. Berry MS, Pentreath VW (1976) Criteria for distinguishing between monosynaptic and polysynaptic transmission. Brain Res 105: 1 20.
53. Dingledine R, Borges K, Bowie D, Traynelis SF (1999) The glutamate receptor ion channels. Pharmacol Rev 51: 7 61.
54. Graham BA, Brichta AM, Callister RJ (2008) Recording temperature affects the excitability of mouse superficial dorsal horn neurons, in vitro. J Neurophysiol 99: 2048 2059.
55. Hille B (2001) Classical Biophysics of the squid giant axon. In: Hille B, ed (2001) Ion channels of excitable membranes. 3rd ed. Sunderland: Sinauer Associates, Inc. pp 25 60.
56. Oren I, Nissen W, Kullmann DM, Somogyi P, Lamsa KP (2009) Role of ionotropic glutamate receptors in long-term potentiation in rat hippocampal CA1 oriens-lacunosum moleculare interneurons. J Neurosci 29: 939 950.

Fourth publication

J Neurophysiol 91: 646–655, 2004.
First published October 1, 2003; 10.1152/jn.00883.2003.

Ionic Basis of Tonic Firing in Spinal Substantia Gelatinosa Neurons of Rat

Igor V. Melnick,[1] Sónia F. A. Santos,[1] Karolina Szokol,[2] Péter Szûcs,[2] and Boris V. Safronov[1]
[1]*Instituto de Biologia Molecular e Celular (IBMC), 4150–180 Porto, Portugal; and* [2]*Department of Anatomy, Histology, and Embryology, Faculty of Medicine, Medical and Health Science Centre, University of Debrecen, Debrecen, H-4012, Hungary*

Submitted 9 September 2003; accepted in final form 25 September 2003

Melnick, Igor V., Sónia F. A. Santos, Karolina Szokol, Péter Szûcs, and Boris V. Safronov. Ionic basis of tonic firing in spinal substantia gelatinosa neurons of rat. *J Neurophysiol* 91: 646–655, 2004.. First published October 1, 2003; First published October 1, 2003; 10.1152/jn.00883.2003. Ionic conductances underlying excitability in tonically firing neurons (TFNs) from substantia gelatinosa (SG) were studied by the patch-clamp method in rat spinal cord slices. Ca^{2+}-dependent K^+ (K_{CA}) conductance sensitive to apamin was found to prolong the interspike intervals and stabilize firing evoked by a sustained membrane depolarization. Suppression of Ca^{2+} and K_{CA} currents, however, did not abolish the basic pattern of tonic firing, indicating that it was generated by voltage-gated Na^+ and K^+ currents. Na^+ and K^+ channels were further analyzed in somatic nucleated patches. Na^+ channels exhibited fast activation and inactivation kinetics and followed two-exponential time course of recovery from inactivation. The major K^+ current was carried through tetraethylammonium (TEA)-sensitive rapidly activating delayed-rectifier (K_{DR}) channels with a slow inactivation. The TEA-insensitive transient A-type K^+ (K_A) current was very small in patches and was strongly inactivated at resting potential. Block of K_{DR} rather than K_A conductance by 1 mM TEA lowered the frequency and stability of firing. Intracellular staining with biocytin revealed at least three morphological groups of TFNs. Finally, on the basis of present data, we created a model of TFN and showed that Na^+ and K_{DR} currents are sufficient to generate a basic pattern of tonic firing. It is concluded that the balanced contribution of all ionic conductances described here is important for generation and modulation of tonic firing in SG neurons.

INTRODUCTION

Dorsal horn of the spinal cord is the first relay station in processing the sensory input from primary afferent terminals. Diversity of sensory modalities in dorsal horn is encoded by the type of peripheral afferent fiber, synaptic connectivity, and intrinsic firing properties of dorsal horn neurons (Brown 1981; Cervero 1987; Willis and Coggeshall 1991). Substantia gelatinosa (SG) is the dorsal horn region where most fine-calibre C- and Aδ-fibers terminate (LaMotte 1977; Light and Perl 1977; Rethelyi 1977; Sugiura et al. 1986) and is therefore considered as an important element of nociceptive processing system. Several types of SG neurons are distinguished on the basis of their intrinsic firing properties (Grudt and Perl 2002; Lopez-Garcia and King 1994; Thomson et al. 1989; Yoshimura and Jessell 1989). Among them, tonically firing neurons (TFNs) were described as exhibiting little spiking frequency adaptation during sustained depolarization. In functional terms, a majority of TFNs was shown to be either wide-dynamic-range or nociceptive-specific neurons (Lopez-Garcia and King 1994). According to their somatodendritic organization TFNs in SG belong to several distinct morphological types (Grudt and Perl 2002), suggesting that the intrinsic firing behavior might be mostly determined by the properties of ionic conductances present in the membrane. However, the knowledge about major types of ion channels specifically expressed in TFNs as well as their role in sustained firing is insufficient. Therefore we carried out this study and created a computer model to elucidate the ionic basis of tonic firing in SG neurons.

METHODS

Tight-seal recordings were done using 300-μm parasagittal slices prepared from the lumbar enlargement of the spinal cord of 2- to 5-wk-old rats (Bentley and Gent 1994; Chery et al. 2000; Edwards et al. 1989). The animals were killed in accordance with the local guidelines. After the anesthesia by intraperitoneal injection of pentobarbital sodium (30 mg/kg) the vertebral column was quickly cut out and immersed in ice-cold oxygenated artificial cerebrospinal fluid (ACSF). The 5- to 7-mm-long segment of the lumbar enlargement was dissected and glued to the stage of the tissue slicer (Leica VT 1000S). Four parasagittal slices (2 from each half of the spinal cord) were prepared and incubated for 30–60 min in ACSF at 33°C. SG (lamina II) was identified as a translucent band in the dorsal horn.

ACSF contained (in mM) 115 NaCl, 5.6 KCl, 2 $CaCl_2$, 1 $MgCl_2$, 11 glucose, 1 NaH_2PO_4, and 25 $NaHCO_3$ (pH 7.4 when bubbled with 95% O_2-5% CO_2). In some cases, 2 mM kynurenic acid was added to ACSF during preparation. Low-Ca^{2+}, high-Mg^{2+} solution (ACSF*) was obtained from ACSF by setting [Ca^{2+}] to 0.1 mM and [Mg^{2+}] to 5 mM. In some experiments K^+ currents were recorded in Na^+-free choline–Cl solution containing (in mM) 135 choline-Cl, 1.1 KCl, 0.1 $CaCl_2$, 5 $MgCl_2$, 11 glucose, and 10 HEPES. The pH value was adjusted to 7.4 by KOH (final [K^+] was 5.6 mM). Apamin and charybdotoxin were dissolved in ACSF with 0.05% BSA.

Standard pipette solution contained (in mM) 6 NaCl, 128 KCl, 2 $MgCl_2$, 10 EGTA, and 10 HEPES. The solution with low Ca^{2+} buffering capacity contained (in mM) 6 NaCl, 145 KCl, 2 $MgCl_2$, 1 EGTA, and 10 HEPES. The pH value in both solutions was adjusted to 7.3 with KOH (final [K^+] was 160.5 mM). Pipette solution for studying Na^+ channels contained (in mM) 4 NaCl, 131 CsCl, 2 $MgCl_2$, 10 EGTA, and 10 HEPES. The pH value was adjusted to 7.3 by CsOH (final [Cs^+], 153 mM) and NaOH (final [Na^+], 6 mM). All chemicals were purchased from Sigma.

The patch pipettes were pulled from thick-walled borosilicate glass tubes (Modulohm, Denmark; 1.50 mm OD/0.86 mm ID) and had a resistance of 3–5 MΩ after fire-polishing. The EPC-9 amplifier (HEKA, Lambrecht, Germany) was used in all experiments. The effective corner frequency of the low-pass filter was 3 kHz. The frequency of digitization was 10 kHz. Transients and leakage currents were digitally subtracted using standard P/n protocol. Offset potentials were nulled directly before formation of a seal. Liquid junction potentials were calculated and corrected for in all experiments. In

Address for reprint requests and other correspondence: B. V. Safronov, Instituto de Biologia Molecular e Celular (IBMC), Rua do Campo Alegre 823, 4150–180 Porto, Portugal (E-mail: safronov@ibmc.up.pt).

The costs of publication of this article were defrayed in part by the payment of page charges. The article must therefore be hereby marked "*advertisement*" in accordance with 18 U.S.C. Section 1734 solely to indicate this fact.

neurons subjected to detailed analysis the series resistance measured in the whole cell mode was 6–20 MΩ and was compensated by ≥60%. Action potentials were recorded using the fast current-clamp mode of the EPC-9 amplifier. Input resistance (R_{IN}) was measured in voltage-clamp mode using negative 10- to 40-mV pulses from a holding level of −80 mV. Only cells with a resting potential (V_R) negative to −60 mV were included into this study.

Ion channels were studied in two types of isolated structures: nucleated patches excised from somatic membrane (Sather et al. 1992) or entire somata (Safronov et al. 1997). Nucleated patches were usually obtained from deep neurons or larger superficial neurons and had diameters ranging from 5 to 8 μm. From the majority of superficial neurons, however, the entire soma with a diameter of 8–10 μm was isolated. We did not distinguish between those two structures and in the following text will refer them to as nucleated patches. For estimation of the current densities in isolated patches their mean diameter was assumed to be 7.5 μm.

The current–voltage (*I-V*) relationship for Na^+ channels was fitted with equation: $G_0/[1 + \exp((V_{50} - V)/k)] \times (V - V_{REV})$, where G_0 is the maximum conductance, V_{50} is the potential of half-maximum channel activation, k is a steepness factor, and V_{REV} is the reversal potential. V_{REV} obtained by fitting for each *I-V* curve was 10–20 mV more negative than a theoretical V_{Na} (+79 mV) due to appearance of outward Cs^+ current through delayed-rectifier K^+ channels incompletely blocked by 1 mM TEA. K^+ conductances were calculated assuming V_{REV} equal to V_K of −84 mV, in agreement with the data shown in Fig. 4*D*. The activation and steady-state inactivation characteristics were fitted with Boltzmann function: $1/(1 + \exp[(V_{50} - V)/k])$. The time course of Na^+ channel recovery from inactivation was fitted with a two-exponential function: $1 - A \times \exp(-t/\tau_F) - (1 - A) \times \exp(-t/\tau_S)$, where τ_F and τ_S are the fast and slow time constants and A is the relative amplitude of the fast component.

All numbers are given as mean ± SE. The values obtained by data fitting with a linear or nonlinear least-squares procedure are given as mean ± SE. In all figures the error bars are given when exceeding the symbol size. The present study is based on recordings from 266 SG neurons, 187 of which were classified as TFNs, and from 65 nucleated patches. All experiments were carried out at 22–24°C.

In some experiments, 0.5% biocytin (Sigma) was included in the pipette solution for later cell reconstruction. Following the recording session, the slices with biocytin-filled TFNs were transferred into a fixative containing 4% paraformaldehyde, 1.25% glutaraldehyde, and 0.2% picric acid in 0.1 M phosphate buffer (pH 7.4) for 7–10 days. After resectioning at 60 μm, slices were treated according to the avidin-biotinylated horseradish peroxidase method (Extravidin, diluted 1:1000, Vector Labs, Burlingame, CA) and the reaction was completed with a diaminobenzidine (Sigma, St. Louis, MO) chromogen reaction. Sections were counterstained with toluidine blue, dehydrated, and mounted with DPX (Fluka, Buchs, Switzerland). The somata as well as the dendritic and axonal arbors of labeled neurons were reconstructed from serial sections using a camera lucida with a ×100 oil immersion objective.

Computer simulations were done using NEURON software (Hines 1993; Hines and Carnevale 1997) with an integration step of 50 μs. Model consisted of the axon initial segment (AIS) and soma connected to an equivalent dendrite. This allowed us to construct a model of TFN independent of its belonging to one of three morphological groups described below. Parameters of the equivalent dendrite were calculated using standard procedure (Rall 1959, 1969; Dodge and Cooley 1973) on the basis of our recordings from six TFNs with R_{IN} = 1.7 ± 0.3 GΩ. Electrotonic length of the cylinder was calculated from the equation $L = \pi/(\tau_0/\tau_1 - 1)^{0.5}$, where τ_0 = 91 ± 10 ms (n = 6) and τ_1 = 4.1 ± 0.3 ms (n = 6) were the two slowest membrane time constants obtained by exponential "peeling" from the averaged (500 episodes) low-amplitude (<2 mV) passive decay transients evoked in current-clamp mode by short (1 ms) hyperpolarizing current pulses (not shown). Calculated L value was 0.68, indicating a compact electrotonic structure of TFNs. Assuming a uniform membrane capacitance (C_m) of 1 μF/cm^2, the specific membrane resistivity, $R_m = \tau_0/C_m$, was estimated to be 91 kΩcm^2. Using standard equations describing a passive cable, $\lambda^2 = DR_mR_i^{-1}/4$, $R_{IN} = 4\lambda R_i\pi^{-1}D^{-2}\coth L$ and $l = L\lambda$, where λ is a characteristic length, D is a diameter of the equivalent dendrite, R_i is an axial resistance, l is a length of the equivalent cylinder, and, assuming R_i of 80 Ωcm (Barrett and Crill 1974; Thurbon et al., 1998) and R_{IN} of 1.7 GΩ, one could estimate the dimensions of the equivalent dendrite, l = 1371 μm and D = 1.4 μm. The soma was considered a 10-μm-long cylinder with a 10-μm diameter. AIS was 30 μm long and linearly tapered in diameter from 1.0 μm at base to 0.5 μm at its distal end (Gobel et al. 1980). The C_m, R_m, and R_i values in the soma and AIS were the same as in the dendrite. The soma, AIS, and equivalent dendrite consisted of 10, 30, and 50 compartments, respectively. V_R in the model was −70 mV.

The models of Na^+ and K_{DR} currents were developed on the basis of our recordings. Na^+ current was described by a Hodgkin–Huxley style equation $g_{Na}m^3h(V - V_{Na})$, where g_{Na} was the Na^+ conductance, m and h were the variables of activation and inactivation, respectively, and V_{Na} was +60 mV. The steady-state activation variable (m_∞) and the time constant of activation (τ_m) were determined as $m_\infty = \alpha_m/(\alpha_m + \beta_m)$ and $\tau_m = 1/(\alpha_m + \beta_m)$, where $\alpha_m = 0.182(V + 33)/\{1 - \exp[-(V + 33)/9]\}$ and $\beta_m = -0.124(V + 33)/\{1 - \exp[(V + 33)/9]\}$ were reaction rates. The time constant of inactivation (τ_h) was determined as $\tau_h = 1/(\alpha_h + \beta_h)$ with $\alpha_h = -0.0018(V + 82)/\{1 - \exp[(V + 82)/18]\}$ and $\beta_h = 0.061(V + 46)/\{1 - \exp[-(V + 46)/3]\} + 0.0166$. The steady-state inactivation variable was given as $h_\infty = 1/\{1 + \exp[(V + 75)/9]\}$. K_{DR} current was described as $g_Kn^4h(V - V_K)$, where g_K was the K_{DR} conductance, n was the variable of activation, and V_K was −84 mV. The parameters were $n_\infty = \alpha_n/(\alpha_n + \beta_n)$, $\tau_n = 1/(\alpha_n + \beta_n)$, $\alpha_n = 0.035(V + 15)/\{1 - \exp[-(V + 15)/9]\}$, $\beta_n = 0.014\exp[-(V - 12)/46]$, $h_\infty = \alpha_h/(\alpha_h + \beta_h)$, $\tau_h = 1/(\alpha_h + \beta_h)$, $\alpha_h = 0.0083\{1 + 1/[\exp((V + 20)/10) + 1]\}$ and $\beta_h = 0.0083/\{\exp[-(V + 20)/10] + 1\}$.

K_{DR} current density in the soma was adjusted in agreement with our present measurements. Those in the dendrite and AIS were determined by simulating the experiments from Wolff et al. (1998), which showed that the ratio of somatic/dendritic/AIS components of K_{DR} current recorded in voltage-clamp mode with electrode placed on the soma was 15/47/38. These conditions were satisfied if g_K was 34, 4.3 and 76 mmho/cm^2 for the dendrite, soma, and AIS, respectively. Inactivating Na^+ channels were only inserted in the soma and AIS (Safronov 1999). On the basis of our present results g_{Na} was set to 8 mmho/cm^2 for the soma. In AIS g_{Na} was set to 1800 mmho/cm^2 to reach the maximum velocity of spike depolarization of 229 V/s (mean value for 70 TFNs). At a V_R of −70 mV, the density of available Na^+ channels with a conductance of 11.6 pS (Safronov et al. 1997) was 0.55 μm^{-2} in the soma and 124 μm^{-2} in AIS. Since the K_A current in TFNs was small and almost completely inactivated at V_R, it was not included into the model.

RESULTS

TFNs were identified in SG as neurons able to support sustained firing during 500-ms depolarization evoked by an injection of inward current. Of a total of 266 SG neurons tested, 187 (70%) were TFNs with V_R of −67 ± 1 mV (n = 117) and R_{IN} of 1.14 ± 0.08 GΩ (n = 117). In all TFNs the firing frequency progressively increased with stimulation intensity (Fig. 1*A*). Frequency-current (*f-I*) curves for the first interspike interval (instantaneous) and the last few intervals (steady-state) as well as the instantaneous firing frequency as a function of time (*f-t* plot) are shown in Fig. 1*B*. The steady-state *f-I* characteristic was nonlinear with an initial slope of 0.61 ± 0.08 Hz/pA (n = 8).

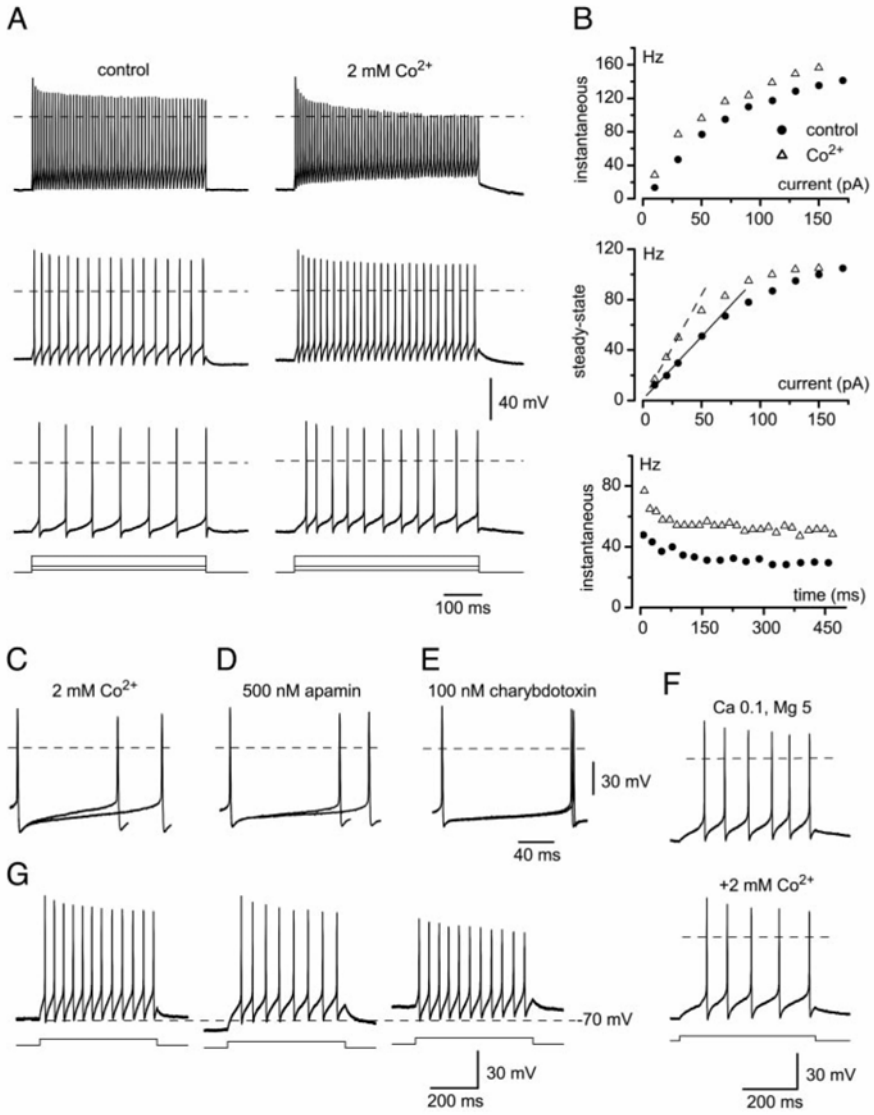

FIG. 1. Effects of Ca^{2+} and V_R on firing pattern. *A*: tonic firing evoked in control [artificial cerebrospinal fluid (ACSF), 2 mM Ca^{2+}] and after an equimolar substitution of Co^{2+} for Ca^{2+}. Dashed lines indicate 0 mV. Depolarizing current pulses of 10, 30, and 130 pA were applied for 0.5 s. *B*: plots of the instantaneous and the steady-state firing frequency characteristics as functions of injected current (*f-I*) and the instantaneous firing frequency at 30 pA stimulation as function of time (*f-t*). Effects of 2 mM Co^{2+} (*C*), 500 nM apamin (*D*), and 100 nM charybdotoxin (*E*) on interspike potentials during sustained firing. Each superimposed pair of traces was recorded at the same stimulation intensity. *F*: tonic firing in ACSF* (0.1 Ca^{2+}–5 Mg^{2+}) before and after addition of 2 mM Co^{2+}. Current protocol is the same for both traces. *G*: trains of action potentials evoked in a tonically firing neuron (TFN) at varying V_R, which was set to –70, −80, and –60 mV by injecting a steady-state in- or outward current (<15 pA) through the recording pipette.

Ca^{2+}-dependent conductances

Blockers of Ca^{2+} and K_{CA} channels were tested to study the role of Ca^{2+}-dependent conductances. In these experiments intracellular solution containing 1 mM EGTA was used. After equimolar substitution of 2 mM Ca^{2+} in ACSF by inorganic Ca^{2+} channel blockers Co^{2+} ($n = 8$) or Mn^{2+} ($n = 5$), several modifications of firing pattern were observed. At low stimulation intensities, the firing frequencies increased (Fig. 1, *A* and *B*, shown for Co^{2+}), so that the initial slope of the steady-state *f-I* curve reached 1.14 ± 0.12 Hz/pA ($n = 8$). At strong stimulation, however, the steady-state frequency was similar to control value, but pronounced spike attenuation within the train appeared in Co^{2+} or Mn^{2+}. Thus the block of Ca^{2+} influx into the neuron led to a left-shift in the *f-I* characteristics and a reduction of firing stability. The effects of Co^{2+} or Mn^{2+} on TFN firing resulted from a reduction of a slow afterhyperpolarization (Fig. 1*C*). Similar effects were also seen in ACSF after addition of 500 nM apamin (Fig. 1*D*; $n = 5$) but not 100 nM charybdotoxin (Fig. 1*E*; $n = 4$), indicating the involvement of small conductance apamin-sensitive, rather than big conductance K_{CA} channels. It could be therefore concluded that *1*) Ca^{2+}-dependent conductances are involved in regulation of firing frequency in TFNs, but *2*) the basic pattern of tonic firing is generated by voltage-gated Na^+ and K^+ channels.

The following study of Na^+ and K^+ channels was carried out in ACSF* (0.1 mM Ca^{2+}–5 mM Mg^{2+}) with 10 mM EGTA in pipette solution to minimize the contribution of Ca^{2+}-dependent conductances. Under these conditions, TFNs showed sustained firing, but addition of 2 mM Co^{2+} did not shorten intervals between spikes (Fig. 1*F*, $n = 5$). Further substitution of internal EGTA with fast Ca^{2+} chelator BAPTA (10 mM) did not change the pattern recorded in ACSF* ($n = 5$; not shown). Thus a combination of external ACSF* and internal 10 mM EGTA, used in all of the following experiments, was adequate for minimizing Ca^{2+}-dependent conductances.

An appearance of tonic firing did not depend on V_R in the range between −80 and −60 mV (Fig. 1*G*). Hyper- or depolarization of TFN by injection of sustained current did not prevent generation of tonic firing evoked by depolarizing cur-

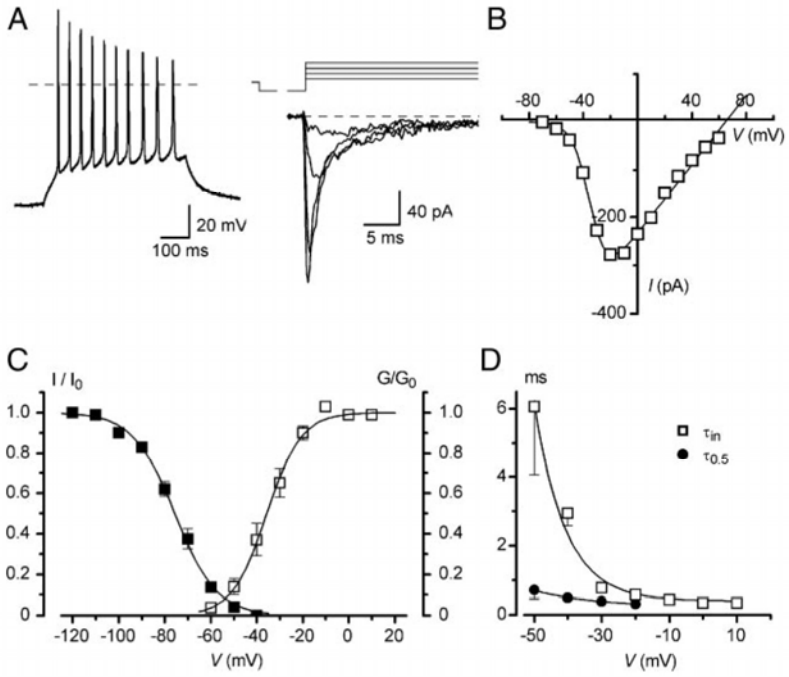

FIG. 2. Activation and inactivation of Na^+ channels. *A*: identification of a TFN in current-clamp mode a few seconds after the membrane rupture with a pipette containing Cs^+ solution. *B*: Na^+ currents activated in a nucleated patch by depolarization to –50, −40, −30, and –20 mV following a 50-ms prepulse to –120 mV, holding potential −80 mV. Current-voltage (*I-V*) curve is shown for the same neuron. *C*: steady-state activation and inactivation characteristics of Na^+ channels. Fitting parameters are given in the text. *D*: the rise time of a half-maximum current ($\tau_{0.5}$) and inactivation time constants (τ_{in}) as a function of membrane potential ($n = 6$).

rent pulses ($n = 25$). Therefore in current-clamp experiments all neurons were uniformly kept at –70 mV by injecting the holding current, which did not exceed 45 pA.

Na^+ channels

Na^+ channels were studied in nucleated patches using pipette solution in which K^+ was substituted with Cs^+. Since neurons could not keep V_R and tonic firing without internal K^+, their characterization was done during the first 10–15 s after membrane was broken, before pipette Cs^+ substituted intracellular K^+ (Fig. 2*A*). For Na^+ current recording in patches, 1 mM TEA was added to ACSF* to reduce outward K^+ current. Na^+ channels began to activate at –50 mV and had fast opening kinetics (Fig. 2, *B* and *D*). Their activation characteristic fitted with Boltzmann equation had $V_{50} = -35.7 \pm 0.6$ mV and $k = 7.5 \pm 0.5$ mV (Fig. 2*C*, $n = 6$). The steady-state inactivation of Na^+ channels, studied with 50-ms conditioning prepulses, revealed a half-maximum inactivation at -75.5 ± 0.1 mV and $k = -9.1 \pm 0.1$ mV (Fig. 2*C*, $n = 5$).

The kinetics of Na^+ channel inactivation was studied by fitting the current decay. Whenever possible, a monoexponential function was used. In cases where two-exponential fitting was needed, the time constant of the dominating fast component was considered as the inactivation time constant (τ_{in}) of Na^+ current. The τ_{in} changed from 6.1 ± 2.1 ms at –50 mV to 0.39 ± 0.04 ms at +10 mV (Fig. 2*D*, $n = 6$). The time course of Na^+ channel recovery from inactivation at potentials close to V_R was studied using a standard two-pulse protocol (Fig. 3*A*). The membrane was held at −80 mV and two 25-ms voltage pulses to –30 mV with varying intervals were applied. Recovery of channels from inactivation followed a double-exponential time course. The time constants, fast and slow, were $\tau_F = 21.8 \pm 1.7$ ms (63%) and $\tau_S = 793 \pm 92$ ms (37%), respectively (Fig. 3*B*, $n = 7$).

Recovery from inactivation seemed to be too slow to explain firing frequencies about 100 Hz (10-ms spike intervals) observed in experiments from Fig. 1*A*. To understand the reason for this apparent discrepancy we analyzed a degree of Na^+

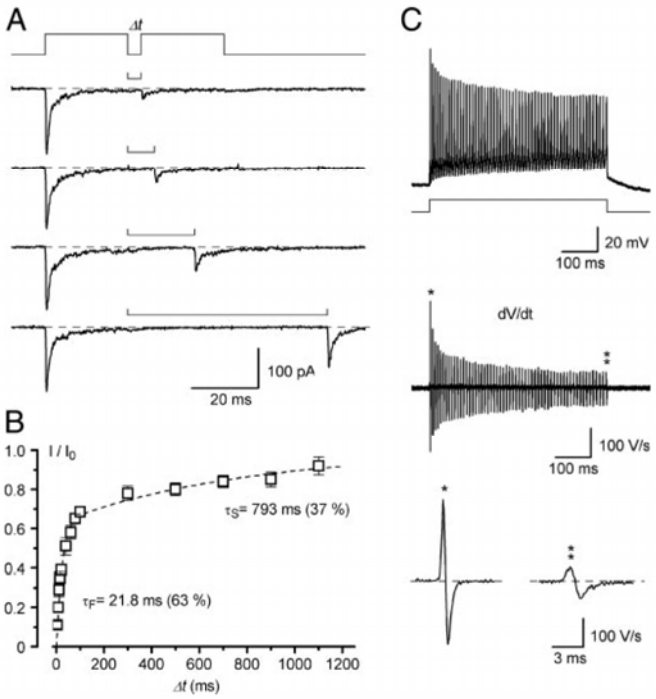

FIG. 3. Kinetics of Na^+ channel recovery from inactivation. *A*: Na^+ currents activated by pairs of 25-ms pulses from –80 to –30 mV with varying intervals (4, 8, 20, and 60 ms). *B*: time course of Na^+ channel recovery from inactivation at –80 mV ($n = 7$). The data are fitted using a double-exponential function. *C*: estimation of Na^+ channel inactivation during sustained firing. Train of action potentials recorded in the presence of 2 mM Co^{2+} (taken from Fig. 1*A*) was differentiated to give a rate of membrane polarization as derivative d*V*/d*t*. **Derivatives of the first and last spikes are given below at expanded time scale.

channel inactivation during a high-frequency firing in the presence of 2 mM Co^{2+}. The top trace from Fig. 1*A* (right) was differentiated (Fig. 3*C*). The inward current charging the membrane is proportional to the depolarization rate according to an equation $I = C(dV/dt)$, where C is a membrane capacitance. Each positive peak of the differentiated trace reflected maximum Na^+ current depolarizing the neuron during the corresponding spike. Within the train the depolarization rate was reduced from 290 V/s at the first spike to 58 V/s at the last one. In five neurons recorded either in the presence of 2 mM Co^{2+} or in ACSF*, the amplitude of Na^+ current contributing to the last spike in a train was 0.22 ± 0.04 of the first spike. This is in good agreement with a value of 0.24 predicted from a fitting curve in Fig. 3*B* for a recovery time of 10 ms. Thus a high-frequency firing can be generated with only about one-fifth of available (noninactivated) Na^+ channels.

Delayed-rectifier K^+ (K_{DR}) channels

The major voltage-gated K^+ current found in TFNs was a slowly inactivating K_{DR} current (Fig. 4*A*). Patch was held at −80 mV and depolarizing voltage pulses were applied after a 150-ms prepulse to −60 mV inactivating transient A-type K^+ (K_A) currents. The threshold of K_{DR} current was −40 mV and conductance reached saturation at +20 mV (Fig. 4*B*). The fitting of the activation characteristic with Boltzmann equation gave $V_{50} = -19.8 \pm 0.4$ mV and $k = 9.9 \pm 0.4$ mV ($n = 13$). To describe the activation kinetics we measured the rise time of a half-maximum current ($\tau_{0.5}$). At potentials positive to +30 mV, the $\tau_{0.5}$ became shorter than 1 ms (Fig. 4*B*, $n = 9$). Thus gating kinetics of K_{DR} current was sufficiently fast for its involvement in spike repolarization.

Starting from –20 mV, a partial inactivation of K_{DR} current with a monoexponential time course developed. The τ_{in} was weakly voltage dependent, changing from 79.8 ± 12.5 ms at –10 mV to 59.0 ± 3.2 ms at +60 mV (Fig. 4*C*, $n = 9$). V_{REV} for K_{DR} conductance was estimated from tail currents evoked by voltage return from +40 mV to different levels (Fig. 4*D*). The tail current changed almost linearly with a voltage and reversed its polarity near to V_K of −84 mV ($n = 5$).

Tail currents were also used to measure the closing rate of K_{DR} channel at −60 mV. They were recorded after short and long depolarizing pulses to +60 mV (Fig. 4*E*). The short pulse of 3–5 ms was adjusted to terminate at a peak of the current giving the tails corresponding to the total (noninactivated) K_{DR} current. This tail current decayed monoexponentially with a time constant of 5.9 ± 1.3 ms ($n = 6$). Similar measurement was also done after a 200-ms pulse, for a partially inactivated K_{DR} current. The tail currents became smaller but decayed monoexponentially with a similar time constant of 5.3 ± 1.1 ms. The observed fast closing rate of K_{DR} channel correlated well with high frequencies of tonic firing seen in current-clamp experiments.

In 1 mM TEA, K_{DR} current was blocked to 20.3 ± 1.5% (Fig. 4*F*, $n = 4$). The kinetics of control and remaining currents were very similar, which was better seen when the traces were normalized and superimposed (Fig. 4*F*, *bottom*). In 10 mM TEA, the current was reduced to 8.4 ± 1.3% ($n = 5$) but the current kinetics remained unchanged (not shown).

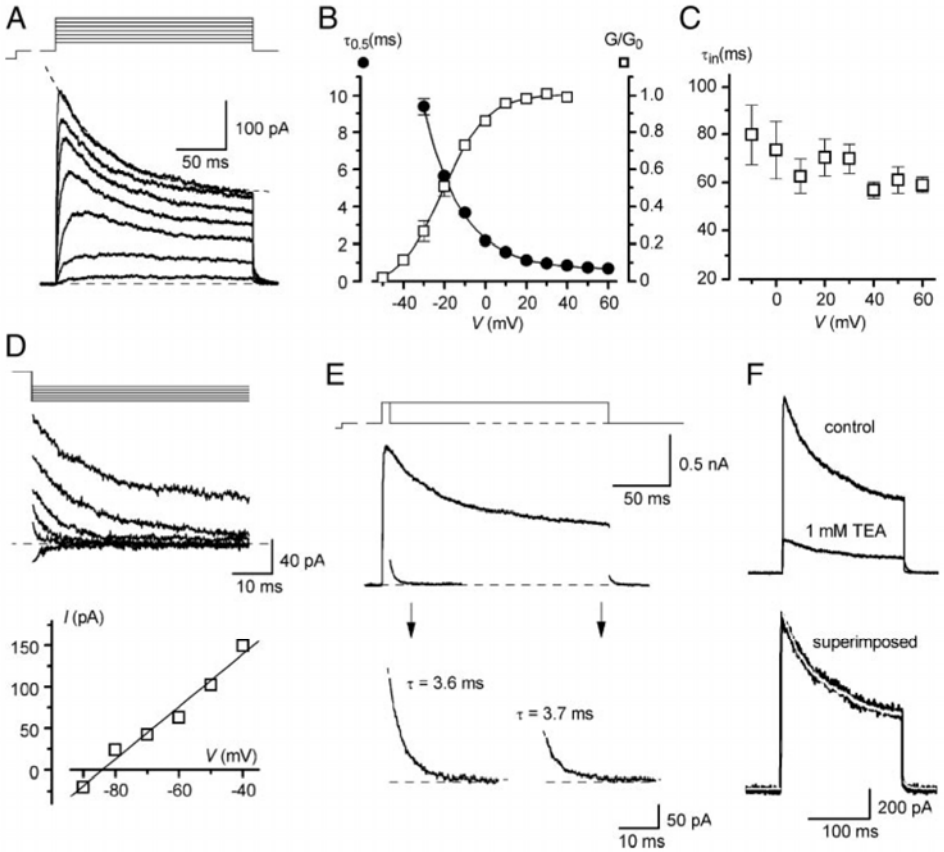

FIG. 4. K_{DR} current in nucleated patches. *A*: K_{DR} currents activated by 200-ms depolarizing pulses (from −40 mV to +20 mV in 10-mV steps) following a 150-ms prepulse to −60 mV. Holding potential, −80 mV. Decay of the current at +20 mV is fitted with a monoexponential function. *B*: steady-state activation curve and the rise time of a half-maximum current ($\tau_{0.5}$). *C*: τ_{in} at different potentials. *D*: measurements of V_{REV} for K_{DR} current. Tail currents at potentials between −40 and –90 mV in 10-mV steps. *I-V* relationship for these tail currents is shown below. *E*: closing rate of K_{DR} current. Tail currents recorded at −60 mV after a short (3 ms) and long (200 ms) depolarization pulses to +60 mV (prepulse: 150 ms, −60 mV; holding potential, −80 mV). The tail currents are shown below enlarged. Superimposed dashed lines are monoexponential fittings. *F*: K_{DR} current in control solution and in the presence of 1 mM tetraethylammonium (TEA). Both traces were normalized and are shown superimposed below. The control trace is given by white color. Pulse protocol: holding potential, −80 mV; prepulse, −60 mV, 150 ms; depolarizing pulse, +60 mV, 200 ms.

K_A current

In somatic patches from TFNs, a transient K_A current was much smaller than K_{DR} current. K_A current could not be separated using a standard procedure with two prepulses (to −120 and −60 mV), since the difference trace was always dominated by the slowly inactivating K_{DR} current, the amplitude of which also depended on the prepulse. Therefore we recorded K^+ currents elicited by a voltage step from –120 to +60 mV before and after addition of 10 mM TEA (Fig. 5*A*). In control solution no fast inactivating component could be revealed and a monoexponential fitting with a slow τ_{in} typical for K_{DR} current adequately described inactivation. In 10 mM TEA, K_{DR} current decreased (Fig. 5*A*, *left*) and the fast inactivating component could be resolved in the remaining current (*right*, the same trace is shown amplified). A double-exponential fitting revealed the fast component of inactivation, $\tau_A = 6.6 \pm 0.8$ ms at +60 mV ($n = 8$).

Because of its small amplitude in nucleated patches and lack of possibility of clear separation, some properties of K_A current were studied in a whole cell mode. K_A current was activated by pulses from –120 mV to –60 or –55 mV, voltages subthreshold for activation of Na^+ current. Since, in the majority of TFNs, K_A current was too small to be studied, we chose seven cells with the largest current ranging between 40 and 250 pA for analysis. The steady-state inactivation of K_A current with $V_{50} = -96.3 \pm 1.2$ mV and $k = -7.2 \pm 0.8$ mV (Fig. 5*B*, $n = 5$) showed that it was almost completely inactivated at V_R. The whole cell recordings were also used to study the sensitivity of K_A current to 10 mM TEA. For control of TEA diffusion into the slice we also monitored a reduction of K_{DR} current activated by a voltage step from −60 to –20 mV (Fig. 5*C*). K_A current was resistant to 10 mM TEA, the remaining part being 0.99 ± 0.17 ($n = 5$) of the control current.

Densities of Na^+ and K^+ currents

For estimation of the current densities the mean diameter of nucleated patch was assumed to be 7.5 μm giving a membrane area of 177 μm^2. The maximum amplitude of Na^+ current activated after a 50-ms prepulse to –120 mV was 208 ± 31 pA ($n = 15$), corresponding to a density of 1.18 pA μm^{-2}. The

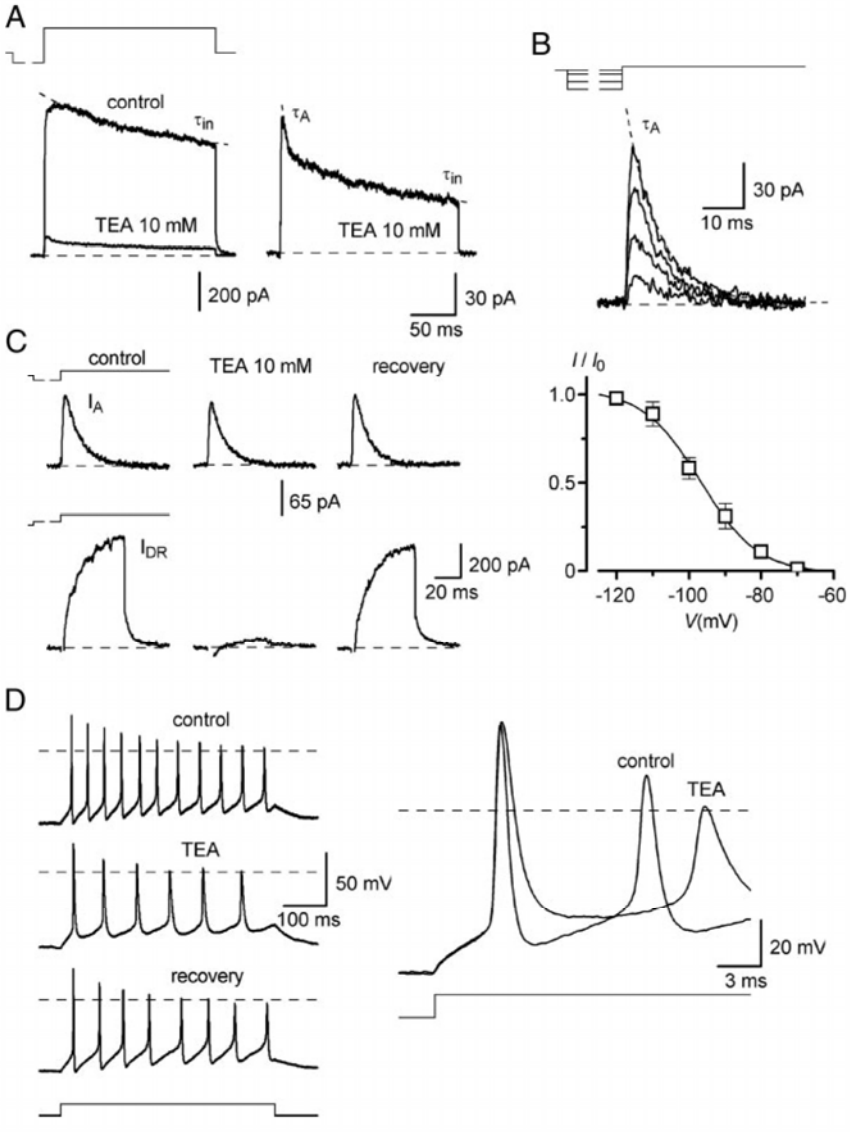

FIG. 5. K_A currents in patches and TFNs. *A*: total K^+ current activated in a nucleated patch by a voltage step from –120 (150 ms) to +60 mV (200 ms) in the presence and absence of 10 mM TEA. Holding potential, −80 mV. The trace in TEA is shown at higher magnification (*right*). The amplitude of K_A current was obtained from a double-exponential fitting of the decay kinetics as the amplitude of the fast component (τ_A). *B*: steady-state inactivation. Whole cell K_A currents recorded at −60 mV after a 150 ms prepulse to varying potentials (–130, −110, −90 and −80 mV). Holding potential, −80 mV. Steady-state inactivation characteristic was fitted with Boltzmann equation. *C*: effects of 10 mM TEA on K_A and K_{DR} currents. Holding potential, −80 mV. K_A currents were activated by step from –120 to −60 mV, whereas K_{DR} currents by a voltage step from −60 to –20 mV. *D*: firing frequency at 10 pA stimulation is reduced in 1 mM TEA (*left*). *Right*, slowing down the spike repolarization in 1 mM TEA (stimulation, 190 pA).

amplitude of K_{DR} current measured at a voltage step from −60 to +60 mV was 1049 ± 193 pA (n = 8), giving a mean current density of 5.9 pA μm^{-2}. It should be noted the K_{DR} channels were inactivated to some degree at −60 mV. The total K^+ current seen after a –120 mV prepulse was larger by a factor of 1.23 ± 0.05 (n = 11), but it represented a mixture of the K_{DR} and K_A currents that could not be clearly separated.

Based on our whole cell recordings, it could be assumed that K_A currents in patches were not substantially reduced in 10 mM TEA. At the voltage step from –120 to +60 mV, the amplitude of K_A current estimated by the fitting was 123.1 ± 34.6 pA (n = 8), giving a density of 0.7 pA μm^{-2}. It should be noted that the K_A current formed only 8.6 ± 1.6% (n = 8) of a total (K_{DR} + K_A) current when recorded after a –120-mV prepulse and became negligible when depolarization was applied after prepulses close to the V_R level.

Role of K_{DR} current in tonic firing

An involvement of K_{DR} channels in tonic firing was tested in current-clamp mode by comparing the patterns recorded in the presence and absence of 1 mM TEA, which partially blocked K_{DR}, but not K_A, current. The firing frequency and stability, at a given stimulation strength, were reduced in 1 mM TEA (Fig. 5*D*, n = 6). These effects resulted from slowing down the spike repolarization and disappearance of fast afterhyperpolarization (Fig. 5*D*, *right*). Thus a reduction of K_{DR} rather than K_A current was critical for generation of repetitive firing.

Morphology of TFNs

Twelve biocytin-filled TFNs were reconstructed and six of them are shown in Fig. 6. On the basis of their dendritic arborization and appearance, TFNs could be divided into three major groups. The cells belonging to the first group (Fig. 6*A*, n = 5) had triangular/pyramidal somata with three to four main dendrites passing the border between lamina II (SG) and III. The axon, when reconstructed, stayed at the level of the cell body and was extensive in a rostrocaudal orientation. Neurons with a similar appearance were classified as stalked cells (Eckert et al. 2003; Gobel 1978; Todd 1988). The second group of neurons (Fig. 6*B*, n = 3) was characterized by smaller fusiform somata, dendrites bearing large beads, and axon branching around the cell body. The cells from the final group (Fig. 6*C*, n = 4) had rounded somata with multiple extensively branching dendrites either in a multipolar or a bipolar organization. The axons were recovered mainly in lamina II (SG). Neurons with similar features were referred to as islet cells (Eckert et al. 2003; Gobel 1978; Todd 1988). The neurons from all three groups had similar electrophysiological parameters: V_R, −70 ± 2, −73 ± 3, and −71 ± 4 mV; R_{IN}, 1.25 ± 0.30, 1.16 ± 0.26, and 1.17 ± 0.15 GΩ; τ_0, 94.4 ± 9.3, 98.3 ± 23.4, and 102.7 ± 7.4 ms for the first (n = 5), second (n = 3), and third (n = 4) group TFNs, respectively.

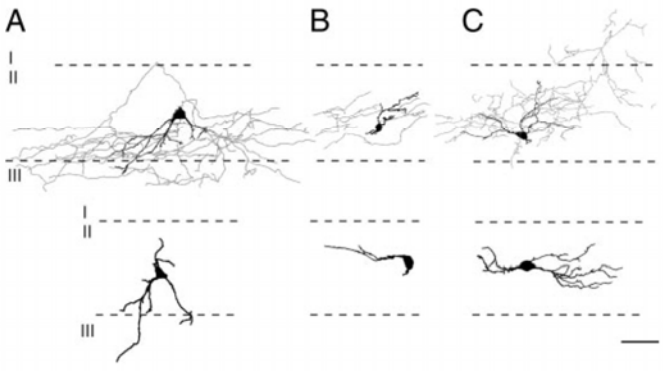

FIG. 6. Camera lucida reconstruction of biocytin-filled TFNs from SG (lamina II). Somata and dendrites were reconstructed from serial sections. The axon, shown only at *top*, was reconstructed from a single section and is therefore not considered as complete. Some shrinkage is likely to have occurred during the histological processing, which is apparent from the undulating appearance of the dendrites. *A*: neurons with triangular/pyramidal soma and dendrites extending into lamina III. *B*: neurons with smaller somata and dendrites bearing large dendritic beads. *C*: neurons with multiple extensively branching dendrites and rich axonal arbor occupying mainly lamina II. Dashed lines represent the borders between lamina I, II, and III. Scale bar = 50 μm.

Computer simulation

To test our assumption about the role of Na^+ and K_{DR} currents in the generation of tonic firing, we built a computer model of TFN. Inclusion of these conductances was sufficient to provide firing in a broad range of frequencies (Fig. 7*A*). The steady-state firing *f-I* characteristic of the model with the initial slope of 1.5 Hz/pA (Fig. 7*B*) was very similar to that recorded in TFNs. At high-frequency firing the degree of interspike recovery of Na^+ channels from inactivation was about one-fifth of the resting level seen before the first spike (Fig. 7*C*), indicating that a high safety factor for the spike generation is important for the appearance of high-frequency firing.

To study the interplay between Na^+ and K_{DR} channels, we plotted the variables h (Na^+) and n^4 (K_{DR}) during the steady-state firing (Fig. 7*D*). At low frequencies (*left*), both parameters returned to their interspike level 10–20 ms after each spike and the delay to the next one was mostly determined by the passive membrane properties. At maximum frequencies, however, the next spike was generated just after the major part of K_{DR} conductance, preventing membrane depolarization, was deactivated (*right*). The degree of Na^+ channel recovery from inactivation, in turn, determined the spike overshoots, which were reduced to 0 mV at maximum frequencies. The kinetics of the Na^+ channel activation was much faster (m^3, Fig. 7*D*), indicating that it did not limit the firing rate. Removal of Na^+ channels from the soma reduced the single spike overshoot by <0.5 mV and did not affect the tonic firing.

DISCUSSION

Tight-seal recordings from TFNs in SG were performed to study ionic mechanisms of tonic firing. TFNs represented the most frequent SG cell type able to fire spikes during sustained depolarization without remarkable frequency adaptation and amplitude attenuation. Our data support most reports describing this abundant type of neuron in superficial dorsal horn (Grudt and Perl 2002; Lopez-Garcia and King 1994; Prescott and De Koninck 2002; Thomson et al. 1989), but conflict with Ruscheweyh and Sandkuhler (2002) who have not found TFNs in rat lamina II (SG). According to cutaneous afferent input, most TFNs were shown to be either wide-dynamic-range or nociceptive-specific neurons (Lopez-Garcia and King 1994). The intrinsic tonic firing seems to be an important property of this class of neurons, allowing them to fire bursts of spikes in response to synaptic stimulation (Thomson et al. 1989).

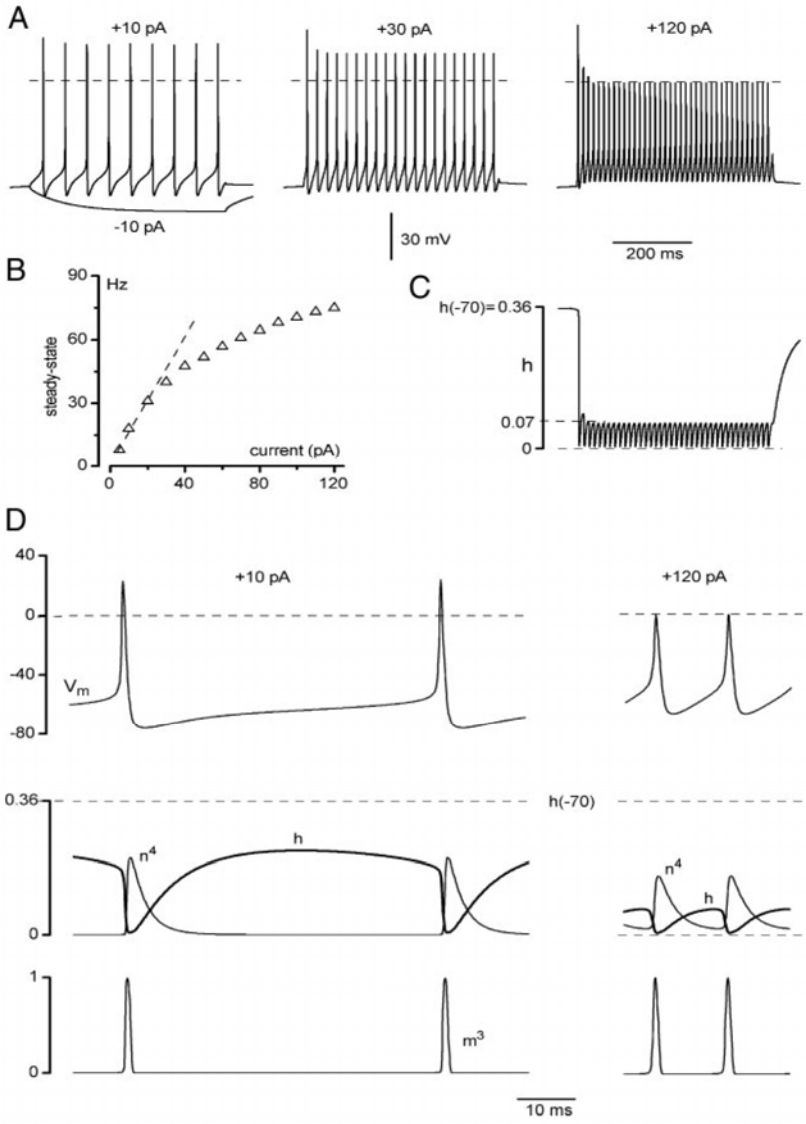

FIG. 7. Computer simulation of tonic firing. *A*: tonic firing evoked by 500-ms current pulses of +10, +30, and +120 pA. A negative (–10 pA) current pulse evoked a passive response. Dashed line indicates 0 mV. *B*: steady-state firing frequency (*f-I*) characteristic of the model neuron. *C*: changes in Na^+ channel inactivation variable *h* during tonic firing evoked by +120 pA current pulse. *D*: dynamics of n^4, *h* (Na^+), and m^3 during steady-state firing at low and high frequencies. All variables are shown for the middle point of AIS.

The present study determined the role of major conductances in excitability of TFNs. Both Ca^{2+} and K_{CA} currents are involved in modulation of firing frequency. The effect is based on activation of apamin-sensitive K_{CA} channels, regulating the slow component of afterhyperpolarization as was shown for several types of neurons (Barrett and Barrett 1976; Nishimura et al. 1989; Savic et al. 2001; Schwindt et al. 1988; Smith et al. 2002; Viana et al. 1993). Activation of K_{CA} channels by entering Ca^{2+} reduced the firing at a given depolarization strength and therefore modified the input–output characteristic of the neuron. Thus Ca^{2+}-dependent conductances play an important modulatory and stabilizing role in firing of SG neurons, but they are unlikely to be responsible for the appearance of the basic form of tonic firing. In similar manner, the variation of V_R does not change the pattern of tonic firing but regulates the strength of stimulation needed to evoke it. Therefore the voltage-gated Na^+ and K^+ channels are mostly responsible for the appearance of tonic firing.

The activation kinetics of Na^+ channels was sufficiently fast to provide spike depolarization. A low channel density found in the soma supports previous observations that the major part of Na^+ conductance necessary for the spike generation in spinal neurons is located in AIS (Alessandri-Haber et al. 1999; Safronov et al. 1999a,b). In addition, our simulations showed that removal of somatic channels did not change the spike overshoot. Rapid inactivation of Na^+ channels at positive potentials ($\tau_{in} < 0.4$ ms at +10 mV), in combination with fast K_{DR} channel opening ($\tau_{0.5} < 0.9$ ms at +40 mV), is critical for the spike repolarization. Double-exponential recovery of Na^+ channels from inactivation was similar to that observed in rat motoneurons (Safronov and Vogel 1995) and hippocampal neurons (Martina and Jonas 1997). About one-fifth of the channels reprimed within the first 10 ms, which corresponds to interspike intervals at 100 Hz firing. However, our recordings and model showed that this amount of Na^+ channels is sufficient to support firing. Thus a high safety factor for the spike generation (see also Eckert 1978) plays a critical role in maintaining the tonic firing under conditions in which most Na^+ channels are inactivated.

K_{DR} channel underlies the major type of K^+ conductance in TFNs. Delayed activation and a high sensitivity to TEA allowed us to attribute it to a family of delayed-rectifier K^+

channels. Its inactivation was by an order of magnitude slower than that of K_A channels. Moreover, in contrast to the K_A component, K_{DR} current did not show inactivation kinetics at potentials below −10 mV. K_{DR} current was proportionally reduced in 1 and 10 mM TEA, indicating homogeneity of the channel population with respect to its sensitivity to the blocker. The study of the tail currents at −60 mV did not provide any evidence for existence of a channel subpopulation, which was active at the beginning of the pulse but inactivated at the end of 200 ms depolarization. Thus, based on analysis of tail currents and sensitivity to TEA, which are used as standard tools for separating delayed-rectifier current components (Dubois 1981; Safronov et al. 1996; Stühmer et al. 1989), we assume that K_{DR} current is carried through a one-channel type highly permeable for K^+. Somatic density of K_{DR} current of 5.9 pA μm^{-2} found here is much higher than one calculated from Wolff et al. (1998) for nonidentified dorsal horn neurons of 3- to 7-day-old rats (240 pA for the 10 μm soma, corresponding to 0.76 pA μm^{-2}). This difference can be explained if it is assumed that the neuronal development during the first postnatal month is accompanied by somatic expression of K_{DR} channels, in contrast to the Na^+ channels that are exclusively expressed in AIS (Safronov et al. 1999b).

The activation of K_{DR} current was sufficiently rapid to provide membrane repolarization during an action potential. The channel closing with a time constant of <6 ms, in turn, was important for sustained firing at high frequencies. An involvement of K_{DR} channels in both processes was confirmed by a spike prolongation and reduction of firing frequency seen in 1 mM TEA (see also Olschewski et al. 2001).

K_A current was very small in somatic patches and strong inactivation at V_R would further reduce it, making its participation in tonic firing unlikely. It appears that lack of K_A channels is critical for appearance of sustained firing, since a pronounced K_A current in dorsal horn neurons was shown to result in delayed firing onset, irregular bust-like firing, or frequency adaptation (Grudt and Perl 2002; Ruscheweyh and Sandkuhler 2002; Yoshimura and Jessell 1989).

Our model has confirmed that a combination of Na^+ and K_{DR} channels is sufficient for appearance of a basic pattern of tonic firing. The model could reproduce the firing in a broad range of frequencies. The maximum firing rates were determined by biophysical properties of the channels in such a way that at a given stimulus strength the closing of K_{DR} channels determined the length of the interspike interval, whereas the recovery of Na^+ channels from inactivation determined the spike amplitude. Our model was not based on the specific anatomy of any particular type of neurons and, therefore, it can be useful for studying the mechanisms of firing adaptation or appearance of delayed-firing patterns in other types of SG neurons.

The population of TFNs was morphologically inhomogeneous and at least three groups of neurons were distinguished on the basis of their somatodendritic organization. Our results support the observations of others that tonic firing can be generated by several anatomical groups of SG neurons (Grudt and Perl 2002). Moreover, neurons belonging to one group could show firing patterns with differing degrees of adaptation (Grudt and Perl 2002), implying the absence of strict correlation between the firing pattern and cell morphology in SG. It can be therefore suggested that the balanced expression of ion channels described here is responsible for appearance of tonic firing in morphologically distinct types of SG neurons. We could not combine a nucleated patch recording with staining in the same neuron, because the isolation of the nucleus usually resulted in a deterioration of relatively small SG neuron and did not allow us to obtain a sufficiently good staining. Nevertheless, in more than 60 nucleated patches from TFNs, we recorded ion channels with similar properties, suggesting their presence in cells of all three subtypes.

In conclusion, a balanced system of ionic conductances underlies tonic firing in SG neurons. Voltage-gated Na^+ current in combination with a pronounced K_{DR} but small K_A currents generate a basic firing pattern, while Ca^{2+}-dependent conductances stabilize tonic firing, efficiently regulate discharge frequency, and modulate an input–output characteristic in a neuron.

ACKNOWLEDGMENT

We thank H. Pereira for technical assistance.

GRANTS

The work was supported by a grant from the Portuguese Foundation for Science and Technology (Fundação para a Ciência e a Tecnologia).

REFERENCES

Alessandri-Haber N, Paillart C, Arsac C, Gola M, Couraud F, and Crest M. Specific distribution of sodium channels in axons of rat embryo spinal motoneurones. *J Physiol* 518: 203–214, 1999.

Barrett EF and Barrett JN. Separation of two voltage-sensitive potassium currents, and demonstration of a tetrodotoxin-resistant calcium current in frog motoneurones. *J Physiol* 255: 737–774, 1976.

Barrett JN and Crill WE. Specific membrane properties of cat motoneurones. *J Physiol* 239: 301–324, 1974.

Bentley GN and Gent JP. Electrophysiological properties of substantia gelatinosa neurones in a novel adult spinal slice preparation. *J Neurosci Methods* 53: 157–162, 1994.

Brown AG. *Organization in the Spinal Cord.* Berlin: Springer-Verlag, 1981.

Cervero F. Dorsal horn neurones and their sensory inputs. In: *Spinal Afferent Processing*, edited by TL Yaksh. New York: Plenum, 1987, p. 197–216.

Chery N, Yu XH, and De Konink Y. Visualization of lamina I of the dorsal horn in live adult rat spinal cord slices. *J Neurosci Methods* 96: 133–142, 2000.

Dodge FA and Cooley JW. Action potential of motoneuron. *IBM J Res Dev* 17: 219–229, 1973.

Dubois J-M. Evidence for the existence of three types of potassium channels in the frog Ranvier node membrane. *J Physiol* 318: 297–316, 1981.

Eckert R. Nerve cells and signals. In: *Animal Physiology*, edited by R Eckert and D Randall. San Francisco, CA: Freeman, 1978, p. 148–192.

Eckert WA, McNaughton KK, and Light AR. Morphology and axonal arborization of rat spinal inner lamina II neurons hyperpolarized by μ-opioid-selective agonists. *J Comp Neurol* 458: 240–256, 2003.

Edwards FA, Konnerth A, Sakmann B, and Takahashi T. A thin slice preparation for patch clamp recordings from neurones of the mammalian central nervous system. *Pflügers Arch* 414: 600–612, 1989.

Gobel S. Golgi studies of the neurons in layer II of the dorsal horn of the medulla (trigeminal nucleus caudalis). *J Comp Neurol* 180: 395–414, 1978.

Gobel S, Falls WM, Bennet GJ, Abdelmoumene M, Hayashi H, and Humphrey E. An EM analysis of the synaptic connections of horseradish peroxidase-filled stalked cells and islet cells in the Substantia Gelatinosa of adult cat spinal cord. *J Comp Neurol* 194: 781–807, 1980.

Grudt TJ and Perl ER. Correlations between neuronal morphology and electrophysiological features in the rodent superficial dorsal horn. *J Physiol* 540: 189–207, 2002.

Hines ML. Neuron: a program for simulation of nerve equation. In: *Neural Systems: Analysis and Modeling*, edited by FH Eeckman. Boston, MA: Kluwer, 1993, p. 127–136.

Hines ML and Carnevale NT. The NEURON simulation environment. *Neural Comput* 9: 1179–1209, 1997.

LaMotte C. Distribution of the tract of lissauer and the dorsal root fibers in the primate spinal cord. *J Comp Neurol* 172: 529–561, 1977.

Light AR and Perl ER. Differential termination of large-diameter and small-diameter primary afferent fibers in the spinal dorsal gray matter as indicated by labelling with horse-radish peroxidase. *Neurosci Lett* 6: 59–63, 1977.

Lopez-Garcia JA and King AE. Membrane properties of physiologically classified rat dorsal horn neurons *in vitro*: correlation with cutaneous sensory afferent input. *Eur J Neurosci* 6: 998–1007, 1994.

Martina M and Jonas P. Functional differences in Na^+ channel gating between fast-spiking interneurones and principal neurones of rat hippocampus. *J Physiol* 505: 593–603, 1997.

Nishimura Y, Schwindt PC, and Crill WE. Electrical properties of facial motoneurons in brainstem slices from guinea pig. *Brain Res* 502: 127–142, 1989.

Olschewski A, Hempelmann G, Vogel W, and Safronov BV. Suppression of potassium conductance by droperidol has influence on excitability of spinal sensory neurons. *Anesthesiology* 94: 280–289, 2001.

Prescott SA and De Koninck Y. Four cell types with distinctive membrane properties and morphologies in lamina I of the spinal dorsal horn of the adult rat. *J Physiol* 539: 817–836, 2002.

Rall W. Branching dendritic trees and motoneuron membrane resistivity. *Exp Neurol* 1: 491–527, 1959.

Rall W. Time constants and electrotonic length of membrane cylinders and neurons. *Biophys J* 9: 1483–1508, 1969.

Rethelyi M. Preterminal and terminal axon arborizations in the substantia gelatinosa of cat′s spinal cord. *J Comp Neurol* 172: 511–521, 1977.

Ruscheweyh R and Sandkuhler J. Lamina-specific membrane and discharge properties of rat spinal dorsal horn neurones in vitro. *J Physiol* 541: 231–244, 2002.

Safronov BV. Spatial distribution of Na^+ and K^+ channels in spinal dorsal horn neurones: role of the soma, axon and dendrites in spike generation. *Prog Neurobiol* 59: 217–241, 1999a.

Safronov BV, Bischoff U, and Vogel W. Single voltage-gated K^+ channels and their functions in small dorsal root ganglion neurones of rat. *J Physiol* 493: 393–408, 1996.

Safronov BV and Vogel W. Single voltage-activated Na^+ and K^+ channels in the somata of rat motoneurones. *J Physiol* 487: 91–106, 1995.

Safronov BV, Wolff M, and Vogel W. Functional distribution of three types of Na^+ channel on soma and processes of dorsal horn neurones of rat spinal cord. *J Physiol* 503: 371–385, 1997.

Safronov BV, Wolff M, and Vogel W. Axonal expression of sodium channels in rat spinal neurones during postnatal development. *J Physiol* 514: 729–734, 1999b.

Sather W, Dieudonné S, MacDonald JF, and Ascher P. Activation and desensitization of *N*-methyl-D-aspartate receptors in nucleated outside-out patches from mouse neurones. *J Physiol* 450: 643–672, 1992.

Savic N, Pedarzani P, and Sciancalepore M. Medium afterhyperpolarization and firing pattern modulation in interneurons of stratum radiatum in the CA3 hippocampal region. *J Neurophysiol* 85: 1986–1997, 2001.

Schwindt PC, Spain WJ, Foehring RC, Stafstrom CE, Chubb MC, and Crill WE. Multiple potassium conductances and their functions in neurons from cat sensorimotor cortex in vitro. *J Neurophysiol* 59: 424–449, 1988.

Smith MR, Nelson AB, and Lac S. Regulation of firing response gain by calcium-dependent mechanisms in vestibular nucleus neurons. *J Neurophysiol* 87: 2031–2042, 2002.

Stühmer W, Ruppersberg JP, Schröter KH, Sakmann B, Stocker M, Giese KP, Perschke A, Baumann A, and Pongs O. Molecular basis of functional diversity of voltage-gated potassium channels in mammalian brain. *EMBO J* 8: 3235–3244, 1989.

Sugiura Y, Lee CL, and Perl ER. Central projections of identified, unmyelinated (C) afferent fibers innervating mammalian skin. *Science* 234: 358–361, 1986.

Thomson AM, West DC, and Headley PM. Membrane characteristics and synaptic responsiveness of superficial dorsal horn neurons in a slice preparation of adult rat spinal cord. *Eur J Neurosci* 1: 479–488, 1989.

Thurbon D, Luscher HR, Hofstetter T, and Redman SJ. Passive electrical properties of ventral horn neurons in rat spinal cord slices. *J Neurophysiol* 80: 2485–2502, 1998.

Todd AJ. Electron microscope study of Golgi-stained cell in lamina II of the rat spinal dorsal horn. *J Comp Neurol* 275: 145–157, 1988.

Viana F, Bayliss DA, and Berger AJ. Multiple potassium conductances and their role in action potential repolarization and repetitive firing behavior of neonatal rat hypoglossal motoneurons. *J Neurophysiol* 69: 2150–2163, 1993.

Willis WD and Coggeshall RE. *Sensory Mechanisms of the Spinal Cord.* New York: Plenum, 1991.

Wolff M, Vogel W, and Safronov BV. Uneven distribution of K^+ channels in soma, axon and dendrites of rat spinal neurones: ffunctional role of the soma in generation of action potentials. *J Physiol* 509: 767–776, 1998.

Yoshimura M and Jessell TM. Membrane properties of rat substantia gelatinosa neurons in vitro. *J Neurophysiol* 62: 109–118, 1989.

Fifth publication

Mechanism of spike frequency adaptation in substantia gelatinosa neurones of rat

Igor V. Melnick[1], Sónia F. A. Santos[1,2] and Boris V. Safronov[1,2]

[1] *Instituto de Biologia Molecular e Celular, Rua do Campo Alegre 823, 4150-180 Porto, Portugal and* [2] *Instituto de Histologia e Embriologia, Faculdade de Medicina, Universidade do Porto, Alameda Professor Hernâni Monteiro, 4200-319 Porto, Portugal*

Using tight-seal recordings from rat spinal cord slices, intracellular labelling and computer simulation, we analysed the mechanisms of spike frequency adaptation in substantia gelatinosa (SG) neurones. Adapting-firing neurones (AFNs) generated short bursts of spikes during sustained depolarization and were mostly found in lateral SG. The firing pattern and the shape of single spikes did not change after substitution of Ca^{2+} with Co^{2+}, Mg^{2+} or Cd^{2+} indicating that Ca^{2+}-dependent conductances do not contribute to adapting firing. Transient K_A current was small and completely inactivated at resting potential suggesting that adapting firing was mainly generated by voltage-gated Na^+ and delayed-rectifier K^+ (K_{DR}) currents. Although these currents were similar to those previously described in tonic-firing neurones (TFNs), we found that Na^+ and K_{DR} currents were smaller in AFNs. Discharge pattern in TFNs could be reversibly converted into that typical of AFNs in the presence of tetrodotoxin but not tetraethylammonium, suggesting that lower Na^+ conductance is more critical for the appearance of firing adaptation. Intracellularly labelled AFNs showed specific morphological features and preserved long extensively branching axons, indicating that smaller Na^+ conductance could not result from the axon cut. Computer simulation has further revealed that down-regulation of Na^+ conductance represents an effective mechanism for the induction of firing adaptation. It is suggested that the cell-specific regulation of Na^+ channel expression can be an important factor underlying the diversity of firing patterns in SG neurones.

(Resubmitted 13 April 2004; accepted after revision 25 June 2004; first published online 2 July 2004)
Corresponding author Boris V. Safronov: Instituto de Biologia Molecular e Celular, Rua do Campo Alegre 823, 4150-180 Porto, Portugal. Email: safronov@ibmc.up.pt

The dorsal horn of the spinal cord is the first relay station processing the sensory input from primary afferent terminals. The diversity of sensory modalities in dorsal horn is encoded by the type of peripheral afferent fibre, synaptic connectivity and intrinsic firing properties of dorsal horn neurones (Brown, 1981; Cervero, 1987; Willis & Coggeshall, 1991). The substantia gelatinosa (SG) is the dorsal horn region where most fine-calibre C- and Aδ-fibres terminate (Rethelyi, 1977; LaMotte, 1977; Light & Perl, 1977; Sugiura *et al.* 1986) and is therefore considered to be a key element in the nociceptive processing system.

Several classes of SG neurones are distinguished on the basis of their intrinsic firing properties (Yoshimura & Jessell, 1989; Thomson *et al.* 1989; Lopez-Garcia & King, 1994; Grudt & Perl, 2002). A major criterion widely used for such a classification is a degree of spike frequency adaptation observed during sustained membrane depolarization. While some neurones were characterized by a tonic firing, the others exhibited a strong adaptation generating short bursts of spikes or just a single spike. A degree of spike frequency adaptation in a neurone correlates with a type of its cutaneous afferent input (Lopez-Garcia & King, 1994) and therefore the cell-specific regulation of firing adaptation can underlie diverse modalities of sensory encoding in SG. In spite of its importance, the mechanism of spike frequency adaptation in SG neurones is not well understood.

Recently we described the ion basis of tonic (non-adapting) firing in a group of SG neurones and created a computer model of the SG neurone (Melnick *et al.* 2004). The voltage-gated Na^+ and delayed-rectifier K^+ channels were shown to generate the basic pattern of tonic firing, while the Ca^{2+}-dependent conductances stabilized firing and regulated discharge frequency. The present study was carried out to elucidate the major

I. V. Melnick and S. F. A. Santos contributed equally to this work.

factors responsible for the appearance of spike frequency adaptation in SG neurones.

Methods

Tight-seal recordings were performed using both 200 μm transverse and 300 μm parasagittal slices prepared from the lumbar enlargement of the spinal cord of 2- to 7-week-old rats (Edwards *et al.* 1989; Bentley & Gent, 1994; Chery & De Konink, 2000). The animals were killed in accordance with national guidelines (Direcção Geral de Veterinária, Ministério da Agricultura). After anaesthesia by intraperitoneal injection of sodium pentobarbital (30 mg kg^{-1}) the vertebral column was quickly cut out and immersed in ice-cold oxygenated artificial cerebrospinal fluid (ACSF). The 5–7 mm segment of the lumbar enlargement was dissected and the slices were prepared using a tissue slicer (Leica VT 1000S). The slices were then incubated for 30–60 min in ACSF at 33°C. SG (lamina II) was identified as a translucent band in the dorsal horn (Fig. 2*A*). Neurones were localized during recording according to a position of the pipette tip on the video-image of SG.

ACSF contained (mM): NaCl 115, KCl 5.6, $CaCl_2$ 2, $MgCl_2$ 1, glucose 11, NaH_2PO_4 1, $NaHCO_3$ 25 (pH 7.4 when bubbled with a 95% O_2–5% CO_2). To block Ca^{2+}-dependent conductances Co^{2+} (2 mM), Cd^{2+} (0.1 mM) and Mg^{2+} (5 mM) were used. Co^{2+} was equimolarly substituted for Ca^{2+}. In experiments with Cd^{2+}, Ca^{2+} was omitted and $[Mg^{2+}]$ was increased to 3 mM. In 5 mM Mg^{2+} solution the concentration of Ca^{2+} was reduced to 0.1 mM. The last solution was also used for studying Na^+ and K^+ channels and is referred to as ACSF*. Standard pipette solution contained (mM): NaCl 15, KCl 120, $MgCl_2$ 1, EGTA 10 and Hepes 10 (pH 7.3 adjusted with KOH, final $[K^+]$ was 151 mM). The solution with low Ca^{2+} buffering capacity contained (mM): NaCl 5, KCl 147, $MgCl_2$ 1, EGTA 1 and Hepes 10 (pH 7.3, adjusted with KOH, final $[K^+]$ was 155 mM). The pipette solution for studying Na^+ channels contained (mM): NaCl 4, CsCl 131, $MgCl_2$ 2, EGTA 10 and Hepes 10 (pH 7.3 adjusted by CsOH and NaOH, final $[Cs^+] = 153$ mM and $[Na^+] = 6$ mM). All chemicals were purchased from Sigma.

The patch pipettes were pulled from thick-walled borosilicate glass tubes (Modulohm, Denmark) and had after fire-polishing a resistance of 3–5 MΩ. The EPC-9 amplifier (HEKA, Lambrecht, Germany) was used in all experiments. The effective corner frequency of the low-pass filter was 3 kHz. The frequency of digitization was 10 kHz. Transients and leakage currents were digitally subtracted using standard P/n protocol. Offset potentials were nulled directly before formation of a seal. Liquid junction potentials were calculated and corrected for in all experiments. In neurones subjected to detailed analysis the series resistance measured in the whole-cell mode was 6–20 MΩ and was compensated by at least 60%. Input resistance was measured in both current- and voltage-clamp modes. Ion channels were studied in nucleated patches excised from somatic membrane (Sather *et al.* 1992). To calculate the density of somatic channels, the diameter of each patch was measured.

Action potentials were recorded using the fast current-clamp mode of the EPC-9 amplifier. The accuracy of the voltage measurements done with this patch-clamp amplifier was tested in the experiments shown in Fig. 1. A current pulse (2 nA, 3 ms) was applied to a model circuit containing a capacitor (C_m, 22 pF) and a resistor (R_m, 500 MΩ) connected in series with another resistor (R_S, 5.1 MΩ). A theoretically calculated response (continuous line) was compared with the averaged trace of 500 recordings (dashed line). Time derivatives of both theoretical and recorded voltage traces (dV/dt) are shown on the right. In the initial phase of depolarization, the fast current-clamp mode of the EPC-9 amplifier produced less distortion of the recorded signal than the normal (slow) current-clamp mode of the EPC-7 amplifier (see Fig. 3*C* from Magistretti *et al.* 1996, 1998) and it appears to be more suitable for measurements of voltage changes and polarization velocities.

The current–voltage (I–V) relationship for Na^+ channels was fitted using the equation: $G_0/(1 + \exp((V_{50} - V)/k))(V - V_{rev})$, where G_0 is the maximum conductance, V_{50} is the potential of

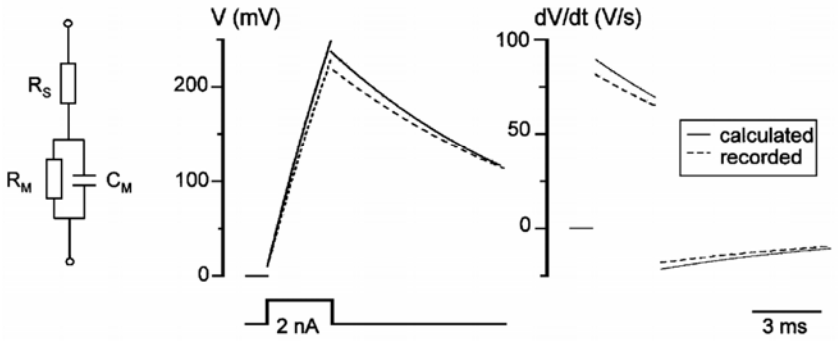

Figure 1. Test of the voltage change measurements made using the fast current-clamp mode of the EPC-9 amplifier
Parameters of the model circuit: $C_m = 22$ pF, $R_m = 500$ MΩ and $R_S = 5.1$ MΩ. Current pulse: 2 nA, 3 ms. Continuous line, a theoretically calculated response; dashed line, an average of 500 recorded traces. Right, time derivatives of calculated and recorded voltage traces (dV/dt). Points corresponding to instantaneous voltage changes on R_S at the beginning and end of the pulse are removed from both dV/dt graphs.

half-maximum channel activation, k is a steepness factor and V_{rev} is the reversal potential obtained by fitting for each I–V curve. K^+ conductances were calculated assuming $V_{rev} = E_K = -84$ mV, where E_K is the equilibrium potential for K^+. The activation and steady-state inactivation characteristics were fitted with a Boltzmann function: $1/(1 + \exp((V_{50} - V)/k))$. The time course of Na^+ channel recovery from inactivation was fitted using a two-exponential function: $1 - A \exp(-t/\tau_F) - (1 - A) \exp(-t/\tau_S)$, where τ_F and τ_S are the fast and slow time constants, A is the relative amplitude of the fast component.

All numbers are given as mean ± standard error of the mean (S.E.M.). The values obtained by data fitting with a linear or non-linear least-squares procedures are given as mean ± standard error (S.E.M.). In all figures the error bars

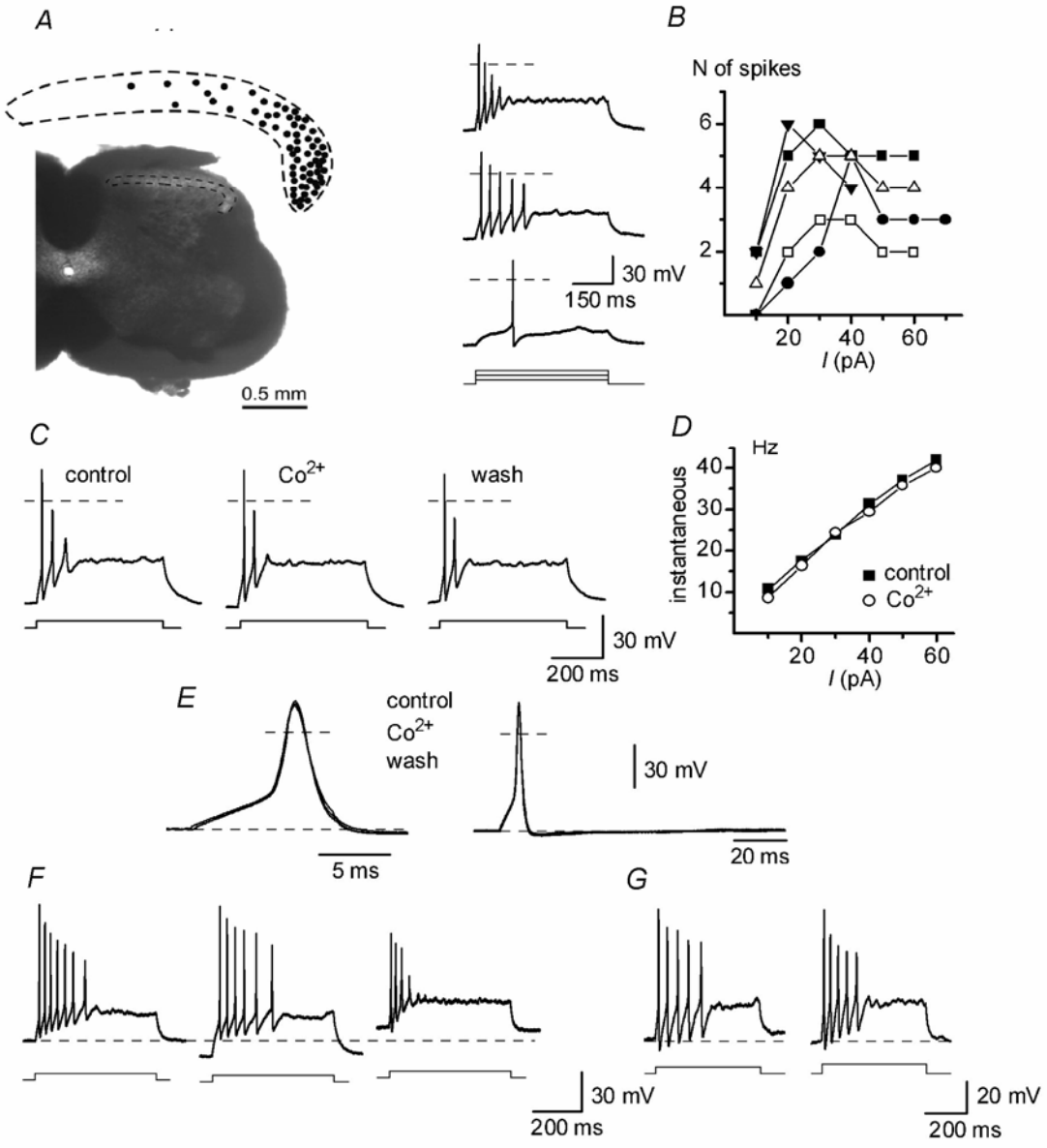

Figure 2. Discharge properties of adapting-firing neurones (AFNs) in ACSF (2 mM Ca^{2+}) and Ca^{2+}-free solutions

A, localization of AFNs ($n = 65$) in SG. Transverse section of the spinal cord of 19-day-old rat. *B*, bursts of spikes evoked in an AFN by 0.5 s depolarizing current pulses of 10, 30 and 50 pA in ACSF. Dashed lines, 0 mV. Right, the number of spikes as a function of injected current plotted for 5 AFNs. *C*, firing patterns in ACSF (control and wash) and Co^{2+}-containing solution. The stimulation strength was 20 pA in all recordings. *D*, instantaneous frequency–current (*f*–*I*) characteristics of AFNs in ACSF and Co^{2+}-containing solution. *E*, single spikes activated by 10 ms current pulses in ACSF and Co^{2+}-containing solution. *F*, discharge patterns in an AFN at varying membrane potentials, −70 mV (dashed line), −80 and −60 mV. *G*, firing patterns recorded in ACSF with external 2.5 mM K^+ at room temperature (left) and 35–37°C (right). Current pulses: 20 and 30 pA, respectively.

Table 1. Comparison of single spike parameters in control and 2 mM Co^{2+}

Spike parameters	Units	Control	Co^{2+}	Wash	*t* test
Width at 0 mV	ms	1.2 ± 0.1	1.2 ± 0.1	1.1 ± 0.1	n.s.
Width at −30 mV	ms	2.3 ± 0.2	2.4 ± 0.2	2.5 ± 0.2	n.s.
Amplitude[a]	mV	95.2 ± 3.0	90.5 ± 2.9	86.3 ± 2.7	n.s.
AHP, maximum[b]	mV	68.1 ± 1.2	69.2 ± 1.1	69.6 ± 1.1	n.s.
AHP, at 40 ms[c]	mV	67.1 ± 1.0	67.8 ± 0.7	68.6 ± 0.9	n.s.

[a]The spike amplitude was measured from a membrane potential of −70 mV. [b]The largest after-hyperpolarization (AHP, maximum) was measured within the first 8–15 ms after beginning of the spike. [c]The second measurement of AHP was 40 ms after the beginning of the spike. Data from 10 neurones. Student's paired *t* test was used to compare control parameters with those obtained in Co^{2+}. n.s., non-significant difference with $P > 0.25$.

are shown when exceeding the symbol size. The parameters were compared by paired or independent Student's *t* test. The present study is based on recordings from 113 adapting-firing neurones (AFNs), 232 tonic-firing neurones (including 187 from Melnick *et al.* 2004) and 68 nucleated patches obtained from AFNs. All experiments, except those in Fig. 2*G* (right), were carried out at room temperature 22–24°C.

Ten AFNs were filled with 0.5% biocytin during recording for later cell visualization. Following the recording session, the slices with biocytin-filled neurones were transferred into a fixative containing 4% paraformaldehyde, 0.3% picric acid in 0.1 M phosphate buffer (pH 7.4) for one night. The slices were then washed in 0.1 M phosphate buffer saline (PBS) and treated with 30% sucrose for one night. After re-sectioning at 50 μm, slices were serially collected in PBS. After repeated washing (10 min each) in PBS containing 0.3% Triton X-100 (PBST), slices were incubated in an Alexa Streptavidin 594 antibody solution (1 : 1000 PBST, Molecular Probes, The Netherlands) at 4°C for 48 h. Slices were mounted in glycerol/PBS (3 : 1). Serial confocal optical sections were obtained with 1 μm steps at maximum pixel intensity. Images of labelled cells show the summed *Z* projection.

Computer simulations were done using NEURON software (Hines, 1993; Hines & Carnevale, 1997) and a model of a TFN described previously (Melnick *et al.* 2004). This universal model was created for SG neurones with diverse dendritic organizations. The input resistance and membrane time constants of the model were close to those described here for AFNs. Only three parameters of the model were varied in the present study: the Na^+ conductance (g_{Na}) in the axon initial segment and the voltage dependencies of Na^+ channel activation and inactivation. The g_{Na} was changed from a control value of 1800 mS cm^{-2} (1.0) to 730 mS cm^{-2} (0.41) and 521 mS cm^{-2} (0.29). The voltage dependencies were modified by uniformly shifting all equations describing Na^+ channel activation and inactivation by +5 and +11 mV, respectively.

Results

Adapting-firing neurones (AFNs) were mostly found in the lateral part of SG (Fig. 2*A*). In ACSF they showed a resting potential of −69.9 ± 0.6 mV ($n = 102$), an input resistance of 1.3 ± 0.1 GΩ ($n = 102$) and a membrane time constant of 84.5 ± 5.0 ms ($n = 20$). Unless otherwise stated, in the following current-clamp experiments the membrane potential was adjusted to −70 mV. AFNs were usually able to support firing only during the first 100–250 ms of depolarization evoked by an injection of 0.5 s pulses of inward current (Fig. 2*B*). The number of generated spikes depended on the pulse strength. In a narrow range of 10–40 pA it increased to a maximum of 3–6 spikes, but then became lower at stronger stimulation.

Ca^{2+}-dependent conductances

A contribution of Ca^{2+}-dependent conductances to firing in AFNs was studied by using the inorganic blockers of Ca^{2+} channels Co^{2+}, Cd^{2+} and Mg^{2+}. The concentration of internal EGTA in these experiments was reduced to 1 mM. In the presence of 2 mM Co^{2+} ($n = 10$), 0.1 mM Cd^{2+} ($n = 8$) or 5 mM Mg^{2+} ($n = 9$), no changes in firing pattern or the instantaneous frequency–current (*f–I*) characteristic, calculated for the first interspike interval, were observed (Fig. 2*C* and *D*, shown for Co^{2+}). The shape of single spikes was also unchanged by the blockers (Fig. 2*E*, shown for Co^{2+}). For 10 neurones recorded in control and Co^{2+}-containing solutions, several parameters of the single spike were compared and no significant difference was found (Table 1). The amplitude of after-hyperpolarization (fast and slow) was also not

reduced by Co^{2+} ($n = 10$). Thus, it could be concluded that Ca^{2+}-dependent conductances do not contribute to discharge pattern in AFNs. In the following experiments we used the 10 mM EGTA pipette solution and both ACSF and ACSF* (0.1 mM Ca^{2+} and 5 mM Mg^{2+}) as bath solution.

The effect of membrane potential on the firing pattern was studied in experiments where it was changed from −70 to −80 or −60 mV. Varying the potential in this range did not change the adapting firing patterns in either ACSF or ACSF* (Fig. 2*F*, shown for ACSF*, $n = 34$).

In 11 AFNs we tested whether lower external K^+ and increase in temperature to 35–37°C can change the basic pattern of intrinsic firing. In all these neurones a typical pattern of adaptation was seen in external 2.5 mM K^+ at room temperature (Fig. 2*G*, left) as well as after increasing the temperature to 35–37°C (Fig. 2*G*, right).

Na^+ channels

Na^+ channels were studied using the Cs^+-containing pipette solution. The identification of a firing pattern in a neurone was done during the first few seconds after membrane rupture, before Cs^+ replaced intracellular K^+ (Melnick *et al.* 2004). Na^+ currents were recorded in nucleated patches in ACSF* containing 1 mM TEA to reduce outward K^+ current (Fig. 3*A*). Their activation curve fitted with a Boltzmann equation had $V_{50} = -30.3 \pm 0.2$ mV and $k = 7.1 \pm 0.2$ mV (Fig. 3*B*, $n = 10$). The steady-state inactivation of Na^+ channels, studied with 50 ms conditioning prepulses, revealed a half-maximum inactivation at -64.2 ± 0.9 mV and $k = -9.6 \pm 0.8$ mV (Fig. 3*B*, $n = 10$, test pulses to −30 or −20 mV). The inactivation kinetics of Na^+ channels could be fitted using a mono-exponential function with the time constant changing from 5.9 ± 1.5 ms at −40 mV to less than 0.5 ms at positive potentials (Fig. 3*C*, $n = 7$). Recovery of Na^+ channels from inactivation at −80 mV was studied by applying two 25 ms voltage pulses to −30 mV with varying intervals (Fig. 3*D*). The time course of recovery was double-exponential (Safronov & Vogel, 1995; Martina & Jonas, 1997; Melnick *et al.* 2004) with time constants of 21.2 ± 2.2 ms (57%) and 674 ± 95 ms (43%) ($n = 7$). The density of somatic Na^+ current in AFNs was 0.84 ± 0.16 pA μm^{-2} ($n = 8$).

Voltage-gated K^+ channels

The major K^+ current found in AFNs was a slowly inactivating delayed-rectifier (K_{DR}) current (Fig. 4*A*). For its recording the patch was held at −80 mV and depolarizing voltage pulses were applied after a 150 ms prepulse to −60 mV inactivating a fast transient K^+ (K_A) current. Half-maximum activation of K_{DR} conductance was observed at $V_{50} = -18.0 \pm 0.6$ mV ($k = 9.3 \pm 0.5$ mV, $n = 11$, Fig. 4*B*). The activation kinetics of the current was described by plotting the rise time of a half-maximum current ($\tau_{0.5}$) as a function of potential (Fig. 4*B*). The $\tau_{0.5}$ value became close to 1 ms at potentials positive to +30 mV (Fig. 4*B*, $n = 11$), indicating involvement of K_{DR} current in spike repolarization. Starting from −20 mV a partial inactivation of K_{DR} current developed. The time course and degree of inactivation were only weakly voltage dependent (Fig. 4*C*, $n = 11$). The reversal potential for K_{DR} current, estimated from instantaneous tail currents, was close to E_K of −84 mV ($n = 5$, not shown). In 10 mM TEA the current was blocked to $7.9 \pm 1.0\%$ ($n = 9$, not shown).

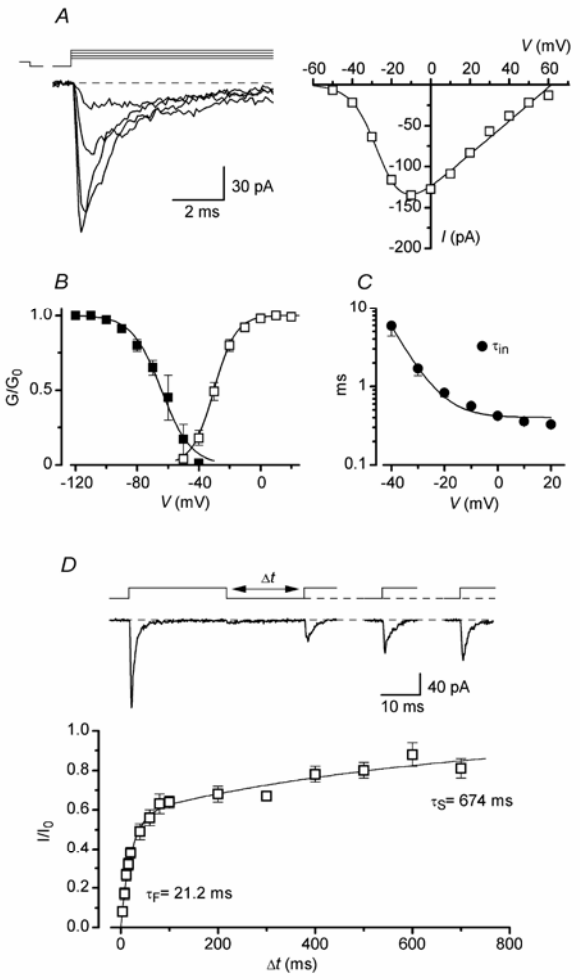

Figure 3. Properties of Na^+ channels in nucleated patches from AFNs

A, Na^+ currents activated by depolarization to −40, −30, −20 and −10 mV following a 50 ms prepulse to −120 mV. Holding potential, −80 mV. *I–V* curve is shown for the same neurone. *B*, steady-state activation and inactivation characteristics. Fitting parameters are given in the text. *C*, the inactivation time constant (τ_{in}) as a function of membrane potential. *D*, kinetics of Na^+ channel recovery from inactivation. Na^+ currents activated by pairs of 25 ms pulses from −80 to −30 mV with varying intervals. The time course of Na^+ channel recovery from inactivation was fitted using a double-exponential function.

The density of somatic K_{DR} current in AFNs at +60 mV was 3.7 ± 0.3 pA μm^{-2} ($n = 18$).

The K_A component was not seen in nucleated patches when K^+ current was activated by a voltage step from −120 to +60 mV, but it could be separated after addition of 10 mM TEA as the fast inactivating component of the remaining current (Fig. 4*D*). The inactivation time constant of K_A current was 10.5 ± 1.2 ms ($n = 10$). The amplitude of K_A current, estimated from the double-exponential fitting of the inactivation kinetics of the remaining current, gave the somatic current density of 0.60 ± 0.17 pA μm^{-2} at +60 mV ($n = 10$). Because of its low density in nucleated patches, the steady-state inactivation of K_A current was studied in whole-cell mode. The whole-cell K_A current evoked after a conditioning prepulse to −120 mV by a voltage step to potentials subthreshold for Na^+ channel activation (between −60 and −50 mV) ranged from 0 to 220 pA. The steady-state inactivation of K_A current ($V_{50} = -96.3 \pm 1.2$ mV; $k = -7.2 \pm 0.8$ mV; $n = 5$) showed that it was completely inactivated at −70 mV (Fig. 4*E*). To reveal a possible contribution of K_A current to setting the firing threshold in AFNs, the current-clamp responses of AFNs to depolarization were compared with membrane passive responses (Fig. 4*F*). A hyperpolarization evoked by a −10 pA current injection was considered as a passive response, which was appropriately scaled (dashed curves) and compared with cell responses to +10 and +20 pA depolarization (Fig. 4*F*). In agreement with our data about complete K_A current inactivation at resting potential, a subthreshold depolarization was found to be passive and not affected by activation of K_A conductance ($n = 28$).

By comparing the present results for AFNs with those recently reported for tonic-firing neurones (TFNs) from Melnick *et al.* (2004), it was possible to conclude that both neurone types possess Na^+ and K_{DR} currents as well as negligible K_A current. The ranges of K_{DR} channel activation were very similar (V_{50}, −18.0 mV for AFNs *versus* −19.8 mV for TFNs). The kinetics of Na^+

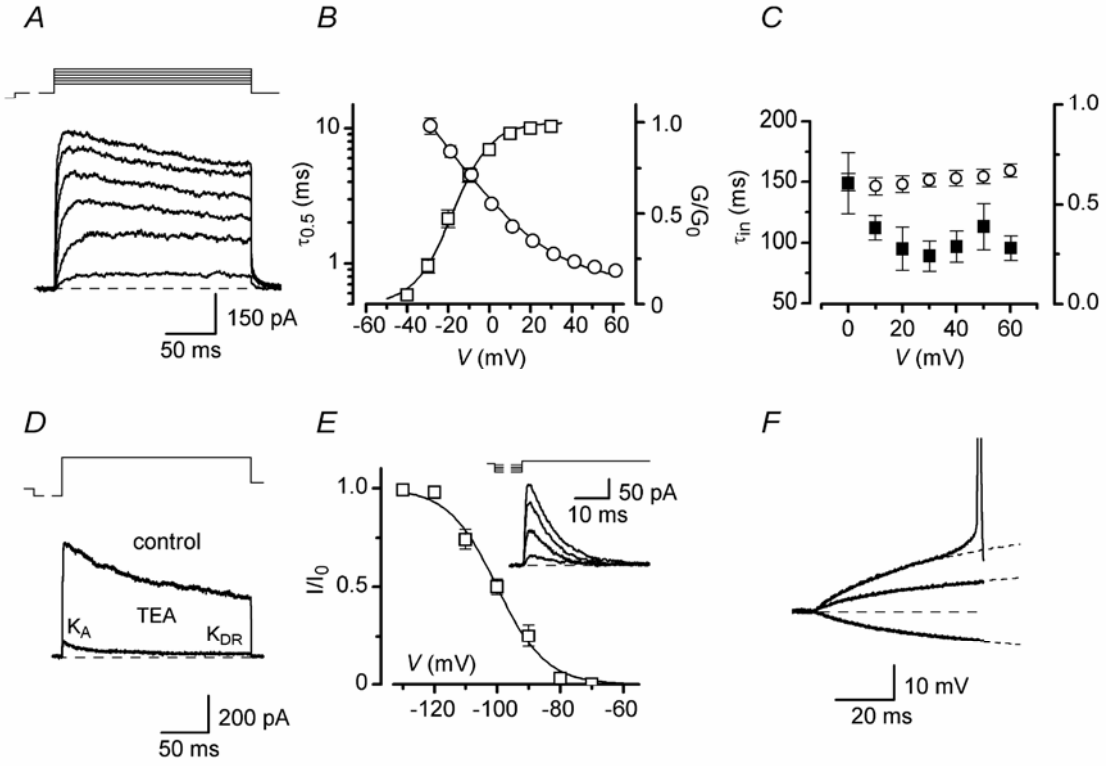

Figure 4. Voltage-gated K^+ channels in AFNs
A, K_{DR} currents in patches activated in ACSF* by 200 ms depolarizing pulses (from −30 mV to +20 mV in a 10 mV step) following a 150 ms prepulse to −60 mV. Holding potential, −80 mV. These traces were off-line low-pass filtered at 1 kHz. *B*, steady-state activation curve (□) and the rise time of a half-maximum current ($\tau_{0.5}$, ○). *C*, the time constant of inactivation (■) and the ratio of currents measured at peak and at the end of the pulse (○) at different potentials. *D*, separation of transient K_A currents in patches. Total K^+ current activated in a nucleated patch by a voltage step from −120 (150 ms) to +60 mV (200 ms) in the presence and absence of 10 mM TEA. Holding potential, −80 mV. *E*, steady-state inactivation of K_A current. Whole-cell K_A currents were recorded at −50 mV after a 150 ms prepulse to varying potentials (−130, −110, −100 and −90 mV). Holding potential, −80 mV. *F*, analysis of subthreshold current-clamp responses to injection of current pulses. AFN was stimulated by −10, +10 and +20 pA currents. A response to −10 pA current was considered as passive. It was digitally multiplied by factors of −1 and −2 (shown by dashed curves) and shown superimposed on the other two traces.

channel recovery from inactivation in both cell types were two-exponential with the time constants: 21.2 ms (57%) and 674 ms (43%) for AFNs *versus* 21.8 ms (63%) and 793 ms (37%) for TFNs. The activation characteristics of Na^+ channels were insignificantly different (V_{50}, −30.3 mV for AFNs *versus* −35.7 mV for TFNs; $P < 0.1$). However, the density of somatic Na^+ and K_{DR} currents in AFNs was lower and the Na^+ channel inactivation was shifted to more positive potentials by 11 mV (V_{50}, −64.2 mV for AFNs *versus* −75.5 mV for TFNs; $P < 0.02$). The following experiments were done to find out which of these factors played a critical role in the appearance of firing adaptation.

Block of Na^+ rather than K_{DR} channels in TFNs induces adaptation typical of AFNs

Since somatic Na^+ current represents only few per cent of the total Na^+ current in a spinal neurone (Safronov *et al.* 1997, 1999; Alessandri-Haber *et al.* 1999), a comparison of total Na^+ conductances in AFNs and TFNs was done by measuring maximum spike depolarization rates. The histogram of distributions of maximum de- and repolarization rates obtained by digital differentiation of the first spike in a train are shown in Fig. 5*A* for 102 AFNs and 232 TFNs. The mean maximum depolarization rates of $103.7 \pm 2.8\ V\ s^{-1}$ for AFNs ($n = 102$) and $208.3 \pm 3.4\ V\ s^{-1}$ for TFNs ($n = 232$) were significantly different ($P < 0.0001$). Since the depolarization rate is proportional to the inward current charging the membrane according to the equation: $I = C(dV/dt)$, where C is membrane capacitance, our results imply relatively lower Na^+ conductance in AFNs in comparison with TFNs. In addition, the velocity of repolarization was also lower in AFNs ($61.2 \pm 1.5\ V\ s^{-1}$, $n = 102$, for AFNs *versus* $99.9 \pm 1.9\ V\ s^{-1}$, $n = 232$, for TFNs, $P < 0.0001$).

In 10 TFNs, the effect of partial K_{DR} current block on firing pattern was studied in ACSF*. In 5 of them an addition of 1 mM TEA resulted in the appearance of spike doublets in the train (Fig. 5*B*, left). In the other 5 TFNs, 1 mM TEA prolonged spikes, reduced the after-hyperpolarization and stability of firing, so that the amplitude of spikes progressively decreased during the train (Fig. 5*B*, right). However, both modified firing patterns were obviously different from those of AFNs.

In 21 TFNs the effect of TTX on pattern was studied in ACSF*. In all TFNs tested, the tonic firing changed to adapting and then to strongly adapting with a single spike when perfusion of the slice with 40 nM TTX-containing solution was started (Fig. 5*C*). Wash out of TTX was done just after the pattern modification occurred (before 40 nM TTX completely diffused into the slice). Differentiation of the voltage traces has shown that the appearance of adaptation correlated with a reduction of Na^+ current (Fig. 5*C*, bottom). In control solution, Na^+ current (estimated from derivatives) decreased during tonic firing due to the channel inactivation (Melnick *et al.* 2004) but still remained sufficiently large to support firing. After a partial Na^+ current block by TTX, only the first few spikes could be generated before inactivation further reduced Na^+ current to the level below that necessary for the spike generation (dashed line). It should be noted that the block of Na^+ conductance also resulted in a reduction in the rate of spike repolarization, probably because of lesser activation of K_{DR} channels by spikes with reduced overshoots. A transition from tonic to adapting firing occurred at 40–60% block of Na^+ conductance (Fig. 5*D*). Thus, block of Na^+ rather than K_{DR} channels in TFNs modified a firing pattern to that typical of AFNs.

Anatomy of AFNs

In order to test whether the smaller Na^+ conductance observed in AFNs might result from the cutting of the axon during the preparation of slices, AFNs were labelled by including biocytin in the patch pipette ($n = 10$). Because of their predominant location in the lateral part of SG (Fig. 2*A*), AFNs were rarely seen in sagittal sections typically used for anatomical studies. Therefore, the labelling was performed in transverse slices. All AFNs had small rounded somata and dense dendritic trees mostly staying within SG. Dendritic arbors exhibited spines and a limited spread in the medio-lateral or dorso-ventral dimensions. The axon was identified as a thinner process with constant diameter lacking spines. The axons branched extensively and entered laminae I and III. In some AFNs labelled axon branches had a total length of several hundreds of micrometres (Fig. 6*A* and *B*). Thus it could be concluded that the axon initial segment in AFNs was not cut during the preparation of slices.

Computer simulation

Computer simulations were done to study how a reduction in Na^+ current and a shift in its activation and inactivation characteristics to more positive potentials can influence firing in a model neurone (Fig. 7). A control model of a TFN (Melnick *et al.* 2004) generated sustained firing with frequency increasing with stimulation intensity (Fig. 7, 1/0/0). The maximum depolarization rate of the first spike in a train was $231\ V\ s^{-1}$ when measured at +30 pA stimulation. By reducing the Na^+ conductance (g_{Na}) to 0.41 it was possible to induce firing adaptation (0.41/0/0). The maximum depolarization rate of the first spike in a burst was reduced to $132\ V\ s^{-1}$ (+30 pA stimulation). If the activation characteristics of Na^+ channels were shifted by +5 mV, a strong adaptation appeared in the model already at the control g_{Na} value (1/+5/0). After

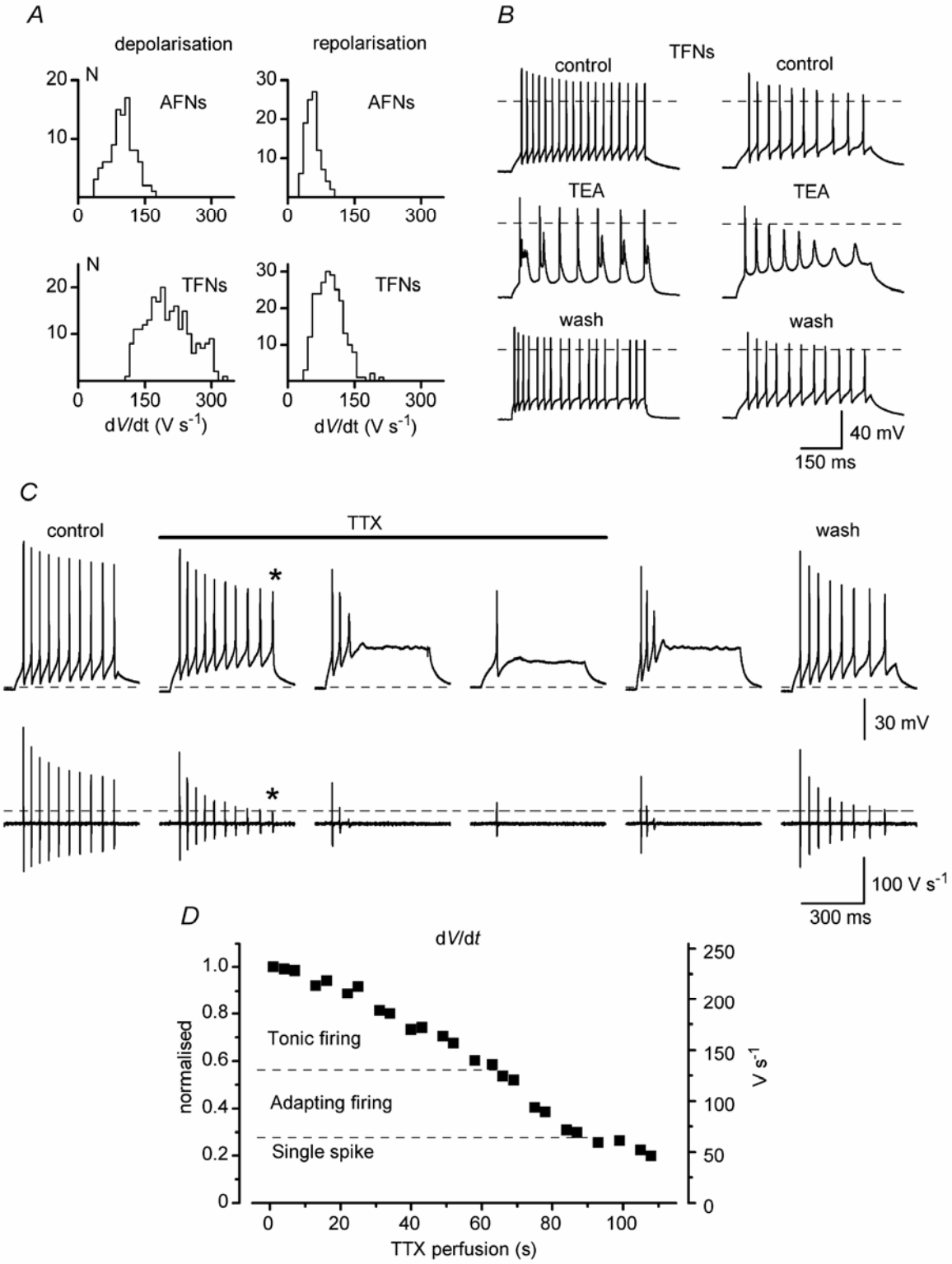

Figure 5. TTX but not TEA can induce adaptation in tonic-firing neurones (TFNs)
A, histograms of distribution of de- and repolarization rates in AFNs and TFNs. Bin width, 10 V s^{-1}. *B*, modifications of discharge patterns in TFNs by 1 mM TEA. *C*, induction of adaptation in a TFN during perfusion of the slice with 40 nM TTX. Bottom traces are derivatives of voltage traces (d*V*/d*t*). The baselines are 0 V s^{-1}. Dashed line shows the maximum depolarization rate for the reduced spike with the overshoot close to 0 mV (indicated by asterisks). *D*, modification of firing pattern from tonic to adapting as a function of Na^+ channel block during slice perfusion with 40 nM TTX. The maximum depolarization rate of the first spike in a train (right axis) is also shown as normalized to the control value (left axis).

the inactivation was shifted by +11 mV, the model again generated tonic firing (1/+5/+11). In the model with both activation and inactivation shifted to positive potentials a stronger reduction in g_{Na} to 0.29 was needed for the induction of adaptation in the whole stimulation range (0.29/+5/+11). In this case the maximum depolarization rate of the first spike became 147 V s^{-1} (+ 30 pA stimulation). Thus, both a reduction in g_{Na} and a positive shift in activation characteristics promote spike frequency adaptation, while a positive shift in inactivation has an opposite effect.

Discussion

This study has shown that reduced expression of Na^+ channels is a critical factor determining the appearance of spike frequency adaptation in SG neurones. Therefore, regulation of the intrinsic firing pattern in a SG neurone through modulation of Na^+ channels may represent an important element of spinal sensory encoding.

The degree of spike frequency adaptation is a criterion most frequently used for electrophysiological classification of superficial dorsal horn neurones (Thomson *et al.* 1989; Lopez-Garcia & King, 1994; Grudt & Perl, 2002; Prescott & De Koninck, 2002; Ruscheweyh & Sandkuhler, 2002; Hu & Gereau, 2003). Adapting-firing neurones (AFNs) which generate a short burst of spikes at the beginning of depolarization were also called phasic-, burst- or transient-type neurones. Most were physiologically classified as nociceptive-specific neurones (Lopez-Garcia & King, 1994). AFNs from lamina II (SG) receive monosynaptic input from slowly conducting primary C-type afferents (Grudt & Perl, 2002). Our data support a number of reports showing that adapting firing patterns are generated by only a subpopulation of neurones (Thomson *et al.* 1989; Lopez-Garcia & King, 1994; Grudt & Perl, 2002; Hu & Gereau, 2003; Melnick *et al.* 2004) rather than by all neurones in SG (lamina II) as proposed by Ruscheweyh & Sandkuhler (2002).

The present study shows that Ca^{2+}-dependent conductances do not contribute to the discharge pattern in AFNs. In this respect AFNs differ from tonic-firing neurones (TFNs), where Ca^{2+}-dependent slow after-hyperpolarization (AHP) regulated discharge rate and stabilized the basic form of tonic firing generated by voltage-gated Na^+ and delayed-rectifier K_{DR} currents (Melnick *et al.* 2004). The present finding can also explain a difference in the shape of the AHP seen between TFNs (prolonged and polyphasic) and AFNs (short and monophasic) (Thomson *et al.* 1989; Prescott & De Koninck, 2002).

Voltage-gated K^+ channels are similar in both AFNs and TFNs. Fast inactivating K_A current was found to be very small and strongly inactivated at resting potential and it was also not activated by a subthreshold depolarization. The lack of K_A current appears to be important for the generation of typical discharge patterns in AFNs as well as

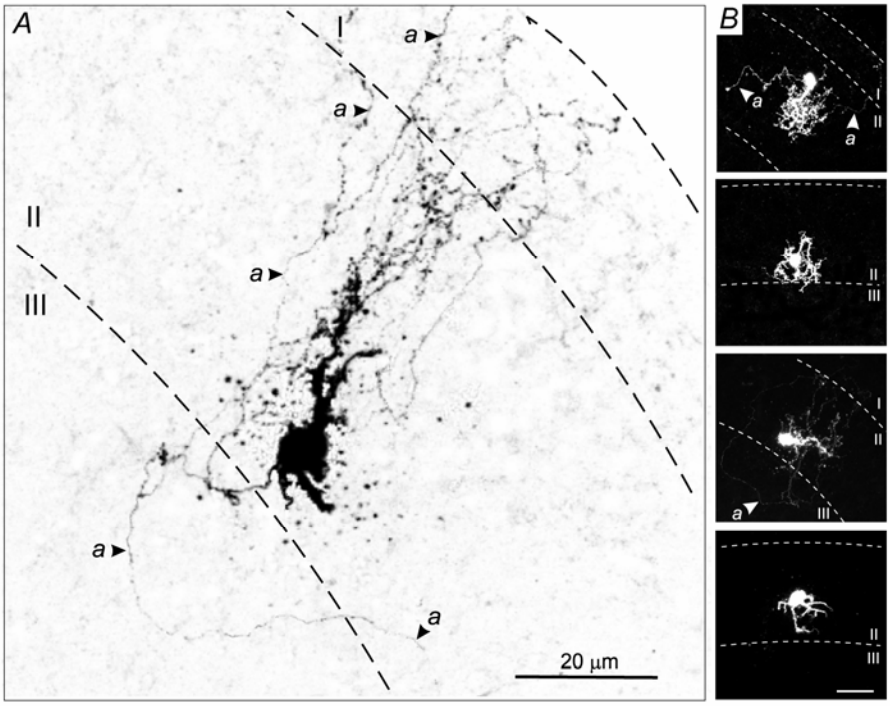

Figure 6. Confocal images of AFNs labelled with biocytin
A, inverted image of AFN with extensive axonal collaterals indicated by arrows. *B*, images of another four AFNs two of which have extensive axonal collaterals. Calibration bar, 20 μm. Dashed lines represent the borders between laminae I, II (SG) and III.

TFNs, since the expression of large K_A currents was shown to result in delayed-onset firing or irregular bust-like discharges (Yoshimura & Jessell, 1989; Grudt & Perl, 2002; Ruscheweyh & Sandkuhler, 2002). K_{DR} current formed a major K^+ conductance in both AFNs and TFNs and had similar kinetics and activation ranges. Although K_{DR} channels are necessary for the maintenance of sustained firing in TFNs (Melnick *et al.* 2004), their partial block by TEA did not result in the appearance of the typical pattern of spike frequency adaptation seen in AFNs. Thus, K_A and K_{DR} currents are unlikely to be responsible for the firing adaptation in SG neurones studied here.

Although the basic properties of Na^+ channels in AFNs were similar to those in TFNs (Melnick *et al.* 2004), their

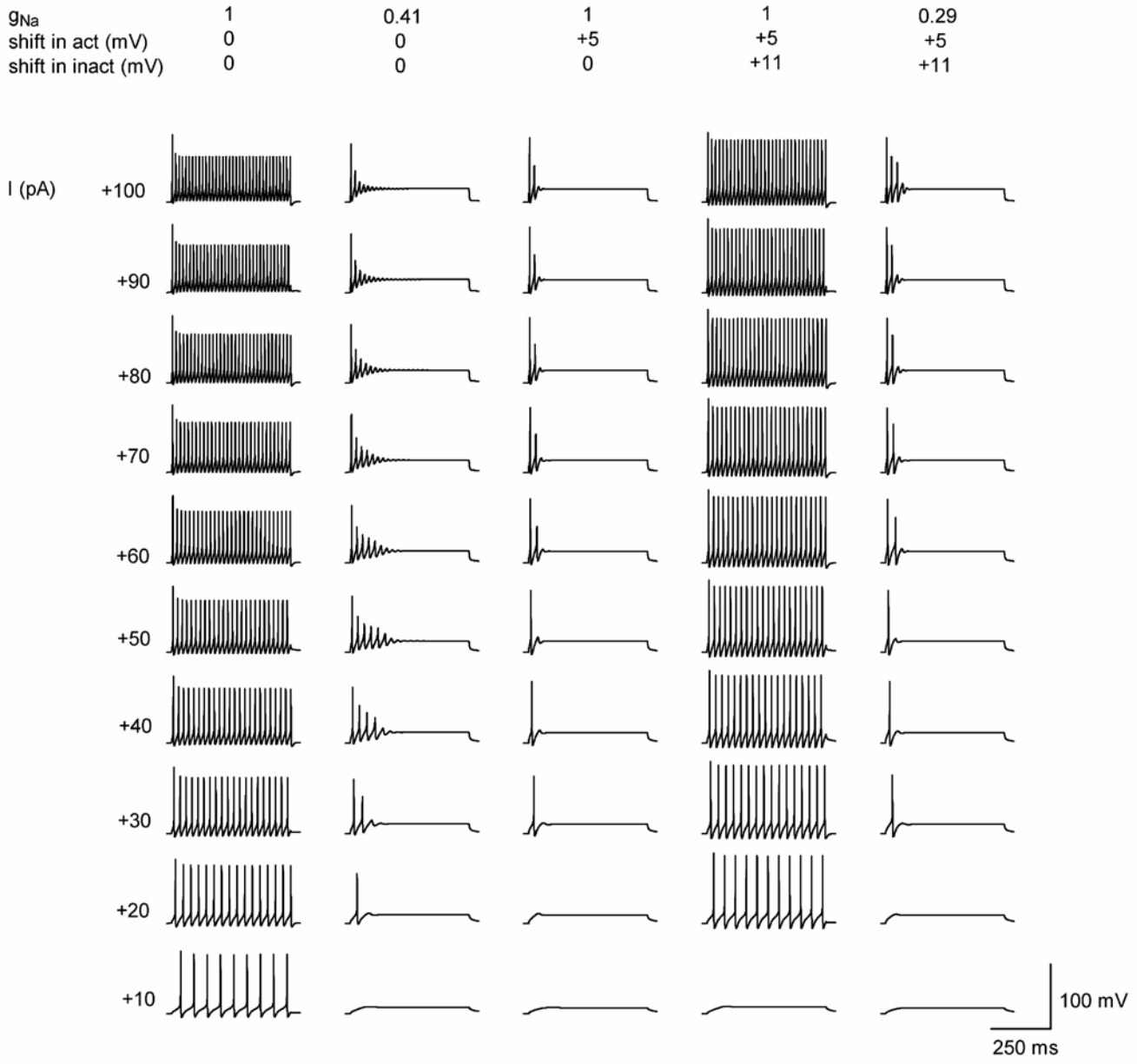

Figure 7. Computer simulation of firing adaptation in SG neurone
A basic model of TFN from Melnick *et al.* (2004). Repetitive firing evoked by 500 ms current pulses of increasing intensity in a basic model (1/0/0). Reduction of Na^+ conductance (g_{Na}) in the axon initial segment to 0.41 induced firing adaptation (0.41/0/0). An activation shift by +5 mV, without lowering g_{Na}, resulted in a strong firing adaptation (1/+5/0). A +11 mV shift in inactivation characteristics restored tonic firing in a model with control g_{Na} (1/+5/+11). Reduction in g_{Na} to 0.29 induced spike frequency adaptation in a model with shifted activation and inactivation characteristics (0.29/+5/+11). The resting potential was −70 mV in all simulations.

expression was lower and voltage dependency was slightly shifted to more positive potentials. Experiments with TTX and computer simulations have shown that a reduction in Na^+ conductance is critical for the appearance of adaptation. Simulations have also revealed a dual effect of a positive shift in voltage dependency of Na^+ channels on firing behaviour. Although the activation shift promoted spike frequency adaptation, a stronger shift in inactivation characteristics had an opposite effect. Thus, a lower Na^+ conductance seems to be a major factor introducing adaptation in SG neurones.

It is possible that Na^+ channels in AFNs and TFNs are formed by different combinations of principal (α) and auxiliary ($\beta1$ and $\beta2$) subunits (Black *et al.* 1994; Waxman *et al.* 1999; Blackburn-Munro & Fleetwood-Walker, 1999). In this case, the change in subunit expression as well as the up-regulation of Na^+ channels associated with neuropathic pain (Waxman *et al.* 1999; Blackburn-Munro *et al.* 1999; Hains *et al.* 2003) can lead to hyperexcitability of dorsal horn neurones via the induction of long-term plasticity of their intrinsic firing properties. Besides, a regulation of Na^+ channels through an integration of cell-specific G-protein-coupled synaptic inputs (Ma *et al.* 1994; Carr *et al.* 2003) may introduce a short-term modulation of intrinsic firing and thus dynamic modification of spinal sensory encoding.

The smaller Na^+ conductance in AFNs is unlikely to result from axonal injury during the slicing procedure, as all AFNs labelled with biocytin possessed extensively branching axons crossing the borders with neighbouring laminae I and III. Labelled parts of axons were considerably longer than the 25 μm needed for spike generation in SG neurones (Safronov, 1999; Safronov *et al.* 1999). AFNs studied here belonged to one morphological class with its predominant localization in the lateral part of SG. The dendritic tree of AFNs has probably a rostro-caudal orientation within SG. Morphologically, AFNs were similar to islet cells (Gobel, 1978; Gobel *et al.* 1980; Todd, 1988; Eckert *et al.* 2003), although a strict conclusion could not be drawn based on neuronal images in transverse sections.

In conclusion, we suggest that different expression of Na^+ channels may be responsible for variation in the degree of spike frequency adaptation in SG neurones. The present results also imply that a modulation of Na^+ channels can represent an effective mechanism altering the firing behaviour of SG neurones. In addition to metabolic regulation of inwardly rectifying and A-type K^+ channels (Derjean *et al.* 2003; Hu & Gereau, 2003), a cell-specific modulation of Na^+ conductance provides one more mechanism of sensory, i.e. nociceptive, encoding and processing in the spinal cord.

References

Alessandri-Haber N, Paillart C, Arsac C, Gola M, Couraud F & Crest M (1999). Specific distribution of sodium channels in axons of rat embryo spinal motoneurones. *J Physiol* **518**, 203–214.

Bentley GN & Gent JP (1994). Electrophysiological properties of substantia gelatinosa neurones in a novel adult spinal slice preparation. *J Neurosci Meth* **53**, 157–162.

Black JA, Yokoyama S, Higashida H, Ransom BR & Waxman SG (1994). Sodium channel mRNAs I, II and III in the CNS: cell-specific expression. *Brain Res Mol Brain Res* **22**, 275–289.

Blackburn-Munro G & Fleetwood-Walker SM (1999). The sodium channel auxiliary subunits beta 1 and beta 2 are differentially expressed in the spinal cord of neuropathic rats. *Neuroscience* **90**, 153–164.

Brown AG (1981). *Organization in the Spinal Cord*. Springer-Verlag, Berlin, Heidelberg.

Carr DB, Day M, Cantrell AR, Held J, Scheuer T, Catterall WA & Surmeier DJ (2003). Transmitter modulation of slow, activity-dependent alterations in sodium channel availability endows neurons with a novel form of cellular plasticity. *Neuron* **39**, 793–806.

Cervero F (1987). Dorsal horn neurones and their sensory inputs. In *Spinal Afferent Processing*, ed. Yaksh TL, pp. 197–216. Plenum Press, New York.

Chery N, Yu XH & De Konink Y (2000). Visualization of lamina I of the dorsal horn in live adult rat spinal cord slices. *J Neurosci Meth* **96**, 133–142.

Derjean D, Bertrand S, LeMasson G, Landry M, Morisset V & Nagy F (2003). Dynamic balance of metabotropic inputs causes dorsal horn neurons to switch functional states. *Nature Neurosci* **6**, 274–281.

Eckert WA, McNaughton KK & Light AR (2003). Morphology and axonal arborization of rat spinal inner lamina II neurons hyperpolarized by μ-opioid-selective agonists. *J Comp Neurol* **458**, 240–256.

Edwards FA, Konnerth A, Sakmann B & Takahashi T (1989). A thin slice preparation for patch clamp recordings from neurones of the mammalian central nervous system. *Pflugers Arch* **414**, 600–612.

Gobel S (1978). Golgi studies of the neurons in layer II of the dorsal horn of the medulla (trigeminal nucleus caudalis). *J Comp Neurol* **180**, 395–414.

Gobel S, Falls WM, Bennet GJ, Abdelmoumene M, Hayashi H & Humphrey E (1980). An EM analysis of the synaptic connections of horseradish peroxidase-filled stalked cells and islet cells in the substantia gelatinosa of adult cat spinal cord. *J Comp Neurol* **194**, 781–807.

Grudt TJ & Perl ER (2002). Correlations between neuronal morphology and electrophysiological features in the rodent superficial dorsal horn. *J Physiol* **540**, 189–207.

Hains BC, Klein JP, Saab CY, Craner MJ, Black JA & Waxman SG (2003). Upregulation of sodium channel Nav1.3 and functional involvment in neuronal hyperexcitability associated with central neuropathic pain after spinal cord injury. *J Neurosci* **23**, 8881–8892.

Hines ML (1993). NEURON – a program for simulation of nerve equation. In *Neural Systems: Analysis and Modeling*, ed. Eeckman FH, pp. 127–136. Kluwer Academic Publishers, Boston.

Hines ML & Carnevale NT (1997). The NEURON simulation environment. *Neural Comput* **9**, 1179–1209.

Hu H-J & Gereau RW (2003). ERK integrates PKA and PKC signaling in superficial dorsal horn neurons. II. Modulation of neuronal excitability. *J Neurophysiol* **90**, 1680–1688.

LaMotte C (1977). Distribution of the tract of Lissauer and the dorsal root fibers in the primate spinal cord. *J Comp Neurol* **172**, 529–561.

Light AR & Perl ER (1977). Differential termination of large-diameter and small-diameter primary afferent fibers in the spinal dorsal gray matter as indicated by labelling with horse-radish peroxidase. *Neurosci Lett* **6**, 59–63.

Lopez-Garcia JA & King AE (1994). Membrane properties of physiologically classified rat dorsal horn neurons *in vitro*: correlation with cutaneous sensory afferent input. *Eur J Neurosci* **6**, 998–1007.

Ma JY, Li M, Catterall WA & Scheuer T (1994). Modulation of brain Na^+ channels by a G-protein-coupled pathway. *Proc Natl Acad Sci U S A* **91**, 12351–12355.

Magistretti J, Mantegazza M, de Curtis M & Wanke E (1998). Modalities of distortion of physiological voltage signals by patch-clamp amplifiers: a modeling study. *Biophys J* **74**, 831–842.

Magistretti J, Mantegazza M, Guatteo E & Wanke E (1996). Action potentials recorded with patch-clamp amplifiers: are they genuine? *Trends Neurosci* **19**, 530–534.

Martina M & Jonas P (1997). Functional differences in Na^+ channel gating between fast-spiking interneurones and principal neurones of rat hippocampus. *J Physiol* **505**, 593–603.

Melnick IV, Santos SFA, Szokol K, Szucs P & Safronov BV (2004). Ionic basics of tonic firing in spinal substantia gelatinosa neurons of rat. *J Neurophysiol* **91**, 646–655.

Prescott SA & De Koninck Y (2002). Four cell types with distinctive membrane properties and morphologies in lamina I of the spinal dorsal horn of the adult rat. *J Physiol* **539**, 817–836.

Rethelyi M (1977). Preterminal and terminal axon arborizations in the substantia gelatinosa of cat's spinal cord. *J Comp Neurol* **172**, 511–521.

Ruscheweyh R & Sandkuhler J (2002). Lamina-specific membrane and discharge properties of rat spinal dorsal horn neurones *in vitro*. *J Physiol* **541**, 231–244.

Safronov BV (1999). Spatial distribution of Na^+ and K^+ channels in spinal dorsal horn neurones: role of the soma, axon and dendrites in spike generation. *Prog Neurobiol* **59**, 217–241.

Safronov BV & Vogel W (1995). Single voltage-activated Na^+ and K^+ channels in the somata of rat motoneurones. *J Physiol* **487**, 91–106.

Safronov BV, Wolff M & Vogel W (1997). Functional distribution of three types of Na^+ channel on soma and processes of dorsal horn neurones of rat spinal cord. *J Physiol* **503**, 371–385.

Safronov BV, Wolff M & Vogel W (1999). Axonal expression of sodium channels in rat spinal neurones during postnatal development. *J Physiol* **514**, 729–734.

Sather W, Dieudonné S, MacDonald JF & Ascher P (1992). Activation and desensitization of *N*-methyl-D-aspartate receptors in nucleated outside-out patches from mouse neurones. *J Physiol* **450**, 643–672.

Sugiura Y, Lee CL & Perl ER (1986). Central projections of identified, unmyelinated (C) afferent fibers innervating mammalian skin. *Science* **234**, 358–361.

Thomson AM, West DC & Headley PM (1989). Membrane characteristics and synaptic responsiveness of superficial dorsal horn neurons in a slice preparation of adult rat spinal cord. *Eur J Neurosci* **1**, 479–488.

Todd AJ (1988). Electron microscope study of Golgi-stained cells in lamina II of the rat spinal dorsal horn. *J Comp Neurol* **275**, 145–157.

Waxman SG, Dib-Hajj S, Cummins TR & Black JA (1999). Sodium channels and pain. *Proc Natl Acad Sci U S A* **96**, 7635–7639.

Willis WD & Coggeshall RE (1991). *Sensory Mechanisms of the Spinal Cord*. Plenum Press, New York.

Yoshimura M & Jessell TM (1989). Membrane properties of rat substantia gelatinosa neurons in vitro. *J Neurophysiol* **62**, 109–118.

Acknowledgements

We would like to thank Ms Helena Pereira for technical assistance. The work was supported by a grant from the Portuguese Foundation for Science and Technology (FCT).

III. FINAL REMARKS

Understanding of pain and chronic pain conditions critically relies on evaluation of sensory processing in the spinal cord, where the nociceptive information is integrated and transmitted to the brain. The SG is involved in pain conduction (Rethelyi, 1977; Light & Perl, 1979; Sugiura *et al*., 1986; Cervero, 1987) and in the system of pain control (Merchenthaler *et al*., 1986; Ribeiro-da-Silva *et al*., 1991; Arvidson *et al*., 1995a,b).

By the time we started this experimental work, little was known about SG sensory processing. The physiological characteristics of SG neurons involved in pain conduction or in pain control, and their functional synaptic organization had not yet been studied.

In the *first publication*, we studied the neuron types involved in the endogenous enkephalinergic antinociception. Since previously it was shown that there is no correlation between neuron morphology and sensitivity to MORs agonists (Light & Wilcockson, 1999; Eckert *et al*., 2003) and the actions of opioids on neurons with different firing patterns had not been compared so far, we tested sensitivity to DAMGO of neurons with different firing patterns. It became necessary to create uniform classification criteria in order to distinguish neuronal groups on the basis of their firing. This study showed that only one of the three types of SG neurons was sensitive to the MOR agonist. TFNs were selectively inhibited by the drug and, as a functional consequence, their firing pattern was modified. Since the majority of SG neurons expressing MORs do not contain GABA or glycine and therefore are excitatory interneurons (Kemp *et al*., 1996) we suggested in this study a possible excitatory nature for TFNs.

For technical reasons, a systematic physiological study of synaptically connected SG interneurons had never been done, and therefore, it was for a long time believed that the SG is mostly formed by GABAergic inhibitory interneurons participating in both pre- and postsynaptic inhibition. In addition, there was a generalized idea that the SG could be considered in terms of the 'gate control theory' (Melzack & Wall, 1965) emphasising the role of inhibitory circuits, and perhaps for this reason, organization of excitatory circuits was less studied (Graham *et al*., 2007). Therefore, we developed a novel technique which allowed routine recording from pairs of synaptically connected SG neurons and characterization of their excitatory or inhibitory function. This development resulted in the *second publication* showing that sensory integration in the SG neuronal network is dominated by excitatory interneurons.

Our finding revised the classical view on the sensory processing in the SG and indicated a vital importance of investigating unknown yet basic properties of synaptic connections formed by

excitatory interneurons. Therefore, in the *third publication*, we studied a range of functional properties and signaling in glutamatergic synapses as well as the efficacy of synaptic transmission.

Finally, in the *fourth* and *fifth publications*, we studied the ionic basis of generation of cell-specific firing in major types of SG neurons, to better understand their intrinsic integrative properties.

1. Postsynaptic inhibition by MOR agonist

The results obtained in the *first publication* have shown that, in agreement with several patch clamp studies (Grudt & Perl, 2002; Lu & Perl, 2003; Hu & Gereau, 2003), SG neurons can be separated into three groups, according to their firing type - TFNs, AFNs and DFNs. This separation was based on several criteria, such as firing threshold, presence/absence of K_A current and degree of inward rectification.

Each group of neurons had its specific distribution pattern within SG: TFNs were relatively homogeneously distributed over the whole length of SG, AFNs were mostly localized in a lateral part, especially SG ventral part, and DFNs could be found in all regions, with higher densities in the medial and lateral parts.

To study the spinal mechanisms of opioidergic analgesia, the action of a MOR agonist, DAMGO, on SG neurons with different intrinsic firing properties was tested.

Within the SG, the sensitivity of a neuron to DAMGO depended on its type rather than its location. In fact, there was a striking correlation between the firing pattern of SG neurons and their sensitivity to DAMGO: at 1 μM concentration, this MOR agonist selectively hyperpolarized all TFNs tested, whereas none of the AFNs nor DFNs were affected. The DAMGO effect on TFNs was due to activation of G protein–coupled inward-rectifier K^+ conductance (GIRK) (Yoshimura & North, 1983; Grudt & Williams, 1994; Schneider *et al*., 1998; Light & Willcockson, 1999). Although all three types of neurons possessed GIRK conductance, which could be blocked by 500 μM Ba^{2+} and 500 μM Cs^+ but increased by 50 μM baclofen (Sodickson & Bean, 1996; Svoboda & Lupica, 1998), only TFNs showed hyperpolarization and, as a functional consequence of DAMGO action, a majority of TFNs changed their pattern of intrinsic firing from tonic to adapting. This selective inhibition means that the input–output characteristics of the neurons were modified in such a way that stronger synaptic input could no longer be converted into increasing numbers of generated spikes.

Since postsynaptic MORs, located in somatodendritic domains (Dado *et al*., 1993; Grudt & Williams, 1994; Arvidson *et al*., 1995a,b) are specifically targeted to excitatory SG interneurons (Kemp *et al*., 1996), it was suggested that TFNs can function as excitatory interneurons. Besides,

DAMGO-sensitive interneurons from SG send some of their axons to lamina I and V (Eckert *et al*., 2003), where most projection neurons that target supraspinal regions are located (Trevino *et* al., 1973; Lima, 1998) and cells expressing MORs are located in close proximity to enkephalinergic terminals (Arvidson *et al*., 1995b; Song & Marvizon, 2003). This means that TFNs may represent a primary postsynaptic target for both administered opioids and endogenous enkephalins in the spinal cord and may contribute to profound and prolonged relief of pain with virtually no motor blockade (Hu & Rubly, 1983; Bräu *et al*., 2000; Wolff *et al*., 2004).

The suggested excitatory nature of TFNs could only be proven if to identify pairs of monosynaptically coupled neurons in which the presynaptic neuron would be a TFN. However, the probability of finding monosynaptically connected neurons in slices of the superficial dorsal horn by using a conventional double patch clamp recording technique was, at that time, very low (Lu & Perl, 2003; 2005).

2. Excitatory interneurons and sensory processing in the SG

In the *second publication* we described an efficient method for identifying synaptically coupled neurons in rat spinal cord slices and characterizing their excitatory or inhibitory nature. Using tight-seal whole-cell recordings and a cell-attached stimulation technique, we routinely tested about 1500 SG neurons, classifying 102 of them as monosynaptically connected to neurons in lamina I–III.

The striking finding of our study was that 85% of SG neurons are excitatory interneurons having synapses on somata and dendrites of neurons located in laminae I, II (SG) and III. This was surprising, since after appearance of the ‘gate-control-theory’ by Melzack and Wall in the middle of the last century, the neurons in the SG were mostly considered in terms of GABAergic inhibition of primary afferent terminals and neighbouring spinal neurons. In contrast, we have shown that excitatory interneuron circuitries dominate the sensory network processing in the SG.

We also showed that this excitatory synapses are glutamatergic and the fast synaptic transmission in these synapses is mediated through AMPA and/or kainate receptors, since EPSCs were completely blocked by CNQX, the antagonist for those receptors. Under our experimental conditions, activation of kainate receptors was unlikely because it required much higher intensity of stimulation (Frerking *et al.*, 1998; Lee *et al.*, 2004), and EPSCs mediated by kainate receptors should have much slower kinetics (Frerking *et al.*, 1998; Cossart *et al.*, 2002). The involvement of AMPA receptors suggested by our study is in agreement with observations of others that AMPA receptors are highly

expressed in the superficial dorsal horn synapses (Tachibana *et al.*, 1994; Tolle *et al.*, 1995; Petralia *et al.*, 1997) and modulate spinal synaptic plasticity and inflammatory pain (Hartmann *et al.*, 2004).

Considering that some inhibitory neurons may form presynaptic axoaxonic synapses, and therefore cannot be detected by our technique, this results are in good agreement with previous morphological studies (Todd & Sullivan, 1990; Landry *et al.*, 2004). However, to make sure that the low frequency of recording from inhibitory SG interneurons was not due to limitations in the experimental protocol, we performed control experiments by changing several parameters and specifically searched for inhibitory interneurons. We took several precautions: i) increase of slices thickness to 500–600 μm in order to ensure a complete preservation of distal dendrites; ii) change of the amplitude of the first step in the testing voltage command to −120 mV, to increase the driving force for inhibitory postsynaptic currents (IPSCs) and therefore their resolution; iii) recorded from presumably not connected neuron pairs in the presence of CNQX, to ensure that IPSCs in these pairs were not masked by glutamate-mediated EPSCs of the same magnitude, and iiii) recorded from pairs of neurons located in the centre of the SG near the interface of laminae IIi and IIo, where inhibitory GABAergic connections were found (Lu & Perl 2003). Under these conditions, we confirmed the low percentage of inhibitory connections and a predominantly glycinergic nature of inhibitory presynaptic neurons, what is in accordance with observations that spontaneous miniature IPSCs in lamina I neurons were almost exclusively mediated through strychnine-sensitive glycine receptors (Chéry & De Koninck, 1999). One can explain this results if to assume that in the majority of inhibitory synapses formed by SG neurons, $GABA_A$ receptors can be extrasynaptic and therefore coreleased GABA and glycine predominantly evoke glycine-mediated IPSCs (Chery & De Koninck, 1999), and/or that some GABAergic neurons in the SG are involved in presynaptic inhibition of primary afferent terminals (reviewed by Lima, 1996), and thus cannot be identified by simultaneous recording from neuronal pairs.

We have also demonstrated that intrinsic firing of a SG neuron correlates with its function in such a way that a vast majority of TFNs and AFNs are excitatory interneurons, whereas DFNs could be both excitatory and inhibitory interneurons. As a rule, excitatory interneurons form intralaminar connections, while those of inhibitory SG neurons are mostly interlaminar. The majority of excitatory DFNs made connections within the SG with local TFNs while inhibitory DFNs formed most connections with lamina I TFNs. AFNs appear to be mostly involved in the intralaminar excitatory processing within the lateral SG. The vast majority of TFNs were excitatory glutamatergic interneurons which could be directly suppressed by opioid agonists, as shown in the *first publication*. This strongly supports the idea of specific targeting of postsynaptic MORs to excitatory SG interneurons (Kemp *et al.*, 1996). Because of their numerous excitatory connections throughout the

superficial dorsal horn, a selective inhibition of TFNs may underlie the analgesic postsynaptic effects of endogenous enkephalins and administered opioids (Duggan *et al.*, 1977; Johnston & Duggan, 1981).

These findings offered new, conceptually different view on sensory processing in the SG neuronal network and called for a close attention to the nociceptive integration in excitatory synapses of SG interneurons.

3. Transmission efficacy and plasticity in excitatory synapses

In the *third publication* it was our purpose to study the mechanisms of signal processing in synapses of glutamatergic excitatory interneurons that form the majority of the SG neuron population.

To describe the functional organization and efficacy of excitatory synapses, we did non-invasive recordings from 183 pairs of monosynaptically connected SG neurons. An intact presynaptic SG excitatory interneuron was specifically stimulated through the cell-attached pipette while the evoked EPSCs or excitatory postsynaptic potentials (EPSPs) were recorded through perforated-patch from a postsynaptic neuron (laminae I-III). This way, we studied monosynaptic connections of excitatory interneurons and tried to give detailed answers to the questions mentioned in 'work objectives'.

3.1. Mechanism of postsynaptic spike initiation

The first step was to describe the efficacy of excitatory transmission at spinal interneuron-interneuron synapses, by studying the threshold of spike initiation in an SG neuron and the EPSP efficacy in evoking spikes.

By using independent electrodes for stimulation and recording from one and the same neuron, we observed that short depolarizations induced by the cell-attached stimulation were sufficient to elicit spike in the AIS which, in turn, propagated in two directions: orthodromically, towards the axon terminals, and antidromically, to the soma (Safronov *et al*., 1999; Safronov *et al*., 2000).

Stimulating a neuron via a cell-attached pipette allowed us to avoid injections of large currents that would distort recording at the moment of spike initiation. This way, we were able to correctly measure the true latency of the postsynaptic response (by excluding the time needed for the antidromic

spike propagation from the AIS to the soma) and the threshold of spike initiation, both important parameters for evaluation of efficacy of synaptic transmission.

3.2. Time course and latency of EPSCs

We analysed the latency, rise time and the decay time constant of the postsynaptic EPSCs evoked by synaptic release from the excitatory SG interneurons.

The longest latencies observed in our experiments could hardly be explained by the time needed for the spike propagation in the axon of the presynaptic neuron and transmitter release. Therefore, we did computer simulations to test whether such a delay might be caused by the electrotonic propagation of the EPSC in the postsynaptic neuron, when the activated synapses were located in the distal part of the dendritic tree. In addition, we studied whether the different locations of synapses along the somatodendritic domain of the postsynaptic neuron could explain the range of variations of the rise times and the decay time constants reported.

Simulations were done using the model of SG neuron from the *fourth publication*. Recording electrode in both voltage- and current-clamp simulations was placed at the soma, while an excitatory synapse was added to the model and moved along the somatodendritic domain to simulate proximal and distal inputs. Based on our data, we modelled a fast synapse described by the conductance rise and decay time constants of 0.5 ms and 5 ms, respectively.

In voltage-clamp simulation, the proximal EPSC showed expected fast decay kinetics but, when the same synapse was moved to the distal part of the dendrite, the EPSC reaching the soma became much smaller and slower. We also studied how the electrotonic delay of the EPSC appearance at the soma depends on the synapse location on the dendrite. Both the electrotonic delay and the EPSC rise time increased progressively with the synapse location, from the somatic to the distal synapse.

Also in current-clamp, the distal EPSP had slower rising phase and the electrotonic delays increased when release occurred at more distal synapses.

Our voltage-clamp recordings combined with computer simulations have shown that, in the majority of cases, the variations in the rise and decay kinetics could be explained by different locations of the fast synapse along the somatodendritic domain of the postsynaptic neuron. Electrotonic delay of 3.51 ms predicted by the model for the distal EPSCs, may explain experimentally observed long latencies of 4-5 ms, if 1 ms allowance for the spike propagation and transmitter release in the presynaptic neuron were done.

Thus, the variations in the EPSC kinetics and latencies reflected a broad somatodendritic distribution of synapses in the postsynaptic neuron.

3.3. Transmission efficacy and synaptic plasticity

We studied the efficacy of synaptic transmission in 22 connections and grouped the results according to the classification of the SG presynaptic excitatory interneuron input. Only in 3/22 connections the input was subthreshold and neither single nor summed EPSPs elicited spikes. In 11/22 connections the input was either at the level of firing threshold (3/11) or was suprathreshold (8/11) and, in both cases, spikes could also be evoked by the EPSP summation, although with a different probability (below 20% or above 67%, respectively). In the remaining 8 connections, spontaneous synaptic plasticity was observed and single EPSPs became suprathreshold after EPSC increase.

Although several studies concluded that excitatory connections between dorsal horn neurons are weak and not sufficient to elicit postsynaptic spikes (Lu & Perl, 2005; Schneider, 2008), our experiments have shown that, in the majority of cases, the synaptic release from the individual excitatory SG interneurons produces a substantial depolarization of the postsynaptic neuron and individual or summed EPSPs can frequently elicit spikes. It seems that in those studies the true efficacy of excitatory transmission was underestimated due to low-R_{IN} recordings from a postsynaptic neuron, reducing the amplitude of depolarization, and dialysis of the presynaptic neuron with subsequent reduction in its capacity of transmitter release.

We also show that synaptic transmission from the excitatory SG interneurons can undergo spontaneous increase in the strenght, in this case, those neurons may reach the functional state in which they can effectively evoke postsynaptic spikes.

Having recorded several cases of spontaneous plasticity, we also did experiments trying to induce functional plasticity in the synapses of the excitatory SG interneurons. We focused on two forms of plasticity 1) short-term, induced in the sub-second range and 2) long-term, lasting tens of minutes. Short-term plasticity was induced in 7 connections using a standard paired-pulse protocol and no interaction between the paired responses was seen for intervals up to 160 ms. At longer intervals (320 ms and 640 ms), a depression of the second response was observed but was not associated to a change in the failure rate. Long-term plasticity was induced by stimulating SG excitatory interneurons at 1 Hz, 10 Hz and 100 Hz. In these conditions both, a significant and irreversible increase in synaptic strength, LTP, or depression, LTD, were induced.

3.4. Multiple synapses formed by the axon of an SG excitatory interneuron

Analysis of composite EPSCs, computer simulations and labelling experiments indicated that the axon of an SG excitatory interneuron forms multiple synapses on a postsynaptic neuron.

3.4.1. Electrophysiological paired recordings of composite EPSCS

In the majority of connections, at least two components elicited by one presynaptic spike could be clearly distinguished on the rising phase of the evoked EPSCs. These EPSC components could be explained in two different ways:

1) The axon of the excitatory SG interneuron can form several synapses along the somatodendritic domain of the postsynaptic neuron. The composite EPSCs would result of the simultaneous transmitter release in synapses located at different electrotonic distances, therefore, reaching the soma with different delays.

2) For connections with large time intervals (>1 ms) between components, the pre- and postsynaptic neurons could be also connected indirectly via an intercalated excitatory neuron.

We measured latency, time interval between each EPSC component and their variation. In both parameters, variations were within 1 ms, showing that each EPSC component could be independently identified as monosynaptic, based on the standard criterion of latency stability. Assuming that initiation time is the most critical factor determining the delay on an intercalated neuron (Berry & Pentreath, 1976), we also analysed spike initiation time values and their variations to test the possibility of involvement of an intercalated neuron. We concluded that the spike initiation time and its variation in the intercalated neuron were substantially larger than the time interval between each EPSC component and its variation. Therefore, one could conclude that the appearance of the EPSC components is most probably caused by the existence of multiple synapses between connected neurons.

3.4.2. Computer simulations and labeling experiments

We also did computer simulations to test whether composite EPSCs could be modelled by a simultaneous transmitter release from two synapses inserted at different locations along the somatodendritic domain of the postsynaptic neuron. We saw that simultaneous activation of both synapses gave composite EPSCs, and time interval between each component increased with the distance between the synapses.

Labelling experiments allowed us to show close appositions, indicating putative synaptic contacts, and suggesting an anatomical basis for the composite EPSCs.

Thus, paired recordings, computer simulation and biocytin labelling experiments suggested that the composite EPSCs with several components on the rising phase could be evoked by the simultaneous transmitter release from multiple synapses formed by one presynaptic neuron along the somatodendritic domain of the postsynaptic neuron.

3.5. Role of individual synapses in induction of functional plasticity

In some connections it was possible to analyse the individual components of the composite EPSC and, therefore, to directly estimate the release probability in individual synapses and follow the changes in properties of individual synapses.

The induction of LTP could be associated with 1) an increase in the release probability for one of the synapses involved; activating silent synapses and 2) an increase in the magnitude of already active synapses.

To elucidate the type of postsynaptic receptors activated by the transmitter release from the excitatory SG interneurons, we studied the effects of several specific blockers. These experiments allowed us to conclude that 1) transmitter released from excitatory SG interneurons acts on postsynaptic AMPA-type glutamate receptors and 2) the transmission involves both the GluR2-lacking Ca^{2+}-permeable AMPA receptors and the GluR2-containing Ca^{2+}-impermeable AMPA receptors. These results are in agreement with immunocytochemistry and electron microscopy studies which have also revealed that excitatory synapses in the superficial dorsal horn express both GluR2 subunities of AMPA receptors (Nagy *et al*., 2004; Larsson & Broman, 2006; Antal *et al*., 2008; Polgar *et al*., 2008) involved in several signalling pathways (Liu & Cull-Candy, 2005; Plant *et al*., 2006; Guire *et al*. 2008; Terashima *et al*., 2008; Park *et al*., 2009).

3.6. Functional balance between the excitatory and inhibitory inputs

Correct estimation of relative contributions of excitatory and inhibitory interneurons to the sensory processing in the dorsal horn is crucially important for understanding the organization of the spinal nociceptive circuitries. Studies using *in situ* hybridization (Landry *et al*., 2004), immunocytochemistry (Todd & Sullivan, 1990) and the high-R_{IN} paired voltage-clamp recordings (*second* and *third publications*) have shown that the majority of SG interneurons are excitatory glutamatergic neurons, whereas the inhibitory interneurons form a minority. These conclusions were opposed by the studies based on the low-R_{IN} current-clamp recordings which have found more numerous inhibitory connections (Lu, 2008; Schneider, 2008); it was suggested that the difference was due to inability of voltage-clamp method to detect weak distal inhibitory inputs.

Because of its critical importance for the entire research field dealing with both spontaneous and evoked synaptic inputs in superficial dorsal horn neurons (which are mostly studied in voltage-clamp), we did thorough analysis of the resolution power of voltage- and current-clamp techniques for detection of synaptic responses. For both recording configurations the ability to detect synaptic response depends on 1) the level of membrane noise at the potential used for the recording, 2) neuronal R_{IN} and the location of the synapse (proximal *versus* distal) on the dendritic tree, and 3) the driving force for the carrier ion. The first three factors were subjected to experimental study by combining the tight-seal recordings and computer simulations.

3.6.1. Membrane noise

Subthreshold voltage or current noise seen in an experiment is the sum of the actual membrane (biological) noise and the instrumental (non-biological) noise (i.e. due to non-zero access resistance) (Sherman-Gold, 1993; Marty & Neher, 1995). The membrane noise consists of synaptic noise, resulting from spontaneous quantal transmitter release, and the ion channel noise, caused by stochastic opening and closing of background K^+ channels (determining R_{IN}) and voltage-gated Na^+ and K^+ channels. At subthreshold and near-threshold potentials, the ion channel noise increases dramatically with depolarization, because of activation of voltage-gated Na^+ and K^+ conductances and an increased driving force for the background and voltage-gated K^+ channels (Diba *et al*., 2004; Jacobson *et al*., 2005). Therefore, we measured membrane noise at several potentials used to reveal the synaptic responses. Voltage-clamp identification of synaptic responses in the *second* and *third publications* was done with triple pulse protocol, where the low-membrane-noise potentials of -80 mV and -100 mV

were generally used to detect EPSCs (E_{Rev} = 0 mV) and IPSCs (E_{Rev} = E_{Cl} = -82 mV), respectively, whereas a pulse to -60 mV was applied to confirm the reversion of the IPSCs. For comparison, the entire identification of synaptic responses in current-clamp mode was done at -50 mV and -60 mV by Lu and Perl (2003, 2005) and at -60 mV by Schneider (2008). For this reason, we compared the current noise in neurons voltage-clamped at -80 mV and -100 mV with the voltage noise in neurons current-clamped at -60 mV and -55 mV.

We analyzed noise in the frequency range between 10 Hz (determined by the trace length) and 3 kHz (determined by the low-pass filter frequency, voltage-clamp). The noise was presented as the root mean square (r.m.s.) noise, or σ, which is also identical to the square root of the variance (Diba *et al*., 2004). In voltage-clamp, the current noise (σ_I) was measured and the mean σ_I value was similar at -80 mV and at -100 mV but increased at -60 mV. The voltage noise (σ_V) was also measured in the same neurons by switching the amplifier to the current-clamp recording mode and the mean σ_V value was low at -80 mV, where voltage-gated Na^+ and K^+ channels were not active, but increased dramatically with depolarization to -60 mV and -55 mV. In agreement with other studies, an additional voltage noise which appeared at -60 mV and -55 mV showed frequency above 100 Hz and was caused by subthreshold activity of Na^+ channels (Diba *et al*., 2004).

We concluded that our measurements adequately describe the magnitude and voltage-dependence of membrane noise in SG neurons studied in spinal cord slices with unblocked synaptic inputs, since σ_I and σ_V values are in excellent agreement with those reported for cultured hippocampal neurons with blocked synaptic inputs (Diba *et al*., 2004). Besides the measurement of the σ (r.m.s.), the resolution limit for the EPSC and EPSP detection is also dependent on the spectral composition of the noise at a given potential and the time course of synaptic response. To determine the resolution limits, we added computer simulated EPSCs and EPSPs to our original recordings of current noise at -80 mV and voltage noise at both -60 mV and -55 mV. The amplitudes of simulated EPSCs and EPSPs were expressed in the σ values measured for the corresponding noise recordings; σ, 2 σ and 3 σ. In voltage-clamp traces (-80 mV; 3 kHz) the EPSC could be already detected at 2 σ_I amplitude, and was clearly resolved at 3 σ_I amplitude. Detection of EPSP was more difficult in current-clamp at -60 mV and -55 mV, where the Na^+-channel-dependent component of the voltage noise with its characteristic frequency above 100 Hz (Diba *et al*., 2004) masked EPSP.

Analysis of membrane noise allowed us to determine the smallest EPSC and EPSP which could be reliably resolved with the same signal-to-noise ratio. Assuming that in both voltage- and current-clamp the resolution starts at the 3 σ level, one could conclude that an EPSC of 5 pA recorded at -80 mV is as well resolved as an EPSP of 0.9 mV at -60 mV or 1 mV at -55 mV.

3.6.2. Neuronal R_{IN} and location of the synapse

R_{IN} in a postsynaptic neuron is critical for detection of synaptic inputs, since increase in membrane conductance associated with its drop will unavoidably shunt the distal synaptic responses recorded at the soma. The R_{IN} values reported for SG neurons in the literature differ by an order of magnitude, implying that they are mostly determined by the choice of experimental conditions. R_{IN} is high when measured in perforated-patch mode or in the whole-cell mode when intracellular solution with 1 mM BAPTA as Ca^{2+}-chelator is used (*second* and *third publications*, respectively). It becomes much lower when internal solutions without Ca^{2+}-chelators are used to increase the probability of synaptic release (Lu & Perl, 2003, 2005; Hantman *et al*., 2004; Schneider, 2008). Therefore, we analyzed effect of the R_{IN} variation on detection of both distal and proximal synaptic responses.

We used the basic model of SG neuron presented in the *fourth publication* and introduced two synapses, proximal (soma) and distal (dendrite 0.95). For both synapses, the g_M values were adjusted to give the EPSCs of 5 pA when measured with a voltage-clamp electrode placed at the soma. This basic model with the smallest proximal and distal EPSCs resolved under our experimental conditions (each above the 3 σ_I level) was used to analyze how the drop in R_{IN} would change the amplitude of the recorded signal in relation to the resolution limit in both voltage- and current–clamp.

The voltage-clamp simulation showed that the drop in R_{IN} to values below 500 MΩ critically reduced the resolution of the distal EPSCs. In current-clamp, the proximal EPSP was just below the 3 σ_V level in the basic model and progressively diminished as R_{IN} dropped while the distal EPSP could only be well resolved for R_{IN} values higher than 500 MΩ. Thus, lowering R_{IN} dramatically reduced the amplitude of the distal EPSP in relation to the resolution limit.

Our simulations have shown a critical importance of high R_{IN} for adequate recording of distal synaptic events in both voltage- and current-clamp. In contrast to Lu (2008) and Schneider (2008) about the lower resolution power of the voltage-clamp technique, we have found that, for both proximal and distal synaptic inputs, the high-R_{IN}-voltage-clamp recordings at -80 mV and -100 mV have considerably higher signal-to-noise ratio than the low-R_{IN}-current-clamp recordings at -60 mV and -50 mV (Lu & Perl, 2003, 2005; Hantman *et al*., 2004). Furthermore, the efficacy of distal EPSPs in depolarizing the soma membrane is dramatically reduced with the drop in R_{IN}, implying that low-R_{IN}-current-clamp-recording substantially underestimates the efficacy of distal synapses in evoking somatic spikes.

We have shown that the high-R_{IN} voltage-clamp mode is better suitable for the detection, recording and biophysical analysis of synaptic inputs in the superficial dorsal horn. Therefore, the low proportion of excitatory inputs reported by Lu (2008) is most probably due to inability of low-R_{IN}

current-clamp recording to resolve distal dendritic inputs. Indeed, the largest latencies measured in current-clamp for IPSPs (3.3 ms; Lu & Perl, 2003) and for EPSPs (2.1 ms; Lu & Perl, 2005) were short and clearly indicated that none of these inputs originated from the distal part of the dendritic tree. Recent analysis of the receptor distributions in SG neurons done by the laser scanning photostimulation technique has shown that the inhibitory receptors are confined to the narrow peri-somatic region while the glutamate receptors are more widespread (Kato *et al.*, 2007). Therefore, inability of low-R_{IN} current-clamp to record weak distal dendritic inputs (Lu, 2008), which are mostly excitatory (Kato *et al.*, 2007), led to a crucial underestimation of excitatory connections and, therefore, of the percentage of excitatory SG interneurons.

Also, recording at uncontrolled membrane potential and reporting IPSPs with amplitudes smaller than the resolution limit question conclusions about the high frequency of inhibitory connections (Schneider, 2008).

4. Basic conductances and structural elements responsible for appearance of cell-specific tonic- and adapting-firing patterns in SG neurons

Using tight-seal recordings from rat spinal cord slices, intracellular labelling and computer simulation, we analysed the mechanisms of tonic firing and spike frequency adaptation in SG neurons.

4.1. Ca^{2+}-dependent K^+ conductances

Blockers of Ca^{2+}- and Ca^{2+}-dependent K^+ (K_{CA}) channels were tested to study the role of Ca^{2+}-dependent conductances. In TFNs the block of Ca^{2+} influx into the neuron led to a left-shift in the frequency–current characteristics and a reduction of firing stability. These effects resulted from a reduction of a slow afterhyperpolarization, shown for several types of neurons (Barrett & Barrett, 1976; Schwindt *et al*., 1988; Nishimura *et al*., 1989; Viana *et al*., 1993; Savic *et al*., 2001; Smith *et al*., 2002), and also seen in the presence of apamin but not charybdotoxin, indicating the involvement of small conductance apamin-sensitive, rather than big conductance K_{CA} channels.

Blockers of Ca^{2+}- and K_{CA} channels were also tested in AFNs and no changes in firing pattern or the instantaneous frequency–current characteristic, calculated for the first interspike interval, were observed. The shape of single spikes was also unchanged by the blockers and the amplitude of afterhyperpolarization (fast and slow) was also not reduced by Co^{2+}.

Thus, it could be concluded that Ca^{2+}-dependent conductances do not contribute to discharge pattern in AFNs and are only involved in regulation of firing frequency in TFNs. The basic tonic firing and adapting firing should be, instead, generated by voltage-gated Na^+ and K^+ channels.

4.2. Voltage-gated Na^+ and K^+ currents

In the case of TFNs, Na^+ channels exhibited fast activation and inactivation kinetics and followed two-exponential time course of recovery from inactivation. The study of recovery from inactivation also showed that such a high frequency firing can be generated with only about one-fifth of available Na^+ channels.

The major K^+ current was carried through tetraethylammonium (TEA)-sensitive rapidly activating delayed-rectifier (K_{DR}) channels with a slow inactivation and sufficiently fast gating kinetics for its involvement in spike repolarization.

The TEA-insensitive transient A-type K^+ (K_A) current was very small in patches and was strongly inactivated at resting potential. Block of K_{DR} rather than K_A conductance by TEA lowered the frequency and stability of firing.

By comparing the results for AFNs with those for TFNs, it was possible to conclude that both neuron types possess Na^+ and K_{DR} currents as well as negligible K_A current. The lack of K_A current appears to be important for the generation of typical discharge patterns in both, AFNs and TFNs, since the expression of large K_A currents was shown to result in delayed-onset firing or irregular burst-like discharges (Yoshimura & Jessell, 1989; Grudt & Perl, 2002; Ruscheweyh & Sandkuhler, 2002). The ranges of K_{DR} channel activation and the kinetics of Na^+ channel recovery from inactivation were very similar and the activation characteristics of Na^+ channels were insignificantly different. However, the density of somatic Na^+ and K_{DR} currents in AFNs was lower and the Na^+ channel inactivation was shifted to more positive potentials by 11 mV. Thus, the next step was to perform experiments that would allow us to find out which of these factors played a critical role in the appearance of firing adaptation.

4.3. Block of Na^+ rather than K_{DR} channels in TFNs induces adaptation typical of AFNs

Since somatic Na^+ current represents only few per cent of the total Na^+ current in a spinal neuron (Safronov *et al.,* 1997, 1999; Alessandri-Haber *et al.,* 1999), a comparison of total Na^+ conductances in AFNs and TFNs was done by measuring maximum spike depolarization rates. AFNs showed a slower Na^+ conductance in comparison with TFNs. In addition, the velocity of repolarization

was also lower in AFNs. Lower Na^+ conductance seemed to be more critical for the appearance of firing adaptation than K_{DR} current since discharge pattern in TFNs could be reversibly converted into that typical of AFNs in the presence of TTX but not TEA. In fact, in all TFNs tested, the tonic firing changed to adapting and then to strongly adapting with a single spike when perfusion of the slice with TTX-containing solution was started. These results were also confirmed by differentiation of the voltage traces which showed that the appearance of adaptation correlated with a reduction of Na^+ current and the transition from tonic to adapting firing occurred at 40–60% block of Na^+ conductance. Thus, block of Na^+ rather than K_{DR} channels in TFNs modified a firing pattern to that typical of AFNs.

In order to test whether the smaller Na^+ conductance observed in AFNs might result from the cutting of the axon during the preparation of slices, AFNs were labelled by including biocytin in the patch pipette. Intracellularly labelled AFNs showed specific morphological features and preserved long extensively branching axons, indicating that smaller Na^+ conductance could not result from the axon cut.

We also performed computer simulations to study how a reduction in Na^+ current and a shift in its activation and inactivation characteristics to more positive potentials could influence firing in a model neuron. The control model of a TFN showed in the *fourth publication* was used and we saw that, by reducing the Na^+ conductance (gNa) to 0.41, it was possible to induce firing adaptation. If the activation characteristics of Na^+ channels were shifted by +5mV, a strong adaptation appeared in the model already at the control gNa value. After the inactivation was shifted by +11 mV, the model again generated tonic firing. If both activation and inactivation shifted to positive potentials, a stronger reduction in gNa to 0.29 was needed for the induction of adaptation in the whole stimulation range. Thus, although the activation shift promoted spike frequency adaptation, a stronger shift in inactivation characteristics had an opposite effect.

These results showed that, in addition to metabolic regulation of inwardly rectifying and A-type K^+ channels (Derjean *et al.,* 2003; Hu & Gereau, 2003), a down-regulation of Na^+ conductance represents an effective mechanism for the induction of firing adaptation and it was suggested that the cell-specific regulation of Na^+ channel expression can be an important factor underlying the diversity of firing patterns in SG neurons.

References

Alessandri-Haber N, Paillart C, Arsac C, Gola M, Couraud F & Crest M (1999). Specific distribution of sodium channels in axons of rat embryo spinal motoneurones. *J Physiol* **518**: 203–214.

Antal M, Fukazawa Y, Eordogh M, Muszil D, Molnar E, *et al*. (2008). Numbers, densities, and colocalization of AMPA- and NMDA-type glutamate receptors at individual synapses in the superficial spinal dorsal horn of rats. *J Neurosci* **28**: 9692-9701.

Arvidson U, Dado RJ, Riedl M, Lee J-H, Law P-Y, Loh HH, Elde R & Wessendorf MW (1995a). δ-Opioid receptor immunoreactivity: Distribution in brainstem and spinal cord, and relationship to biogenic amines and enkephalin. *J Neurosci* **15**: 1215–1235.

Arvidson U, Riedl M, Chakrabarti S, Lee J-H, Nakano AH, Dado RJ, Loh HH, Law P-Y, Wessendorf MW & Elde R (1995b). Distribution and targeting of a μ-opioid receptor (MOR1) in brain and spinal cord. *J Neurosci* **15**: 3328–3341.

Barrett EF & Barrett JN (1976). Separation of two voltage-sensitive potassium currents, and demonstration of a tetrodotoxin-resistant calcium current in frog motoneurones. *J Physiol* **255**: 737–774.

Berry MS & Pentreath VW (1976). Criteria for distinguishing between monosynaptic and polysynaptic transmission. *Brain Res* **105**: 1-20.

Bräu ME, Koch ED, Vogel W & Hempelmann G (2000). Tonic blocking action of meperidine on Na^+ and K^+ channels in amphibian peripheral nerves. *Anesthesiology* **92**: 147–155.

Cervero F (1987). Dorsal horn neurons and their sensory inputs, Spinal Afferent Processing. (Yaksh TL, ed) New York, Plenum Press, pp 197–216.

Chéry N & De Koninck Y (1999). Junctional versus extrajunctional glycine and GABAA receptor-mediated IPSCs in identified lamina I neurons of the adult rat spinal cord. *J Neurosci* **19**: 7342–7355.

Cossart R, Epsztein J, Tyzio R, Becq H, Hirsch J, Ben-Ari Y & Crepel V (2002). Quantal release of glutamate generates pure kainate and mixed AMPA/kainate EPSCs in hippocampal neurons. *Neuron* **35**: 147–159.

Dado RJ, Law PY, Loh HH & Elde R (1993). Immunofluorescent identification of a delta (delta)-opioid receptor on primary afferent nerve terminals. *Neuroreport* **5**: 341–344.

Derjean D, Bertrand S, LeMasson G, Landry M, Morisset V & Nagy F (2003). Dynamic balance of metabotropic inputs causes dorsal horn neurons to switch functional states *Nature Neurosci* **6**: 274–281.

Diba K, Lester HA & Koch C (2004). Intrinsic noise in cultured hippocampal neurons: experiment and modeling. *J Neurosci* **24**: 9723-9733.

Duggan AW, Hall JG & Headley PM (1977). Suppression of transmission of nociceptive impulses by morphine: selective effects of morphine administered in the region of the substantia gelatinosa. *Br J Pharmacol* **61**: 65–76.

Eckert WA, McNaughton KK & Light AR (2003). Morphology and axonal arborization of rat spinal inner lamina II neurons hyperpolarized by μ-opioid-selective agonists. *J Comp Neurol* **458**: 240–256.

Frerking M, Malenka RC & Nicoll RA (1998). Synaptic activation of kainate receptors on hippocampal interneurons. *Nat Neurosci* **1**: 479–486.

Graham BA, Brichta AM & Callister RJ (2007). Moving from an averaged to specific view of spinal cord pain processing circuits. *J Neurophysiol* **98**: 1057-1063.

Grudt TJ & Perl ER (2002). Correlations between neuronal morphology and electrophysiological features in the rodent superficial dorsal horn. *J Physiol* **540**: 189–207.

Grudt TJ & Williams JT (1994). μ-Opioid agonists inhibit spinal trigeminal substantia gelatinosa neurons in guinea pig and rat. *J Neurosci* **14**: 1646–1654.

Guire ES, Oh MC, Soderling TR & Derkach VA (2008). Recruitment of calcium-permeable AMPA receptors during synaptic potentiation is regulated by CaM-kinase I. *J Neurosci* **28**: 6000-6009.

Hantman AW, van den Pol AN, Perl ER (2004). Morphological and physiological features of a set of spinal substantia gelatinosa neurons defined by green fluorescent protein expression. *J Neurosci* **24**: 836–842.

Hartmann B, Ahmadi S, Heppenstall PA, Lewin GR, Schott C, Borchardt T, Seeburg PH, Zeilhofer HU, Sprengel R & Kuner R (2004). The AMPA receptor subunits GluR-A and GluR-B reciprocally modulate spinal synaptic plasticity and inflammatory pain. *Neuron* **44**: 637–650.

Hu H-J & Gereau RW (2003). ERK integrates PKA and PKC signaling in superficial dorsal horn neurons: II. Modulation of neuronal excitability. *J Neurophysiol* **90**: 1680–1688.

Hu S & Rubly N (1983). Effects of morphine on ionic currents in frog node of Ranvier. *Eur J Pharmacol* **95**: 185–192.

Jacobson GA, Diba K, Yaron-Jakoubovitch A, Oz Y, Koch C, Segev I & Yarom Y (2005). Subthreshold voltage noise of rat neocortical pyramidal neurones. *J Physiol* **564**: 145-160.

Johnston SM & Duggan AW (1981). Evidence that opiate receptors of the substantia gelatinosa contribute to the depression, by intravenous morphine, of the spinal transmission of impulses in unmyelinated afferents. *Brain Res* **207**: 223–228.

Kato G, Kawasaki Y, Ji RR & Strassman AM (2007). Differential wiring of local excitatory and inhibitory synaptic inputs to islet cells in rat spinal lamina II demonstrated by laser scanning photostimulation. *J Physiol* **580**: 815-833.

Kemp T, Spike RC, Watt C & Todd AJ (1996). The μ-opioid receptor (MOR1) is mainly restricted to neurons that do not contain GABA or glycine in the superficial dorsal horn of the rat spinal cord. *Neurosci* **75**: 1231–1238.

Landry M, Bouali-Benazzouz R, El Mestikawy S, Ravassard P & Nagy F (2004). Expression of vesicular glutamate transporters in rat lumbar spinal cord, with a note on dorsal root ganglia. *J Comp Neurol* **468**: 380-394.

Larsson M & Broman J (2006). Pathway-specific bidirectional regulation of Ca^{2+}/calmodulindependent protein kinase II at spinal nociceptive synapses after acute noxious stimulation. *J Neurosci* **26**: 4198-4205.

Lee CJ, Labrakakis C, Joseph DJ & Macdermott AB (2004). Functional similarities and differences of AMPA and kainate receptors expressed by cultured rat sensory neurons. *Neuroscience* **129**: 35–48.

Light AR & Perl ER (1979). Spinal termination of functionally identified primary afferent neurons with slowly conducting myelinated fibers. *J Comp Neurol* **186**: 133–150.

Light AR & Willcockson HH (1999). Spinal laminae I-II neurons in rat recorded in vivo in whole cell, tight seal configuration: Properties and opioid responses. *J Neurophysiol* **82**: 3316–3326.

Lima D (1996). Endogenous pain modulatory system in the light of the gate control theory. *Pain Forum* **5**: 31–39.

Lima D (1998). Anatomical basis for the dynamic processing of nociceptive input. *Eur J Pain* **2**: 195–202.

Liu SJ & Cull-Candy SG (2005). Subunit interaction with PICK and GRIP controls Ca^{2+} permeability of AMPARs at cerebellar synapses. *Nat Neurosci* **8**: 768-775.

Lu Y (2008). Synaptic wiring in the deep dorsal horn. Focus on "Local circuit connections between hamster laminae III and IV dorsal horn neurons". *J Neurophysiol* **99**: 1051-1052.

Lu Y & Perl ER (2003). A specific inhibitory pathway between substantia gelatinosa neurons receiving direct C-fiber input. *J Neurosci* **23**: 8752–8758.

Lu Y & Perl ER (2005). Modular organization of excitatory circuits between neurons of the spinal superficial dorsal horn (laminae I and II). *J Neurosci* **25**: 3900-3907.

Marty A & Neher E (1995). Tight-seal whole-cell recording. In: Sakmann B, Neher E, editors. Single-channel recording 2nd ed. New York: Kluwer Academic/Plenum Publishers. pp. 31-52.

Melzack R & Wall PD (1965). Pain mechanisms: a new theory. *Science* **150**: 971-979.

Merchenthaler I, Maderdrut JL, Altschuler RA & Petrusz P (1986). Immunocytochemical localization of proenkephalin-derived peptides in the central nervous system of the rat. *Neurosci* **17**: 325–348.

Nagy GG, Al-Ayyan M, Andrew D, Fukaya M, Watanabe M, *et al*. (2004). Widespread expression of the AMPA receptor GluR2 subunit at glutamatergic synapses in the rat spinal cord and phosphorylation of GluR1 in response to noxious stimulation revealed with an antigen730 unmasking method. *J Neurosci* **24**: 5766-5777.

Nishimura Y, Schwindt PC & Crill WE (1989). Electrical properties of facial motoneurons in brainstem slices from guinea pig. *Brain Res* **502**: 127–142.

Park JS, Voitenko N, Petralia RS, Guan X, Xu JT, *et al*. (2009). Persistent inflammation induces GluR2 internalization via NMDA receptor-triggered PKC activation in dorsal horn neurons. *J Neurosci* **29**: 3206-3219.

Petralia RS, Wang YX, Mayat E & Wenthold RJ (1997). Glutamate receptor subunit 2-selective antibody shows a differential distribution of calcium-impermeable AMPA receptors among populations of neurons. *J Comp Neurol* **385**: 456–476.

Plant K, Pelkey KA, Bortolotto ZA, Morita D, Terashima A, McBain CJ, Collingridge GL & Isaac JT (2006). Transient incorporation of native GluR2-lacking AMPA receptors during hippocampal long-term potentiation. *Nature Neurosci* **9**: 602-604.

Rethelyi M (1977). Preterminal and terminal axon arborizations in the substantia gelatinosa of cat's spinal cord. *J Comp Neurol* **172**: 511–521.

Ribeiro-da-Silva A, Pioro EP & Cuello AC (1991). Substance P- and enkephalin-like immunoreactivities are colocalized in certain neurons of the substantia gelatinosa of the rat spinal cord: An ultrastructural double-labeling study. *J Neurosci* **11**: 1068–1080.

Ruscheweyh R & Sandkuhler J (2002). Lamina-specific membrane and discharge properties of rat spinal dorsal horn neurones in vitro. *J Physiol* **541**: 231–244.

Safronov BV, Wolff M & Vogel W (1997). Functional distribution of three types of Na^+ channel on soma and processes of dorsal horn neurones of rat spinal cord. *J Physiol* **503**: 371–385.

Safronov BV, Wolff M & Vogel W (1999). Axonal expression of sodium channels in rat spinal neurones during postnatal development. *J Physiol* **514**: 729-734.

Safronov BV, Wolff M & Vogel W (2000). Excitability of the soma in central nervous system neurons. *Biophys J* **78**: 2998-3010.

Savic N, Pedarzani P & Sciancalepore M (2001). Medium afterhyperpolarization and firing pattern modulation in interneurons of stratum radiatum in the CA3 hippocampal region. *J Neurophysiol* **85**: 1986–1997.

Schneider SP (2008). Local circuit connections between hamster laminae III and IV dorsal horn neurons. *J Neurophysiol* **99**: 1306-1318.

Schneider SP, Eckert WA & Light AR (1998). Opioid-activated postsynaptic, inward rectifying potassium currents in whole cell recordings in substantia gelatinosa neurons. *J Neurophysiol* **80**: 2954–2962.

Schwindt PC, Spain WJ, Foehring RC, Stafstrom CE, Chubb MC & Crill WE (1988). Multiple potassium conductances and their functions in neurons from cat sensorimotor cortex in vitro. *J Neurophysiol* **59**: 424–449.

Sherman-Gold R (1993). The axon guide for electrophysiology and biophysics laboratory techniques. Axon Instruments, Foster City, CA.

Smith MR, Nelson AB & Lac S (2002). Regulation of firing response gain by calcium-dependent mechanisms in vestibular nucleus neurons. *J Neurophysiol* **87**: 2031–2042.

Sodickson DL & Bean B (1996). $GABA_B$ receptor-activated inwardly rectifying potassium current in dissociated hippocampal CA3 neurons. *J Neurosci* **16**: 6374–6385.

Song B & Marvizon JC (2003). Peptidases prevent mu-opioid receptor internalization in dorsal horn neurons by endogenously released opioids. *J Neurosci* **23**: 1847–1858.

Svoboda KR & Lupica CR (1998). Opioid inhibition of hippocampal interneurons via modulation of potassium and hyperpolarization-activated cation (I_h) currents. *J Neurosci* **18**: 7084–7098.

Sugiura Y, Lee CL & Perl ER (1986). Central projections of identified, unmyelinated (C) afferent fibers innervating mammalian skin. *Science* **234**: 358–361.

Tachibana M,Wenthold RJ, Morioka H & Petralia RS (1994). Light and electron microscopic immunocytochemical localization of AMPA-selective glutamate receptors in the rat spinal cord. *J Comp Neurol* **344**: 431–454.

Terashima A, Pelkey KA, Rah JC, Suh YH, Roche KW, Collingridge GL, McBain CJ & Isaac JT (2008). An essential role for PICK1 in NMDA receptor-dependent bidirectional synaptic plasticity. *Neuron* **57**: 872-882.

Tolle TR, Berthele A, ZieglgansbergerW, Seeburg PH & WisdenW (1995). Flip and Flop variants of AMPA receptors in the rat lumbar spinal cord. *Eur J Neurosci* **7**: 1414–1419.

Todd AJ & Sullivan AC (1990). Light microscope study of the coexistence of GABA-like and glycine-like immunoreactivities in the spinal cord of the rat. *J Comp Neurol* **296**: 496-505.

Trevino DL, Coulter JD & Willis WD (1973). Location of cells of origin of spinothalamic tract in lumbar enlargement of the monkey. *J Neurophysiol* **36**: 750–761.

Viana F, Bayliss DA & Berger AJ (1993). Multiple potassium conductances and their role in action potential repolarization and repetitive firing behavior of neonatal rat hypoglossal motoneurons. *J Neurophysiol* **69**: 2150–2163.

Wolff M, Olschewski A, Vogel W & Hempelmann G (2004). Meperidine suppresses the excitability of spinal dorsal horn neurons. *Anesthesiology* **100**: 947–955.

Yoshimura M & Jessell TM (1989). Membrane properties of rat substantia gelatinosa neurons in vitro. *J Neurophysiol* **62**: 109–118.

Yoshimura M & North RA (1983). Substantia gelatinosa neurones hyperpolarized in vitro by enkephalin. *Nature* **305**: 529–530.

IV. SUMMARY AND CONCLUSIONS

It is known that diverse sensory modalities are encoded in the SG by the types of terminating afferents, neuronal firing properties and synaptic connectivity. However, although several groups of SG neurons with distinct intrinsic firing properties were characterized, little is known about major types of ion channels specifically expressed in SG neurons as well as their synaptic connections. Besides, although the SG is an important element in the system of antinociception, little is known about the types of neurons serving as specific postsynaptic targets for opioid action within this region.

To better understand how nociceptive information is processed within the superficial dorsal horn, it is essential to study firing patterns of SG interneurons, their synaptic connections and sensitivity to opioid agonists.

The present work was done to study these questions in the rat and divided in the following independent points:

1. To study the spinal mechanisms of opioidergic analgesia, we compared the action of MOR agonist, DAMGO, on SG neurons with different intrinsic firing properties. Reliable identification criteria were created in order to correctly classify the different intrinsic firing patterns and study neuronal distribution and sensitivity to DAMGO.

DAMGO selectively hyperpolarized all TFNs tested and this effect was due to activation of GIRK conductance and, as a functional consequence, a majority of TFNs changed their pattern of intrinsic firing from tonic to adapting. It was therefore suggested that TFNs are primary postsynaptic targets for administered and endogenous opioid agonists in the spinal SG. Indeed, the functional transition from tonic to adapting firing mode may represent an important mechanism facilitating opioidergic analgesia. It is also suggested that TFNs would presumably function as excitatory interneurons. This suggestion could only be tested if to study synaptic connections established by SG neurons.

(Santos, Melnick & Safronov, 2004; *Anesthesiology* **101**: 1177-1183)

2. We implemented a novel approach for efficiently identifying monosynaptic connections and studied discharge properties of excitatory and inhibitory SG interneurons. This approach combined a tight-seal whole-cell recording from postsynaptic neuron with a specific cell-attached stimulation of presynaptic neuron.We focused on two critical aspects of SG network organization: (1) the functional balance between the excitatory and inhibitory modes of sensory processing, and (2) whether and how neuronal firing properties correlate with their synaptic connections. We have characterized synaptic

connections for SG neurons with different firing patterns and found that signalling within the SG network is dominated by excitatory glutamatergic interneurons.

(Santos, Rebelo, Derkach & Safronov, 2007; *J Physiol* **581**: 241-254)

3. To study functional organization and activity-dependent modification of glutamatergic synapses of SG excitatory interneurons, we combined paired recording (non-invasive recordings through perforated-patch from a postsynaptic neuron and stimulation of an intact presynaptic SG excitatory interneuron through the cell-attached pipette), computer simulation and biocytin-labelling techniques. We found that: 1) Action potentials could be rapidly initiated in an SG neuron by a short depolarization of about 10 mV; 2) Glutamate released from the terminals of an excitatory SG interneuron acts on both the GluR2-lacking Ca^{2+}-permeable AMPA receptors and the GluR2-containing Ca^{2+}-impermeable AMPA receptors; 3) The EPSCs elicited by stimulating excitatory SG interneurons are fast, and the variation in their kinetics indicates broad distribution of excitatory synapses over the somatodendritic domain of the postsynaptic neuron; 4) Many excitatory interneurons are able alone to initiate spike in the postsynaptic neuron; 5) Synapses formed by the excitatory SG interneurons can undergo different forms of spontaneous and induced plasticity, thus, changing their functional state and increasing efficacy of transmission; 6) The axon of the excitatory SG interneuron forms multiple functional synapses on the dendrites of the postsynaptic neuron; 7) The high-R_{IN} recording from the postsynaptic neuron is important for correct study of synaptic transmission, since artificial lowering of R_{IN} dramatically reduces both the magnitude and the functional efficacy of the distal synaptic inputs.

(Santos, Luz, Szucs, Lima, Derkach & Safronov; *PlosOne* **4**: e8047, pp1-18)

4. To determine the ionic basis underlying tonic- and adapting- firing patterns we did patch-clamp recordings, intracellular staining with biocytin and created a computer model of a SG neuron.

We concluded that a balanced system of ionic conductances underlies tonic firing in SG neurons. Voltage-gated Na^+ current in combination with a pronounced K_{DR} but small K_A currents generate a basic firing pattern, while Ca^{2+}-dependent conductances stabilize tonic firing, efficiently regulate discharge frequency, and modulate an input–output characteristic in a neuron.

(Melnick, Santos, Szokol, Szucs & Safronov, 2004; *J Neurophysiol* **91**: 646-655)

In the case of AFNs, although currents were similar to those present in TFNs, we found that Na^+ and K_{DR} currents were smaller. Discharge pattern in TFNs could be reversibly converted into that typical of AFNs in the presence of TTX but not TEA, suggesting that lower Na^+ conductance is more critical for the appearance of firing adaptation. Intracellularly labelled AFNs showed specific morphological features and preserved long extensively branching axons, indicating that smaller Na^+ conductance could not result from the axon cut. Computer simulation has further revealed that down-regulation of Na^+ conductance represents an effective mechanism for the induction of firing adaptation suggesting that the cell-specific regulation of Na^+ channel expression can be an important factor underlying the diversity of firing patterns in SG neurons.

(Melnick, Santos & Safronov, 2004; *J Physiol* 559: 383-394)

In conclusion, the data presented in this dissertation allowed us to provide a new knowledge on the functional connectivity of different types of SG interneurons and the modulation of their intrinsic firing via synaptic inputs. This knowledge is essential for better understanding the functioning of spinal nociceptive circuitry.

We characterized TFNs, AFNs and DFNs as excitatory or inhibitory interneurons, determined their distribution, transmitters they release and the type of postsynaptic receptors they act on. We also have shown that a MOR agonist selectively suppress TFNs, indicating that they could function as excitatory interneurons. This implies a strong relationship between the intrinsic firing and function of SG neurons and strongly supports the idea of specific targeting of postsynaptic MORs to excitatory SG interneurons. Moreover, MOR agonists acting via GIRK channels could switch firing mode of TFNs. Because of their numerous excitatory connections throughout the superficial dorsal horn, a selective inhibition of TFNs may underlie the analgesic postsynaptic effects of endogenous enkephalins and administered opioids.

We further studied the excitatory interneuron as an important processing element in the spinal SG. As a rule, the axon of an excitatory SG interneuron forms multiple synapses on the soma and

dendrites of a postsynaptic neuron. Many of those synapses have functional Ca^{2+}-permeable AMPA receptors. The excitatory transmission is frequently very effective and one excitatory SG interneuron can elicit spike in a postsynaptic neuron. The excitatory synapses are dynamic and can change their functional state showing diverse forms of spontaneous and induced plasticity which further increase synaptic efficacy.

V. RESUMO E CONCLUSÕES

Sabe-se que as diversas modalidades sensoriais na SG são codificadas pelos tipos de terminações de aferentes primários, propriedades de disparo e conectividade sináptica neuronial. Contudo, apesar de vários grupos de neurónios da SG com distintas propriedades de disparo terem sido caracterizados, sabe-se muito pouco sobre os principais tipos de canais iónicos expressos nos neurónios da SG, assim como as conexões sinápticas que estabelecem. Para além disso, apesar da SG ser um importante elemento do sistema antinociceptivo, pouco é sabido sobre os tipos de neurónios que servem de alvos pós-sinápticos específicos para a acção dos opioides nesta região espinhal.

Desta forma, para melhor compreendermos o processamento da informação nociceptiva no corno dorsal superficial, é essencial o estudo do tipo de disparos intrínsicos dos neurónios da SG, da sua conectividade e sensibilidade a agonistas de receptores opioides.

De forma a facilitar o estudo destas questões, o presente trabalho foi dividido em vários pontos independentes:

1. Para o estudo dos mecanismos espinhais de analgesia opioidérgica, comparámos a acção do agonista de receptores opioides do tipo μ, DAMGO, em neurónios da SG com diferentes propriedades de disparo intrínsico. Foram criados critérios de identificação fiáveis de forma a classificar correctamente os diferentes padrões intrínsicos e estudar a distribuição neuronial e sensibilidade ao DAMGO.

O DAMGO hiperpolarizou selectivamente todos os neurónios de disparo tónico testatos e o seu efeito ficou a dever-se à activação da condutância GIRK e, como consequência funcional, a maioria destes neurónios modificou o seu padrão de disparo de tónico para adaptativo. Consequentemente, foi sugerido que estes neurónios são alvos pós-sinápticos principais para agonistas de opioides endógenos e administrados exogenamente na SG. De facto, a transição funcional de disparo tónico para adaptativo poderá representar um importante mecanismo facilitador de analgesia mediada por opioides. É ainda sugerido que os neurónios de disparo tónico funcionam, presumivelmente, como interneurónios excitatórios.

(Santos, Melnick & Safronov, 2004; *Anesthesiology* **101**: 1177-1183)

2. Implementámos uma nova técnica para identificação eficiente de conexões mono-sinápticas e estudo das propriedades de descarga dos interneurónios excitatóros e inibitórios da SG. Esta estratégia combinou o registo apertado em 'whole-cell' do neurónio pós-sináptico com a estimulação específica em 'cell-attached' do neurónio pré-sináptico. Focámo-nos em dois aspectos

críticos e desconhecidos da rede organizacional da SG: (1) o balanço funcional entre os modos de processamento sensoriais excitatório e inibitório e (2) se e como as propriedades de disparo neuroniais se correlacionam com as sinapses estabelecidas. Caracterizámos as conexões sinápticas dos neurónios da SG com diferentes padrões de disparo e verificámos que a sinalização na SG é dominada por interneurónios excitatórios glutamatérgicos.

(Santos, Rebelo, Derkach & Safronov, 2007; *J Physiol* **581**: 241-254)

3. De forma a estudar a organização funcional das sinapses glutamatérgicas dos interneurónios excitatórios da SG, combinámos técnicas de registo duplo de patch-clamp (registos não invasivos mantendo o neurónio pós-sináptico em 'perforated-patch' e estimulando o neurónio pré-sináptico intacto com a pipeta em 'cell-attached'), simulações computacionais e processamento de células em conexão coradas com biocitina. Concluímos que: 1) Os potenciais de acção podem ser rapidamente iniciados no neurónio da SG por uma despolarização de apenas cerca de 10 mV; 2) O glutamato libertado dos terminais de um neurónio excitatório da SG actua em ambos os receptores AMPA, sem a subunidade GluR2 (permeáveis ao Ca^{2+}), e com a subunidade GluR2 (impermeáveis ao Ca^{2+}); 3) As EPSCs evocadas pela estimulação dos interneurónios excitatórios da SG são rápidas e a variação na sua cinética indica a ampla distribuição das sinapses excitatórias ao longo do domínio somatodendrítco do neurónio pós-sináptico; 4) Vários interneurónios excitatórios são capazes de iniciar o potencial no neurónio pós-sináptico; 5) As sinapses formadas pelos interneurónios da SG podem ser submetidas a diferentes formas de plasticidade espontânea e induzida, alterando o seu estado funcional e aumentando a sua eficácia de transmissão; 6) O axónio do interneurónio excitatório da SG forma múltiplas sinapses funcionais nas dendrites do neurónio pós-sináptico; 7) A alta R_{IN} do neurónio pós-sináptico é importante para o correcto estudo da transmissão sináptica, uma vez que a redução da R_{IN} reduz dramaticamente, quer a magnitude, quer a eficácia funcional dos inputs distais.

(Santos, Luz, Szücs, Lima, Derkach & Safronov; *PlosOne* **4**: e8047, pp1-18)

4. De forma a determinar a base iónica subjacente aos disparos tónico e adaptativo fizemos registos em patch-clamp, coloração intracelular com biocitina e criámos um modelo computacional do neurónio da SG.

Concluímos que existe um equilíbrio de condutâncias iónicas subjacente ao disparo tónico nos neurónios da SG. As correntes de Na^+ dependentes de voltagem em combinação com uma pronunciada corrente K_{DR} e negligenciável corrente K_A geram o padrão básico de disparo, enquanto as condutâncias dependentes de Ca^{2+} estabilizam o disparo tónico, regulam a frequência de descarga e modulam as características neuroniais input–output.

(Melnick, Santos, Szokol, Szucs & Safronov, 2004; *J Neurophysiol* **91**: 646-655)

No caso dos neurónios de disparo adaptativo, apesar das correntes de Na^+ e K_{DR} serem semelhantes às observadas nos neurónios de disparo tónico, são menores. O padrão de disparo nos TFNs pode ser reversivelmente convertido no típico disparo adaptativo na presença de TTX mas não de TEA, sugerindo que uma menor condutância de Na^+ é crítica para o aparecimento da adaptação do disparo. Os neurónios de disparo adaptativo corados intracelularmente apresentavam características morfológicas específicas com longos axónios preservados, indicando que a condutância menor de Na^+ não é resultado do corte axonal. A simulação computacional revelou ainda que a diminuição da condutância de Na^+ representa um mecanismo efectivo para a indução da adaptação do disparo sugerindo que a regulação celular específica da expressão do canal de Na^+ deverá ser um importante factor subjacente à diversidade dos padrões de disparo na SG.

(Melnick, Santos & Safronov, 2004; *J Physiol* **559**: 383-394)

Em conclusão, os dados desta dissertação permitem-nos providenciar um novo conhecimento sobre a conectividade funcional dos diferentes tipos de interneurónios da SG e sobre a modulação do padrão intrínsico de disparo através dos inputs sinápticos. Este conhecimento é essencial para o melhor entendimento dos circuitos espinhais nociceptivos.

Caracterizámos os neurónios TFNs, AFNs e DFNs como excitatórios ou inibitórios, determinámos a sua distribuição, os neurotransmissores libertados e o tipo de receptores pós-sinápticos em que actuam. Mostrámos ainda que o agonista dos MORs suprime selectivamente os TFNs, indicando que estes podem funcionar como interneurónios excitatórios. Isto implica uma forte relação entre o padrão de disparo e a função dos neurónios da SG e suporta fortemente a ideia da existência de alvos pós-sinápticos específicos para os MORs por parte dos interneurónios excitatórios da SG. Para

além disso, os agonistas dos MORs, que actuam via canais GIRK, podem modificar o tipo de disparo tónico. Dadas as numerosas conexões excitatórias que os TFNs podem estabelecer no corno dorsal espinhal superficial, a sua inibição selectiva poderá estar na base dos efeitos pós-sinápticos das encefalinas endógenas e opioides administrados.

Estudámos ainda o interneurónio excitatório como um importante elemento no processamento espinhal na SG. Como regra, o axónio de um interneurónio excitatório da SG forma múltipas sinapses no soma e dendrites do neurónio pós-sináptico. Várias destas sinapses apresentam receptores AMPA funcionais permeáveis ao Ca^{2+}. A transmissão excitatória é frequentemente muito efectiva e apenas um interneurónio excitatório pode evocar o potencial de acção no neurónio pós-sináptico. As sinapses excitatórias são dinâmicas e podem modificar o seu estado funcional através de diversas formas de plasticidade com consequente aumento da eficácia sináptica.

' O cientista não é o homem que fornece as verdadeiras respostas, é quem faz as verdadeiras perguntas. '

Claude Lévi-Strauss
O Cru e o Cozido

Capa: Revelação histológica de dois neurónios da SG em conexão sináptica.

Júri de Dutoramento

Presidente- Director da Faculdade de Medicina, Prof Dr Agostinho Marques.

Arguentes

Doutor Victor A. Derkach, Físico, Professor do Vollum Institute, Oregon Health & Science University, Portland, USA;

Doutora Ana Maria Ferreira de Sousa Sebastião, Professora Associada da Faculdade de Medicina da Universidade de Lisboa.

Vogais

Doutora Deolinda Maria Valente Alves Lima Teixeira, Médica, Professora Catedrática da Faculdade de Medicina da Universidade do Porto;

Doutor José Manuel Pereira Dias Castro Lopes, Médico, Professor Catedrático da Faculdade de Medicina da Universidade do Porto;

Doutor Rui Manuel Cardoso Vaz, Neurocirurgião, Professor Associado Convidado da Faculdade de Medicina da Universidade do Porto;

Doutora Mónica Luísa Ribeiro Mendes de Sousa, Investigadora Principal do Instituto de Biologia Molecular e Celular.